Evolution of the global productivity of terrestrial ecosystems under constraint linked to nitrogen availability : analysis over the recent historical period and future projections

Jaime Andres Riano Sanchez

THÈSE DE DOCTORAT

NNT : 2023UPASJ012

université PARIS-SACLAY

Evolution of the global productivity of terrestrial ecosystems under constraint linked to nitrogen availability: analysis over the recent historical period and future projections

Évolution de la productivité globale des écosystèmes terrestres sous contrainte liée à la disponibilité en azote : analyse sur la période historique récente et projections futures

Thèse de doctorat de l'université Paris-Saclay

École doctorale n° 129, Sciences de l'Environnement d'Île-de-France (SEIF)
Spécialité de doctorat : Géosciences
Graduate School : Géosciences, climat, environnement et planètes
Référent : Université de Versailles-Saint-Quentin-en-Yvelines

Thèse préparée dans l'unité de recherche **LSCE** (Université Paris-Saclay, CNRS, CEA, UVSQ)
sous la direction de **Nicolas VUICHARD,** chercheur, CEA,
et la codirection de **Philippe PEYLIN**, directeur de recherche, CNRS

Thèse soutenue à Saint-Aubin, le 23 mars 2023, par

Jaime Andres RIANO SANCHEZ

Composition du Jury

Membres du jury avec voix délibérative

Benoît GABRIELLE Professeur des Universités, AgroParisTech	Président du jury
Éric CESCHIA Directeur de recherche, INRAE	Rapporteur & Examinateur
Roland SÉFÉRIAN Ingénieur-Chercheur, CNRM Météo-France	Rapporteur & Examinateur
Alberte BONDEAU Chargée de recherche, CNRS	Examinatrice
Nicolas DELPIERRE Professeur des Universités, Université Paris-Saclay	Examinateur

université PARIS-SACLAY

ÉCOLE DOCTORALE
Sciences de l'Environnement d'Île-de-France (SEIF)

Titre : Évolution de la productivité globale des écosystèmes terrestres sous contrainte liée à la disponibilité en azote : analyse sur la période historique récente et projections futures

Mots clés : Puits de carbone, azote, écosystèmes terrestres, cycle du carbone, changement climatique, fixation biologique de l'azote.

Résumé : Les écosystèmes terrestres absorbent actuellement plus d'un quart des émissions de CO_2 d'origine anthropique, grâce à l'effet de fertilisation associé à l'augmentation du CO_2 atmosphérique. La plupart des modèles de systèmes terrestres utilisés dans les récents travaux du GIEC estiment que les écosystèmes terrestres continueront à se comporter comme un puits de carbone de plus ou moins grande ampleur au XXIe siècle, en fonction des trajectoires futures du CO_2 atmosphérique et du climat. Quelle que soit l'évolution de la concentration de CO_2 atmosphérique, il reste essentiel de déterminer si suffisamment de nutriments (en particulier l'azote) seront disponibles pour soutenir pleinement l'augmentation de la production primaire résultant de l'effet de fertilisation d'un CO_2 élevé. La plupart des modèles globaux des écosystèmes terrestres ne tiennent pas compte du cycle de l'azote et des interactions entre les cycles de l'azote et du carbone. La dernière version du modèle ORCHIDEE développé en France intègre ces nouvelles fonctionnalités

En utilisant ce modèle, l'objectif de la thèse sera d'analyser l'évolution de la productivité terrestre sur la période historique récente et de quantifier l'évolution future de la productivité des écosystèmes terrestres sous l'effet combiné de ces changements globaux : climat, concentration en CO_2, et évolution de la production d'azote réactif, selon différents scénarios socio-économiques.
L'inclusion du cycle couplé de l'azote et du carbone dans ORCHIDEE nécessite également une meilleure approximation d'un apport clé d'azote résultant de la fixation biologique de l'azote qui est actuellement déterminé par l'évapotranspiration. Ceci a été récemment invalidé par une étude de méta-analyse. Le second objectif de cette thèse consiste donc à implémenter un modèle dynamique basé sur les processus pour reproduire la BNF dans ORCHIDEE afin d'améliorer l'estimation des flux de carbone.

Title: Evolution of the global productivity of terrestrial ecosystems under constraint linked to nitrogen availability: analysis over the recent historical period and future projections

Keywords: Carbon sink, Nitrogen, Terrestrial Ecosystems, Carbon cycle, Climate change, Biological Nitrogen Fixation.

Abstract : Terrestrial ecosystems currently absorb more than a quarter of CO_2 emissions of anthropogenic origin, thanks to the fertilization effect associated with the increase in atmospheric CO_2. Most of the terrestrial system models used in recent IPCC work estimate that terrestrial ecosystems will continue to behave like a carbon sink of greater or lesser magnitude in the 21st century, depending on the future trajectories of atmospheric CO_2 and climate. Whatever the evolution of atmospheric CO_2 concentration, it remains critical to determining whether enough nutrients (particularly nitrogen) will be available to fully support the increase in primary production resulting from the fertilization effect of elevated CO_2. Most global models of terrestrial ecosystems do not account for the nitrogen cycle and the interactions between the nitrogen and carbon cycles. The latest version of the ORCHIDEE model developed in France incorporates these new features.

Using this model, the objective of the thesis will be to analyze the evolution of terrestrial productivity over the recent historical period and to quantify the future development of the productivity of terrestrial ecosystems under the combined effect of these global changes: climate, CO_2 concentration, and reactive nitrogen production evolution, according to different socio-economic scenarios.
Including the coupled nitrogen and carbon cycle in ORCHIDEE also requires a better approximation to one key Nitrogen input resulting from Biological Nitrogen Fixation that is currently determined by evapotranspiration. This has been recently invalidated by a meta-analysis study. The second objective of this thesis consists then of implementing a process-based dynamic model for reproducing BNF in ORCHIDEE to improve the estimation of the carbon fluxes.

"*Carbon sequestration is a critical component of our efforts to combat climate change. It is a win-win solution that allows us to reduce emissions while also improving the health and productivity of our forests, grasslands and agricultural lands*".

Tom Vilsack, former Secretary of Agriculture of the United States.

Acknowledgements

I would like to express my deepest gratitude to my research supervisors, Dr. Nicolas Vuichard and Dr. Philippe Peylin for their unwavering support, guidance, and encouragement throughout the course of this research. I would not have been able to complete this work without their mentorship, expertise, and patience. They have been a constant source of inspiration and motivation, and I am forever grateful for their guidance, support, and friendship.

I would also like to thank the members of my Ph.D. committee: Dr. Alberte Bondeau, Dr. Benoît Gabrielle, Dr. Nicolas Delpierre, Dr. Roland Séférian and Dr. Éric Ceschia for their valuable feedback, insights, and suggestions on the manuscript. Their expertise and knowledge in the field have been of great help in shaping the research and making it a success.

I would like to acknowledge the CEA for their financial support of this research. Without their support, this work would not have been possible. I also wish to thank the LSCE for providing the necessary resources and facilities for the research. I am grateful to the staff of the laboratory for their help and support throughout the research. I would like to express my appreciation to my colleagues for their support and helpful discussions. Their camaraderie and feedback have been essential in the progress of this work.

I would like to extend my appreciation to all the body of technical staff for their help and support in providing the necessary resources, materials, and equipment. Their invaluable assistance is greatly appreciated. I also wish to thank the administrative staff for their help and support throughout the research.

I wish to extend a special thanks to my family, especially my parents, my brother and my sister, and friends for their unwavering love and support throughout this journey. Their encouragement and understanding have been invaluable, and I am forever grateful. I would like to express my appreciation for the support provided by my partner, who has been a constant source of love, encouragement, and understanding throughout this journey.

Finally, I would like to acknowledge the countless hours spent reading, editing, and proofreading this manuscript. My gratitude to all those who have helped them in one way or another during this journey cannot be fully expressed in words. I would also like to express my appreciation for the support of my friends and colleagues who have encouraged and motivated me throughout this journey. This work is dedicated to all of them for their love and support. To my grandad who is not among us, and who always wanted me to be a doctor, this is also for you.

¡Reviente, hediondo!

Summary

Terrestrial ecosystems play a crucial role in the global carbon cycle by absorbing more than a quarter of CO_2 emissions of anthropogenic origin. This carbon sequestration in terrestrial ecosystems is primarily due to the fertilization effect associated with the increase in atmospheric CO_2. However, nutrients, in particular nitrogen, also play a key role as their availability may limit or boost the increase in terrestrial productivity resulting from the CO_2 fertilization effect, hence directly controlling the net carbon storage.

The thesis aims at quantifying the role of nitrogen on the global terrestrial productivity over the industrial period and for near-future scenarios. It is based on the use and development of a global terrestrial ecosystem model, named ORCHIDEE, which includes a representation of the nitrogen cycle and of the carbon-nitrogen interactions.

Based on a set of factorial simulations over the industrial period (varying alternatively atmospheric CO_2, nitrogen deposition and/or climate), I estimated that the anthropogenic increase of atmospheric nitrogen deposition on lands was responsible for ~20% of the current land carbon sink, the remaining being mainly due to atmospheric CO_2 increase. The impact of increasing nitrogen deposition is highly variable in space, with a large effect near industrialized regions or intense agricultural activities (with fertilization practices).

In the second part of the thesis, I focus on the projected change in land carbon store (CLCS) over the 21st century under the combined evolution of climate, CO_2 concentration, land-use change and reactive nitrogen production, according to different socio-economic scenarios (derived from the last climate projection inter-comparison project, CMIP6). I estimated that the CLCS spread associated with the uncertainty on the land-use change trajectories is as large as the one associated with atmospheric CO_2, while uncertainty associated with nitrogen depositions is responsible for a spread in CLCS lower by a factor three.

In the third part of my thesis, I implemented a process-based dynamic model of the Biological Nitrogen Fixation (BNF) into ORCHIDEE (in replacement of the initial constant fixation rate) and quantified the impact of this new modeling scheme on the simulated historical and future carbon fluxes. While the default and new BNF models induce similar land carbon fluxes over the past industrial period, significant changes are projected over the 21st century, with an increase of the land carbon store of 70% with the new BNF model for some socio-economic scenarios.

Overall, the thesis provides a comprehensive and integrated analysis of the interactions between the carbon and nitrogen cycles in terrestrial ecosystems in response to global changes, using a state of the art process based land surface model. The results of this thesis will contribute to the development of more accurate and reliable projections of the terrestrial

carbon sequestration potential for near-future climate and may serve for decision-making regarding climate change mitigation and adaptation solutions.

Résumé

Les écosystèmes terrestres jouent un rôle essentiel dans le cycle global du carbone en absorbant plus du quart des émissions de CO_2 d'origine anthropique. Cette séquestration de carbone dans les écosystèmes terrestres est principalement due à l'effet fertilisant lié à l'augmentation du CO_2 atmosphérique. Cependant, les nutriments, en particulier l'azote, jouent également un rôle clé car leur disponibilité peut limiter ou amplifier l'augmentation de la productivité terrestre résultant de l'effet de fertilisation du CO_2, contrôlant ainsi directement le stockage net de carbone.

La thèse vise à quantifier le rôle de l'azote sur la productivité terrestre globale sur la période industrielle et pour des scénarios futurs. Il est basé sur l'utilisation et le développement d'un modèle global d'écosystème terrestre, nommé ORCHIDEE, qui inclut une représentation du cycle de l'azote et des interactions carbone-azote.

Sur la base d'un ensemble de simulations factorielles sur la période industrielle (variant alternativement le CO_2 atmosphérique, les dépôts d'azote et/ou le climat), j'ai estimé que l'augmentation anthropique des dépôts d'azote atmosphérique sur les terres était responsable de ~20% du puits de carbone terrestre actuel, le reste étant principalement dû à l'augmentation du CO_2 atmosphérique. L'impact de l'augmentation des dépôts d'azote est très variable dans l'espace, avec un effet important à proximité des régions industrialisées ou des activités agricoles intenses (avec des pratiques de fertilisation).

Dans la deuxième partie de la thèse, je me concentre sur l'évolution projetée du carbone stocké dans les écosystèmes terrestres (ECST) au cours du 21e siècle sous l'évolution combinée du climat, de la concentration en CO_2, du changement d'affectation des terres et de la production d'azote réactif, selon différents scénarios socio-économiques (issus du dernier projet d'intercomparaison des projections climatiques, CMIP6). J'ai estimé que la dispersion de l'ECST associée à l'incertitude sur les trajectoires de changement d'affectation des terres est aussi grande que celle associée au CO_2 atmosphérique, tandis que l'incertitude associée aux dépôts de N est responsable d'une dispersion de l'ECST inférieure d'un facteur trois.

Dans la troisième partie de ma thèse, j'ai implémenté un modèle dynamique de la fixation biologique de l'azote (BNF) dans ORCHIDEE (en remplacement du taux de fixation initial constant au cours du temps) et ai quantifié l'impact de ce nouveau schéma de modélisation sur les flux de carbone simulés. (sur la période historique et pour le futur). Alors que le modèle par défaut et le nouveau modèle de BNF induisent des flux de carbone similaires au cours de la dernière période industrielle, des changements significatifs sont projetés au cours du 21e siècle, avec une augmentation de la réserve de carbone terrestre de 70 % avec le nouveau modèle de BNF pour certains scénarios socio-économiques.

Dans l'ensemble, la thèse fournit une analyse intégrée des interactions entre les cycles du carbone et de l'azote dans les écosystèmes terrestres en réponse aux changements globaux, en utilisant un modèle de surface terrestre basé sur des processus. Les résultats de cette thèse contribueront au développement de projections plus précises et fiables du potentiel de séquestration du carbone terrestre pour le climat futur et pourraient servir à la prise de décision concernant des mesures d'atténuation et d'adaptation au changement climatique.

Table of contents

Table of images

Abbreviations

Carbon (**C**)

Carbon dioxide (***CO_2***)

Elevated CO_2 (***eCO_2***)

Nitrogen (***N***)

Molecular Dinitrogen (***N_2***)

Phosphorous (***P***)

Water (***H_2O***)

Oxygen (**O_2**)

Sugar (**$C_6H_{12}O_6$**)

Nicotinamide Adenine Dinucleotide Phosphate (***NADP***)

Adenosine triphosphate (**ATP**)

Nitrate (***NO_3-***)

Nitrite (***NO_2-***)

Nitrous Oxide (***N_2O***)

Nitric Oxide (**NO**)

Amino group (**NH_2-**)

Alpha Ketone Acid (***$C_4H_6O_3$***)

Carboxyl group (***-COOH***)

Ammonia (***NH_3***)

Ammonium (***NH_4+***)

Acetylene Reduction Assay Method (***ARA***)

Acetylene (**C_2H_2**)

Gram (***g***)

Kilogram (***kg***)

Tera-gram (**Tg**)

Peta-gram (***Pg***)

Gigaton (***Gt***)

Parts per million (**ppm**)

Gross Primary Productivity (***GPP***)

Net Primary Production (***NPP***)

Net Ecosystem Productivity (***NEP***)

Net Biospheric Production (***NBP***)

Dynamic Global Vegetation Model (***DGVM***)

Land Surface Model (***LSM***)

Earth System Model (***ESM***)

Climate Research Unit (***CRU***)

Oak Ridge National Laboratory (***ORNL***)

Community Land Model (***CLM***)

Community Land Model 4.0 (**CLM4**)

Organizing Carbon and Hydrology in Dynamic Ecosystems (***ORCHIDEE***)

Food and Agriculture Organization (***FAO***)

Soil Carbon Pool (***SCP***)

Land Use Change (***LUC***)

Land-Use Change and Forestry (***LULUCF***)

Fossil fuel emission (***EFOS***)

Net land use change emission (***ELUC***)

Atmospheric growth (***GATM***)

Ocean sink (***SOCEAN***)

Land sink (***SLAND***)

Free Air CO_2 Enrichment (***FACE***)

Stomatal conductance (***SWC***)

Couple Model Intercomparison (***CMIP***)

Fifth Phase of the Couple Model Intercomparison (***CMIP5***)

Sixth Phase of the Couple Model Intercomparison (***CMIP6***)

Land Use Model Intercomparison Project (***LUMIP***)

Plant Functional Type (***PFT***)

Soil Organic Matter (***SOM***)

Leaf Area Index (***LAI***)

Normalized Difference Vegetation Index (***NDVI***)

Global Carbon Budget (***GCB***)

Trends in Land carbon cycle (***TRENDY***)

Terrestrial Ecosystem Carbon (***TEC***)

Land Use Land Cover Change (***LULCC***)

Input datasets for Model Intercomparison Project (***Input4MIPS***)

Atmospheric CO_2 Use Efficiency (***ACUE***)

Integrated Assessment Models (***IAM***)

Gross Domestic Product (***GDP***)

Shared Socio-economic Pathways (***SSP***)

Institute Pierre Simon Laplace (IPSL)

Scenario Model Intercomparison Project (***ScenarioMIP***)

Radiative Concentration Pathway (***RCP***)

Change in land Carbon Store (***CLCS***)

Greenhouse gases (***GHG***)

Dissolved Organic Carbon (***DOC***)

Nitrogen Use Efficiency (***NUE***)

Biological Nitrogen Fixation (***BNF***)

Nitrogen deposition (***Ndep***)

Free-living nitrogen fixation (***FLNF***)

Reduced nitrogen reactive compounds (***NHx***)

Nitrogen oxides (***NOy*** or ***NOx***)

Yu and Zhuang BNF Model (***Y&Z***)

Dynamic Biological Nitrogen Fixation (***dBNF***)

Static Biological Nitrogen Fixation (**sBNF**)

Atmospheric Nitrogen Deposition Use Efficiency (***ANDUE***)

"*Carbon sequestration, by which carbon dioxide is removed from the atmosphere and stored, is an important way to combat climate change*".
Al Gore, former Vice President of the
United States and Climate Activist

CHAPTER 1

Carbon and nitrogen cycles, interactions, limitations, and modeling.

1.1 Global carbon cycle

Carbon is a vital element on Earth. It forms the structure of all life on the planet, thus representing almost 50% of the dry weight of all living organisms. Carbon compounds are a fundamental source of energy. Plants transform the radiant energy into chemical energy in the form of sugars, starches and other organic molecules that support food chains and so living beings' metabolisms. Its fossil form is used for heating, transportation and generation of electricity (Houghton, 2003), sustaining global economic development.

The carbon exchange between biotic and abiotic reservoirs through the biosphere, pedosphere, geosphere, hydrosphere, and atmosphere of the Earth, is defined as the global biogeochemical carbon cycle. Numerous chemical, physical, geological, and biological processes all contribute to the flow of carbon across reservoirs (Friedlingstein et al., 2022). The continental crusts and upper mantle contain the most carbon on Earth, with 122,576,000 PgC (1 Pg = 1 Gt = 1 billion metric tons = $1*10^{15}$ g) (Kayler et al., 2017), followed by carbon in the

seas, with 39,495 PgC (in the forms of dissolved carbon compounds (organic and inorganic), particulate carbon, surface sediments). The third largest reservoir is carbon trapped in soils and permafrost, which accounts for 3,100 PgC, in addition to fossil fuel reserves of around 895 PgC. It is only followed by carbon in the atmosphere (875 PgC) and carbon in plants (450 PgC). (Figure 1.1) (Friedlingstein et al., 2022).

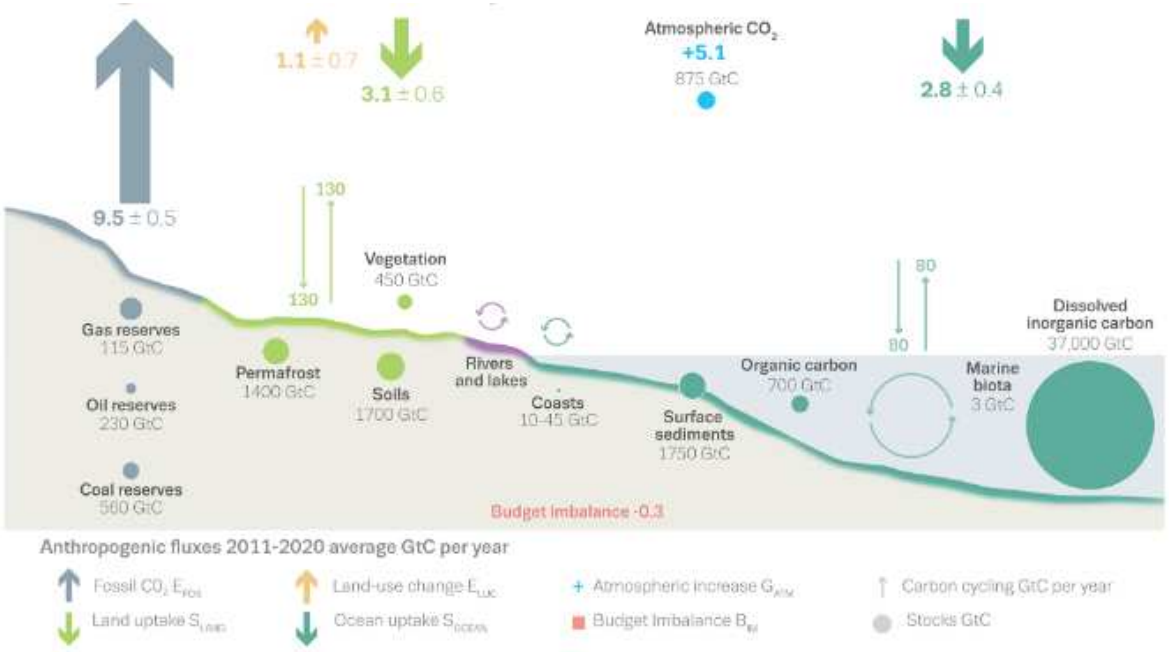

Figure 1.1 - Global carbon cycle: Schematic representation of the overall perturbation of the global carbon cycle caused by anthropogenic activities, averaged globally for the decade 2011–2020 in PgC (Friedlingstein et al., 2022).

Carbon in the atmosphere exists in two main forms: carbon dioxide (CO_2) and methane (CH4). These two gasses are to some extent responsible for the greenhouse effect because they retain and absorb the heat emitted from Earth. CO_2 is the dominant gas with a current concentration of 420 ppm (NOAA, 2022) corresponding approximately to a mass of 875±5 PgC (Canadell et al., 2021). Plants assimilate atmospheric CO_2 through photosynthesis. They produce organic molecules cycled through plant tissues, litter, and soil that can be released back into the atmosphere by autotrophic (plant) and heterotrophic (soil microbial and animal) respiration (Ciais et al., 2013). Organic carbon remaining in soil had turned into fossil fuels over the millions of years by exposure to heat and pressure in the Earth's crust (Canadell et al., 2021). A portion of the terrestrial carbon is also carried from the soil to rivers and streams, where it is expelled as CO_2. Another fraction is submerged in organic freshwater sediments (Ciais et al., 2013) and the remaining part passes through rivers to the coastal ocean in the form of dissolved inorganic carbon, dissolved organic carbon and particulate organic carbon (Tranvik et al., 2009).

Carbon also enters the ocean mainly through CO_2 dissolution through gas exchange driven by the partial CO_2 pressure difference between the air and the sea. This carbon is converted by organisms into organic carbon by photosynthesis and can be transfer throughout the food chain or precipitated into the ocean's deeper layer where is available predominantly as Dissolved Inorganic Carbon with a mass of around 37,173 ± 23 PgC (carbonic acid, bicarbonate and carbonate ions) and Dissolved Organic Carbon of around 700 PgC (Canadell et al., 2021), from which an important fraction has a turnover time of 1000 years or longer (Hansell et al., 2009). Without human involvement, carbon stocks would be generally steady since the natural movements of carbon between the atmosphere, ocean, terrestrial ecosystems, and sediments are balanced with relatively small net fluxes between these reservoirs.

1.1.1 Natural terrestrial carbon cycle

Terrestrial ecosystems play a significant role in the carbon balance at the *biosphere - atmosphere - pedosphere* confluence through physical and biogeochemical processes. In natural ecosystems, the carbon balance is mainly driven by photosynthesis and respiration. Photosynthesis (Equation 1.1) is a biological process through which plants, algae, and some bacteria transform radiative energy into chemical energy, splitting H_2O to liberate O_2, and fixating CO_2 into sugars $C_6H_{12}O_6$. It occurs in two stages, in the first one or so-called light-dependent reactions (Equation 1.2), the radiative energy is captured to make the hydrogen carrier NADPH and the molecule ATP that stores the energy. This complex process is controlled by environmental factors such as solar irradiance, humidity of the boundary layer, ambient temperature, atmospheric CO_2 concentration, nutrient availability and soil water availability (Govind & Kumari, 2014) mainly affect the second stage or light-independent reactions.

$$6CO_2 + 6H_2O + energy \rightarrow C_6H_{12}O_6 + 6O_2 \quad (1.1)$$

$$2H_2O + 2NADP^+ + 3ADP + 3Pi + light \rightarrow 2NADPH^+ + 2H + 3ATP + O_2 \quad (1.2)$$

During the second stage or light-independent reactions, these products are used to capture and reduce the carbon dioxide into carbohydrates (Whitmarsh & Gonvindjee, 1999). Globally, gross photosynthesis accounts for around 113 PgC yr^{-1} for pre-industrial era (Canadell et al., 2021). Part of this assimilated carbon is subsequently allocated above and belowground biomass, contributing to the global vegetation stock of 450 PgC (Janowiak et al., 2017).

Forests account for 92% of all terrestrial biomass, storing 400 PgC quite heterogeneously around the globe as a result of the different climates. Tropical forests account for two-thirds of all terrestrial biomass or 262 PgC, while temperate forests account for 47 PgC and boreal forests 54 PgC (Pan et al., 2013). The amount of carbon stored in aboveground organs such as

leaves, branches and stems depend also on climates. In the wet and warm region of the Tropics, there is more carbon stored above than below ground whereas for colder zones like the boreal regions there are enormous belowground carbon stores (Pan et al., 2013). Some of the distributions of carbon storage in forest for other ecosystems can be observed in (Figure 1.2).

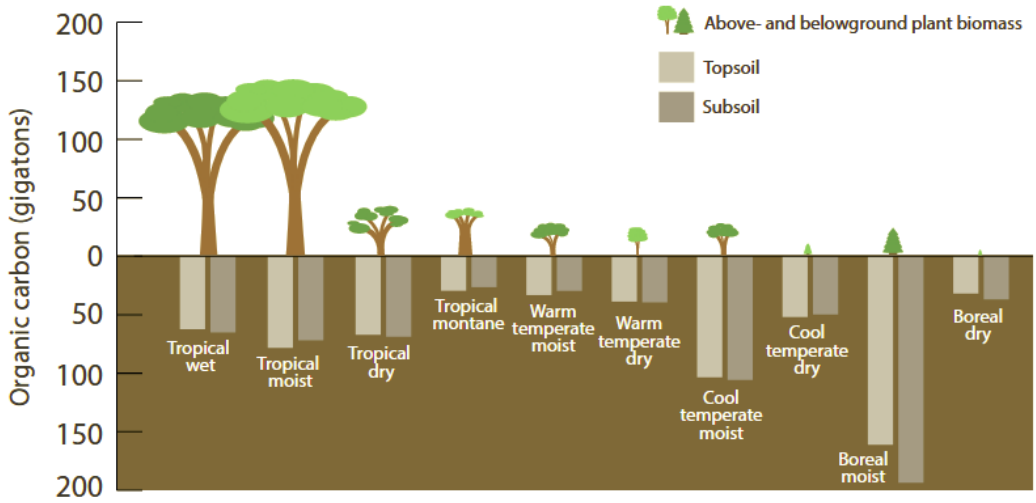

Figure 1.2 - Carbon stored in forest by ecosystems in gigatons of carbon GtC (Kayler et al., 2017).

The organic carbon present in plants and any living organism is then transferred to soil as litter to the different soil carbon pools (SCPs). Carbon stored as organic matter in active soil pools amounts to 1700 PgC while permafrost totals another 1700 PgC (Canadell et al., 2021). At a very slow rate that operates over millions of years, part of this carbon is sequestered into fossil reservoirs . Global stocks of fossil carbon are of around 900 PgC from which 580 correspond to coal, 230 PgC to oil and 118 PgC to gas (Canadell et al., 2021).

The biggest natural terrestrial emission of CO_2 corresponds to respiration and wildfires. While photosynthesis is a process of reduction of carbon dioxide to carbohydrates, cellular respiration (Equation 1.3) is the oxidation of carbohydrates to carbon dioxide to produce energy (in the form of ATP and NADPH) liberating CO_2 in the process.

$$C_6H_{12}O_6 + 6O_2 \rightarrow 6CO_2 + 6H_2O + energy \quad (1.3)$$

On the other hand, combustion (Equation 1.4), like respiration, is the process in which a carbon molecule is reduced by an oxidant (usually atmospheric oxygen) producing CO_2, water and heat. Fires in nature are both natural and human induced. Natural fires are the result of dry climate, lightning, climate variability and volcanic eruptions while human induced fires are the result of human activities such arson or burning methods for cleaning the fields followed by electricity transportation in power lines (Liu et al., 2013).

$$CxHy + \left(x + \frac{y}{4}\right) O_2 \rightarrow xCO_2 + \left(\frac{y}{2}\right) H_2O + energy \quad (1.4)$$

In total, terrestrial ecosystems emitted before the industrial era around 111 PgC yr^{-1} (Canadell et al., 2021) through respiration and natural fires. The difference between the photosynthesis, respiration, and fire fluxes makes a slightly positive net land flux, equilibrated by the loss of carbon through the riverine network. Nevertheless, since the industrial era there have been anthropogenic perturbations in the carbon cycle that have led to a change in the global carbon balance and therefore in the strength of the terrestrial carbon sinks.

1.1.2 Anthropogenic carbon cycle perturbation and its impacts on terrestrial ecosystems

1.1.2.1 Anthropogenic CO_2 emissions

Carbon circulates between the reservoirs of the atmosphere, ocean, and terrestrial biosphere on timescales varying from sub-daily to millennia, while exchanges with geologic reservoirs occur at longer timescales (Archer et al., 2009). This intricate circulation can be disturbed by natural processes such as wildfires, droughts, changes in the orbit of the Earth amongst others, or by humans included activities such as land use change and so agriculture, wildfire suppression and fossil fuel emission occurring in a much smaller timescale.

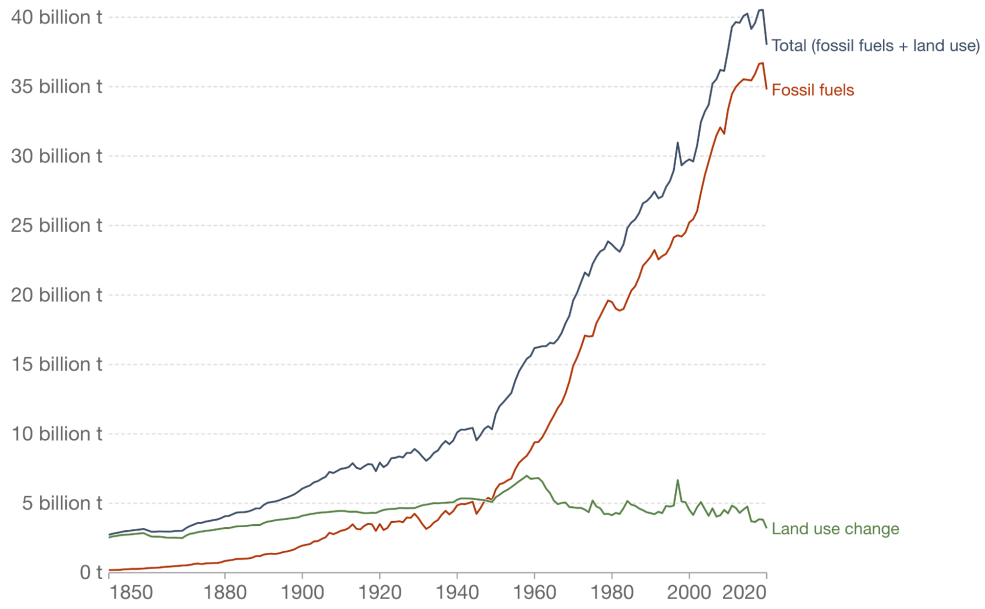

Figure 1.3 - CO_2 increase. Global CO_2 (in $PgCO_2$ yr^{-1}) emission from fossil fuels and land use change. Data adapted from (Friedlingstein et al., 2022) showcased by OurWorldInData.

Global CO_2 emissions have risen sharply since the beginning of the industrial revolution, owing primarily to the use of fossil fuels, followed by agriculture, deforestation, and other related

land use changes, as shown in (Figure 1.3), from 0.73 PgC yr^{-1} in 1850 to 8.03 PgC yr^{-1} in 2000. Anthropogenic emissions were dominated by land-use change emissions up to 1940-1950. Emissions from burning fossil fuels have surged during the 1950s, whereas emissions from land use change have tended to plateau and drop after 1960. Anthropogenic emissions disrupt the global carbon cycle (Figure 1.4) and hence drive climate change.

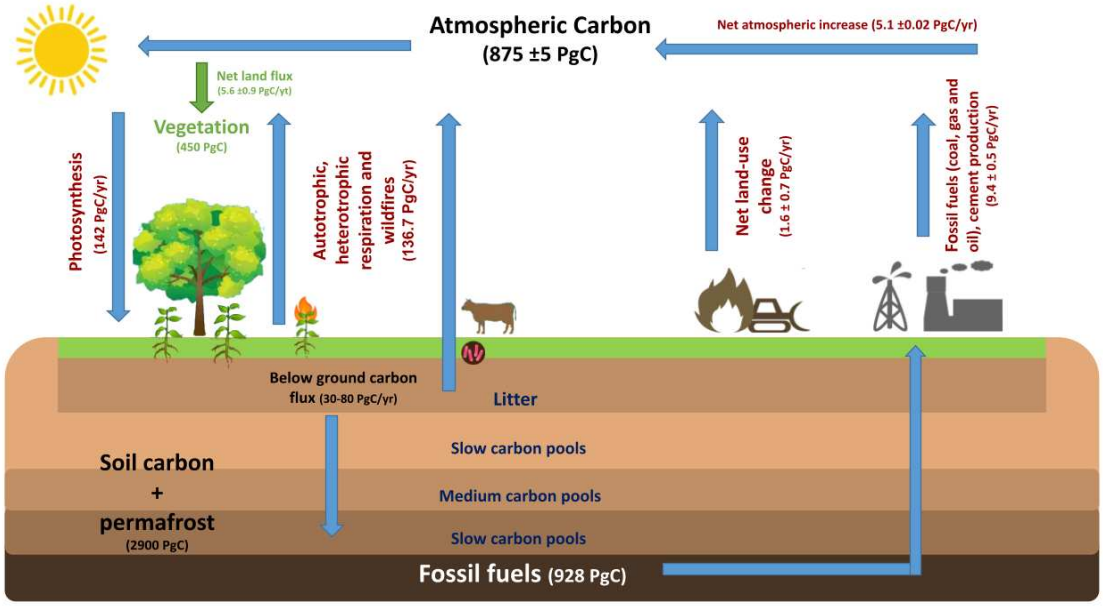

Figure 1.4 - Simplified terrestrial Carbon cicle and carbon budget (2010–2019), adapted from (Ciais et al., 2013).

<u>Perturbations due to fossil fuel burning emissions:</u>

Carbon released from hundreds of millions of years of geological storage from the burning of fossil fuels and cement production is the main contributor to anthropogenic CO_2 emissions. Anthropogenic emissions from fossil fuel emissions started before the industrial era and have become the dominant source of emissions to the atmosphere from around 1950, increasing significantly until the present (Friedlingstein et al., 2022). Fossil fuel emissions corresponded to 65% of the anthropogenic CO_2 emitted between 1750 and 2019, and for the last decade the percentage increased to 85%.

Over the past decade (2010–2019), 11 ±0.9 PgC yr–1 were emitted from human activities from which 9.4 ±0.5 PgC yr^{-1} corresponded to fossil fuel exploitation which were distributed between three Earth system reservoirs: 46% accumulated in the atmosphere (5.1 ± 0.02 PgC yr–1), 23% was taken up by the ocean (2.5 ± 0.6 PgC yr–1) and 31% was stored by vegetation in terrestrial ecosystems (3.4 ± 0.9 PgC yr–1) (Canadell et al., 2021).

By 2019, (Ritchie et al., 2020) reported anthropogenic emissions by sector. From 1990 to 2019,45% of the emissions corresponded to electricity and heat production, followed by manufacturing and construction (18%), transport (18%), buildings (8%), industry (4%),

unallocated fuel combustion (2%), fugitive emission from energy production (1%) as seen in (Figure 1.5).

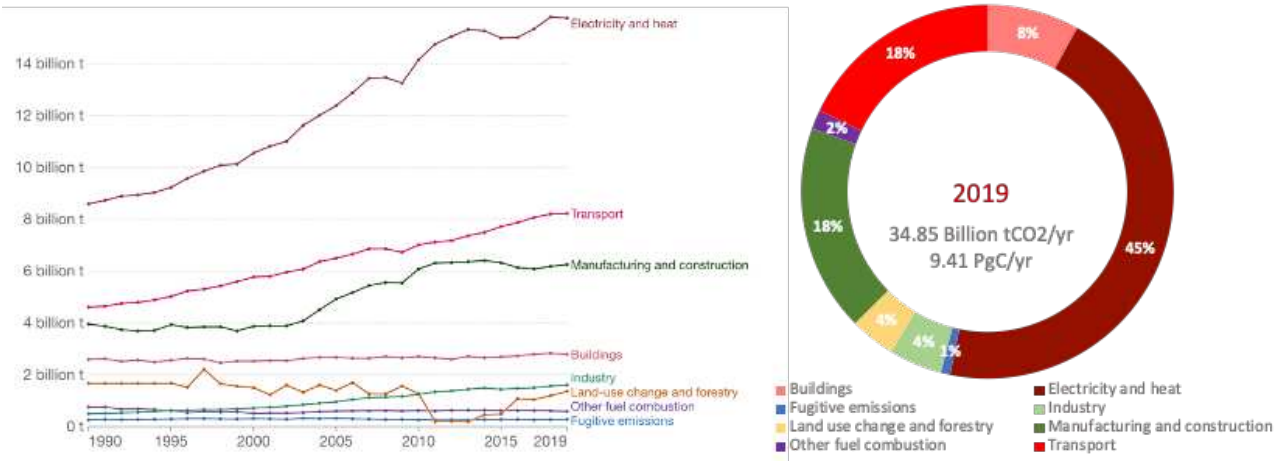

Figure 1.5 - Total CO_2 emission by sectors. (Right) evolution of the global anthropogenic CO_2 emissions by sectors from 1990 to 2019. (Left) percentage by sector in 2019 adapted from (Ritchie et al., 2020).

Perturbations due to land use change emissions:

The second anthropogenic source of emission of carbon stored for decades or centuries in vegetation and soil is due to deforestation and agricultural development. Human activities have altered land cover for thousands of years, but the intensity and magnitude have accelerated in recent centuries. Historically, 10% of the earth's surface has been converted from natural vegetation, releasing 182-199 PgC into the atmosphere (DeFries et al., 1999) from 1850 onwards.

Land use change emissions ranged from around 0.6 PgC yr^{-1} in 1850 to about 1.0 PgC yr^{-1} in the 1930s and never increased much (Houghton & Castanho, 2022). Over the past decade (2010–2019), 1.1 ± 0.7 PgC yr^{-1} were emitted from land use change. By 2020 alone, Land Use Change emission accounted for 0.9 ± 0.7 PtC yr^{-1}, or 2-8% of the total anthropogenic carbon emissions (Friedlingstein et al., 2022) over the 4% of the total carbon emissions by 2019 as reported by (Ritchie et al., 2020).

Houghton & Castanho, (2022) updated a long-term (1850-2020) series of yearly national carbon emissions from LULUCF (Houghton & Nassikas, 2017), based mostly after 1960 on land use information from the United Nations Food and Agriculture Organization (FAO). They found that the three tropical regions had the highest net emissions (a mean of 0.50, 0.41, and 0.31 PgC yr^{-1} for South and Southeast Asia, SubSaharan Africa, and Latin America, respectively). In comparison, four regions (Europe, North America, the Former Soviet Union (FSU), and China) had net sinks of about -0.09, -0.07, -0.05, and -0.02 PgC yr^{-1}, respectively. Individual area net negative emissions (carbon sinks) initially occurred in the 1920s, peaked at around -0.3 PgC

yr^{-1} in the 1970s, and stayed almost constant after that, though the sink appears to have fallen somewhat since 2005 (Figure 1.6).

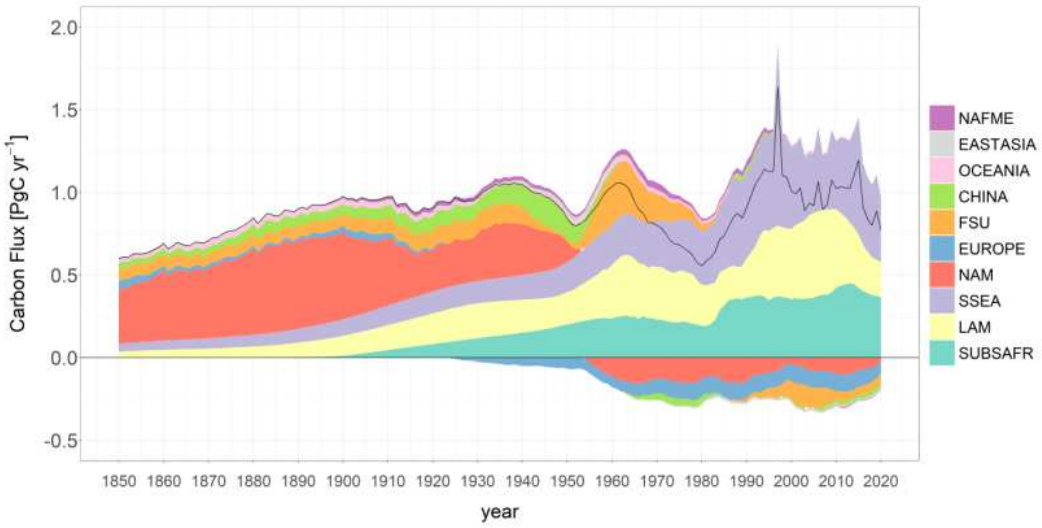

Figure 1.6 - Net annual emissions of carbon by regions (in PgC/yr) The black line represents the global net 316 annual emissions (Houghton & Castanho, 2022).

Global gross emissions (3.38 PgC yr^{-1}) were more than three times greater than net emissions (0.96 PgC yr^{-1}) between 2011 and 2020 (Houghton & Castanho, 2022), whereas gross removals averaged 2.42 PgC yr^{-1}. Gross emissions mainly were (69%) concentrated in three tropical regions (Latin America, tropical Africa, and South and Southeast Asia), whereas gross sinks were approximately evenly distributed between tropical (46%) and non-tropical (54%). The disparity is primarily due to greater rates of deforestation in the tropics. Rotational land uses, such as shifting agriculture and wood harvesting, have substantially lower net emissions than deforestation since gross emissions and removals (due to forest regeneration) are generally offsetting.

1.1.2.2 Emissions partitioning among the atmosphere, ocean, and land:

Over the industrial era from 1750 to 2019, almost 41% of combined anthropogenic CO_2 emissions (fossil fuel plus land use) have remained in the atmosphere. This has made the carbon dioxide CO_2 concentration in the atmosphere increased from 277 parts per million (ppm) in the beginning of the industrial era in 1750 (or a total stock of 591 PgC) (Joos & Spahni, 2008) to current concentration of 420 ppm (875 ± 5 PgC) (NOAA, 2022). Changes in atmospheric carbon content, and hence climate change, have in return also impacted the magnitudes of both ocean and terrestrial carbon balances.

Oceans are estimated to have removed 26% of the anthropogenic CO_2 emitted since 1850, while terrestrial ecosystems have taken approximately 30% (or 230 ± 60 PgC). Over the last six decades, the efficiency of ocean and land to remove CO_2 from the atmosphere have remained nearly constant with ocean and land fractions of respectively 26% and 30%. The land sink is

mainly driven by the fertilizing effect of increasing atmospheric CO_2 (Friedlingstein et al., 2019) which is further described hereafter as could be seen in (Figure 1.7).

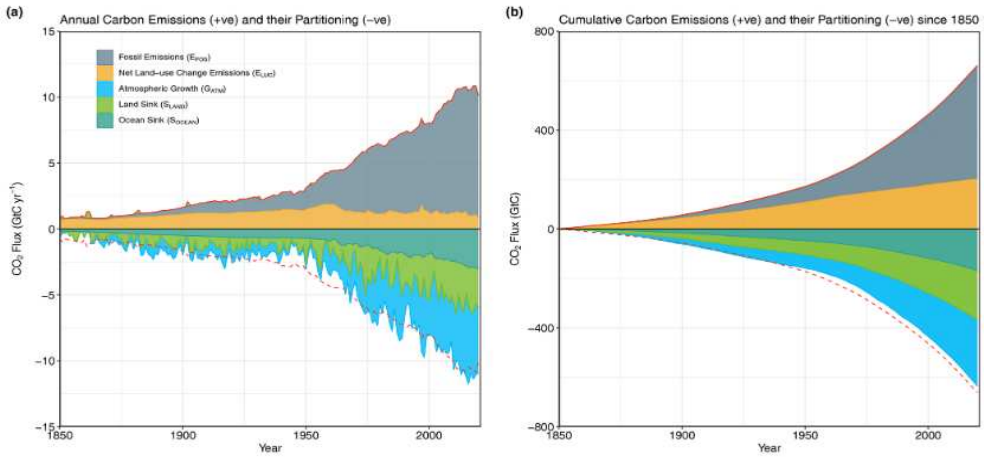

Figure 1.7 - Combined components of the global carbon budget. Fossil CO_2 emissions (EFOS, including a small sink from cement carbonation; gray) and emissions from land-use change (ELUC; brown), as well as their partitioning among the atmosphere (GATM; cyan), ocean (SOCEAN; blue), and land (SLAND; green) (Friedlingstein et al., 2022).

1.1.2.3 CO_2 fertilization effect:

The CO_2 fertilization effect, also known as the carbon fertilization effect, corresponds to an increase in carbon assimilation through photosynthesis while also limiting plant transpiration. Both processes are the result of rising carbon dioxide levels in the atmosphere (CO_2). Carbon fertilization has varying effects depending on plant type, air and soil temperature, and water and nutrient availability. Carbon fertilization has a favorable impact on Net Primary Production (NPP) (Kolby Smith et al., 2016). Thanks to the CO_2 fertilization effect, terrestrial ecosystems have thus lowered the human-induced rise of atmospheric CO_2 levels, therefore mitigating the consequences of climate change.

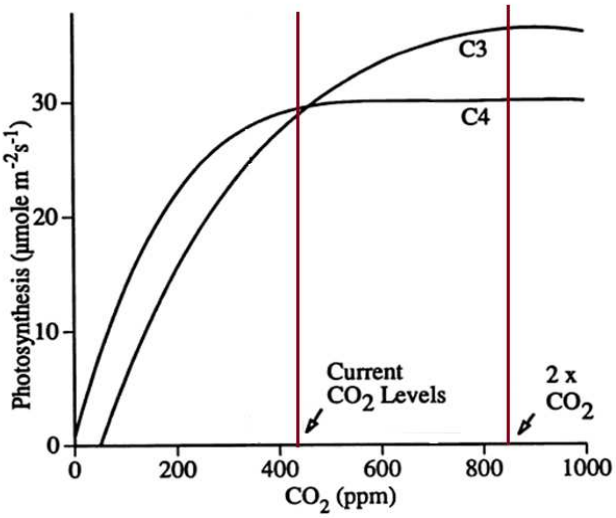

Figure 1.8 - Photosynthesis response to CO_2 concentration. Adapted from (Vivian, 1994).

A more detailed study shows for instance that for most C3 plants[1] the maximal photosynthetic rate is reached at 1000 ppm (more than twice current CO_2 concentration) while for C4 plants[2] it is reached at around 450 ppm (closer to current CO_2 concentration) (Körner et al., 2007) (Figure 1.8). This means that a substantial increase of terrestrial productivity may occur for the 21st century following the projected increase of CO_2 concentration.

The increase in leaf photosynthesis with rising CO_2 plays a dominant role in the current and projected global land carbon sink (Sitch et al., 2008) estimated by global terrestrial biogeochemical models. Recent studies from different modeling groups have shown important carbon sinks on terrestrial ecosystems of around 200 ± 65 GtC over the 1850-2020 period (Friedlingstein et al., 2022) with a major contribution from the rise of atmospheric CO_2 (O'Sullivan et al. 2022).

Since the early 1980s, the Earth's vegetated areas have become significantly greener, due to climate change and increased CO_2 levels in the atmosphere. However, the direct causes of vegetation greening are still being debated, highlighting the importance of long-term data collecting and study of responses to the influence of carbon fertilization (Albani et al., 2006)**.**

1.1.2.4 Interplay between the CO_2 fertilization effect and other environmental factors:

Plant productivity is also dependent on other elements like water availability, nutrition availability, and light intensity, all of which are intricately interconnected. Nitrogen-based nutrients are especially important since they are required to synthesize biomass from assimilated carbon (Arora et al., 2020a), limiting the effect of CO_2 fertilization.

Experimental infrastructures for studying plant and ecosystem functioning:

In conventional laboratory test experiments, a common effect of exposure to high concentrations of CO_2 is a reduction in nutrient and water uptake per unit of biomass produced (Drake et al., 1997). In other cases in which nutrient uptake is increased under high CO_2 concentrations this will deplete soils in the long term (Finzi et al., 2002). The response to elevated CO_2 levels also depends on the stage of plant development. Young plants have a greater response and therefore greater growth (Loehle, 1995). All of this shows that the ecosystem processes associated with the CO_2 fertilization effect remain uncertain and, therefore, difficult to model. As we will further discuss, the particular limitation due to nitrogen disponibility is widely study to correct past and future carbon stocks on Earth system models (ESMs), land system models (LSMs), and dynamic global vegetation models (DGVMs) (Vuichard et al., 2019; Zaehle, 2013)

[1] Some common C3 plant species include spinach, peanuts, cotton, wheat, rice, barley and most trees and grasses.

[2] Some common C4 plants species include maize (Zea mays), sugarcane (Saccharum officinarum), sorghum (Sorghum bicolor), millets, and switchgrass (Panicum virganum).

To understand the ecosystem response to elevated CO_2, a set of continuous CO_2 flow experiments or Free Air CO_2 Enrichment (FACE) have been conducted over the last decades. Experiments with FACE (with usually a doubling of CO_2 concentration level compared to current ambient level) are essential since most investigations on the effects of increasing CO_2 concentrations have been done in labs, where numerous aspects, like plant competition, were lacking. A new generation of FACE experiments in mature forests in various biomes and across a wide range of climate space and biodiversity was analyzed by Norby et al. (2016) to significantly expand the inference space of these experiments. The studied FACE sites where:

- EucFACE in a mature Eucalyptus stand on highly weathered soil in subtropical Australia
- AmazonFACE in a highly diverse primary rainforest in Brazil
- BIFoR-FACE in a 150-year-old deciduous woodland stand in central England
- SwedFACE in a hemiboreal *Pinus sylvestris* stand in Sweden.

This represented a once-in-a-lifetime opportunity to incorporate a model-data interaction into experimental design and address cross-site science questions on topics such as mature forest responses, interactions with temperature, water stress, and nutrients limitation. Each of these independent experiments had a set of science questions and hypotheses that were specific to the location (Norby et al., 2016). There are also some compelling questions shared by all of these sites that will benefit from a cross-site analysis. Here below are some of the main conclusions from the studies based on FACE experiments.

Water Stress:

Elevated CO_2 could partially alleviate effects of water stress on productivity. Elevated CO_2 might be able to boost Carbon stores or postpone the start of a drought, which could increase forest resilience and lower mortality rates during episodes of episodic drought. This interaction between CO_2 and drought served as the foundation for predictions of the relative responses of various ecosystems to elevated CO_2.

Evidence for decreased stomatal conductance (SWC) in forest FACE sites has been conflicting, even though SWC measurements were typically only taken on near-surface soil. While eCO_2 can reduce water loss in drought conditions, the adverse effects of acute drought on stomatic closure can outweigh the advantages of elevated CO_2 for C assimilation. For instance, during a severe drought and heat wave in ORNL FACE this reduced evaporative cooling, resulting in premature leaf senescence. Other factors like LAI, deeper roots and modifications in hydraulic conductance also affect plant growth and productivity.

Climate change is causing the terrestrial carbon cycle to move into a state of dynamic imbalance. As CO_2 concentrations in the atmosphere rise, most plant species will be ertilize, boosting carbon allocation in tissues and soils via litter breakdown, as previously explained. Aside from the FACE trials, other small-scale studies (for example the study of growth constraints in two barley species from nutrient limitation (Burnett et al., 2018) and on

nodulated pea (*Pisum sativum L*) plants (Gavito, 2000) have shown that nutrient availability (particularly nitrogen and phosphorus) restricts ecosystem production and carbon storage and modifies terrestrial carbon stores. The extent of such an imbalance, however, is intrinsically difficult to quantify directly (Wei et al., 2022).

Temperature:

(Long, 1991) demonstrated that, due to the kinetics of the Rubisco enzyme, the effect of high CO_2 on photosynthesis should be greater at higher temperatures. This interaction is captured in ecosystem models that incorporate the (Farquhar et al., 1980) photosynthesis model, which is shared by the majority of existing global models. Under elevated CO_2, such models predict that canopy photosynthesis will have a higher temperature optimum. Because of this interactive effect on gross photosynthesis, ecosystem models frequently predict that the CO_2 response will be greater in tropical ecosystems than in temperate or boreal ecosystems, and that rising global temperatures will amplify the response to an increase in atmospheric CO_2 concentrations (Norby et al., 2016).

Recent cross-site comparisons for the interaction of CO_2 and temperature are ambiguous. Many factorial CO_2 temperature experiments fail to find a positive interaction , and meta-analyses of such experiments show that the CO_2 response is not higher at higher growth temperatures.

Nutrient limitation:

The Duke of Loblolly Pine experiment in North Carolina, one of the long-term FACE experiments, demonstrated an increase in net primary production (NPP) that was sustained throughout the experiment (doubled CO_2), resulting in a greater accumulation of woody biomass supported by an increase in carbon flux below ground, which stimulated nitrogen absorption. This established a positive feedback cycle since the nitrogen from the trees increased the quantity of nitrogen in the canopy and increased the rate of photosynthesis (U.S. DOE., 2020).

In another FACE experiment, at Oak Ridge National Laboratory (ORNL in Nevada), there was a quick growth above ground at high CO_2 concentrations (doubled) that was not sustained over time. The enhanced production from extra fine roots in deeper soil provided for the NPP's support. Nitrogen availability, on the other hand, has continuously declined, resulting in a loss of photosynthetic rate capacities and consequently a decrease in NPP. This drop was quicker at higher CO_2 levels, lending credence to the concept of progressive nitrogen restriction (U.S. DOE., 2020).

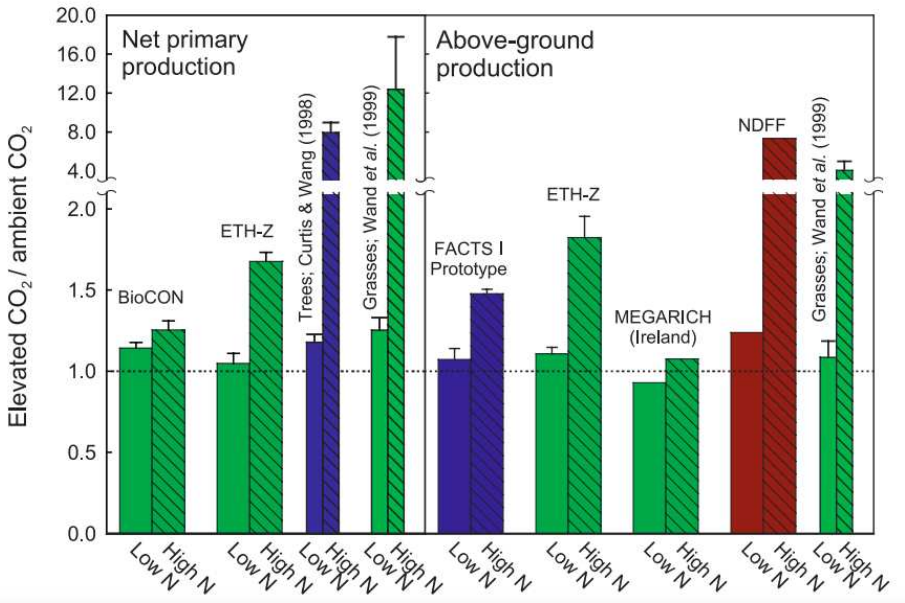

Figure 1.9 - Relative increase in NPP at elevated [CO_2] for different experiments and for two levels (low and high) of Nitrogen availability. Wide, dark-colored bars are results from ecosystem free-air CO_2 enrichment (FACE) experiments whereas narrow, light-colored bars are from meta-analysis of controlled environment and open-top chamber (OTC) experiments (Nowak et al., 2004).

From a meta-analysis study (Nowak et al., 2004) showed that although the impact of high CO_2 on leaf carbon assimilation differed amongst species, two correlations stood out. First, the enhancement of photosynthesis by elevated CO_2 was positively related to the relative change in leaf N content (Figure 1.9). Specifically, plants with reduced leaf nitrogen had smaller increases in carbon assimilation under elevated CO_2, whereas plants with increases in leaf nitrogen had larger increases in carbon assimilation. Second, herbaceous species consistently exhibited lower leaf N-content under high CO_2, resulting in smaller carbon increases than in woody species.

These two key results also suggest that the effects of increasing CO_2 on leaf carbon assimilation are responsive to fertility or increased N deposition and that photosynthesis downregulation may be more common in nitrogen limited situations. The projected rise in productivity with increasing N availability, on the other hand, is primarily supported by FACE data as well as controlled environment.

The first-generation FACE experiments were conducted in Nitrogen limited temperate ecosystems. These experiments have shown that nutrient feedbacks both dampen the CO_2 fertilization response of tree growth through an accelerated decline in N availability and sustain growth responses to elevated CO_2 through enhanced nutrient liberation from soil organic material caused by accelerated C cycling through the root-microbe-soil system (Norby et al., 2010). The interaction of nutrient cycling with eCO_2 on highly weathered soils with low plant-available Phosphorus content is poorly understood. Phosphorus limitation is common in old-growth forests that grow on P-depleted soils, such as those found in much of South

America, Africa, Southeast Asia, and Australia (Figure 1.10). The few field studies on the effect of elevated CO_2 on Phosphorus availability have yielded conflicting results. Model sensitivity experiments, for example, have shown that phosphatase activity and phosphate sorption kinetics can both have a significant impact on Phosphorus availability and determine whether the ecosystem's response to eCO_2 will be sustained.

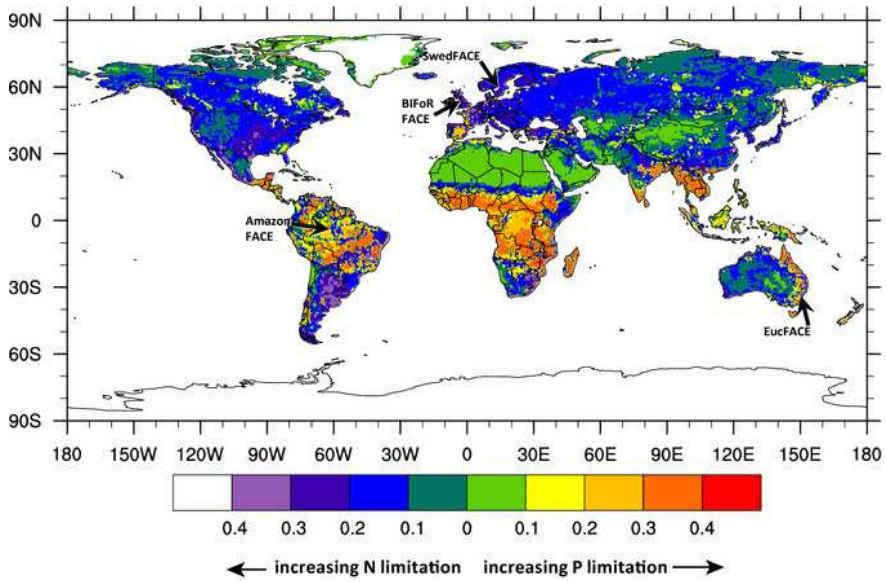

Figure 1.10 - Simulated spatial variation of nutrient limitation (nitrogen (N) and phosphorus (P)) on the global scale using CLM-CNP (Yang et al., 2014). Values plotted are the proportion by which plant growth is reduced due to limitation of that nutrient, following Wang *et al.* (2010).

We have shown that the enhancement of plant productivity due to the CO_2 fertilization may be strongly reduced due to nitrogen limitation. In parallel, the nitrogen cycle experienced a very important human-induced perturbation over the 20th century which indirectly boosted the ecosystem productivity. In the following section, we describe in more detail the nitrogen perturbation and its impact on terrestrial ecosystems.

1.2 Global nitrogen cycle

Nitrogen is a fundamental element for life since it is an essential part of amino acids, made of an amino group (NH_2-) and a carboxyl group (-COOH), a molecular component of proteins. Molecular nitrogen (N_2) or dinitrogen is the most abundant element in the Earth's atmosphere, representing 78% by volume (Williams, 2021). However, organisms cannot make direct use of this inert form (with only a few exceptions, see below). Reactive nitrogen is present in different chemical forms on Earth, but in much lower quantities, including some mineral nitrogen forms such as ammonia (NH_3), ammonium (NH_4+), nitrite (NO_2-), nitrate (NO_3-), nitrous oxide (N_2O) and nitric oxide (NO).

The nitrogen cycle is a biogeochemical cycle in which nitrogen in diverse forms moves within and across air, land, and marine reservoirs (Figure 1.11). Nitrogen transformation from unreactive to reactive forms is accomplished by biological or physical mechanisms. Through a series of microbial modifications, this mechanism makes nitrogen available to plants, which eventually sustains all animal life. The steps are classified as nitrogen fixation, nitrogen assimilation, ammonification, nitrification, and denitrification, and they are not all consecutive.

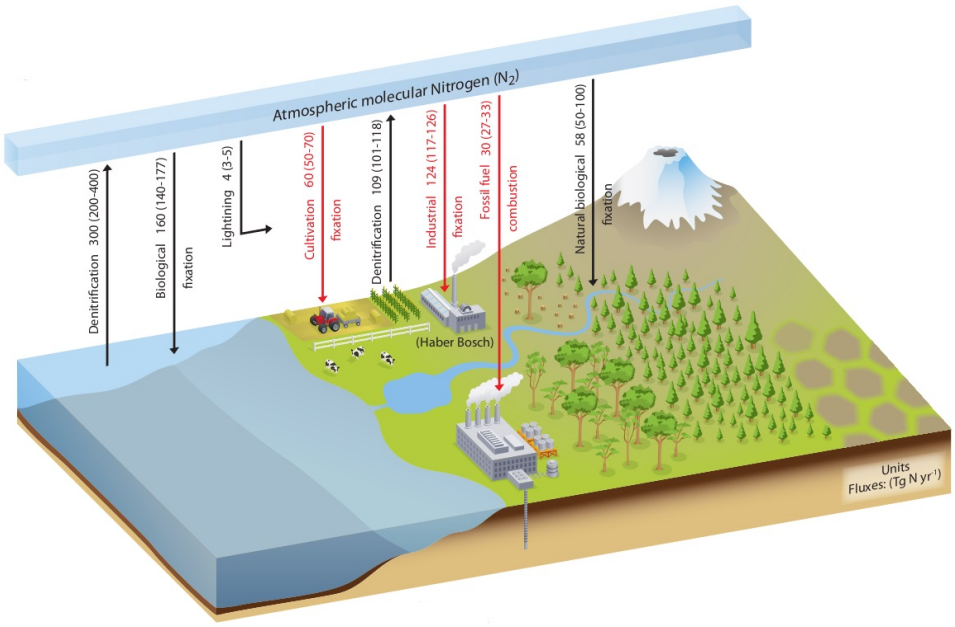

Figure 1.11 - Schematic of the global nitrogen cycle. The natural and anthropogenic processes that create reactive nitrogen and the corresponding rates of denitrification that convert reactive nitrogen back to N2 (Ciais et al., 2013).

Nitrogen in the atmosphere (N_2) is made available to organisms through the natural nitrogen fixation at almost 58 TgN yr^{-1}. In addition to becoming an assimilable form of nitrogen as nitrates by plants and forming the proteins required to sustain the food chain, these reactive forms of nitrogen go through a variety of biological processes, which are covered in further depth below. Nitrates can be denitrified by soil microorganisms and re-emitted into the environment as dinitrogen at the pace of 109 TgN yr^{-1}.

The marine nitrogen cycle is similar to the terrestrial cycle. Nitrogen enters the oceans through precipitation, runoff, or biological fixation of atmospheric nitrogen. More specifically, phytoplankton, like plants, cannot use dinitrogen, it is fixed first by cyanobacteria at a rate of 160 TgN yr^{-1} (Ciais et al., 2013). In this way, phytoplankton mainly use ammonium as a nitrogen source since this does not involve an oxidation-reduction reaction and therefore requires little energy, such as the of the *Prochlorococcus* and some *Synechococcus* phytoplankton family species. Nitrate on the other hand requires oxidation, but being more abundant in the marine environment has led most phytoplankton to adapt to have the necessary nitroreductase enzymes to process nitrogen (Gruber, 2008).

Phytoplankton release ammonia and urea. These are removed from euphotic zones by the downward movement of organic matter and by the sinking of phytoplankton. The introduction of ammonia in the lower areas of the euphotic zone promotes the conversion of ammonia into nitrite and nitrate by the action of nitrifying bacteria. Nitrate can also return to the euphotic zone through vertical mixing where it is absorbed by phytoplankton (Gruber, 2008) and another part is emitted as dinitrogen through denitrification ata rate of 300 TgN yr^{-1} (Ciais et al., 2013), thus closing the cycle.

Ammonium and nitrite show a maximum concentration in the ocean between 50 and 80 m that corresponds to the lower end of the euphotic zone, followed by a decreasing concentration below this depth. This is explained as nitrite and ammonium are intermediate species and are rapidly produced and consumed through the water column (Gruber, 2008).

1.2.1 Natural terrestrial nitrogen cycle

The conversion of dinitrogen into assimilable forms such as nitrates and nitrites through atmospheric and biological processes is called nitrogen fixation. The fixed nitrogen is transformed into amino acids and oxidized compounds by microorganisms, where it is used to create proteins and finally returned to the atmosphere as molecular nitrogen through microbial denitrification in soils (Galloway et al., 2004) (Figure 1.12).

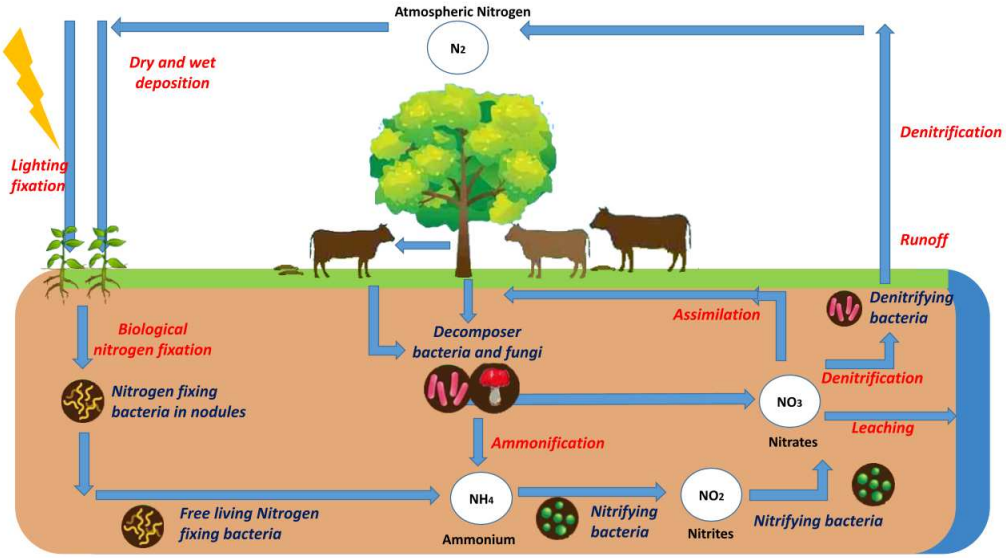

Figure 1.12- Unperturbed terrestrial nitrogen cycle. Adapted from (Galloway et al., 2004).

Biological processes for fixing nitrogen include lighting and biological nitrogen fixation BNF. The electrical energy of the lightning breaks the strong bonds of the atmospheric nitrogen molecule, leaving it alone, which promotes its rapid union with the oxygen molecule, thus forming nitrogen dioxide (NO_2). Nitrogen dioxide dissolves in water creating nitric acid (HNO_3)

and in turn nitrates (NO−3). Nitrates fall to the ground and are consequently absorbed by plants. This accounts for a fixation of around 3 to 5 TgN yr^{-1} (Ciais et al., 2013).

$$N_2 + 8H^+ + 8\,e^- + 16\,Mg\,ATP \rightarrow 2NH_3 + H_2 + 16\,Mg\,ADP + 16\,P_i \quad (1.5)$$

Biological nitrogen fixation BNF (Equation 1.5), discovered in 1901 by Beijerinck (Wagner, 2011), is a biochemical process carried out by specialized prokaryotes to catalyze through the enzyme nitrogenase the conversion of atmospheric nitrogen (N_2) to ammonia (NH_3). Plants can only assimilate NH_3 to produce the forenamed molecules and grow.

These prokaryotes include aquatic organisms, such as cyanobacteria, free-living soil bacteria, such as *Azotobacter*, bacteria that form associative relationships with plants, such as *Azospirillum*, and most importantly, bacteria, such as *Rhizobium* and *Bradyrhizobium*, that form symbiosis with legumes and other plants (Postgate, 1982).

To date, the amount of BNF is estimated to be in the range of 50 to 100 TgN yr^{-1} in natural terrestrial ecosystems (Ciais et al., 2013). Another important biological source of mineral nitrogen comes through the decomposition of organic matter by fungi such as Aspergillus and Penicillium. These organisms break proteins into amino acids that, under the action of a hydrogenase, form an intermediate molecule that in the presence of water in turn forms an alpha ketone acid ($C_4H_6O_3$) plus an ammonium molecule (NH_4^+).

Ammonium is then oxidized to nitrite by aerobic microorganisms that use molecular oxygen (O_2) as an electron acceptor, that is, as an oxidant in a process called nitrification. These microorganisms obtain energy through this oxidation just as heterotrophic organisms do through cellular respiration. Nitrification is carried out through two separate and consecutive processes: nitration, in which nitrite (NO_2–) is obtained from ammonium thanks to the action of bacteria of the genus Nitrosomonas and Nitrosococcus, and nitration through which starting from the nitrite provides nitrate (NO_3-) thanks to the action of bacteria of the Nitrobacter genus. Plants assimilate the nitrates to sustain their growth and metabolism. Part of this assimilated biomass is decomposed entering the nitrogen cycle (Fowler et al., 2013).

The last stage consists of the denitrification, that consists of the reduction of the nitrate ion to molecular nitrogen thanks to the action of heterotrophic bacteria such as *Pseudomonas fluorescens* to obtain energy. This process occurs under anaerobic conditions in which nitrate takes on the role of oxidant (just as oxygen does in cellular respiration) (Fowler et al., 2013), the molecular nitrogen goes back into the atmosphere, closing then the cycle.

1.2.2 Terrestrial nitrogen cycle perturbations

While before the industrial era, reactive nitrogen was produced from N_2 via only two natural processes (lightning and BNF), this balance has been disturbed since the beginning of the

industrial era, by the addition of important anthropogenic sources of production of reactive nitrogen. The anthropogenic production of reactive nitrogen during the last decades has been greater than the natural terrestrial production (Figure 1.13).

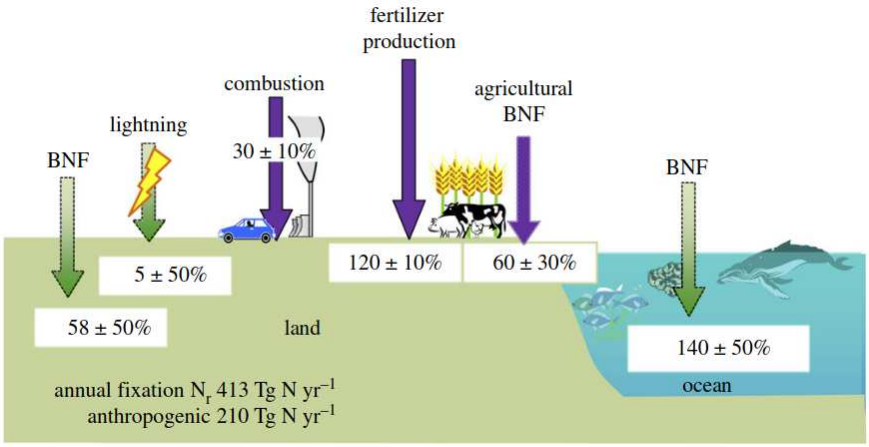

Figure 1.13 - Anthropogenic disturbance nitrogen cycle. Global nitrogen fixation, natural and anthropogenic in both oxidized and reduced forms through combustion, biological fixation, lightning and fertilizer and industrial production through the Haber – Bosch process for 2010 from (Fowler et al., 2013).

The main anthropogenic sources of reactive nitrogen are (Figure 1.14):

1. The Haber-Bosch process that will be further described below, uses energy and a metal catalyst to transform dinitrogen (N_2) into ammonia (NH_3) which is used as nitrogenous fertilizer and as raw material for some industries. Current global production of reactive nitrogen by the Haber-Bosch process is estimated at a rate of around 120 TgN yr^{-1}.
2. The cultivation of leguminous crops that increases the BNF at a rate of around 60 TgN yr^{-1}.
3. The combustion of fossil fuels that emit nitrogen oxides - NOy of around 30 TgN yr^{-1} (Ciais et al., 2013).

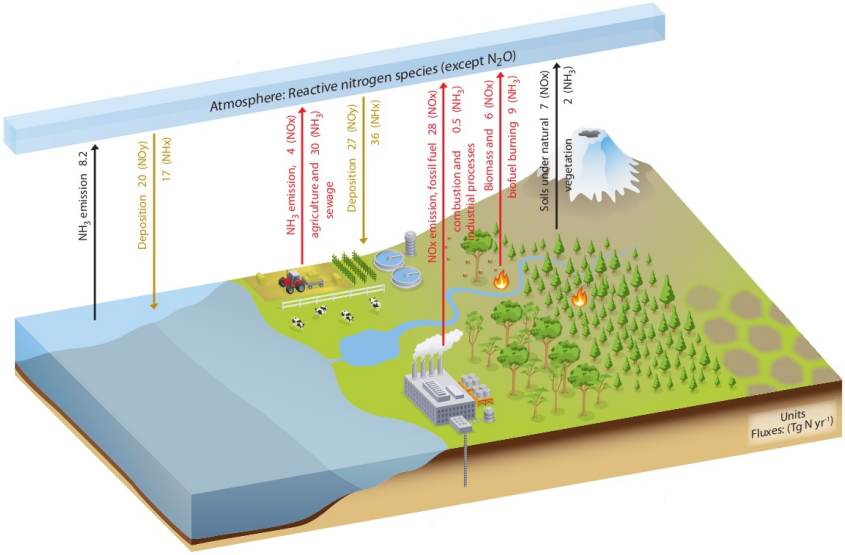

Figure 1.14 - Global nitrogen cycle, flows of the reactive nitrogen species NOy and NHx (Ciais et al., 2013).

These two main groups of atmospheric reactive nitrogen compounds (NHx and NOx or also found as NOy) result from various physicochemical mechanisms as seen in (Figure 1.15). Reduced nitrogen form NH_3 is mostly emitted from agriculture. It is subject to transport and dispersion but also to elimination by dry dispersion and transformation to aerosol bound ammonium (NH_4^+) in reactions with acid gasses and aerosols. Ammonium ions have a long life in the atmosphere and can therefore be transported over long distances of more than 1000 km. Ammonium aerosols are mainly removed by wet deposition (Hertel et al., 2011).

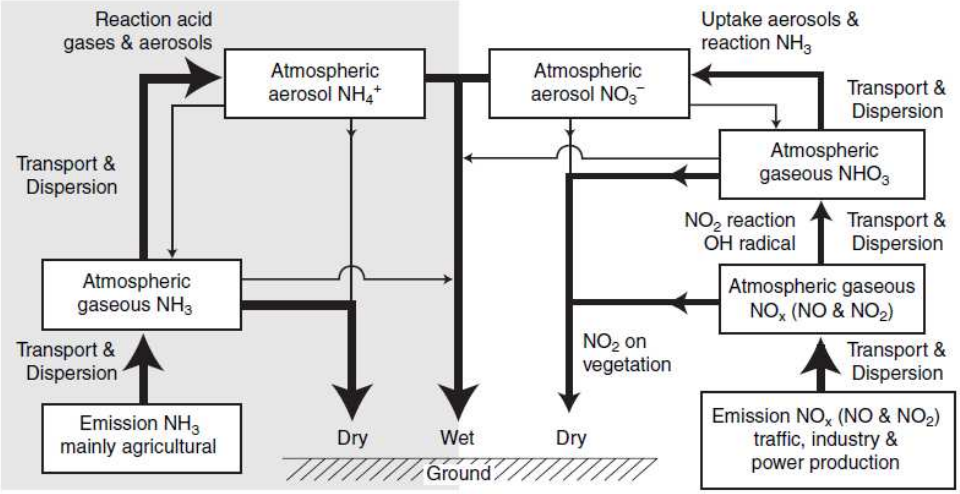

Figure 1.15 - Figure emission and deposition mechanisms for NHx and NOy compounds (Hertel et al., 2011).

On the other hand, nitrogen oxides - NOy, are emitted into the atmosphere as nitrogen monoxide NO and nitrogen dioxide (NO_2), mainly from the combustion of fossil fuels[3] for transportation, industry, and energy production. These species are also objects of transport and dispersal. On the one hand, nitrogen dioxide is deposited dry on vegetation, but it is mainly eliminated in the atmosphere by reaction with the OH radical, forming nitric acid (HNO_3). Nitric acid has a very short lifetime as it is eliminated rapidly by absorption of aerosols with NH_3 or by dry deposition. Uptake in aerosols or formation of new aerosols by the reaction with NH_3 leads to aerosol bound nitrate (NO_3^-). Aerosols containing nitrates NO_3^- and also ammonium NH_4^+ are mainly scavenged by wet deposition (Hertel et al., 2011).

Nitrogen oxides NOy have little impact near sources because their compounds are emitted as nitrogen monoxide NO and nitrogen dioxide NO_2, both with low deposition rates. On the other hand, NH_3 from ammonia has a high impact near sources due to high rates of dry deposition, which implies a greater impact on ecosystems in areas with intense agricultural activities (Hertel et al., 2011). NOx species are deposited over continents at a rate of 27 TgN yr^{-1} while NHx species correspond to 36 TgN yr^{-1} (Ciais et al., 2013). Currently, about 30% of the total

[3] From the reaction among nitrogen and oxygen during combustion of fuels, such as hydrocarbons, in air; especially at high temperatures, such as in car engines.

fixed nitrogen is produced industrially by the Haber-Bosch process (Smith et al., 2004) which uses high temperatures and pressures to convert nitrogen gas and a hydrogen source (natural gas or oil) in ammonia (NH_3) (Equation 1.6). Industrial fixation via the Haber Bosch process accounts for 117 to 126 TgN yr^{-1}.

$$N_2(g) + 3\,H_2(g) \rightleftharpoons 2\,NH_3(g) + \Delta H \quad (1.6)$$

Estimated anthropogenic consumption of nitrogenous fertilizers throughout the 21st century is based on five criteria (population growth, animal protein consumption, improvement of agricultural efficiency and additional production of biofuels) (Figure 1.16). It is estimated that at the end of the 21st century the nitrogen fertilization will range from 90 to 190 TgN yr^{-1}, reaching almost double the current use. This will increase world agricultural production (+82% for 2000–2050) and livestock production (+115%) (Ciais et al., 2013).

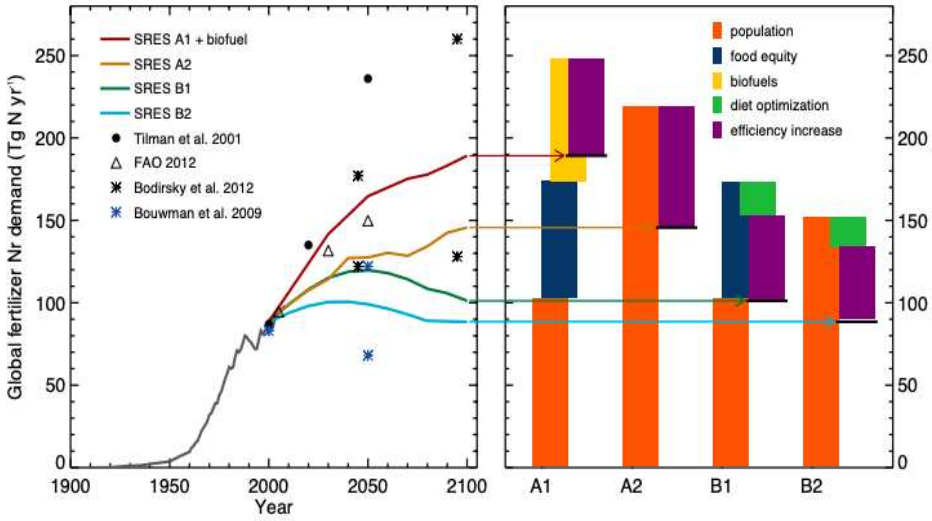

Figure 1.16 -Global nitrogen fertilizer consumption scenarios. (left) and the impact of individual drivers on 2100 consumption (right). This resulting consumption is always the sum (denoted at the end points of the respective arrows) of elements increasing as well as decreasing nitrogen consumption. Other relevant estimates are presented for comparison. The A1, B1, A2 and B2 (Ciais et al., 2013).

There has been an important increase of N deposition rate in North America, Europe, Southern Asia and Africa, since 1850 (Figure 1.17). The global mean pre-industrial nitrogen deposition over land was 0.12 gN m^{-2} yr^{-1} while deposition in 2006 reached 0.43 gN m^{-2} yr^{-1} (around 73.1 TgN yr^{-1}) (Bala et al., 2013).

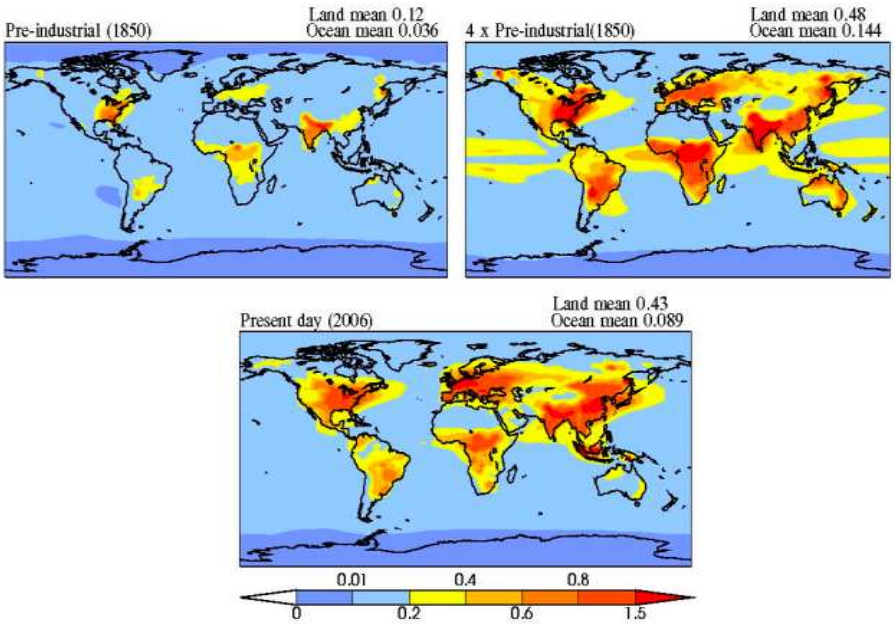

Figure 1.17 - Spatial distribution of N deposition (gN m^{-2} yr^{-1}) in the pre-industrial period (1850; top left panel), four times the pre-industrial N deposition case (4N; top right panel) and present-day (2006; bottom panel) in the input data sets of CLM4 (Bala et al., 2013).

At the regional level, decreases in NHx and NOx deposition are projected for the 21st century in North America and Northern Europe, and increases in Asia and increased nitrogen deposition in large tropical areas such as the Americas, southern Africa, China, and India. Field experiments have shown that tropical forests have higher nitrogen oxide emissions than N-limited forests and this can reduce productivity due to indirect effects on acidity and availability of phosphorus and cations (Matson et al., 2002).

Coupled model intercomparison project -CMIP scenarios projected up to the end of the 21st century a doubling in atmospheric nitrogen deposition in some global biodiversity hotspots with significant deposition rates greater than 15 kg N ha^{-1} yr^{-1} in at least 10% of their total area (Bleeker et al., 2011). Overall, the main changes are explained by an increase in NHx emissions in large regions of the world for all future trajectories (Figure 1.18).

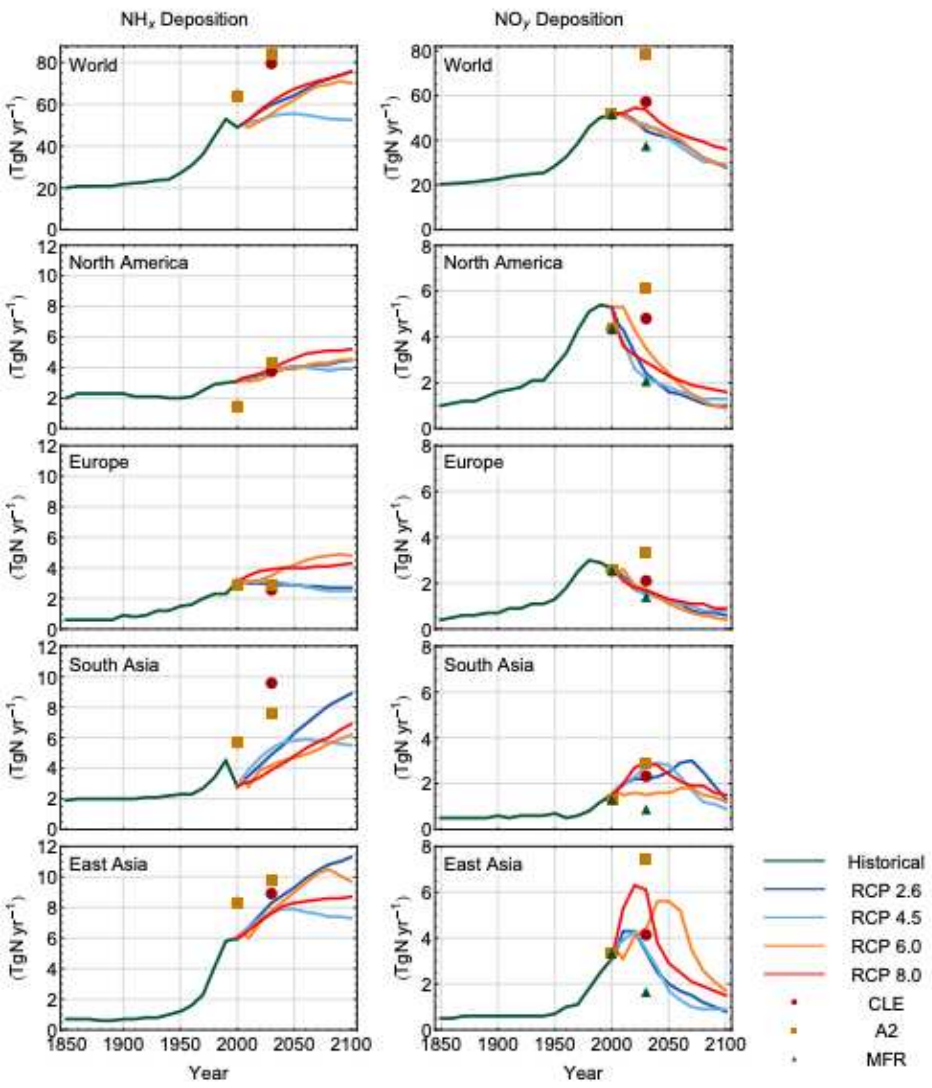

Figure 1.18 - Deposition of NHx and NOy (TgN yr–1) from 1850 to 2000 and projections of deposition to 2100 under the four RCP emission scenarios (Ciais et al., 2013).

Anthropogenic nitrogen addition will continue to have a significant influence on the global carbon cycle. Because nitrogen is one of the most important nutrients for plant development, changing the amount of reactive nitrogen can limit or stimulate future carbon absorption. However, there are still uncertainties in our knowledge and modeling of changes in reactive nitrogen emissions, transport, and deposition processes, which may lead to low confidence in future deposition fluxes (particularly in isolated places) and hence carbon absorption forecasts (Dentener et al., 2006).

1.3 Carbon and Nitrogen interactions and limitations

There is a very tight coupling between the terrestrial nitrogen and carbon cycles. Nitrogen availability is fundamental in controlling the productivity, structure, and dynamics of terrestrial

ecosystems. A perturbation in one cycle will have consequences on the other and vice versa (Zaehle, 2013). Mineral nitrogen in soils comes from mineralization of organic matter and biological and anthropogenic fixation and atmospheric deposition of reactive nitrogen (NHx and NOy). The nitrogen in the soil impacts the carbon cycle directly through plant absorption by the roots, allowing photosynthesis to occur due to the production of Rubisco protein. As shown in (Figure 1.19) absorbed carbon is turned into leaf litter, while part of the nitrogen in leaves and other tissues is degraded and recycled before returning to the soil via mineralization.

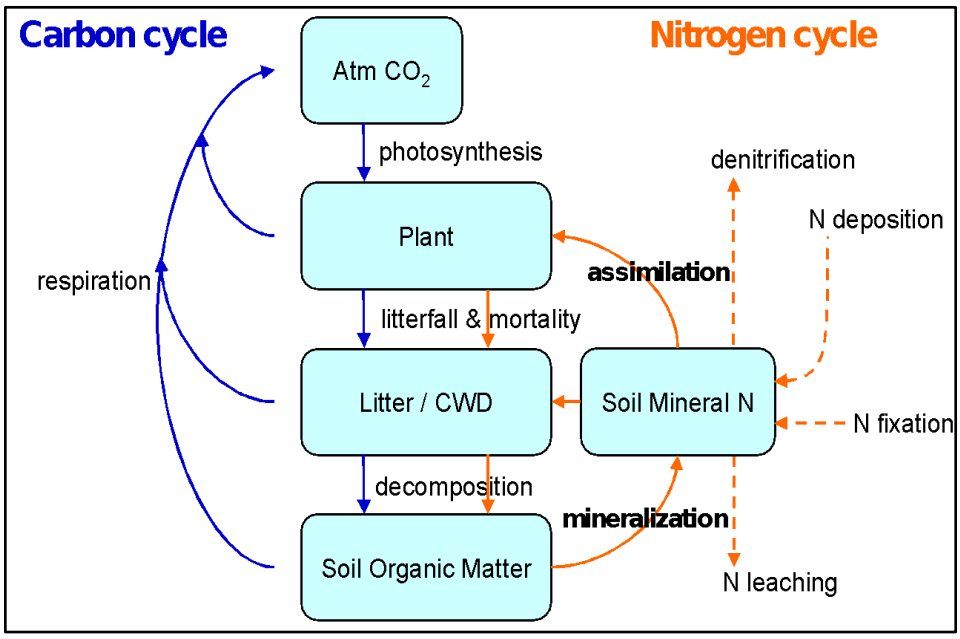

Figure 1.19 - Carbon and nitrogen cycles interactions from the The Community Earth System Model (Danabasoglu et al., 2020).

The limited flexibility of ecosystem C:N stoichiometry reveals the close relationship between the nitrogen and carbon cycles. As shown in the (Figure 1.20), the values of stoichiometric ratios of carbon and nitrogen in both plant and soil are key to quantify the dynamics of plant biomass and of organic matter in soils. Because the amount of nitrogen required to carry out photosynthesis is significantly less than that one available in soils, and because the carbon in the atmosphere is becoming more abundant (due to CO_2 increase), and because living organisms compete for this element, nitrogen is regarded as the limiting component.

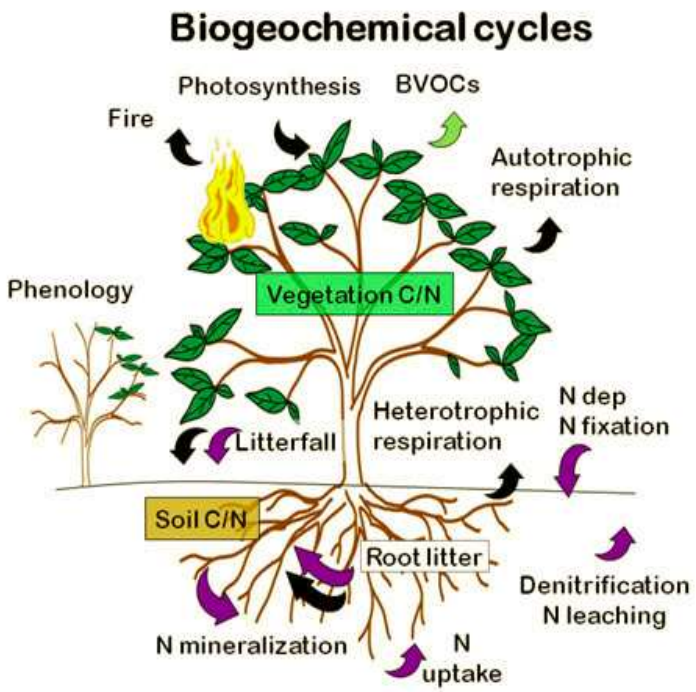

Figure 1.20 - Biogeochemical cycles interaction from the Community Earth System Model (Danabasoglu et al., 2020).

The C:N ratio in both soil and vegetation directly impacts the photosynthetic ability of plants. The quantity of nitrogen and carbon in the soil influences nitrogen absorption by the root. Carbon is required as an energy source for both organic matter breakdown and mineralization, while nitrogen is required as an intermediary in protein synthesis. Without any of these components, mineralization ceases and, consequently, plant production does not have the essential nutrients for structural growth. A higher C:N ratio in woody vegetation than in soil promotes ecosystem carbon storage because reactive nitrogen absorption transfers nitrogen from soil to plant (Melillo et al., 2011). For instance, in response to climate warming, the increase of decomposition of soil organic matter increases the mineralization that enhances the reactive nitrogen uptake and thus favors carbon storage by vegetation.

Thus, through the study of this biogeochemical limitation, it is projected that due to the increase in nitrogen deposition there will be a positive impact on carbon sinks as a result of the high C:N ratio, particularly in mid-latitude forests in the northern hemisphere, where nitrogen deposition is high and nitrogen limitation is common (Holland et al., 2005), but may also be important in tropical regions (Elser et al., 2007; J. B. Fisher et al., 2012).

Therefore, any additional nitrogen added to the terrestrial biosphere could increase carbon storage directly by alleviating nitrogen limitation on plant productivity and indirectly by allowing greater plant response to CO_2 fertilization also referred to as carbon-nitrogen synergy. Synergistic effects can arise when high CO_2 concentrations cause nitrogen limitation, which is alleviated by simultaneous increases in nitrogen deposition. Recent studies indicate

an increase in terrestrial carbon uptake in the range of 0.2-0.5 Pg yr^{-1} (Churkina et al., 2009; Zaehle, 2013) due to the direct effect of increased terrestrial nitrogen deposition from anthropogenic activities. This increase in terrestrial carbon uptake would be equivalent to 10-20% of the total modern carbon sink.

1.4 Global terrestrial ecosystem modeling

The earth's surface is directly affected by humans, animals, and plants. The biogeochemical processes that take place on the earth's surface drive climate impacts on societies and ecosystems. Therefore, an accurate representation of these processes is essential for the understanding of climate and climate change. Land surface models (LSM) are numerical models that resolve the interconnected fluxes of water, energy, and carbon between the earth's surface and the atmosphere, under a set of direct and indirect human forcings and ecological dynamics. LSMs thus provide prognostic variables related to land-mediated feedbacks between the different global biogeochemical cycles (R. A. Fisher & Koven, 2020).

LSMs are likely the most sophisticated tools available to humankind for forecasting land surface properties in the following years. LSM were first established by atmospheric and climatic modeling centers and forecasting operations that required physical information in terms of energy partitioning, surface roughness, and albedo, to reflect the effect of the earth on meteorological processes. LSMs are being used to anticipate plant biophysical responses to increased CO_2, and to represent the linkage of climate and carbon cycle which might significantly modulate the rate of global warming (Cox et al., 2000).

The LSMs have gradually added the representation of physical, biological, and chemical processes relevant to the dynamics of the flows mentioned above. Currently these represent the dynamics of highly interconnected processes such as surface hydrological processes, the functioning of stomata, the heterogeneity of the earth's surface, the carbon cycle in plants and soils, the dynamic distributions of vegetation, fires, urban environments, cover and land management, nitrogen cycle (Lawrence et al., 2019). More recently, some LSMs include a modeling of plant demographic processes (R. A. Fisher et al., 2018; Weng et al., 2017), phosphorus cycle (Goll et al., 2017) and plant hydraulics (Kennedy et al., 2019).

Carbon cycle feedbacks provide a fundamental demonstration of system dependency. Changes in land usage are influenced by environmental influences such as drought and fires, which are mediated by plant biophysics to high CO_2, which is regulated by nutritional restrictions in growth, such as nitrogen availability (R. A. Fisher & Koven, 2020). The integration of these feedbacks is crucial for a better representation of the different processes. For example, the restricted natural availability of N lowers the terrestrial biosphere's carbon storage capability. On the opposite, human-induced Nr atmospheric deposition increases the terrestrial forest carbon sequestration and so slows down the rate at which anthropogenic CO_2 builds up in the atmosphere (Zaehle, 2013).

Terrestrial ecosystems currently remove about one third of anthropogenic carbon emissions from the atmosphere (Friedlingstein et al., 2020), although future projections of carbon uptake will depend on the availability of nutrients such as nitrogen, particularly under conditions of high atmospheric concentrations of carbon dioxide (CO_2). This has led to a recent representation of the nitrogen cycle in the ESM to improve estimates of historical, present, and most importantly future carbon uptake by terrestrial ecosystems. Some of the current main processes studied in ESM are shown in the (Figure 1.21) from (Tharammal et al., 2019).

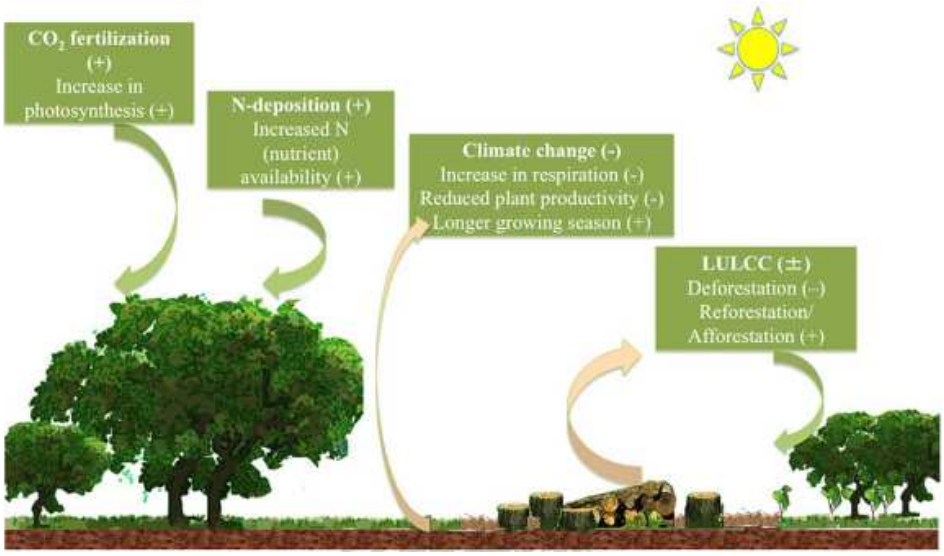

Figure 1.21- CO_2 fertilization, nitrogen (N)-deposition, climate change, and land use and land cover changes—LULCC) of land carbon uptake. Downward arrows represent the carbon flux into the ecosystem. Upward arrows represent the carbon flux from the land to the atmosphere. Positive (+) and negative (–) signs denote the effect of the factor on the land carbon uptake (Tharammal et al., 2019).

Among the land surface models participating in the CMIP5 exercises (Ciais et al., 2013), only two did account for the nitrogen limitation and carbon-nitrogen interactions. The modeled accumulated sink of carbon for the 21st century, was estimated on the order of 120-270 GtC (depending on CO_2 trends and underlying socioeconomic scenarios) over the 2010-2100 period, by this ensemble of models. As a consequence, it is likely that accounting for a N-limitation would lower the carbon sequestration to 40 to 80% of the original estimated range (Zaehle et al., 2015).

The uncertainty associated with this nitrogen limitation on the terrestrial carbon sink depends on the evolution of anthropogenic reactive nitrogen production and subsequent atmospheric nitrogen deposition, which varies depending on the socioeconomic scenario (Ciais et al., 2013). At least ten ESMs contain a description of the nitrogen cycling among the newest generation of models, giving findings to CMIP6 (Arora et al., 2020a). The introduction of a N cycle appears to have increased the dispersion of findings of net land carbon uptake across various ESMs, according to preliminary analysis (C. D. Jones & Friedlingstein, 2020) as could be seen in the

evolution of the biogeochemically coupled evolution of the atmospheric land flux for the CMIP6 and CMIP5 models in the (Figure 1.22).

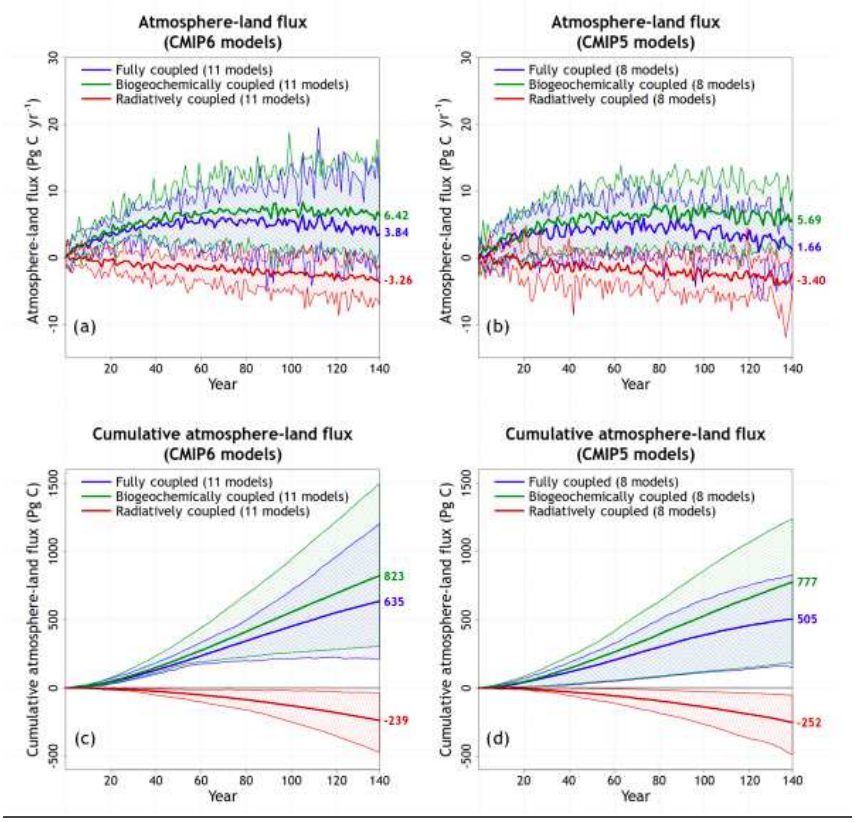

Figure 1.22 - Model mean values and the range across models for annual simulated atmosphere–land CO_2 flux (a, b) and their cumulative values (c, d) for participating CMIP6 (a, c) and CMIP5 (b, d) models from the fully, biogeochemical, and radiatively coupled versions of the 1pctCO_2 experiment (Arora et al., 2020a).

It is therefore critical to continue assessing the impact of nitrogen restriction in terrestrial carbon absorption. Quantifying changes in terrestrial carbon and nitrogen budgets is essential not only for understanding the destiny of anthropogenic reactive nitrogen and its cascade impacts, but also for understanding the climate system.

1.5 Thesis motivation and selected experiments

We highlighted how, due to the well-known CO_2 fertilization effect, atmospheric CO_2 has grown dramatically anthropogenically since 1970, resulting in greater rates of carbon uptake in plants. Plants' improved capacity to sequester carbon is restricted to other essential elements such as nitrogen and phosphorus (Goll et al., 2017) (mainly seen as a limiting nutrient in the tropics). Plants, in particular, require nitrogen to produce proteins and tissues. Plants may only utilize reduced forms of NHx or NOy, which are mostly emitted by the combustion and energy sectors, fertilizer usage, and biological nitrogen fixation. Because of industrial expansion and the discovery of the Bosch process, nitrogen deposition (NHx and NOy) has

also grown dramatically since 1950, contributing to the limitation or enhancement of the carbon assimilation.

It is critical in this setting to examine the influence of nitrogen availability on plant production and carbon storage using cutting-edge process-based models. Given that only a few LSMs have truly embedded a mechanistic description of the Nitrogen cycle (and their impact on the Carbon cycle), and that these LSMs still show very different responses of future terrestrial Carbon sink, it is critical to further investigate these interactions and feedbacks using one state-of-the-art process-based model, namely ORCHIDEE.

The proposed study and investigations were made possible because a complete and state-of-the-art description of the Nitrogen cycle was introduced in the most recent version of the ORCHIDEE LSM (Vuichard et al., 2019); we expected that in depth analysis and use of this new model version, combined with novel factorial experiments, would bring important and possibly new knowledge.

Following this context and previous advancements, my thesis was inspired by a set of questions aimed at providing supplementary and novel insights into the history and destiny of terrestrial carbon fluxes and stocks:

1. To what degree did the rise in atmospheric CO_2, nitrogen deposition, and their synergy contribute to the change in terrestrial carbon storage throughout the historical era, from 1850 to present-day?
2. What will be the effects of climate change, land use change, nitrogen deposition and fertilization on changes in terrestrial carbon storage throughout the 21st century ?
3. Knowing that nitrogen content is crucial in carbon absorption ability, what is the impact of improving biological nitrogen fixation modeling on the estimated terrestrial carbon storages from the post-industrial period through the end of the 21st century?

Beyond continuing the evaluation and analysis of the evolution of terrestrial productivity simulated by ORCHIDEE over the recent historical period, the goal is also to quantify the future and historical evolution of terrestrial ecosystem productivity under the combined effect of climate change, increased atmospheric CO_2 concentration, and the evolution of reactive nitrogen production. It will be a matter of calculating the influence on carbon stocks and fluxes evolutions of numerous sources of uncertainty, including:

- The evolution of the climate according to the different possible socio-economic scenarios.
- The evolution of the use of synthetic and organic fertilizers in the 21st century and the induced changes in atmospheric nitrogen deposition.

- The representation in the model of certain key processes controlling carbon-nitrogen interactions.

For this goal, three simulation axes were suggested using ORCHIDEE in its recent and robustly evaluated version r7267 (Vuichard et al., 2019), which contains a redesigned nitrogen carbon cycle interaction, as indicated in (Figure 1.23):

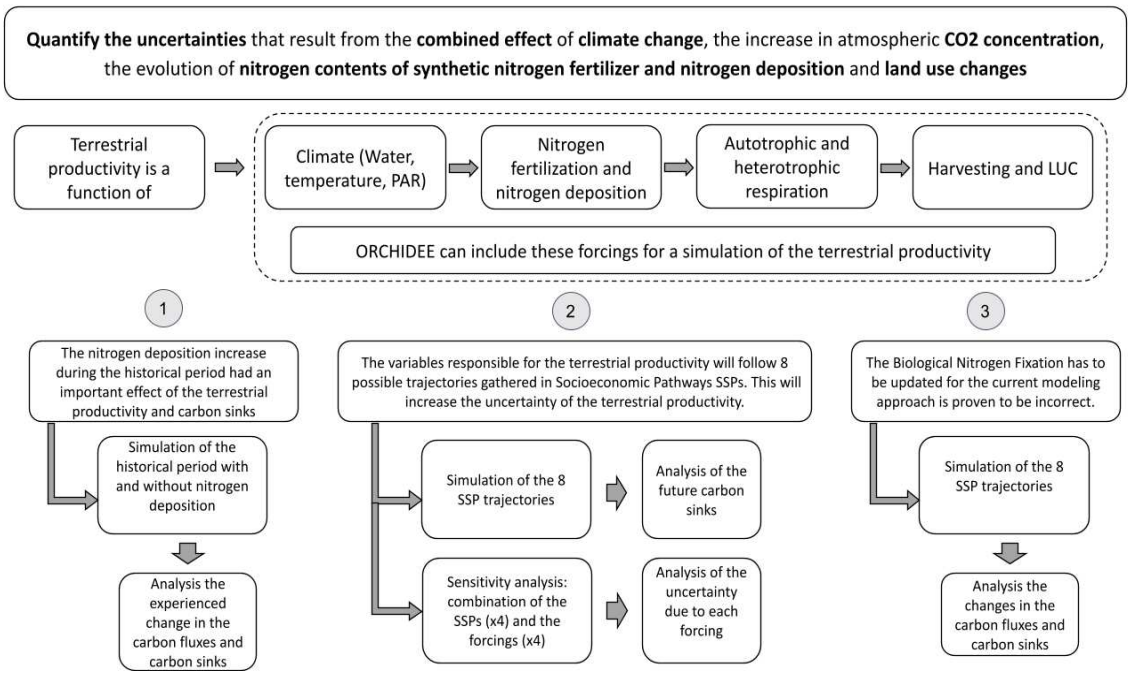

Figure 1.23 - Main axis of the research.

1. The first axis (presented in Chapter 3) is a historical examination of terrestrial and carbon sink productivity with regard to nitrogen deposition and CO_2 concentration evolution from the pre-industrial era to the beginning of the 21st century to explore their single combined contribution.
2. The second axis (presented in Chapter 4) examines land productivity and carbon sinks during the 21st century. We suggest running a factorial simulation to examine the uncertainties associated with the carbon fluxes and carbon sinks arising from the eight alternative paths for nitrogen deposition, climate, and CO_2, and land use change.
3. The third axis (presented in Chapter 5) focuses on Biological Nitrogen Fixation, one of ORCHIDEE's model nitrogen inputs. BNF is implemented in ORCHIDEE using an evapotranspiration-based technique that has recently been rejected by the scientific community, implying an incorrect estimate of carbon fluxes. We developed a novel dynamic BNF process-based model to improve the reactive nitrogen from BNF.

Prior to present these three axes of research, we detail in Chapter 2 the ORCHIDEE model and its capacity at simulating land carbon fluxes.

"*The future of carbon uptake will require a multi-disciplinary approach, including advances in technology, policy, and conservation, if we hope to mitigate the effects of climate change*".

Jane Lubchenco

CHAPTER 2

The ORCHIDEE land surface model

2.1 General description

ORCHIDEE (Organizing Carbon and Hydrology in Dynamic Ecosystems) is the Land Surface component of the Earth System Model - ESM from the Pierre Simon Laplace Institute (IPSL-CM6). It was designed to replicate the behavior of continental vegetation in a mechanistic approach by representing the dynamics governing the water, carbon, nitrogen, and energy balances as explicitly as possible. The modeling structures concentrates on two aspects: the exchanges of energy and water between the atmosphere and the biosphere (Ducoudré et al., 1993), and the carbon cycle dealing with photosynthesis, carbon allocation, litter decomposition, soil carbon dynamics, maintenance and growth respirations, plant phenology (Krinner et al., 2005) and a recent inclusion of carbon-nitrogen interactions (Zaehle and Friend, 2010; Vuichard et al., 2019) on which we will concentrate as the primary topic of our research.

The fundamental unit over which all simulated exchanges occur corresponds to a "mean" plant representative of a plant functional type (PFT) (Table 2.1). The PFT distribution across the globe is defined by a set of state of bio-geophysical characteristics such as plant physiognomy (tree,

herbaceous and other), biogeochemical characteristics such as photosynthesis type (C3 or C4), carbon allocation patterns or phenology (deciduous or evergreen), and climatic characteristics (boreal, temperate or tropical); this concept is made to simplify the large spatial heterogeneity of the land cover into a set of PFTs sharing mainly the same equations for most processes but with different parameters or plant traits.

The time scales taken into consideration in ORCHIDEE vary due to the range of processes modeled: from around 15-30 minutes (depending on the configuration) for the quickest biosphere-atmosphere interactions to yearly timescales for population competitiveness processes. Spatial heterogeneity is treated differently within each grid cell for the energy, water, and carbon cycles. The energy budget is calculated at the grid cell level, without taking into consideration changes across grid cell tiles (i.e. PFTs). Water budgets for three tiles per grid cell are now calculated: one each for bare ground, tree covers, and herbaceous covers. For each tile that is vegetated in a grid cell, the carbon and nitrogen budgets and accompanying fluxes are determined. For each PFT within a grid cell, ORCHIDEE represents carbon and nitrogen for seven plant pools (fine roots, leaves, below- and above-ground sapwood and heartwood and fruits), six litter pools (metabolic, structural, and woody litter for above and below layers) and four soil pools (surface, active, slow, and passive pools).

ORCHIDEE is compelled by an ensemble of input/forcing data, particularly meteorological data (near-surface air temperature, precipitation, short and long-wave incoming radiation, specific air humidity, wind speed), atmospheric CO_2 concentrations, and land cover maps. In terms of nitrogen inputs, ORCHIDEE requires information on atmospheric N deposition (NHx and NOy), N fertilizer rates on managed fields and BNF rate.

PFT acronym	PFT name	NUE ($\mu mol\ CO_2\ s^{-1}\ [g_{Nleaf}]^{-1}$)	$CN_{leaf,min}$ ($g_C\ [g_N]^{-1}$)	$CN_{leaf,max}$ ($g_C\ [g_N]^{-1}$)
TrEBF	Tropical evergreen broadleaved forest	14	16	45.5
TrDBF	Tropical deciduous broadleaved forest	30	16	45.5
TeENF	Temperate evergreen needleleaf forest	20	28	74.8
TeEBF	Temperate evergreen broadleaved forest	33	16	45.5
TeDBF	Temperate deciduous broadleaved forest	38	16	45.5
BoENF	Boreal evergreen needleleaf forest	15	28	74.8
BoDBF	Boreal deciduous broadleaved forest	38	16	45.5
BoDNF	Boreal deciduous needleleaf forest	22	16	45.5
GraC3	C_3 grass	45	16	45.5
GraC4	C_4 grass	45	16	45.5
CroC3	C_3 crop	60	16	45.5
CroC4	C_4 crop	60	16	45.5

Table 2.1 - List of plant functional types (PFTs) used in the ORCHIDEE model and the associated parameter values of nitrogen-use efficiency (NUE) and minimal and maximal leaf C/N ratio (Vuichard et al., 2019).

For this thesis, I have used one version of the model, including the nitrogen cycle, which corresponds to revision r7267 (referred later as ORCHIDEE-r7267). The research specifically carried out in this version relates to the nitrogen dynamics within the soil-plant-atmosphere

continuum, as initially described in Vuichard et al., (2019). This version is also the one that was used in the last two TRENDY model intercomparison for the global carbon budget (Friedlingstein et al., 2022).

Note however that the ORCHIDEE model is developed by a large community of scientists which leads to many different versions evolving over time. After the completion of the first version including the energy, water and carbon cycles in 2005 (Krinner et al., 2005), the model has continuously evolved.

For the recent CMIP6 climate model intercomparison, a version has been used with many improvements regarding the water, energy and carbon transfers compared to Krinner et al. (2005), but without the nitrogen cycle. The first initiative to include the nitrogen cycle started by the work of Zaehle and Friend (2010) which led to a separated model named OCN. Recently, Vuichard et al. (2019) introduced again the nitrogen cycle in the main version of ORCHIDEE (i.e., the Trunk) following mostly the implementation of Zaehle and Friend (2010). However, this version was completed too late to be used in the CMIP6 exercise for climate projections. This thesis thus capitalizes on such recent work. Key features of this new version are:

- The nitrogen cycle, like the carbon cycle, is included at the PFT level.
- There is a parallel nitrogen pool for each carbon pool, with carbon to nitrogen (C:N) ratios varying throughout time.
- The C:N ratio at the leaf level varies as a result of nitrogen supply by roots and biomass allocation requirement.
- The C:N stoichiometry of the remaining live biomass pools (belowground and aboveground sapwood, belowground and aboveground heartwood, fruit, and fine roots) is determined by the C:N ratio of the leaves but multiplied by a pool-dependent factor *fcn*.
- In terms of the Soil Organic Matter (SOM) decomposition, ORCHIDEE follows the scheme in which *C*/*N* ratios of SOM pools are expressed as a function of soil mineral nitrogen content (ammonium and nitrate). This technique makes carbon decomposition rates independent of the C:N ratio of the SOM pools, making possible an analytical approach for estimating the carbon content of SOM pools at equilibrium.

The mineral nitrogen in the soil follows the formulation of the O-CN version of ORCHIDEE by (Zaehle & Friend, 2010). Mineral nitrogen is represented by soil pools of ammonium (NH_3/NH^{+4}), nitrate (NO^{-3}), nitrogen oxides (NO_x), and nitrous oxide (N_2O), and the associated emissions are due to nitrification (the oxidation of NH_3/NH_4^+ in NO_3^-) and denitrification (the reduction of NO_3^- up to the production of N_2). NO_3^- (and NH_4^+) uptake by roots is modeled as a function of the NO_3^- (and NH_4^+) available in the soil, of and the root biomass and of the N plant's requirement.

Mineral nitrogen inputs in the soil-plant system are related to: **1)** Atmospheric nitrogen deposition in the form of NHx and NOy components. **2)** Biological nitrogen fixation (BNF) on any land category. The BNF rates are calculated as a function of evapotranspiration using the (Cleveland et al., 1999) method. In particular, all simulations employ a single evapotranspiration climatology based on a worldwide ORCHIDEE simulation for present-day conditions and **3)** Nitrogen fertilization on croplands.

The new carbon assimilation feature of this carbon-nitrogen version of ORCHIDEE as well as the the main interactions between the carbon and nitrogen cycles are explained in the following sections

2.1.1 Carbon assimilation scheme

The carbon assimilation scheme used in ORCHIDEE (r7267) is based on the Farquhar model (Farquhar et al., 1980) which forecasts the carbon assimilation in C3 plants as a function of the minimum of the Rubisco rate of CO_2 assimilation (A_c) and the electron-transport rate of CO_2 assimilation (A_j). Yin and Struik provide a C4 plant equivalent version of the Farquhar model (Yin & Struik, 2009) with an analytical solution to the equation that connects the net assimilation rate (A, µmol CO_2 $m^{-2}{}_{[leaf]}s^{-1}$), the stomatal conductance to CO_2 ($gs[CO_2]$, mol CO_2 $m^{-2}{}_{[leaf]}s^{-1}$) and the intercellular CO_2 partial pressure (Ci, µmol mol^{-1}).

Both ORCHIDEE versions with and without the C:N interactions kept the majority of the Farquhar model formulations and parameterizations given by (Yin & Struik, 2009). In addition, in the version with the C:N interactions (r7267), the rate of carboxylation of the Rubisco activity ($V_{cmax[leaf]}$, µmol CO_2 m^{-2} s^{-1}) and the maximum rate of electron transport (e^-) under saturated light ($J_{max[leaf]}$, µmol e^-m^{-2} s^{-1}) for C3 plants are expressed as a function of the nitrogen content of the leaves with a parametrization based on the work of (Kattge & Knorr, 2007).

2.1.2 Nitrogen dependency of photosynthesis activity

The photosynthetic activity in the previous versions of ORCHIDEE was unaffected by the leaf nitrogen content. As a result, the value of *Vcmax,ref* of a given canopy layer, was prescribed as a fixed parameter for each PFT. ORCHIDEE r7267 made a step change with the inclusion of nitrogen limitation by implementing the maximum photosynthetic capacity ($Vc_{max,ref}$) (2.1) as a function of the Nitrogen Use Efficiency (NUE) per PFT and the leaf nitrogen content (N_l, $g_{[N]}$ $m^{-2}{}_{[leaf]}$) as proposed by (Kattge et al., 2009).

$$Vc_{max,ref} = NUE_{ref} * N_l \quad (2.1)$$

The leaf nitrogen content (N_l) (2.2) decreases exponentially from top to bottom of the canopy and is consequently expressed as a function of the cumulative LAI from the top of the canopy. The N_l value at a cumulative LAI L (in $m^2_{[leaf]}$ /$m^2_{[ground]}$ from the top to the bottom of the canopy) is defined by (Dewar et al., 2012) with an extinction coefficient k_N, (value of 0.15) as follows:

$$Nl(L) = Nl(0)^{(-k_N * L)} \tag{2.2}$$

where Nl(0) (2.3) is the leaf nitrogen content (N_l) at the top of the canopy (L=0). Nl(0) is expressed as a function of the total nitrogen content (*Ntot*, in g[N] m−2[ground]) and the total LAI of the canopy (*Ltot*):

$$Nl(0) = \frac{k_N * N_{tot}}{1^{-(-k_N * L_{tot})}} \tag{2.3}$$

In our modeling, the leaf nitrogen content variation through the canopy is the result of the variation of the specific leaf area SLA (LAI divided by the leaf mass ($m^2_{[leaf]}$ g^{-1}[C]) while keeping the leaf C:N ratio constant.

2.1.3 Nitrogen allocation in plant reservoirs

The nitrogen cycle is calculated dynamically at the PFT level in the same way as the carbon cycle (labeled CNdyn). For each carbon pool, there is a parallel nitrogen pool with carbon to nitrogen (C:N) ratios changing with time. The leaf C:N ratio changes as a result of the nitrogen supply from the roots and demand of biomass allocation. The C:N stoichiometry of the remaining living biomass pools is determined by the C:N ratio of the leaves, but it is multiplied by a pool dependent factor (*fcn*) (Vuichard et al., 2019).

In the model, the nitrogen required to satisfy the new carbon allocated (GN_{init}, g[N] m^{-2}[ground]) (2.4) to the different reservoirs (*GC*, g[C] m^{-2}[ground] d^{-1}) is obtained following the (Zaehle & Friend, 2010) implementation as follows, under the assumption that *CNleaf* does not vary :

$$G_{N\,init} = \left(\frac{f_l}{CN_{leaf}} + \frac{f_r}{CN_{root}} + \frac{f_f}{CN_{fruit}} + \frac{f_s}{CN_{sap}}\right) * G_c \tag{2.4}$$

Where fi represents the fractions (unitless) of carbon allocated to leaf (l), roots (r), fruit (f) and sapwood or stalks (s) and the CNi denotes the C:N ratios (unitless) for the various biomass pools at the preceding time step. Given that all accessible nitrogen is contained in the labile

pool (*Nlab*, g[N] m^{-2}), the model will check to see whether there is enough nitrogen in the labile pool to meet demand, resulting in a fall in the leaf C:N ratio of the newly allocated biomass (Vuichard et al., 2019).

2.1.4 Nitrogen Uptake

The observed non-linear response of nitrogen adsorption to soil nitrogen availability and soil temperature is accounted for by the formulation reported below based on the work of (H. J. Kronzucker et al., 1996; HerbertJ. Kronzucker et al., 1995). Plant nitrogen uptake (*Nup*, gN m^{-2} d^{-1}) (2.5) is proportional to fine root mass (*Croots*, gC m^{-2}), plant nitrogen status *f(NCplant) (varying between 0 for fulfill-N plants and 1, for highly N-depleted plants)*, soil mineral nitrogen availability (*Nmin*, gN m^{-2}) (assessed for ammonium and nitrate), and soil temperature (*T*).

$$N_{up} = v_{max} * N_{min} * \left(k_{Nmin} + \frac{1}{N_{min} * K_{Nmin}}\right) * f(T) * f\left(NC_{plant}\right) * C_{roots} \qquad (2.5)$$

Where *Vmax* is the parameter representing the maximal plant N uptake in optimal conditions. The nitrogen uptake by the root is governed by an ion transport mechanism governed by Michaelis-Menten kinetics (*K*). From (*kNmin*) to the Michaelis-Menten saturation points, the nitrogen abortion is linear. NCplant is the average nitrogen concentration of the leaf, fine roots, and labile nitrogen stores. The usage of nitrogen concentrations in foliage and roots, as well as labile nitrogen buffers, tends to stabilize plant nitrogen uptake.

2.2 Model evaluation

2.2.1 Simulated Gross Primary Production (GPP)

A precursor version of ORCHIDEE-v3 r7267 (ORCHIDEE-CN r4999) that accounts for carbon-nitrogen interactions has already been partly evaluated at site level and globally with respect to the GPP (Vuichard et al. 2019). The site level evaluation was based on the FluxNet collection of sites where GPP can be derived from net carbon flux measurements (using standard flux partitioning methods). For spatial evaluation, the model simulated GPP can be compared to a standard benchmark product based on a statistical extrapolation of the FluxNet data using satellite vegetation products and meteorological information (Jung et al., 2011). Several products have been derived (Jung et. al. 2020) and we only use here the so-called MTE-GPP. The simulated GPP can satisfactorily mimic the mean seasonal cycle, daily mean fluctuations, and yearly mean data driven GPP for most PFTs. At site level, the mean root square error of the daily GPP flux for any PFT never exceeds the 2.5 g C m^{-2} d^{-1}, for an ensemble of 32 FLUXNET sites.

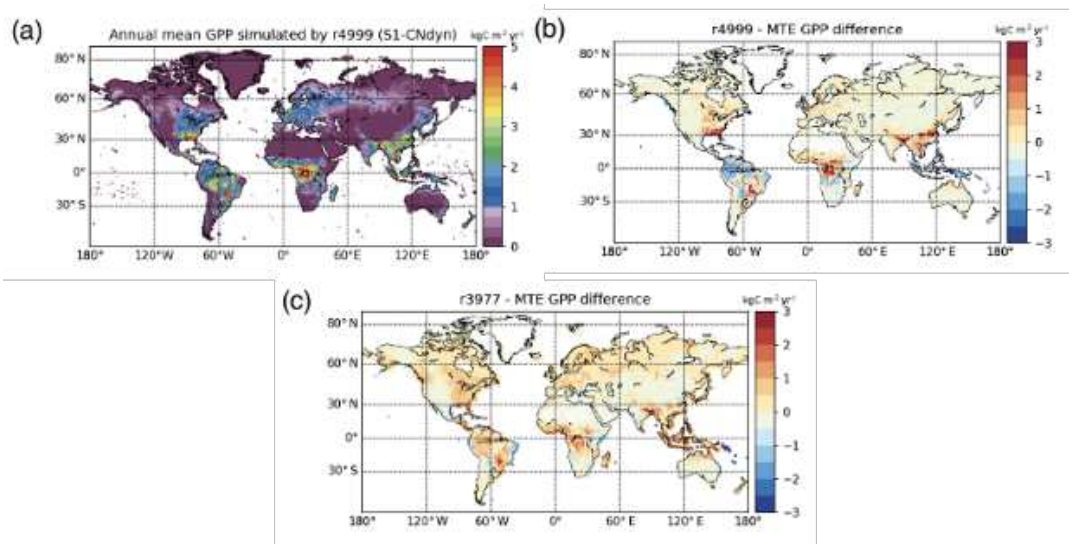

Figure 2.1 - Figure GPP response in ORCHIDEE r4999 Global-scale evaluation of ORCHIDEE against the observation-based MTE-GPP product. (a) Global distribution of the simulated annual mean GPP by ORCHIDEE r4999 (kg C m−2 yr−1) over 2001–2010; (b) global distribution of the difference between the simulated annual mean GPP by ORCHIDEE r4999 and the MTE-GPP product; (c) global distribution of the difference between the simulated annual mean GPP by ORCHIDEE r3977 and the MTE-GPP product. (Vuichard et al., 2019).

Spatially, the yearly mean average GPP over 2001 to 2010 from the r4999 dynamic C:N version provides a greater agreement with the MTE GPP (see figure GPP response in ORCHIDEE) than the previous version of ORCHIDEE r3977 without carbon-nitrogen interactions. Note that climate variability, vegetation greenness index from Normalized Difference Vegetation Index (NDVI), and satellite land cover information are the only factors driving the MTE-GPP. As a result, the MTE-GPP does not directly represent the influence of CO_2 and nitrogen on GPP, but rather indirectly through changes in vegetation greenness, which may explain the GPP positive biases in central Africa and negative biases in Amazonia response.

Overall, the functional responses of ORCHIDEE (r4999) fit better with current photosynthesis knowledge (Figure 2.1) than when the carbon-nitrogen interactions are not considered as shown previously. Note finally that factorial experiments and sensitivity analysis done by (Vuichard et al., 2019) have been supported by several other global terrestrial models responses: the importance of carbon-nitrogen interactions in understanding global terrestrial ecosystem productivity.

2.2.2 Multi-model benchmarking

Using numerous statistical criteria, Seiler et al. (2022), generated benchmark scores that assess the similarity of independently produced reference data, mostly derived from field measurements and satellite photos. Models are deemed to perform well if their model scores meet or exceed the benchmark.

ORCHIDEE-v3 r7267 dynamic C:N version (here referred as ORCHIDEE) scores are usually of comparable magnitude to benchmark scores, showing that our model performance is appropriate given the variety of reference data (Figure 2.2). In particular, ORCHIDEEv3 , scored better than the benchmark than four versions for the NBP *carbonScope* and HLFS *Fluxnet* datasets. ORCHIDEE-v3 scores exceed the multi-model mean values for 22 observational datasets out of 25 (Figure 2.2).

Seiler et al. (2022), also concluded that while all models performance is encouraging, there is still room for improvement, such as reducing a positive leaf area index bias, improving representations of processes that govern soil organic carbon in high latitudes, and assessing the causes of the inter-model propagation of gross primary productivity in boreal regions and humid tropics.

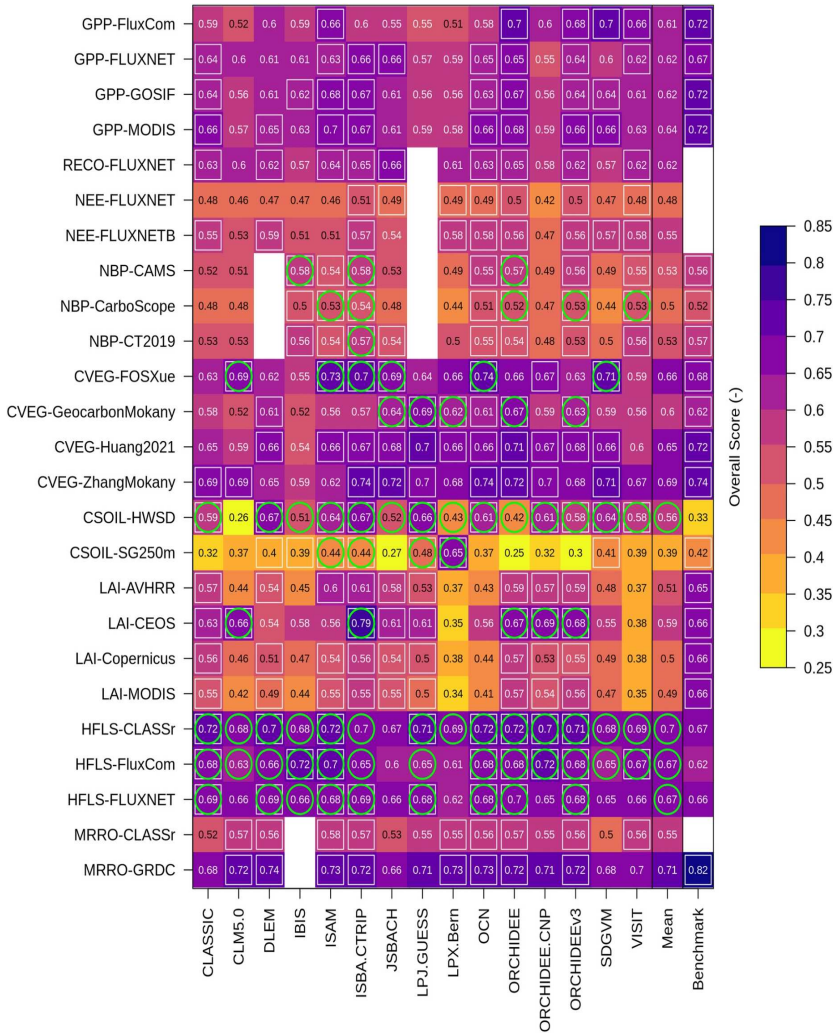

Figure 2.2 - Model and benchmark scores, where green circles denote cases where model scores exceed benchmark scores and white squares present cases where model scores exceed the multi-model mean values. Blank spaces indicate missing data (Seiler et al., 2022).

"*The Earth's carbon sink is a powerful ally in the fight against climate change, but it is also a fragile one. It is therefore our responsibility to do everything in our power to protect it*".

Kofi Annan, former Secretary-General
of the United Nations

CHAPTER 3

Unraveling the contribution of atmospheric CO_2 and Nitrogen deposition to the evolution of land productivity over the historical period

3.1 Introduction

As stated in the introduction chapter, Earth's atmosphere and biosphere have experienced several human-induced changes during the last two centuries. Global CO_2 emissions have risen dramatically, from 2.73 Pg CO_2 yr^{-1} in 1850 to 29.77 Pg CO_2 yr^{-1} in 2000, a total increase of 91%. This perturbation is owed mostly to the use of fossil fuels, followed by land use change emissions from agriculture and deforestation. Emissions from fossil fuels have soared during the 1950s, whereas emissions from land use change have tended to level and drop after 1960. Historical anthropogenic carbon emissions have resulted in an increase of atmospheric CO_2 concentrations from 280 ppm in 1850 to 370 ppm in 2000 (Taylor & Orr, 2000), significantly disturbing the global carbon cycle.

This rapid increase in atmospheric CO_2 has resulted in a boost of terrestrial productivity from the CO_2 fertilization effect. However, as discussed in the introduction chapter, plant

development is also constrained by other elements such as water and nutrients availability, light intensity and temperature among others, elements that are highly interlinked.

Nitrogen is especially important since it is required to synthesize proteins, in particular enzymes such as the Rubisco involved in the photosynthesis., As a consequence, nitrogen availability may potentially limit the CO_2 fertilization effect (Arora et al., 2020a). On the other hand, due to higher anthropogenic emissions from the industrial, transportation and agriculture sectors in the form of NOx and NHx over the historical period (Erisman et al., 2008), the amount of atmospheric reactive nitrogen deposited on land significantly increased, from 30 TgN yr^{-1} in 1850 to 80 TgN yr^{-1} in the 2000s (Lamarque et al., 2013). This increase of the atmospheric nitrogen deposition rates may contribute also to increase land productivity over the historical period.

The contributions on the global terrestrial productivity of the aforementioned factors (CO_2 increase, nitrogen deposition rates increase) but also land use change and climate, have been widely studied in the last decades (Arora et al., 2020a; C. Jones et al., 2013). In the latest Global Carbon Budget, based on a Land surface models ensemble, Friedlingstein et al. (2022) reported that land has acted as a small net source of carbon (5 PgC) over the historical period (1850-2020) although with a high uncertainty on the sign of the net flux.

This nearly neutral budget over 1850-2020 corresponds to the sum of two important opposite fluxes, one related to Land-use change emissions (200 PgC), and one related to the natural land sink driven by atm. CO_2, N deposition and climate (195 PgC). In one of the most recent and comprehensive studies, (O'Sullivan et al. (2022) analyzed the contributions of CO_2 and Ndep, Land-use change and Climate on the net land C flux over 1960-2020. Based on a land models ensemble mean, they report an increase of the net land flux (ie. a higher land C sink) from -0.1 PgC yr^{-1} in 1960's to 1.6 PgC yr^{-1} in 2010's. Atm. CO_2 and Ndep increases are the major contributors to the enhancement of the net land C sink, with an overall contribution going from 1.2 PgC yr^{-1} in the 1960's to 3.5 PgC yr^{-1} in 2010's. CO_2 and Ndep contribution is partially compensated by the land-use change emissions which are nearly constant over 1960-2020 and amount to 1.3 PgC yr^{-1}. The contribution of climate change on the net land C sink is negative but relatively small over 1960-2020 (0.4 PgC yr^{-1} over 1980-2020).

Most of all the multi-model ensemble studies aiming at quantifying the impacts of the different drivers of the net land/atmosphere C flux such as Friedlingstein et al. (2022) or O'Sullivan et al. (2022) are based on the Trends in Land carbon cycle (TRENDY) model intercomparison project.

In the interest of improving the understanding of terrestrial carbon sink patterns over the historical period, TRENDY, an intercomparison of Dynamic Global Vegetation Model (DGVM), is performed each year to feed the the Global Carbon Budget (GCB) of the Global Carbon Project (GCP), by a consortium of Dynamic Global Vegetation Model (DGVM) groups, The aim

is to further investigate spatial and temporal variations in the Net Biome Production (NBP) through a set of DGVM factorial simulations over the recent historical era, using a common protocol applied to all DGVMs.

The protocol was first established solely for terrestrial carbon only models to quantify the relative contributions of CO_2, climate, and LUC to the terrestrial land sink or source, over the industrial period. The protocol consists of a set of four additive simulations. In S0, [CO_2], climate and land-use are set constant to their pre-industrial level. In S1, observed [CO_2] rise is accounted for. In S2, climate change is accounted for, on top of S1. Last, in S3, historical land-use change is also considered. The protocol, however, has been upgraded to include DGVMs modeling the nitrogen cycle and the interactions between the carbon and nitrogen cycles. Effects of the change in nitrogen deposition have been included in S1, in addition to the effect of rising CO_2 levels on terrestrial carbon fluxes. As a result, no study based on the TRENDY protocol is capable of disentangling the fertilization effects of [CO_2] and N deposition. Few studies have attempted to explicitly estimate the specific contribution of the nitrogen deposition increase to global terrestrial carbon fluxes (Bala et al., 2013; Devaraju et al., 2016; O'Sullivan et al., 2019; Tharammal et al., 2019).

(Bala et al., 2013) evaluated the Terrestrial Ecosystem Carbon TEC sensitivity to CO_2 fertilization (referred as βL) and N deposition (referred as δL) through a factorial analysis with twelve experiments with the Community Land Model 4.0 (CLM4). These experiments include 3 sets of 4 simulations of 1000 years each. The first set (1-4) with CO_2 concentration at pre-industrial levels (Control) and nitrogen deposition at respectively pre-industrial levels 1N, twice the preindustrial levels 2N, four times 4N and eight times 8N. The second set (5-8) with $1N_2 \times 2CO_2$, $2N_2 \times 2CO_2$, $4N_2 \times 2CO_2$ and $8N_2 \times 2CO_2$ and the last set (9-12) the same as the second set but with a uniform increase of 2K in atmospheric temperature.

The study has shown that about 242 PgC could have been taken up by land due to the CO_2 fertilization effect and an additional 175 PgC taken up as a result of the increased N deposition since the preindustrial period (1850 to 2005). Climate warming impact (usually referred as γL, the change of land C uptake per unit of increased temperature), on the other hand, could have led to a loss of about 152 PgC during the same period, assuming a warming of about 1K (see Figure 3.1).

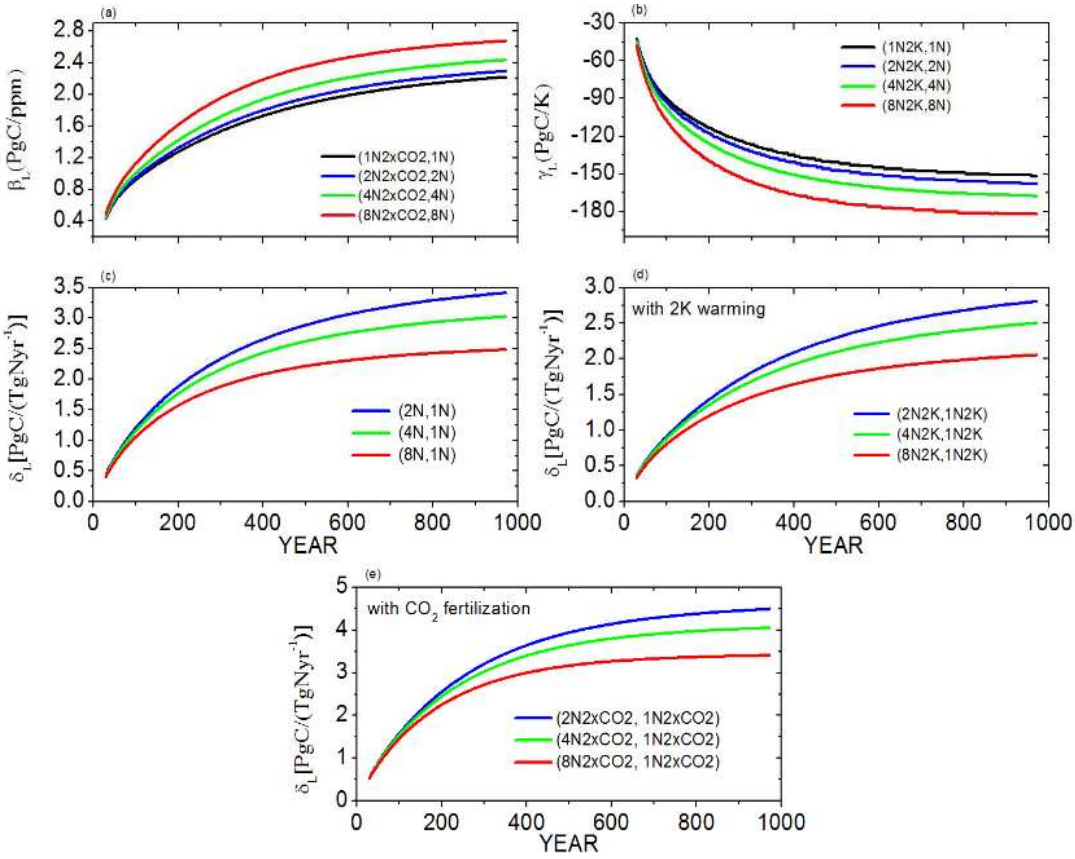

Figure 3.1 - Evolution of terrestrial ecosystem carbon (TEC) storage sensitivity to CO_2, climate warming and increased N deposition in our 1000 yr simulations. TEC sensitivity to (a) atmospheric CO_2 (βL) at different levels of N deposition, (b) temperature (γL) at different levels of N deposition, (c) N deposition (δL), (d) N deposition (δL) in presence of 2K warming and (e) N deposition (δL) in the presence of doubled CO_2 (Bala et al., 2013).

(Devaraju et al., 2016) on the other hand, provided an evaluation of the dominant drivers of the terrestrial carbon uptake by a set of six 156-year experiments from 1850 to 2005 with the Community Land Model 4.0 (CLM4) (see Table 3.1): The experiments use either a transient dataset or a fixed pre-industrial distribution to treat the different forcings: atmospheric CO_2 concentration, climate warming, nitrogen deposition, and LULCC.

Experiment name	CO_2 forcing to land model	CO_2 forcing to atmosphere model	Nitrogen deposition	LULCC	Other GHGs, ozone, aerosols and solar variability
HISTORICAL	Transient	Transient	Transient	Transient	Transient
NO-CO_2-FERT	Pre-industrial	Transient	Transient	Transient	Transient
NO-N-CHANGE	Transient	Transient	Pre-industrial	Transient	Transient
NO-CO_2-CHANGE	Pre-industrial	Pre-industrial	Transient	Transient	Transient
NO-LULCC	Transient	Transient	Transient	Pre-industrial	Transient
NO-CO_2-N-LULCC-CHANGE	Pre-industrial	Pre-industrial	Pre-industrial	Pre-industrial	Transient

Table 3.1 - Summary of experiments performed in (Devaraju et al., 2016).

The study highlighted the CO_2 fertilization and nitrogen deposition as positive factors to the accumulated net land sink during 1850–2005 with +55.39 PgC, 26% contribution and +26.11 PgC, 12% contribution respectively. This in turn was counterbalanced by a large negative contribution due to land use change (−111.57 PgC, 53% contribution) in turn boosted by climate warming (−15.05 PgC, 7% contribution). This has led to a net decline in the land carbon stocks during the studied period of around 45.1 ± 2.4 PgC (see Figure 3.2).

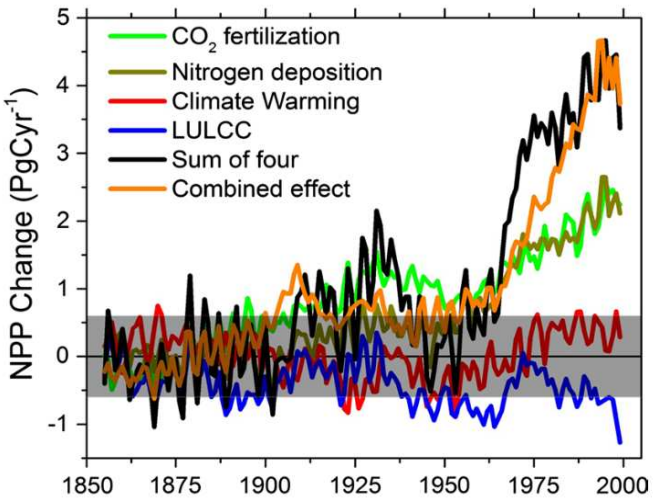

Figure 3.2 - Simulated global- and annual- mean change in NPP (PgCyr−1) due to CO_2 fertilization, nitrogen deposition, climate warming, LULCC, sum of four effects and combined effects during the period 1850–2005. The combined effect is calculated as HISTORICAL simulation results minus the NO-CO_2-N-LULCC-CHANGE results (Devaraju et al., 2016).

(O'Sullivan et al., 2019), performed a set of eight factorial simulations to assess the land carbon cycle response to increasing atmospheric CO_2, nitrogen deposition, and climate changes, as well as the interactions between these driver for period 1901–2016 with the Community Land Model version 4.5 (CLM4.5-BGC) (Table 3.2). The effects of LULCCs were not considered in the study.

Experiment	CO_2	Nitrogen deposition	Climate
S1	C	C	C
S2	T	C	C
S3	C	T	C
S4	C	C	T
S5	T	T	C
S6	T	C	T
S7	C	T	T
S8	T	T	T

Table 3.2 - Summary of Factorial Model Simulations With CLM4.5-BGC (O'Sullivan et al., 2019).

According to the findings of this study, the following components contributed to the rise in NBP between 1901 and 2016: 99% for rising CO_2, 14% for nitrogen deposition, 14% for carbon-nitrogen synergy, 18% for carbon-climate synergy, and -45% for climate change (see Figure 3.3). Based on this study, the contribution of nitrogen deposition appears much smaller than the one reported in other studies (Bala et al., 2013; Devaraju et al., 2016) as a result of the updated version of the model structure and parameterization. CLM4 features a substantial nitrogen downregulation of potential (non-nitrogen restricted) GPP, low soil carbon stocks, a poor CO_2 fertilization response, and a weak terrestrial carbon sink. CLM4.5 on the other hand features enhanced GPP (although still employing the CLM4 nitrogen downregulation idea), vertically resolved soil carbon with considerably higher soil carbon stocks than CLM4, and a greater terrestrial carbon sink than CLM4 (Bonan et al., 2019).

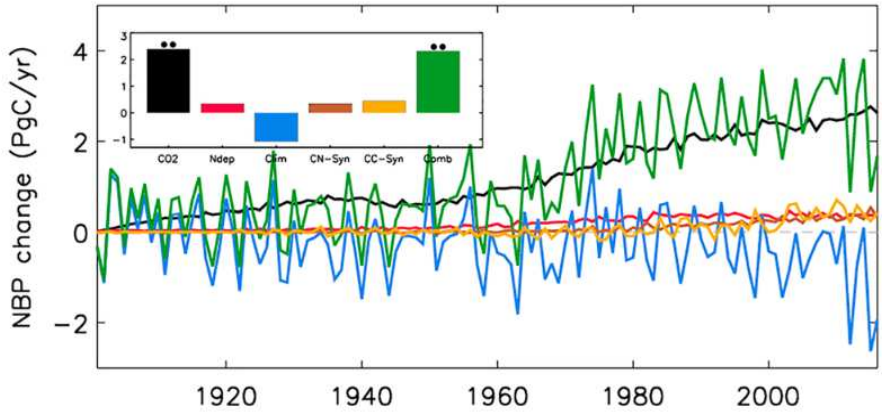

Figure 3.3 - Global, annual mean change in net biome production (Pg C/year) relative to the control simulation (S1) during 1901–2016 due to CO_2 fertilization (CO_2), nitrogen deposition (Ndep), climate change (Clim), the combined effect (Comb), carbon-nitrogen synergy (CN-Syn), and carbon-climate synergy (CC_Syn) (O'Sullivan et al., 2019).

(Tharammal et al., 2019) examined the key drivers of terrestrial carbon absorption compiling the results from different studies, with a relative contribution of CO_2 fertilization to NBP or accumulated NBP (equivalent to the change in Terrestrial Ecosystem Carbon - TEC), ranging from 33% to 85%, with a mean of 55%, and a relative contribution of N deposition ranging from 10% to 24%, with a mean of 16%. In the majority of research, climate change and LULCC cause a loss in terrestrial carbon stocks, with the mean relative contributions of these two causes being 14% and 39%, respectively (see Figure 3.4).

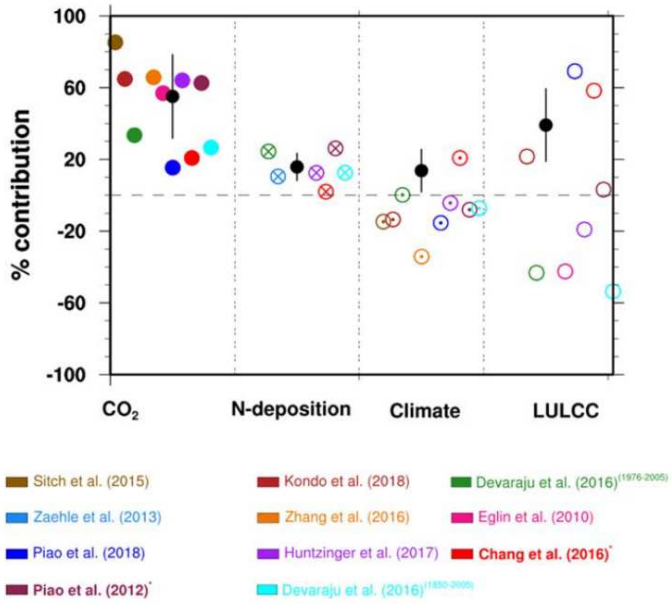

Figure 3.4 - Percent contributions of major drivers of changes in recent-historical (1976–2012) land carbon fluxes and stocks represented by trends or net changes in net biome production (NBP), net ecosystem production (NEP) and total ecosystem carbon (TEC) from various studies. (Tharammal et al., 2019).

Despite these investigations, a wide range of values for the nitrogen contribution to accumulated NBP is found (from 0 to 25% of the flux), indicating that more research into these nutrient-related contributions is required. In the first version of ORCHIDEE including dynamic nitrogen (ORCHIDEE-CN r4999), the relative contributions of the different drivers to the GPP growth over 1861–2016 period were assessed at: 10% for climate change, 50% for CO_2 increase, −13% for land-use change, 20% for nitrogen deposition change and 33% for nitrogen fertilization change (Vuichard et al., 2019). In Vuichard et al,. (2019) no assessment of NBP was performed, and since this initial study substantial improvements of the carbon and nitrogen cycles in ORCHIDEE (r4999) have been made (refer to chapter 2). It is thus of major interest to re-assess the contribution of key factors such as CO_2 and nitrogen deposition, as well as their synergy, on the historical land carbon budget.

To accomplish so, we run a series of factorial simulations, from 1850 to 2010 forced with variable and constant atmospheric CO_2 and nitrogen deposition, inspired by the TRENDY protocol but adding specific runs to separate the C vs N effect. In order to assess the regional contribution of these impacts, we advanced the study of (Vuichard et al., 2019) by examining separately the role of CO_2 rise in the change in gross primary productivity GPP and net biome production NBP in a constant vs variable nitrogen deposition scenario. Similarly, we examined the effect of increased nitrogen deposition on the changes in GPP and NBP for a constant and variable CO_2 concentration trajectory, trying to unravel regional feedback between the two drivers. To this purpose, we will identify some important metrics (linked to C and N fertilization effects) that will enable us to add information to the present state of research based on the

historical era's land carbon dynamic, and we will compare our findings with a few key results and metrics from past studies.

This included a close look at the atmospheric nitrogen deposition use efficiency in European forests over the last decade (response of terrestrial carbon to N deposition), which was compared to a (Flechard, Ibrom, et al., 2020) study based on a mechanist forest growth model in combination with eddy covariance CO_2 exchange fluxes at 22 forest towers across Europe. We finished by the quantification of the sensitivity of terrestrial carbon fluxes (GPP and NBP) to CO_2 and nitrogen deposition change, as described by (Devaraju et al., 2016).

3.2 Methods

3.2.1 Forcing data

ORCHIDEE, as mentioned in the previous chapter, requires meteorological forcing, land cover description, soil texture maps and nitrogen forcings as input datasets. For this study we used the forcings from the TRENDY v.10 GCB 2021 simulations protocol for:

- ***Atmospheric CO_2***: Historical annual atmospheric CO_2 concentration from 1700 to 1959 were derived from ice core CO_2 data. The worldwide increase rate for the period 1959-1979 is based on data of atmospheric CO_2 concentration averaged from the Mauna Loa and South Pole stations (Keeling et al., 1976). The worldwide increase rate for the period 1980-2019 is based on the average of several stations picked from maritime boundary layer locations with well-mixed background air (Ballantyne et al., 2012).
- ***Climate:*** observation-based temperature, precipitation, and incoming surface radiation were obtained from the the merged monthly Climate Research Unit (CRU) and 6-hourly Japanese 55-year Reanalysis (JRA-55) dataset over 1901-2018 on a 0.5∘ × 0.5∘ grid and updated to 2020 (Friedlingstein et al., 2022).
- ***Land use and Land cover changes:*** annual land cover maps from 1700 to 2019 in quarter-degree spatial resolution including cropland/grazing and wood harvest land dataset from the FAO country-level statistics were used. They are constrained spatially based on multi-year satellite land cover maps (ESA-CCI land cover maps; https://www.esa-landcover-cci.org/) and historically by HYDE3.3, History Database of the Global Environment model from The Netherlands environmental agency (Friedlingstein et al., 2022).
- ***Nitrogen inputs***: historical nitrogen fertilizer input datasets were derived from the NMIP project, whereas the historical nitrogen deposition datasets from 1850 to 2014 were taken from input4MIPS (input datasets for Model Intercomparison Projects), a

project that activity seeks to achieve the boundary condition and forcing datasets required for CMIP6 (accessible through the ESGF (G. Hurtt et al., 2017).

3.2.2 Model set-up

In order to specifically study the contribution that both CO_2 and nitrogen deposition had on the terrestrial ecosystem C fluxes over the historical period, four simulations with ORCHIDEE were launched from the spin up run from 1850 up to 2015, in a similar factorial approach than the one of the TRENDY protocol (but not following the same convention). Our model spin-up technique was similar to the multi-model TRENDY approach (Sitch et al., 2015). It included cycling early 20th century climate (1901-1920) with 1700, CO_2 concentration (276.59 ppm) and constant 1700 land cover (crops and pasture distribution).

The simulations were: (***S1***) Simulation with time-varying forcings for all drivers from 1850 to 2015 (i.e. CO_2 level, nitrogen deposition rates, but also LUC and climate change). (***S2***) Simulation with time-varying forcings for all drivers from 1850 to 2015, except CO_2 fixed at its pre-industrial level. (***S3***) Simulation with time-varying forcings for all drivers from 1850 to 2015, except nitrogen deposition fixed at is pre-industrial rate and (***S4***) simulation with constant pre-industrial values for both atmospheric CO_2 and nitrogen deposition rates and time-varying forcings for LUC and climate change. (Table 3.3) resumes these factorial simulations.

Simulation	*CO2*	*Nitrogen deposition*	*LUC*	*Climate*
S1	dynamic	dynamic	dynamic	dynamic
S2	constant	dynamic	dynamic	dynamic
S3	dynamic	constant	dynamic	dynamic
S4	constant	constant	dynamic	dynamic

Table 3.3 - Set-up of the four simulations performed in this study.

Note that the S1 simulation is the same as the S3 simulation used for the 2021 Global Carbon Budget: Land modeling protocol (Trendy-v10) for ORCHIDEE version r4999 with CO_2, climate LUC, N fertilization and deposition all forcing time-varying.

3.2.3 Metrics

<u>Contribution of atmospheric CO_2, nitrogen deposition and their synergy on GPP and NBP fluxes:</u>

We isolate different signals to explain changes in historical production due to rising atmospheric CO_2 and N dep, as well as their interaction or synergy, depending on how the four simulations are combined (Table 3.3). The total contribution due to both CO_2 and N dep increase on gross primary productivity (GPP) and net biome production (NBP) (expressed as

terrestrial ecosystem carbon fluxes: F) (F_{CO_2+Ndep} in gC $m^{-2}yr^{-1}$) is obtained by subtracting the output values of the simulation (***S4***) from (***S1***) (Equation 3.1):

$$F_{CO2+Ndep} = F_{S1} - F_{S4} \quad (3.1)$$

Alike, to isolate the specific contribution of increasing CO_2 on a given carbon flux (F_{CO_2} in gC $m^{-2}\,yr^{-1}$), we subtract the output values of the simulation (***S4***) from (***S3***) (Equation 3.2):

$$F_{CO2} = F_{S3} - F_{S4} \quad (3.2)$$

Similarly, to isolate the contribution of increasing N dep on a given carbon flux (F_{Ndep} in gC $m^{-2}\,yr^{-1}$), it is necessary to subtract the output values of the simulation (***S4***) from (***S2***) (Equation 3.3):

$$F_{Ndep} = F_{S2} - F_{S4} \quad (3.3)$$

If we subtract the individual factor contributions (CO_2 and N dep) from the total contribution of both of them, the remaining value is equivalent to the effect of the synergy between the two, since, as we know, the two biogeochemical cycles interact, limiting or enhancing each other. The synergistic contribution on a given carbon flux (F_{syn} in gC $m^{-2}yr^{-1}$) is then obtained if we subtract from the total effect (***S1-S4***), the contribution due to CO_2 increase (***S3-S4***) and the contribution due to nitrogen deposition increase (***S2-S4***) as follows (Equation 3.4):

$$F_{syn} = F_{CO2+Ndep} - F_{CO2} - F_{Ndep} \quad (3.4)$$

<u>Atmospheric CO_2 Use Efficiency:</u>

We examined how sensitive GPP and NBP were to atmospheric CO_2 growth for the simulated period from 1850 to 2015 under the assumption that nitrogen deposition remained constant. To do so, we computed the Atmospheric CO_2 Use Efficiency ($ACUE_F$ in gC $m^{-2}yr^{-1}$/ppm) as (Equation 3.5):

$$ACUE_F = \frac{F_{CO2}}{\Delta CO2} \quad (3.5)$$

where,

$$\Delta CO2(ppm) = CO2_{S1} - CO2_{S2} = CO2_{S3} - CO2_{S4} \quad (3.6)$$

We also quantified the Atmospheric CO_2 Use Efficiency in an environment where nitrogen deposition varied ($ACUE^+_F$ in gC $m^{-2}\,yr^{-1}$/ppm), thus including the additional contribution from the carbon-nitrogen synergy . This required expressing the contribution of the CO_2 increase on a given carbon flux in a varying nitrogen deposition world by subtracting the output values (***S2***) from (***S1***) (defined as $F^+_{CO_2}$ in gC $m^{-2}\,yr^{-1}$). $ACUE^+_F$ is written as:

$$ACUE_F^+ = \frac{F_{CO2}^+}{\Delta CO2} \tag{3.7}$$

Atmospheric Nitrogen Deposition Use efficiency:

Mirroring the above diagnostic, we also quantified the sensitivity of GPP and NBP to nitrogen deposition increase for the simulated period from 1850 to 2015 under constant CO_2 ($ANDUE_F$ in gC gN^{-1}) as (Equation 3.8):

$$ANDUE_F = \frac{F_{Ndep}}{\Delta Ndep} \tag{3.8}$$

where,

$$\Delta Ndep(gN\,m^{-2}\,yr^{-1}) = Ndep_{S1} - Ndep_{S3} = Ndep_{S2} - Ndep_{S4} \tag{3.9}$$

Similarly, to what has been done for ACUE, we also quantify the Atmospheric Nitrogen Use Efficiency in a CO_2 varying environment ($ANDUE^+_F$ in gC gN^{-1}). , thus including the additional contribution from the carbon-nitrogen synergy . This required defining the contribution of the nitrogen deposition increase on a given carbon flux in a CO_2 varying world by subtracting the output values of (***S3***) from (***S1***) (defined as F^+_{Ndep} in gC $m^{-2}yr^{-1}$). $ANDUE^+_F$ is expressed as (Equation 3.10):

$$ANDUE_F^+ = \frac{F_{Ndep}^+}{\Delta Ndep} \tag{3.10}$$

Land carbon stock changes sensitivity to CO_2 and N dep increase:

We also examine the impact of the different drivers on the change of terrestrial carbon stocks (or cumulated NBP) from 1850 to 2005 to mimic the diagnosis proposed by Devaraju et al. (2016) equivalent to the so-called "beta" analysis (β_{CO_2+} in PgC ppm^{-1}) which is the accumulated NBP due to CO_2 increase ($accNBP_{CO_2}$; see also Equation 3.2) divided by the change in atmospheric CO_2 over the chosen period (Equation 3.11). This is equivalent to equation 5 but integrated over the time of the simulation.

$$\beta_{CO2+} = \frac{accNBP_{CO2}}{CO2_{2015} - CO2_{1850}} \tag{3.11}$$

Similarly, we also study the change of terrestrial carbon stock from 1850 to 2005 due to N dep, via an equivalent "delta" analysis (δ_{Ndep+} in PgC TgN^{-1}) defined as the accumulated NBP due to nitrogen deposition increase ($accNBP_{Ndep}$; see also Equation 3.3) divided by the change in nitrogen deposition in TgN yr^{-1} over the given period (Equation 3.12):

$$\delta_{Ndep+} = \frac{accNBP_{Ndep}}{(Ndep_{2005} - Ndep_{1850})} \quad (3.12)$$

3.3 Results

To study with the ORCHIDEE model how nitrogen deposition, CO_2 fertilization, and their interactions have modified the terrestrial carbon sink, we examined the carbon component fluxes GPP and NBP simulated by the ORCHIDEE r4999 model over the last century, from 1850 to 2015, using the protocol and metrics defined in the previous section. We start by the gross carbon uptake before investigating the net biome production.

3.3.1 GPP

Effect of CO_2, nitrogen deposition and the synergy between the two:

For this diagnosis, we will refer to the global annual mean GPP flux (PgC yr^{-1}) and its evolution over the historical period as shown in Figure 4. Our simulations indicate that simulated global GPP increased significantly from 91.3 PgC yr^{-1} (1950-1955 mean) to 114.3 PgC yr^{-1} (2005-2015 mean), with positive, smooth, and increasing contributions from all evaluated drivers: atmospheric CO_2 increase (GPP_{CO_2} in blue in Figure 3.5), nitrogen deposition increase (GPP_{Ndep} in orange). Regarding the relationship between carbon and nitrogen, the rather low but still positive synergistic contribution of carbon and nitrogen (GPP_{Syn} in green) suggests that the two effects are not solely additive. When nitrogen limitation decreases (through nitrogen deposition), the effectiveness of the CO_2 fertilization on GPP increases, a behavior that was highlighted in the previous study by O'Sullivan et al. (2019).

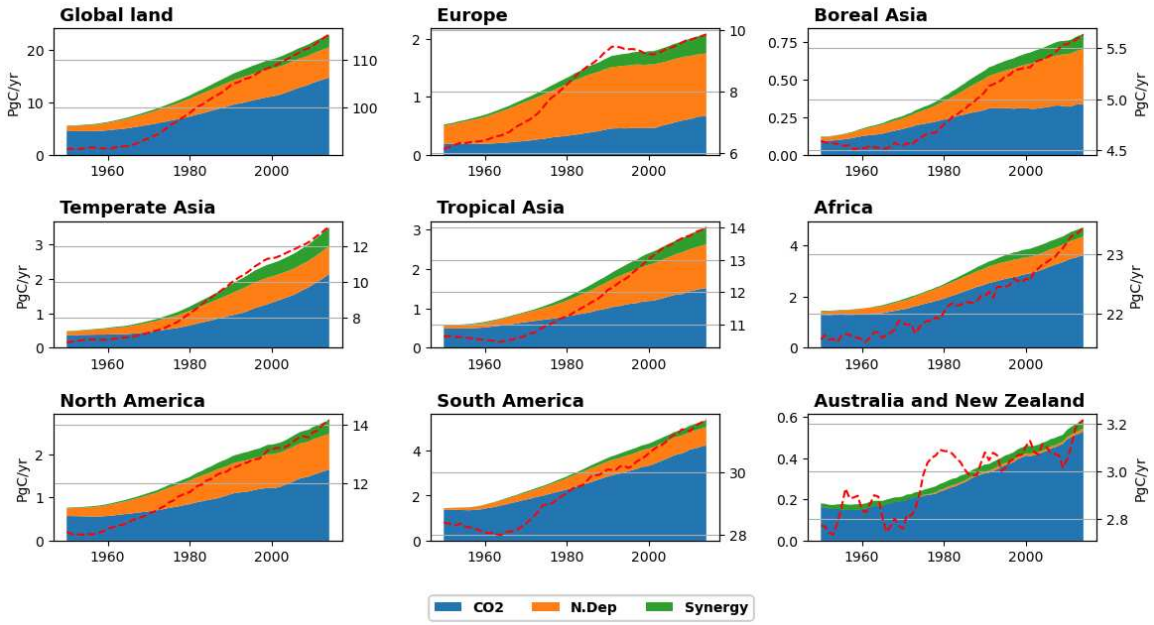

Figure 3.5 - Global and regional contribution of CO_2 increase (GPP_{CO_2} in PgC yr^{-1}), Nitrogen deposition increase (GPP_{Ndep} in PgC yr^{-1}) and the synergy between the two (GPP_{syn} in PgC yr^{-1}) to the total change of GPP (see Equations 3.2 – 3.3 – 3.4). The total GPP flux (S1) in PgC yr^{-1} is represented by the red dashed line and label on the right side of the subpanels. The chosen time period is 1950-2015 as it is from this year that increases in CO_2 and N dep began to have a significant impact on total GPP flux. The curves have been smoothed with a running mean to focus on the overall increase of the contributions and not into the year-to-year variation. The regional surface map is on the (Figure A 1).

By 1950, the worldwide contribution of CO_2 increase to the global GPP (GPP_{CO_2}) had already reached 4.3 PgC yr^{-1}, while GPP_{Ndep} accounted for approximately 0.8 PgC yr^{-1} and GPP_{Syn} 0.1 PgC yr^{-1} (Figure 3.5). Out of the total effect of the two studied factors, GPP_{CO_2} accounted for 83%, while GPP_{Ndep} 15% and GPP_{Syn} the remaining 2%. On the other hand, by 2015, the contribution due to GPP_{CO_2} rose to 14.7 PgC yr^{-1}, and GPP_{Ndep} to 5.7 PgC yr^{-1} which in turn made GPP_{Syn} rose to 2.4 PgC yr^{-1}. In 2015, GPP_{CO_2} accounted for 64% of the total factor's contribution while GPP_{Ndep} accounted for 25% and GPP_{Syn} for 11%, demonstrating how increased nitrogen deposition came to play a larger role in explaining the increase in GPP by the end of the 21st century. As a consequence, this resulted in a significant increase in the carbon-nitrogen synergy contribution.

The relative contributions of GPP_{CO_2} and GPP_{Ndep} to the total GPP growth varied by region (Figure 3.5). Europe, for example, was the only region whose GPP_{Ndep} (51% of total factor contribution by 2015) exceeded GPP_{CO_2} (29%). This pattern was mostly due to a significant increase in atmospheric N deposition (Figure 3.9) caused by industrialization sustained throughout the historical period mostly from 1850 to 1990. In Boreal and Tropical Asia, the GPP_{Ndep} (45% of total factor contribution by 2015) was somewhat equivalent to the GPP_{CO_2} (44%). The regional historical rise in atmospheric nitrogen deposition is significantly lower when compared to the rest of the examined regions (Figure 3.9), indicating that the increase in GPP_{Ndep} is predominantly attributable to the N-limited conditions of these ecosystems. Note

that the total GPP fluxes (red dashed curve in Figure 4; S1 scenario) show temporal variations, especially for some regions (i.e. Australia and New Zealand), while the contribution curves (CO_2, N dep and their synergies) show a smooth increase over time. This is due to the smoothing of the overall flux.

We will now discuss a different metric to quantify the impact of CO_2 fertilization and N deposition on GPP. we choose to express the effect of CO_2, N dep and their synergies for each year of the historical period (increase of GPP as obtained from equations 2-3-4) with respect to the GPP (of the same year) that would have occurred without the CO_2 and N dep effects (S4 simulation). Note that we could have also chosen to express these CO_2 and N dep effects with respect to the overall evolution of the GPP (S1 scenario) including land use and climate effects. We choose S4 as a reference in order to quantify each year the impact of the two effects in percentage of a hypothetical reference GPP that would have evolved only by land use and climate change. (Table 3.4) expresses the value in 2015 for a set of regions (i.e., using the GPP of S4 in 2015 as the reference to compute the percentage), while (see Figure 3.6) show the evolution of that metric over time.

With this new metric, we obtain in 2015 the following impact/change: 15% for CO_2 increase (GPP_{CO_2}), 6% for nitrogen deposition (GPP_{Ndep}), and 3% for carbon-nitrogen synergy (GPP_{Syn}). Individually, CO_2 fertilization and nitrogen deposition induced a smooth and temporary rise in GPP change consistent with the trajectory of the relevant causes explained in the introduction chapter (Figure 1.3 and Figure 3.9).

When these effects are expressed with respect to the change of the GPP flux from 1850 to 2015, this leads to a contribution of 52% for CO_2 rise and 20% for nitrogen deposition change. These values are very similar to those reported by Vuichard et al. (2019) (50% and 20% for CO_2 increase and nitrogen deposition change, respectively) (Table A 2).

	GPP(CO2) (PgC/yr)	*%GPP(S4)*	*GPP(Ndep) (PgC/yr)*	*%GPP(S4)*	*GPP(Syn) (PgC/yr)*	*%GPP(S4)*	*Combined effect (PgC/yr)*	*Combined effect (%)*
1. Global	14,71	15,9	5,74	6,2	2,43	2,63	22,88	24,73
2. Europe	0,68	8,69	1,07	13,78	0,33	4,19	2,08	26,66
3. Boreal Asia	0,34	6,93	0,36	7,5	0,1	2,03	0,8	16,46
4. Temperate Asia	2,14	22,33	0,81	8,42	0,55	5,75	3,5	36,5
5. Tropical Asia	1,51	13,78	1,1	10,06	0,43	3,92	3,04	27,76
6. Africa	3,62	19,28	0,73	3,91	0,36	1,91	4,71	25,1
7. North America	1,65	14,49	0,83	7,28	0,32	2,8	2,8	24,57
8. South America	4,24	16,07	0,81	3,07	0,31	1,16	5,36	20,3
9. Australia and NZ	0,53	20,08	0,01	0,52	0,04	1,52	0,58	22,12

Table 3.4 - Change in GPP due to atmospheric CO_2 increase (GPP_{CO_2} in PgC yr^{-1}), Nitrogen deposition increase (GPP_{Ndep} in PgC yr^{-1}) , the synergistic effects between the two (GPP_{syn} in PgC yr^{-1}) and the combined effect (equal to sum of the previous factors as GPP_{comb} in PgC yr^{-1}) expressed in PgC yr-1 for 2015. Additional columns express these changes as a percentage of the GPP(S4) flux in 2015 (i.e. the GPP that would have only been modified by land use and climate changes).

A more in depth regional study reveals that the CO_2 fertilization impact was the strongest in Temperate Asia in 2015 with 22% of the GPP flux from the -S4 scenario, followed by tropical areas, with relative effects on o the GPP-S4 ranging from 13 to 19% for Tropical Asia and Africa, respectively (see Figure 3.6), and subtropical such as in Australia where the contribution from CO_2 increase reached the 20% by 2015. The equatorial ecosystems with warm temperature and large precipitation benefited the most from CO_2 increase in terms of increase of carbon assimilation.

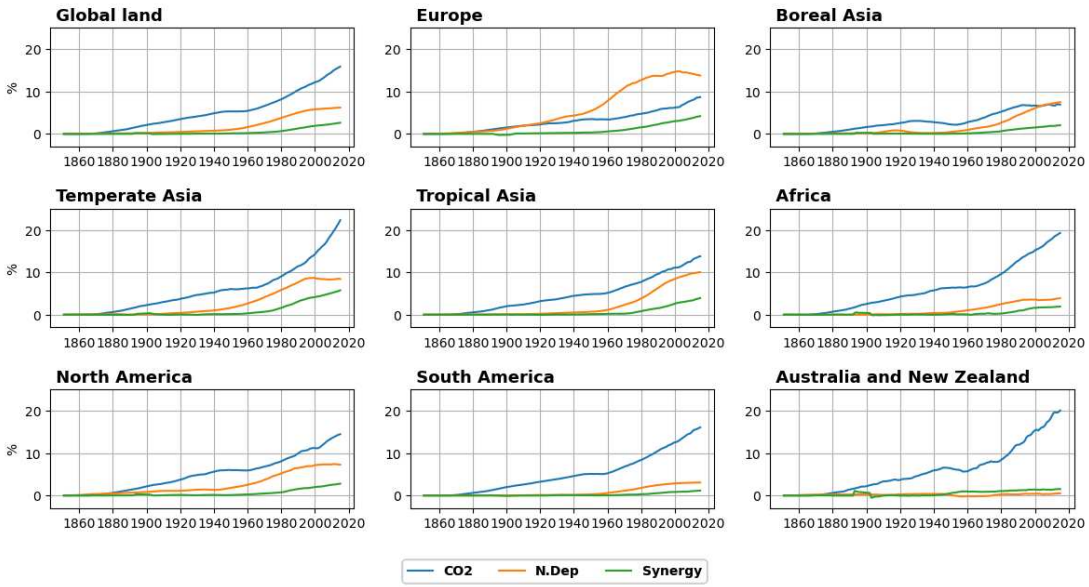

Figure 3.6 - Relative effect on the change GPP(S4) flux in (i.e. the GPP that would have only been modified by land use and climate changes) of CO_2 increase (GPP_{CO_2}), Nitrogen deposition increase (GPP_{Ndep}) and the synergistic effects between the two (GPP_{syn}).

Nitrogen deposition, on the other hand, appeared to be more significant in certain locations than others in terms of relative effect (increment of GPP expressed as a percentage of the GPP S4 flux). These locations correlate to those with high NOy emissions and depositions from transportation and energy combustion, and high NHx emissions and depositions from agricultural lands. Large impacts from nitrogen deposition were quite significant for the end of the 21st century across the industrialized regions in Europe, East Asia, and North America, as well as for the agricultural regions of India and Southeast Asia, making the impact of GPP_{Ndep} to range between 7 to 13% of the selected S4 reference S4 GPP (see figure contributions). While nitrogen deposition related GPP increases have the most impact in industrialized areas, the corresponding GPP response also depends on the ecosystem's nitrogen restriction and status.

We proposed below a further analysis of the atmospheric CO_2 use efficiency (ACUE, see definition on the method section) and nitrogen deposition use efficiency (ANDUE), in order to study the rates of these two effects (i.e., per unit of CO_2 and N dep increase).

GPP Atmospheric CO_2 Use Efficiency (ACUE):

Increase in atmospheric CO_2 concentration during the historical period had a positive and linear effect on the assimilated carbon from photosynthesis as illustrated with a scatter plot between the two variable changes in (Figure 3.7). The global linear relationship for both a constant or variable nitrogen deposition scenario (Blue and orange points in figure 5) appeared to be quite significant during the historical period, with a coefficient of determination (R^2) of 0.998 and 0.993, respectively. This behavior highlights the CO_2's fertilization effect. Most of the plant species are C3 photosynthetic type and remained below the optimal CO_2 concentration for photosynthetic activity during the historical period, which explains the positive response of GPP to CO_2 increase.

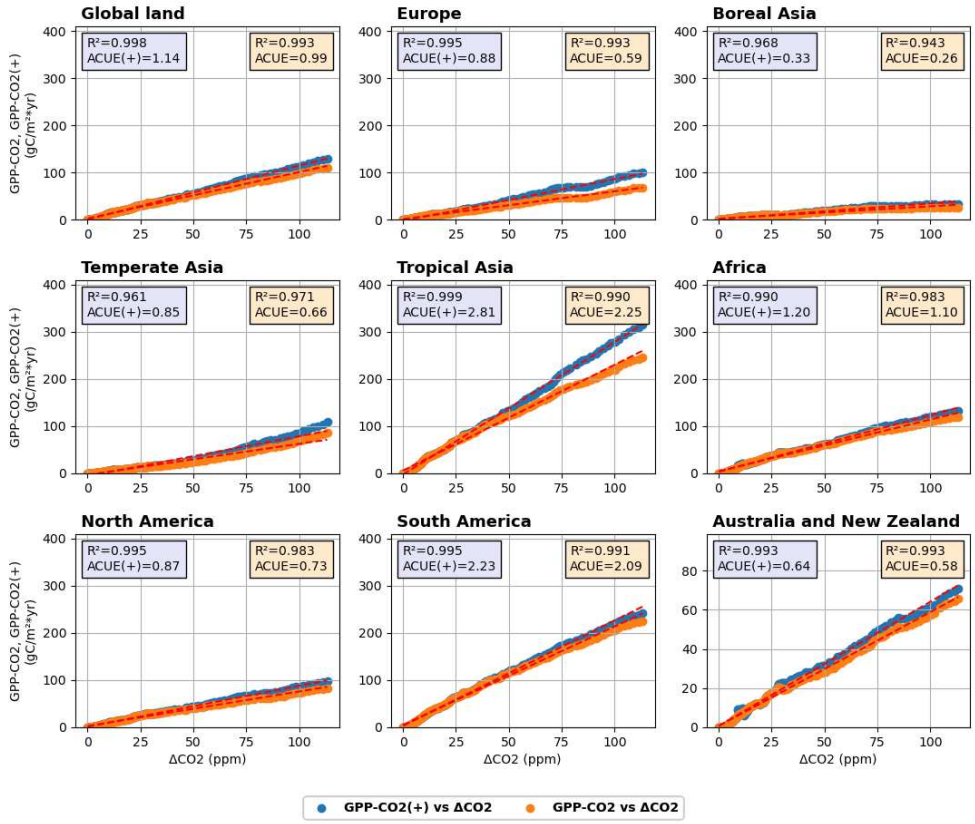

Figure 3.7 - Scatter plot between i) the increase of GPP due to the impact of CO_2 increase (GPP_{CO_2} and $GPPP^{+}_{CO_2}$ in gC $m^{-2}yr^{-1}$) for two scenarios (y axis) and ii) the CO_2 increase (ΔCO_2 in ppm; x-axis).The first scenario (blue points) corresponds to a varying N deposition ($GPP^{+}_{CO_2}$ = GPP_{S1}-GPP_{S2} see Eq. 7) and the second one (orange points) to a constant nitrogen deposition (GPP_{CO_2} = GPP_{S3}-GPP_{S4} see Equation 3.2). The displayed ACUE(+) and ACUE on the text box correspond to the slope of the linear regression applied to the scatter plot (see Equations 3.5 and 3.7).

In Temperate Asia, on the contrary there is a slight enhancement of the effect with high CO_2 increase, which induces a R^2 for $ACUE_{GPP}$ of 0.97 and 0.96 for $ACUE^{+}_{GPP}$. This indicates that there

is higher carbon assimilation for the scenario with varying N dep (Figure 3.7), which changes the linearity of the curve and hence makes R^2 lower. This is due to the vegetation and climatic conditions on this particular ecosystem.

From our results we can identify that the mean global Atmospheric CO_2 Use Efficiency for an increasing nitrogen deposition scenario $ACUE^{+}_{GPP}$ from 1850 to 2015, was equivalent to 1.14 gC m^{-2} yr^{-1}/ppm whereas the mean global Atmospheric CO_2 Use Efficiency for a constant nitrogen deposition scenario $ACUE_{GPP}$ was 0.98 gC m^{-2} yr^{-1}/ppm (see Figure 3.7) with ratio $ACUE^{+}_{GPP}/ACUE_{GPP}$ of 1.16. This global difference of 0.16 gC m^{-2} yr^{-1}/ppm (16% increase) is explained by the addition of reactive nitrogen in the system that boosted the amount of assimilated carbon starting from GPP. $ACUE^{+}_{GPP}$ value is systematically higher than $ACUE_{GPP}$ for any of the eight regions, but with significant differences among regions.

For example, in Europe, Temperate Asia, Boreal Asia, Tropical Asia and North America the ACUE ratios were 1.49, 1.28, 1.26, 1.24 and 1.19 respectively, with Europe benefiting the most with the biggest atmospheric CO_2 use efficiency from increased nitrogen deposition and in overall a significant increase in Asia. The important increase of atmospheric CO_2 use efficiency between the constant and increasing nitrogen deposition scenarios ($ACUE^{+}_{GPP}$ vs. $ACUE_{GPP}$) in these four regions is explained by the substantial increase of nitrogen deposition induced by industrial and/or agricultural sources in these regions.

The difference between $ACUE^{+}_{GPP}$ and $ACUE_{GPP}$ is less important in Australia, South America and Africa, with ACUE ratios of 1.09, 1.07 and 1.06 respectively, explained by a mid-range nitrogen deposition level throughout the historical period, mainly from mid-low economic development and agriculture (Bala et al., 2013).

The R^2 are higher for $ACUE^{+}_{GPP}$ than for $ACUE_{GPP}$ for all regions except for Temperate Asia. This shows that the $ACUE^{+}_{GPP}$ relationship is more linear than that of $ACUE_{GPP}$ (figure 5). Similarly, we can see that although the behavior is linear, there is an asymptotic trend towards the end of the period studied (high CO_2 increase), with a small saturation of the GPP increase. The impact of climate change contributes also to the non-perfect linearity in the GPP_{CO_2} and $GPP^{+}_{CO_2}$ increase versus CO_2 increase (Figure 3.7).

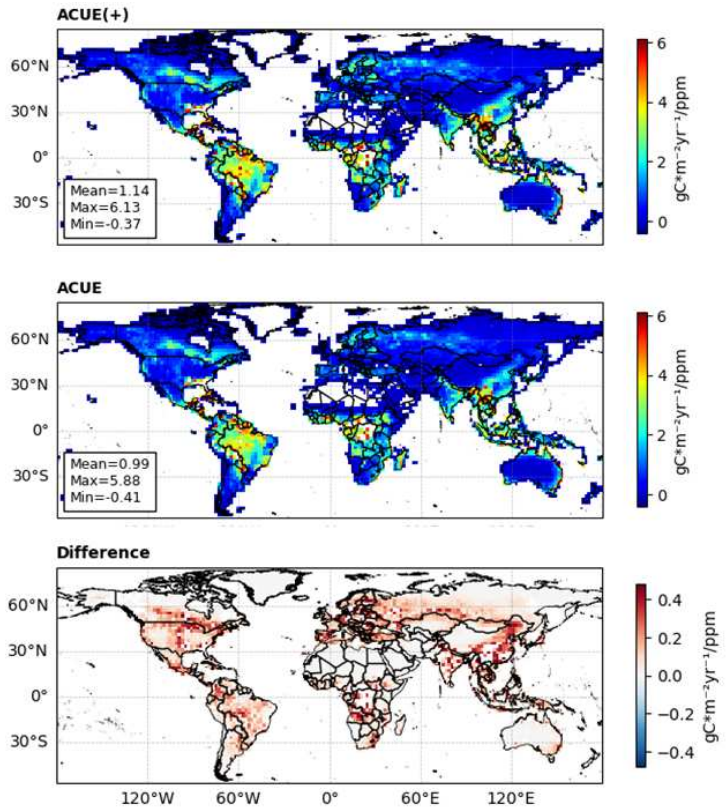

Figure 3.8 - Mean $ACUE^{+}_{GPP}$ (gC m^{-2} yr^{-1}/ppm) and $ACUE_{GPP}$ (gC m^{-2} yr^{-1}/ppm) and difference between the two ($ACUE^{+}_{GPP}$ - $ACUE_{GPP}$ gC m^{-2} yr^{-1}/ppm) from 1850 to 2015 (see Equations 3.5 and 3.7).

The spatial analysis also suggests that the ACUE is strongest in tropical areas of the Amazonia, the Congo Basin, and Southeast Asia followed by productive ecosystems in middle-high latitudes such as Northern Coniferous forests or Taiga in North America and Eurasia (Figure 3.8). In mid-high latitudes, low ACUE is driven by nitrogen-limitation. This means that even when the level of CO_2 is suboptimal, the productivity is limited by the availability of nitrogen. However, in boreal Asia, the addition of CO_2 results in the same increase in GPP. This suggests that another factor, in addition to nitrogen-limitation, is limiting productivity.

The ACUE(+) repones allows us to see that the way in which GPP responds to increased nitrogen deposition varies depending on the nitrogen limitation of an ecosystem. This can be observed in grasslands in Africa and South America, where nitrogen deposition leads to a significant increase in GPP, as well as in industrialized regions of Europe and North America. On the other hand, the positive effects of both carbon and nitrogen are more prevalent in tropical forests and East Asia, which also display high sensitivity to CO_2 fertilization and significant nitrogen deposition from agriculture

The R^2 scores of the linear relationship between the change in GPP and the atmospheric CO_2 are slightly higher for the variable nitrogen deposition scenario than the constant one for all regions except for Temperate Asia. This reflects the slight saturation of the GPP increase at high CO_2 levels in the constant nitrogen deposition scenarios.

GPP Atmospheric Nitrogen Deposition Use Efficiency (ANDUE):

The planet also experienced a significant increase in nitrogen deposition during the historical period. This had in turn an effect on the change in the assimilated carbon from photosynthesis. Similarly, to the previous analysis, (Figure 3.9) displays the scatter plot between the increase of GPP and the change of N deposition, which allows us to estimate the ANDUE (under a constant or an increased scenario of atmospheric CO_2 concentration). Over the historical period, our simulated global mean $ANDUE^{+}_{GPP}$ was 164 gC gN^{-1} while the $ANDUE_{GPP}$ was 124.1 gC gN^{-1} with a ratio $ANDUE^{+}_{GPP}/ANDUE_{GPP}$ of 1.32, showing how the CO_2 increase boosted in turn the nitrogen deposition use efficiency in around 39.8 gC gN^{-1} (a 32% increase). Regions where the differences between $ANDUE^{+}_{GPP}$ and $ANDUE_{GPP}$ are the biggest (such as in Tropical Asia, Europe, and Temperate Asia, see Figure 3.10) are those with the higher GPP increase due to mainly the synergistic effect.

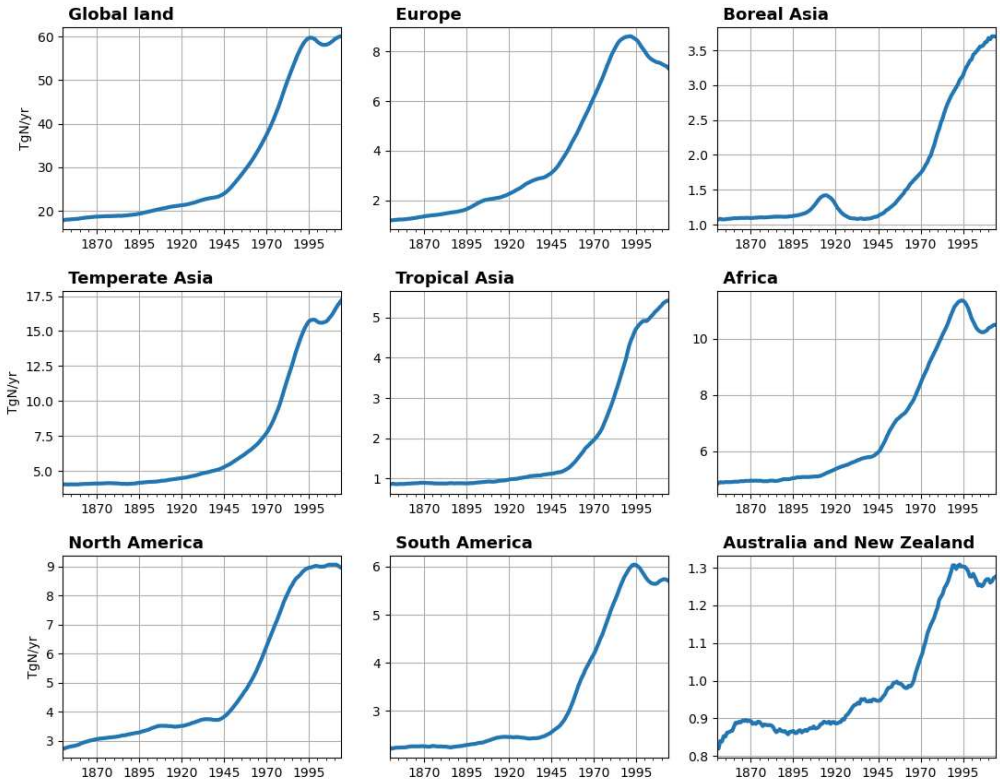

Figure 3.9 - Evolution of nitrogen deposition (in TgN yr^{-1}) for the set of selected regions of study

From our experiment we can see that there was no decline in GPP in any of the regions when N deposition increased. GPP response to nitrogen deposition is not constant across regions as already evidenced by (Flechard, Ibrom, et al., 2020). This is due to the diversity of ecosystems in particular in terms of sensitivity to nitrogen (Nitrogen use efficiency for photosynthesis). Also, although higher nitrogen deposition should translate into higher mineral N available for plant uptake, the relationship between N deposition and mineral N in soils might be region-dependent, function of the water regime and climate. In contrast to the ACUE analysis, the R^2 for the ANDUE is consistently higher than the ANDUE(+) (except for Australia). This means that

the relationship between the GPP increase, and the N deposition rate is more linear in the constant atmospheric CO_2 scenario than in the varying (increasing) one. This implies that the value of $ANDUE^{+}_{GPP}$ slightly increases as atmospheric CO_2 levels rise, while the value of $ANDUE_{GPP}$ is more stable

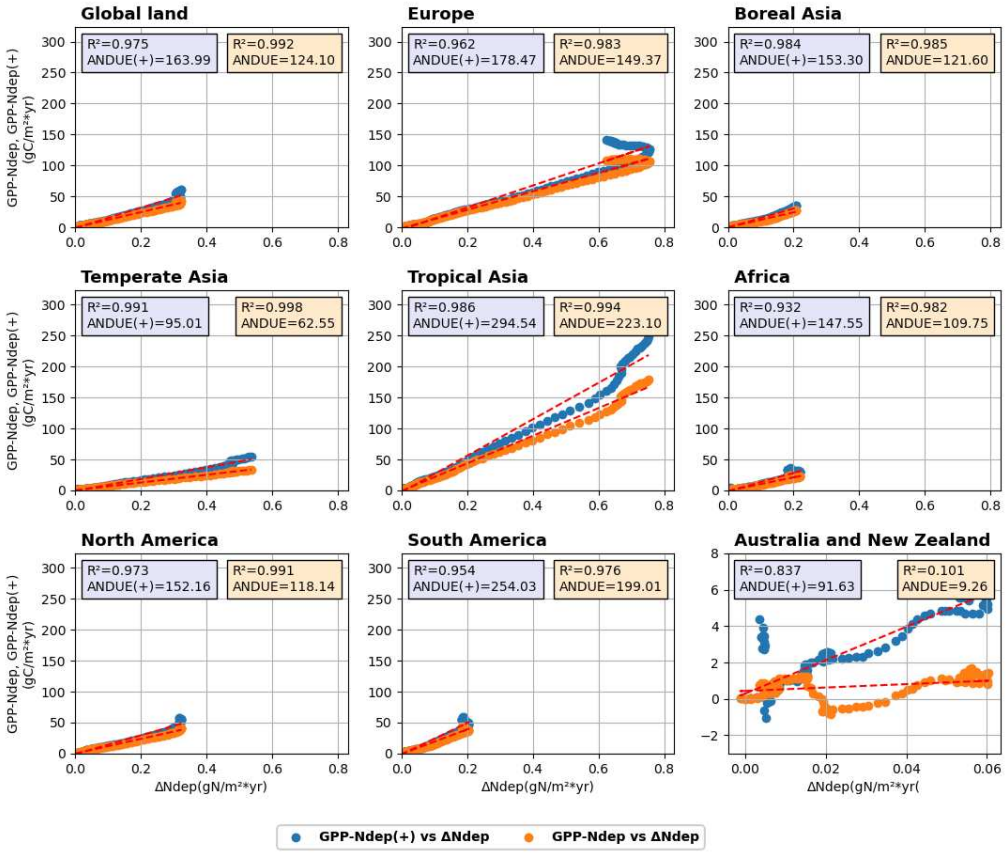

Figure 3.10 - Scatter plot between i) the increase of GPP due to the impact of Nitrogen deposition increase (GPP_{Ndep} and GPP^{+}_{Ndep} in gC $m^{-2}yr^{-1}$) for two scenarios (y axis) and ii) the nitrogen deposition increase (ΔNdep in gN $m^{-2}yr^{-1}$; x-axis). The first scenario (blue points) corresponds to a varying CO_2 world (GPP^{+}_{Ndep}=GPP_{S1}-GPP_{S3}, see Eq. 10) and the second one (orange points) to constant CO_2 world (GPP_{Ndep}=GPP_{S2}-GPP_{S4}, see Eq. 3). The displayed ANDUE(+) and ANDUE on the text box correspond to the slope of the linear regression applied to the scatter plot (see equations 8 and 10).

For the Asian regions, the simulation period shows a linearity that suggests there is no limit on Gross Primary Production (GPP) due to a steady constant increase in nitrogen deposition during the historical period. From 0.6 gN m^{-2} yr^{-1} onwards in both scenarios, there is an important increase in GPP. This increase is more significant in the ACUE(+) scenario, which may be partially attributed to the effects of increasing CO_2, while for the ACUE it may also be attributed to climate change. The change in slope can be explained by all factors that covary in this case, with CO_2 being a major contributor. More specifically, we can see that the $ANDUE^{+}_{GPP}$/$ANDUE_{GPP}$ ratio for Temperate Asia was 1.51, while for Tropical Asia it was 1.32 followed by Boreal Asia of 1.26. The dynamic increase of CO_2 is a key driver of this change in slope.

For the other regions, there is a change in the ANDUE curve for the recent years of the historical period that indicates a decrease in nitrogen deposition, restraining the carbon assimilation (see Figure 3.10). The decrease in the nitrogen deposition occurred around 1995 (except for North America where from 1995 to 2015 the nitrogen deposition was sustained). The $ANDUE^{+}_{GPP}/ANDUE_{GPP}$ ratio for Europe was 1.19, while for North America, 1.28, South America, 1.26 and Africa, 1.34. Apart from Temperate Asia, the tropical regions were the most nitrogen efficient as expected.

In Australia, on the other hand, we can see that the negative values for the change in GPP_{Ndep} (and GPP^{+}_{Ndep} for a few points) may be attributable to a specific climatic event, which generated a substantial decrease in the GPP thus inducing a change in our delta metrics. As revealed by other studies (Poulter et al., 2014), the gross and net ecosystem carbon fluxes of semi-arid ecosystems in Australia show large year to year variability, driven to a large part by El-Niño events.

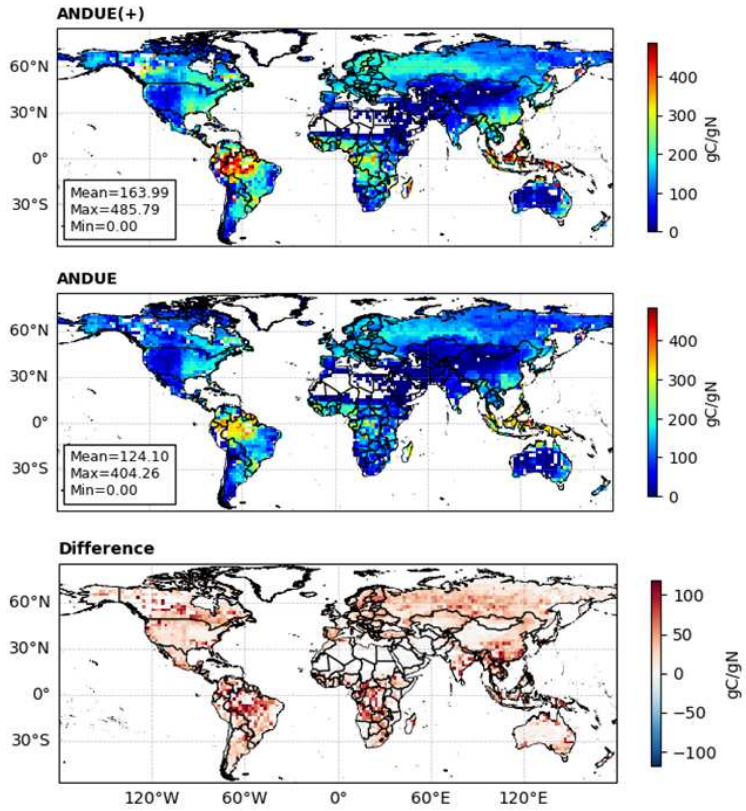

Figure 3.11 - Mean $ANDUE^{+}_{GPP}$ (gC/gN) and $ANDUE_{GPP}$ (gC/gN) and difference (gC/gN) from 1850 to 2015 (see Equations 3.8 and 3.10).

The geographical analysis suggests that the nitrogen deposition effect - ANDUE was strong in the regions where historical nitrogen deposition was showing a larger increase (Figure 3.9 and Figure 1.17), which correspond to the east of North America, Europe and Northern Russia, Southern Asia and as well as in the Amazonia and central Africa (see Figure 3.11). For the increase of CO_2 scenario, the ANDUE(+) is shown to be bigger in the tropical areas mostly from

the synergetic carbon-nitrogen additional contribution. This synergistic contribution occurs when the vegetation requires more nitrogen due to an increase in CO_2 concentrations ever since a bigger carbon contribution also increases nitrogen immobilization by plants and microbiota. This is mostly the case in the Amazon and Southeast Asia.

3.3.2 NBP

We now focus on the analysis of the net ecosystem carbon uptake, following the same approach as the one described above for the gross carbon uptake. Given the complex impacts of N deposition on photosynthesis (GPP), vegetation autotrophic respiration and soil heterotrophic respiration, we do not expect to have the same contributions for NBP as for GPP.

Effect of CO_2, nitrogen deposition and the synergy between the two:
For this diagnosis we will refer to the total global annual mean NBP flux (NBP yr^{-1}) and its evolution over the historical period as shown in Figure 9. Our results show that global NBP went from an emission of -0.3 PgC yr^{-1} (1950-1955 mean) to a carbon sink of 1.4 PgC yr^{-1} (2005-2015 mean) (Figure 3.12, red dash curve), with positive contributions from CO_2 fertilization, nitrogen deposition and carbon-nitrogen synergy. The relative contribution of these drivers to this overall NBP change from 1850 to 2015, amounted 84% from CO_2 enhancement (NBP_{CO_2}), 29% from nitrogen deposition (NBP_{Ndep}) and 19% from carbon-nitrogen synergy (NBP_{Syn}) (Table A 3) in line with previous result gathering the historical contribution from different models of the studied factors (Tharammal et al., 2019). Note that the total contribution is over 100% given that there is also a decrease of NBP due to climate and land use changes.

Other authors have thoroughly investigated this issue and found that land use change has had a significant influence on the carbon stock, leading the land to serve as a carbon source up until 1970 and then acting as a carbon sink until 2015 such as analyzed by Friedlingstein et al. (2014). Other studies have also shown that climatic variations have caused generalized decrease of NBP through an increase of soil respiration such as in the Amazonia, or in the mid latitudes where ecosystem respiration surpassed the NPP flux (O'Sullivan et al., 2019). In line with Friedlingstein et al. (2022), we draw the conclusion from our simulations (accumulated NBP_{S1} see Figure A 20) that the land has been acting as a carbon sink globally since 1970 (with some regional variations, such as in regions like North America since 1960, South America since 1980, temperate and boreal Asia since 1970 and tropical Asia since 1980).

In a similar manner to the GPP, the contributions for the different regions, throughout the 21st century, were consistently positive. While CO_2 fertilization had a steady contribution to NBP changes throughout the period, nitrogen deposition-induced increases became more significant from the 1970-1980 onward (Figure 3.12), a period of increased anthropogenic nitrogen deposition (Lamarque et al., 2013). This was not the case for the most industrially

developed and agriculture-intensive regions such as Europe and North America in which the contribution due to nitrogen deposition started before the mentioned decade.

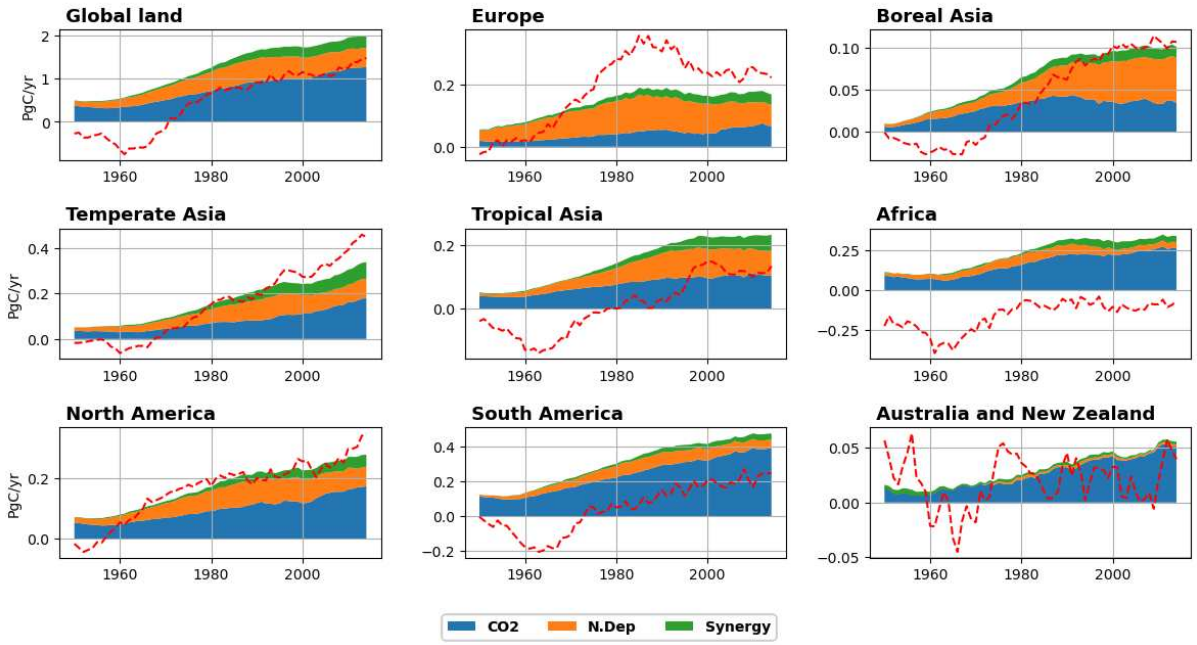

Figure 3.12 - Global and regional contribution of CO_2 increase (NBP_{CO_2} in PgC yr^{-1}), Nitrogen deposition increase (NBP_{Ndep} in PgC yr^{-1}) and the synergy between the two (NBP_{syn} in PgC yr^{-1}) to the total change of NBP (see equations 2 - 3 - 4). The total NBP flux (S1) in PgC yr^{-1} is represented by the red dashed line. The chosen time period is 1950-2015 as it is from this year that increases in CO_2 and N dep began to have a significant impact on total NBP flux. The curves have been smoothed with a running mean to focus on the overall increase of the contributions and not into the year-to-year variation. The regional surface map is on the annexes (annexe global regions).

Historically, by 1950, the worldwide contribution of NBP_{CO_2} reached 0.39 PgC yr^{-1}, while NBP_{Ndep} accounted for approximately 0.09 PgC yr^{-1} and NBP_{Syn} 0.02 PgC yr^{-1} (Figure 3.12). Out of the total effect of the studied factors, NBP_{CO_2} accounted for 78%, while NBP_{Ndep} 18% and GPP_{Syn} the remaining 4%. On the other hand, by 2015, the contribution due to NBP_{CO_2} rose to 1.27 PgC yr^{-1}, and in turn NBP_{Ndep} to 0.44 PgC yr^{-1} and NBP_{Syn} with 0.29 PgC yr^{-1}. NBP_{CO_2} accounted for 53% of the total factor's contribution while NBP_{Ndep} accounted for 34% and NBP_{Syn} for 12%. The increasing synergistic carbon-nitrogen effect shows that the extra nitrogen had a significant beneficial influence on CO_2 fertilization on the NBP as demonstrated by (O'Sullivan et al., 2019). Our synergistic contribution by 2015 is similar to that obtained by O'Sullivan et al. (2019)(0.32 PgC yr^{-1}) and Zaehle & Friend. (2010), (0.4 Pg PgC yr^{-1}). The differences between these estimates are relatively small considering the complex interactions between the carbon and nitrogen cycles and the different model parameterizations.

For the GPP, we discussed these impacts in terms of percentage of the total GPP that would have occurred with only land use and climate change (i.e., the S4 simulation). For the NBP this analysis becomes more complicated since the NBP values are smaller and of varying sign, which leads to highly variable percentages with much less clear interpretation. However, when

performing the analysis with respect to the "full factor simulation" (S1) and the $NBP^{+}_{CO_2}$, NBP^{+}_{Ndep} and NBP^{+}_{Syn} factors we can highlight certain behaviors. For example, the CO_2 fertilization impact was strongest in tropical areas in 2015 following the behavior of the GPP, the carbon entry point for vegetation, with contributions of the change of NBP ranging from 156 to 79% for South America and Tropical Asia, respectively (Table A 3). In Africa, as in South America and Australia, the positive effect of increased CO_2 was greater than the positive effect of increased nitrogen deposition and the carbon-nitrogen synergy, accounting for about one-third of the total factors, due to the primary effect of tropical forests driven by increased CO_2 and low levels of industrialization, resulting in lower levels of nitrogen deposition. Nevertheless, Africa acted as a carbon source from 1950 to 2015, owing to deforestation that occurred during the last century. According to the FAO, Africa lost the most tropical forests of any continent during the 1980s, 1990s, and early 2000s (Boahene, 1998) (Figure A 14).

Increasing nitrogen deposition appeared to have had no strong direct effect on net carbon absorption in tropical forests of South America and Africa (Figure 3.12), a result also obtained in the study of O'Sullivan et al. (2019). On the contrary, in Tropical Asia, the increased nitrogen deposition had an important effect (+57%) on the NBP change, likely due to the large increase in N deposition over this region (due in particular to agricultural practices). The synergistic carbon-nitrogen effects that explain the change in NBP are similar to those that explain the change in GPP, with increases in tropical areas (38% in Tropical Asia and 14% in South America), as well as in mid and high latitude regions, such as 16% in Temperate Asia and 15% in Europe. When there is both a high sensitivity to CO_2 fertilization and a simultaneous removal of nitrogen limitation, these synergistic effects occur. In tropical forests, for example, rising atmospheric CO_2 concentrations increase nitrogen limitation, which is then partly relieved by an increase in nitrogen deposition.

As for the GPP, we propose to conduct a more detailed study of how ecosystem efficiency evolved during the 20th century and to investigate these effects on a regional scale. We analyze the impact of the increase in atmospheric CO_2 and nitrogen deposition, on NBP expressed per unit of CO_2 increase and N deposition increase, using the two metrics defined in the method section: atmospheric CO_2 use efficiency (ACUE) and atmospheric nitrogen deposition use efficiency (ANDUE).

NBP Atmospheric CO_2 Use Efficiency (ACUE):

Like for GPP, figure 10 displays a scatter plot between the changes in NBP and the changes in CO_2. In terms of NBP efficiency to CO_2 increase, we can see a similar pattern to the GPP, with a strong linear relationship between NBP change and CO_2 increase. However, the linearity of relationship between NBP and CO_2 changes appears to be slightly less strong than the one obtained between GPP and CO_2 (R^2 coefficient of 0.96 versus 0.99 for a constant N deposition scenario (Figure 3.7), which reveals the more complex model responses when including the

different respiration terms. As for GPP, there are regional differences in the NBP ACUE estimate, due to large regional differences of ecosystem productivity and nitrogen limitation.

We also note a slightly stronger linear relationship with the increased N deposition scenario ($ACUE^{+}_{NBP}$; R^2 of 0.97) than without ($ACUE_{NBP}$; R^2 of 0.96). The better linear fit for $ACUE^{+}_{NBP}$ is observed in all regions as it was the case for GPP, with the exception of Temperate Asia. This difference in R^2 between the constant and dynamic N deposition scenarios is directly related to a stronger N limitation in constant N deposition scenario. In the Temperate Asia region, the relationship between NBP change and atmospheric CO_2 is slightly exponential, indicating that regional mean ecosystem productivity is not limited by Nitrogen availability in the range of atmospheric CO_2 experienced between 1850 and 2015.

From our results we estimate a mean global Atmospheric CO_2 Use Efficiency for an increasing nitrogen deposition world ($ACUE^{+}_{NBP}$) from 1850 to 2015, equivalent to 0.11 gC m^{-2}/ppm whereas $ACUE_{NBP}$ equals 0.08 gC m^{-2}/ppm. This global difference of 0.03 gC m^{-2}/ppm (37% increase) is explained by the addition of reactive nitrogen in the system that boosted the amount of assimilated carbon as it did for the GPP (see figure 10). We can see that the relative change for a nitrogen varying world on the NBP is twice as big as the increment for GPP (16%). This shows how the NBP flux is more sensitive to nitrogen deposition.

The regional increase in nitrogen deposition enhanced NBP particularly in Europe, Temperate, Tropical and Boreal Asia, where the ACUE ratio corresponded to 1.66, 1.6, 1.41 and 1.33 respectively. The increase in nitrogen deposition did not seem to have had any strong effect on the net carbon sequestration of African and South American ecosystems (Figure 3.13 and Figure 3.14) with a ACUE ratio of 1.1 and 1.0 respectively. As for GPP, this is primarily due to mid-range nitrogen deposition levels throughout the historical period in these regions.

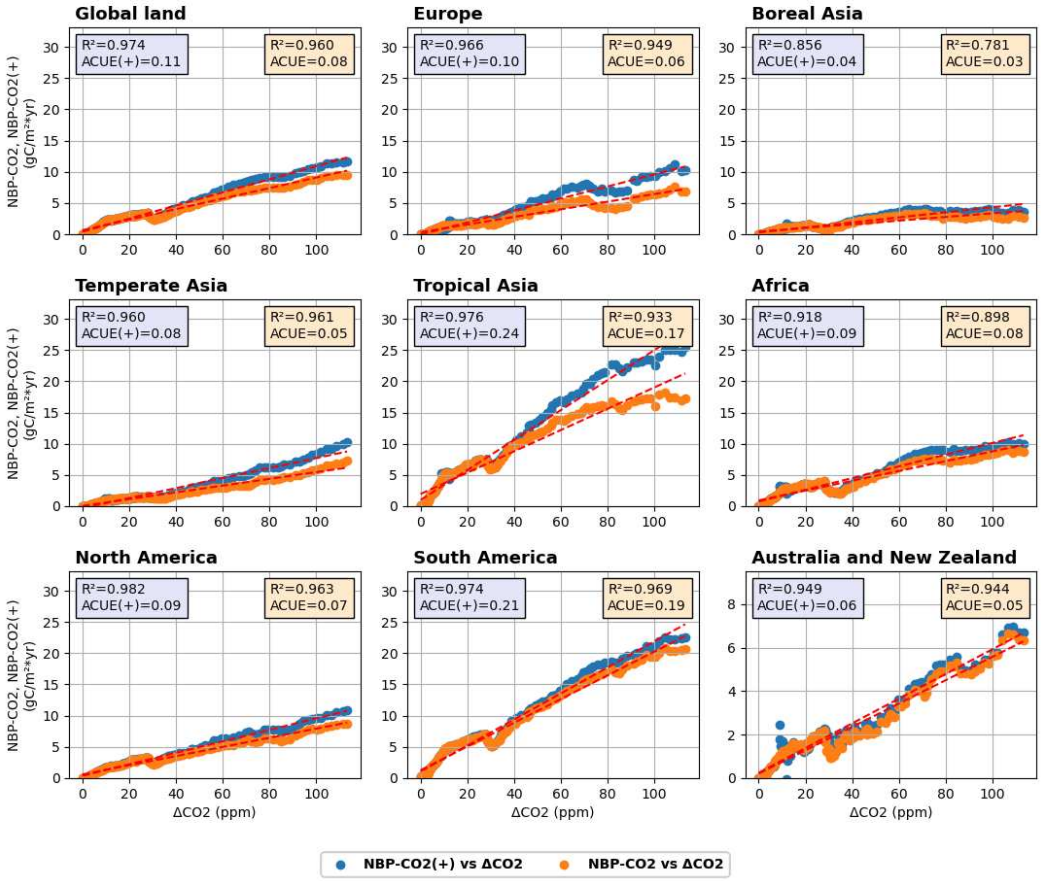

Figure 3.13 - Scatter plot between i) the increase of NBP due to the impact of CO_2 increase (NBP_{CO_2} and $NBP^{+}_{CO_2}$ in gC $m^{-2}yr^{-1}$) for two scenarios (y axis) and ii) the CO_2 increase (ΔCO_2 in ppm; x-axis). The first scenario (blue points) corresponds to a varying N deposition ($NBP^{+}_{CO_2}$ = NBP_{S1}-NBP_{S2} see Eq. 7) and the second one (orange points) to a constant nitrogen deposition (NBP_{CO_2} = NBP_{S3}-NBP_{S4} see Equation 3.2). The displayed ACUE(+) and ACUE on the text box correspond to the slope of the linear regression applied to the scatter plot (see equations 3.5 and 3.7).

For our study it can be seen that by the end of the simulation the ACUE curves tend to flatten especially in South America, Tropical Asia, and Africa similarly to the previous diagnostic for GPP (Figure 3.7). Maximal $ACUE_{NBP}$ values reach 0.6 gC $m^{-2}yr^{-1}$/ ppm. They are located in the most productive regions, in the tropical zone (Amazonia, Central Africa, Southeast Asia). Some regions of the northern Hemisphere (Scandinavia, Canada) have significantly high ACUE values (~0.2 gC m^{-2} yr^{-1}/ppm) relatively to their productivity.

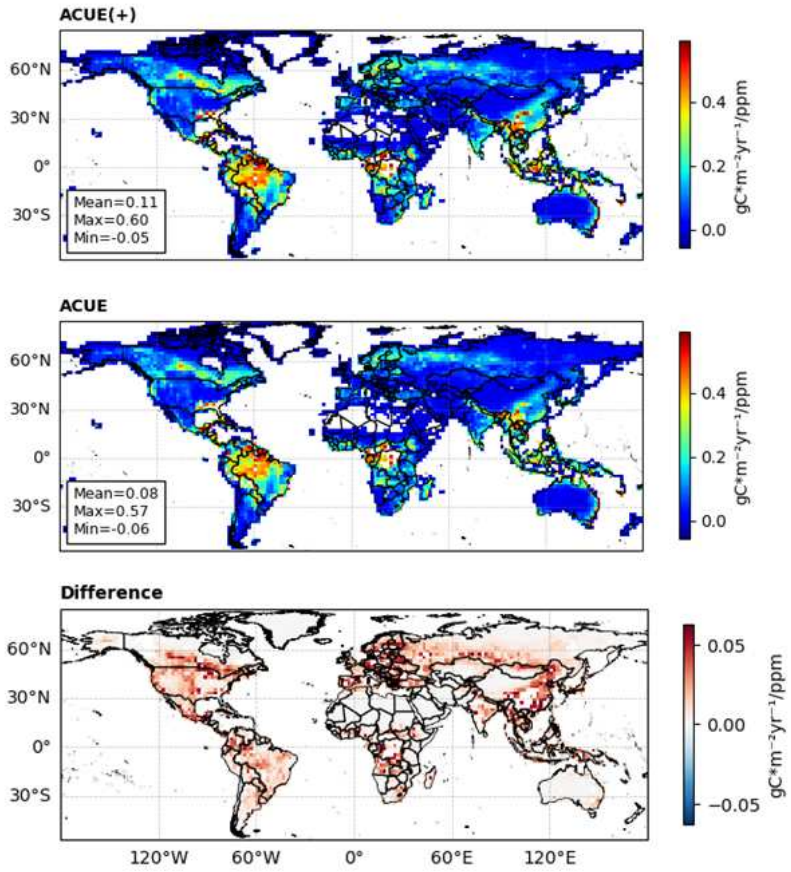

Figure 3.14 - Mean ACUE(+) (gC $m^{-2}yr^{-1}$/ppm) and ACUE (gC $m^{-2}yr^{-1}$/ppm) and their difference (gC $m^{-2}yr^{-1}$/ppm) from 1850 to 2015 (see Equations 3.5 and 3.7).

The differences in hotspot sizes and geographical patterns observed between $ACUE_{GPP}$ (Figure 6) and $ACUE_{NBP}$ (Figure 3.14) may be attributed to factors such as deforestation reemitting the assimilated carbon or the storage of the assimilated carbon not being directly proportional to GPP changes, as suggested by (Flechard, van Oijen, et al., 2020). While some studies have linked these large sinks in temperate regions of Europe and North America to a variety of factors such as reforestation of unused land and previously cleared forests, reduced forest harvesting, CO_2 fertilization, management changes, and long-term forest age structure impacts in Europe (Vilén et al., 2016), the ACUE study only isolates the effect of CO_2 fertilization, and therefore cannot attribute the spatial pattern to this factor due to the lack of supporting elements.

NBP Atmospheric Nitrogen Deposition Use efficiency (ANDUE):

Global mean $ANDUE^{+}_{NBP}$ was 17.68 gC gN^{-1} while the $ANDUE_{NBP}$ was 12.29 gC gN^{-1}, with a $ANDUE^{+}_{NBP}/ANDUE_{NBP}$ ratio of 1.43. This result highlights how the CO_2 increase boosted the net carbon assimilation sensitivity to nitrogen deposition by around 5.39 gC gN^{-1} (43 % increase). Such a pattern was expected from the $ANDUE_{GPP}$ analysis although the ratio is much stronger for NBP (1.43) than for GPP (1.16). The regions with the highest increase in ANDUE from the constant to varying atmospheric CO_2 scenario were the tropical regions, with a ratio of 1.66, 1.42 and 1.39 for Africa, Tropical Asia, and South America respectively, followed by

Temperate Asia with a rate of 1.62 and the rest of the regions between 1.25 and 1.3. One possible reason that explains the larger ratios for NBP than for GPP may be the contribution of croplands vs unmanaged areas. Croplands contribute significantly to GPP but very little to NBP, and croplands are fertilized in parallel, therefore the influence of N deposition (constant vs. rising) on farmland GPP is likely insignificant.

There was less nitrogen deposition in tropical ecosystems, but it had a greater effect in terms of net carbon capture, making these ecosystems very efficient with regards to nitrogen deposition, in turn boosted by increasing CO_2 (Figure 3.15).

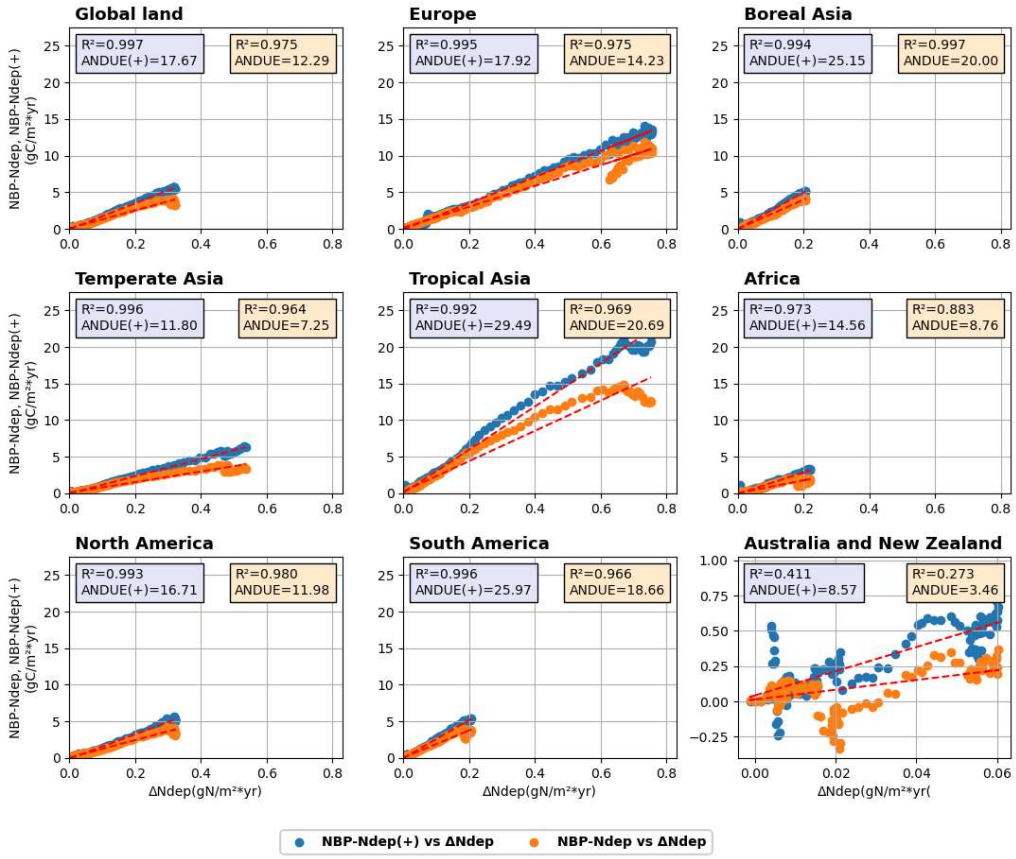

Figure 3.15 - Scatter plot between i) the increase of NBP due to the impact of Nitrogen deposition increase (NBP_{Ndep} and NBP^{+}_{Ndep} in gC $m^{-2}yr^{-1}$) for two scenarios (y axis) and ii) the nitrogen deposition increase (ΔNdep in gN $m^{-2}yr^{-1}$; x-axis). The first scenario (blue points) corresponds to a varying CO_2 world (NBP^{+}_{Ndep}=NBP_{S1}-NBP_{S3}, see Equation 3.10) and the second one (orange points) to constant CO_2 world (NBP_{Ndep}=NBP_{S2}-NBP_{S4}, see Eq. 3). The displayed ANDUE(+) and ANDUE on the text box correspond to the slope of the linear regression applied to the scatter plot (see equations 3.8 and 3.10).

Like the GPP, the ecosystem response of NBP to nitrogen deposition is not homogeneous in space nor linear (Figure 3.15). The R^2 is higher for ANDUE(+) than for ANDUE for all regions except "Boreal Asia". This is an opposite behavior to the ANDUE analysis for the GPP. This indicates that the relationship between NBP and the atmospheric N deposition is slightly more

linear under the scenario of increasing atmospheric CO_2 than compared to the constant scenario. In the Tropical Asia region, the increase of NBP shows a saturation for high N deposition rates, indicating that the ANDUE is decreasing for such high N deposition rates.

This indicates that Tropical ecosystems were not nitrogen constrained during the recent decades (Hedin et al., 2009) under the constant CO_2 scenario, although this may have changed when accounting for the rise in atmospheric CO_2 concentration rise. This behavior should be further studied. Although the curves for a variant and constant CO_2 scenario have different slopes and R^2, they show relatively similar shape.

The change in the form of the $ANDUE_{NBP}$ and $ANDUE^{+}_{NBP}$ curves around the end of the simulation is due to a decrease in nitrogen deposition after 1995, and the direction (going downwards rather than upwards as for the GPP) may be attributed to climate change or other environmental factors in the intermediate fluxes between GPP and NBP that make the NBP delta larger and thus the change in direction near the end of the simulation, but we cannot address their contribution because all of our simulations have been completed. It is worthwhile to examine their contribution using a new set of simulations.

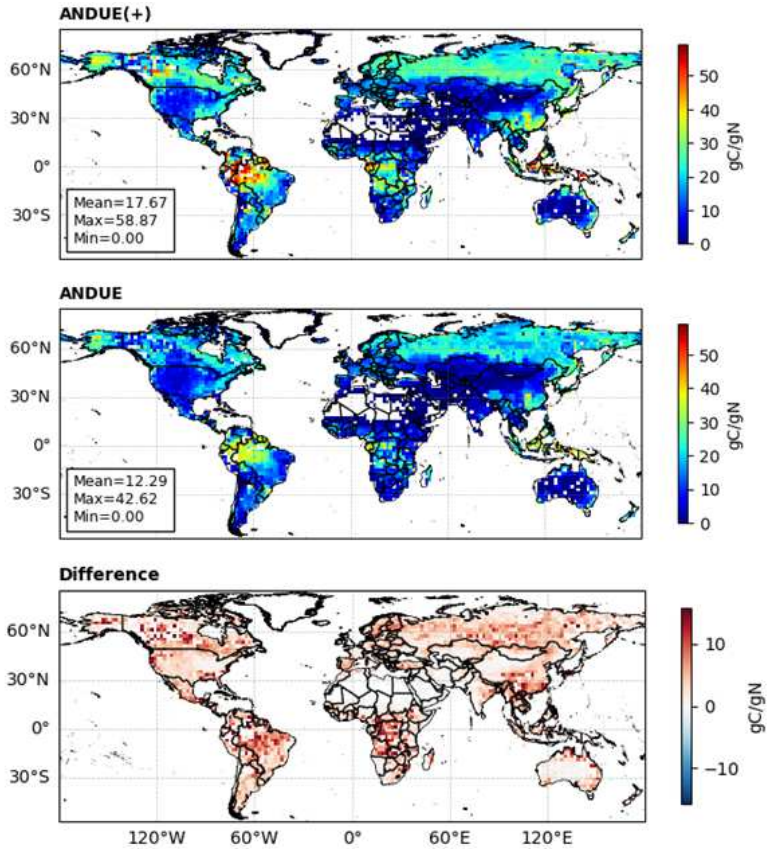

Figure 3.16 - Mean ANDUE(+) (gC/gN), mean ANDUE (gC/gN) and their difference over the period 1850 to 2015 (see Equations 3.8 and 3.10).

From increased nitrogen deposition during the historical era, we can identify large carbon sinks in the Tropics and Boreal ecosystems as well as in the regions associated with large nitrogen

industrial emissions of Europe, North America, and Southern Asia. Tropical areas have the highest $ANDUE^{+}_{NBP}$ values, reaching up to 58 gC gN^{-1}. High $ANDUE^{+}_{NBP}$ levels have also been recorded in the Northern Hemisphere, most notably in Canada, as well as in Scandinavia and Russia (Figure 3.16). The regions with the greatest difference between $ANDUE^{+}_{NBP}$ and $ANDUE_{NBP}$ are those with high $ANDUE^{+}_{NBP}$ values, which are usually found in the tropics and boreal ecosystems. Numerous studies indicate that forests in the Northern Hemisphere operate as a carbon sink mostly due to atmospheric deposition of reactive nitrogen boosted by historical afforestation (Flechard, Ibrom, et al., 2020).

Similarly, it can be seen that the maximum amount of stored carbon in tropical regions increased by about 16 gC gN^{-1}. As in Lu et al. (2021) study for the tropical zones, nitrogen addition significantly increased forest soil carbon and nitrogen stocks in both organic and mineral layers, proving that chronic nitrogen deposition can simulate soil carbon sequestration in the tropical and subtropical forests as found in our results (Figure 3.16).

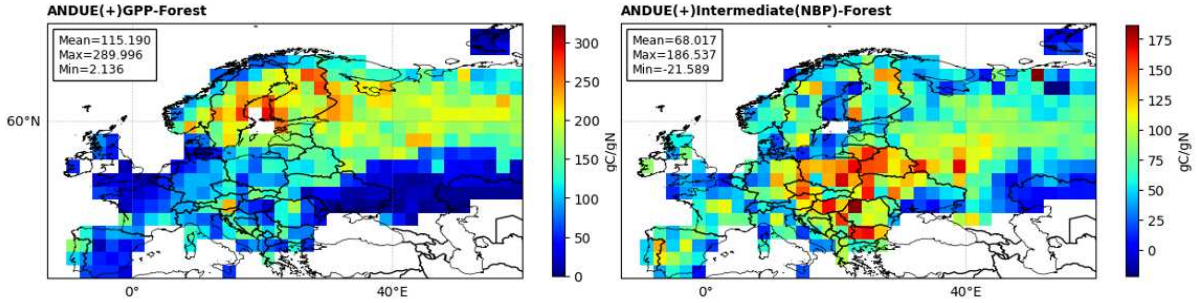

Figure 3.17 - Mean ANDUE(+) (gC/gN) on the forest GPP (left) and NEP (right) from 2004-2010 (see Equation 3.8).

We now compare our results about the carbon productivity and storage sensitivities to nitrogen deposition with those obtained in a recent study for 22 European forest sites between 2004 and 2010 by Flechard, Ibrom, et al. (2020) (Table A 1) with a mean value of 40-50 gC gN^{-1}. Flechard, Ibrom, et al. (2020) used a model of N deposition and CO_2 flux measurements by eddy covariance flux towers.

Our results indicate that there is indeed an important spatial heterogeneity of both the forest GPP and NEP sensitivity to atmospheric N deposition. The regional mean $ANDUE^{+}_{GPP}$ obtained with our model for European forested land was 115.2 gC gN^{-1} (Figure 3.17). There is an important hotspot of $ANDUE^{+}_{GPP}$ over the Nordic region and central and Northwestern Russia corresponding to the boreal forest. These nitrogen-limited ecosystems (Högberg et al., 2017) are highly sensitive to the increased nitrogen deposition, with $ANDUE^{+}_{GPP}$ values around 290 gC gN^{-1}. Likewise, we can observe an important hotspot in the $ANDUE^{+}_{GPP}$ in central Europe with an average value of about 200 gC gN^{-1} (Figure 3.17).

As the study of Flechard, Ibrom, et al. (2020) is focusing on the Net Ecosystem Productivity (NEP), we also based our analysis on the NEP flux. To do so, we computed the weighted average NEP for forested PFTs. We obtained thus a mean $ANDUE^{+}_{NEP}$ between 2004 and 2010

in Europe of 68 gC gN^{-1} quite comparable to the mean reported value of 40-50 gC gN^{-1}, which in turn is claimed to be comparable to previous estimates from inventory data.

This difference might be attributable to the fact that we report the average value over our regional mask of Europe and not over a network of observation sites. The great diversity in terms of forest age, tree species, climate, soils characteristics, fertility and nutrient availability may contribute to the different regional estimate but allows us to see more clearly that there during the 2004-2010 period in Europe, there was an important increase in carbon sequestration in central Europe in partly explained by forest land management.

3.3.4 Carbon stock sensitivity to CO_2 and N deposition increases:

We now investigate the impact of the CO_2 and N deposition on the accumulated NBP between the last decade (1996–2005) and the pre-industrial period (1850), which is equivalent to the total C stock variation and expressed with the β_{CO_2+} and δ_{Ndep+} (see equations 3.11 and 3.12), as illustrated in (Figure 3.18). The sensitivity to CO_2 and nitrogen depositions are in close agreement with previous model estimates. We obtained a β_{CO_2+} of 0.5 PgC ppm^{-1} against 0.5 PgC ppm^{-1} from (Devaraju et al., 2016). Our model estimate of δ_{Ndep+} is equal to 0.5 PgC per TgN yr^{-1} against 0.59 PgC per TgN yr^{-1} from (Devaraju et al., 2016) and within the range of previous model many previous transient simulations of (Thornton et al., 2009; Zaehle & Friend, 2010).

Global sensitivity (expressed in PgC) due to CO_2 increase is equal to the sum of the regions, since the CO_2 increase is experienced globally, while the sensitivity due to nitrogen deposition is local, meaning that the values do not add up to explain the global sensitivity. The tropical regions of South America and Africa account for 56% of the global assimilated carbon followed by the boreal regions of Asia, Europe, and North America with 30% of the global assimilated carbon as expected from the most productive ecosystems of the planet and the CO_2 fertilization effect. As for the sensitivity due to nitrogen deposition, we see the effect in the areas with the highest nitrogen emissions (both from industry and agriculture) and nitrogen deposition corresponding to North America, Europe, South Asia, and South America as shown in (Figure 1.17).

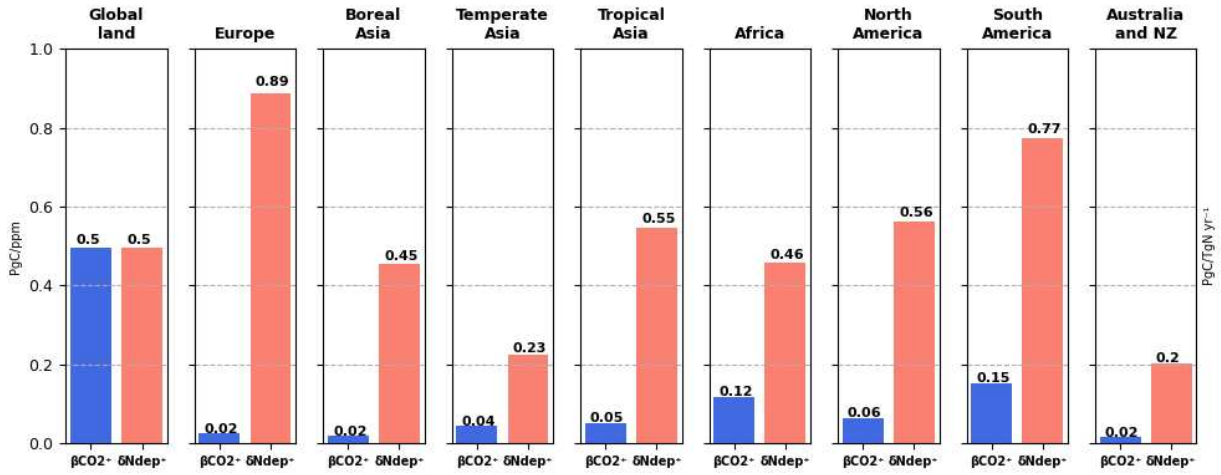

Figure 3.18 - Regional analysis of the sensitivity of the total terrestrial carbon to CO_2 increase (β_{CO_2+} in PgC ppm^{-1}) and of the sensitivity of the total terrestrial carbon to N dep increase (δ_{Ndep+} in PgC per TgN yr^{-1}) from 1850 to 2005.

Uncertainties in the terrestrial carbon cycle can still be addressed by increasing the observational network and modeling processes that are lacking in today's terrestrial models. More data and multi-model comparisons will thus be required to increase our confidence in our knowledge of terrestrial carbon dynamics. On one hand, there is little difference between these sensitivity estimates. However, all models share similar concepts and equations. Despite this, there has been too little evaluation with data to truly determine the effectiveness of these models

3.4 Conclusion

Carbon and nitrogen interactions are crucial for understanding primary production on ecosystems and, as a result, their capacity for carbon storage or release, and hence for comprehending historical and future climate change. Despite the LUC change fluxes that led to a decline in carbon stocks during the historical epoch, the rise in CO_2 and nitrogen deposition, combined with their consequent synergistic impact, produced a positive contribution on both the gross primary flow and the net land carbon. The global increase of GPP due to CO_2 increase, expressed as a percentage of a GPP flux that would have only evolved under land use and climate change (S4 scenario), (GPP_{CO_2}) in 2015 corresponded to 15%, while the impact from nitrogen deposition increase (GPP_{Ndep}) corresponded to 6% and the synergy between carbon and nitrogen (GPP_{Syn}) to 3%, showing how relevant the studied factors were on the carbon assimilation during the last decades. When addressing the contribution to the change in the GPP flux we found that the CO_2 contribution (GPP_{CO_2}) in 2015 corresponded to 53%, while the contribution from nitrogen deposition increase (GPP_{Ndep}) corresponded to 21% and the synergy between carbon and nitrogen (GPP_{Syn}) to 9% in line with literature reported contributions to these factors (O'Sullivan et al., 2019).

In terms of atmospheric carbon and atmospheric nitrogen usage efficiency with respect to GPP flux, we found that our model displays bimodality meaning that there is a reaction to increasing either nitrogen or atmospheric carbon dioxide, but rarely both in equal proportion, as predicted by the work on five distinct models by Davies-Barnard et al. (2020). We found a mean $ACUE^{+}_{GPP}$ from 1850 to 2015 of 1.14 gC $m^{-2}yr^{-1}$/ppm (with the increase N dep scenario) against a $ACUE_{GPP}$ of 0.99 gC $m^{-2}yr^{-1}$/ppm (with the constant N dep scenario), with mostly linear responses for both scenarios. This demonstrates that CO_2 did not limit the productivity of terrestrial ecosystems in most regions during the historical period, because the CO_2 increase occurs at a photosynthetic suboptimal point, which is boosted in turn by increased nitrogen deposition, explaining the difference in the results. One main exception is "Boreal Asia", a region for which the increase in GPP saturates for historical levels of atmospheric CO_2 due to N limitation. In general, nitrogen deposition, however, makes more efficient the efficiency of GPP to CO_2, by systematically yielding a steeper slope for the regional $ACUE^{+}_{GPP}$ curves. Because of the increase in CO_2 levels in the atmosphere, tropical zones continued to be the most productive in the world, followed by boreal ecosystems.

The local increase in nitrogen deposition raised the maximums in the grasslands of South America and Africa, as well as in agriculturally developed regions of South Asia and Europe and North America over the historical era. We found that the $ANDUE+_{GPP}$ between 1850 and 2015 corresponded to 163.99 gC gN^{-1} (scenario with increased atmospheric CO_2) versus an $ANDUE_{GPP}$ of 124.10 gC gN^{-1} (scenario with constant CO_2), attributable to ecosystem diversity and nitrogen deposition evolution. We were able to observe that there are different rates of carbon assimilation for nitrogen saturated soils in the northern hemisphere and no apparent nitrogen limitation in tropical ecosystems. The effect of nitrogen deposition on GPP is more pronounced in regions with higher nitrogen emissions due to industrial development and extensive agriculture (and thus nitrogen deposition in surrounding ecosystems), and the increase of CO_2 enhances the maxima especially in the tropics which, not being nitrogen limited, benefit from a more important carbon-nitrogen synergistic effect.

On the other hand, contribution of CO_2 increase to the overall rise in NBP (NBP_{CO_2}) in 2015 corresponded to 86%, while the contribution from nitrogen deposition increase (NBP_{Ndep}) corresponded to 29% and the synergy between carbon and nitrogen (NBP_{Syn}) to 19% in line with recent results from (O'Sullivan et al., 2019) and (Tharammal et al., 2019). The sum of these factors surpasses 100% because of the other factors, land use and climate change, impact negatively on the NBP.

We found in turn a mean $ACUE^{+}_{NBP}$ from 1850 to 2015 of 0.11 gC m^{-2} yr^{-1}/ppm against a $ACUE_{NBP}$ of 0.08 gC m^{-2} yr^{-1}/ppm with less linear responses for both scenarios as a result of climate change variability, with important hotspots of carbon stocks in the tropical regions followed by boreal ecosystems enhanced by large nitrogen emissions in the northern hemisphere. In parallel our simulations showed an $ANDUE_{NBP}$ of 17.63 gC gN^{-1} versus an

$ANDUE_{NBP}$ of 12.29 gC gN^{-1} with a less linear relationship mostly from nitrogen deposition evolution and nitrogen limitation of different ecosystem types. The difference in the direction of the curve with regards to the $ACUE_{GPP}$ is mostly attributable to the environmental effects on the intermediate fluxes between GPP and NBP (mainly the autotrophic and heterotrophic respirations). Northern ecosystems experience nitrogen saturation which in turn has led to declines in carbon stocks while in the tropical region the synergy between carbon and nitrogen alleviates the nitrogen limitation under rising CO_2.

By 2015, the CO_2 rise lead to a NBP increase of 1.2PgC yr^{-1} while the NBP increase due to nitrogen deposition change lead to 0.41 PgC yr^{-1} and finally the synergistic effect between the two factors contributed to a NBP increase of 0.27 PgC yr^{-1}. Specifically from 1850 to 2005, we obtained a β_{CO_2+} of 0.46 PgC ppm^{-1} and a δ_{Ndep+} of 0.48 PgC per TgN yr^{-1} against a β_{CO_2+} of 0.5 PgC ppm^{-1} and a δ_{Ndep+} of 0.59 PgC per TgN yr^{-1} from (Devaraju et al., 2016) and all within the range of previous model responses (Thornton et al., 2009; Zaehle & Friend, 2010) demonstrating that, although a comparable outcome, it is still important to enhance the comprehension of the interactions between the carbon and nitrogen cycles, as well as with other limiting factors, given the importance of these factor and despite similar estimates to find a better model agreement.

On the other hand, climatic variations may cause changes in carbon storage. Our analysis suggests that climatic variations may be responsible for weakening the carbon sink during the recent period, in particular in the way the sensitivity to CO_2 or Nitrogen deposition may have evolved over time. However, the response of the biosphere to recent climate variations is uncertain, with contradictory conclusions about the magnitude of the change in the carbon sink after the 21st century as suggested by O'Sullivan et al. (2019).

Thus, under the premise of climate change, and possible nutrient limitation in the near future under increased CO_2 demand and regional changes in nitrogen emissions, it is relevant to continue with a more detailed study of the uncertainty of carbon stocks for the 21st century to give more clarity to the possible biogeochemical interactions between carbon and nitrogen in future global change.

"The future of carbon uptake will depend on our ability to protect and restore natural ecosystems, such as wetlands, grasslands and forests, which are major carbon sinks".

Dr. Jane Goodall

CHAPTER 4

Unraveling the contribution of CO_2, land-use and Nitrogen inputs to the future land productivity for different socio-economic scenarios

4.1 Introduction

This increase in atmospheric CO_2 concentrations leads to higher leaf photosynthesis rates and plant water use efficiency. Current CO_2 concentrations are close to optimal for photosynthesis in plants with C4 metabolism, while for the plants with C3 metabolism, an increase of the productivity will still take place with higher CO_2 concentrations (Hamilton III et al., 2008). Owing to this increase of productivity and the fact that C3 plants are dominant, terrestrial ecosystems currently act as a carbon sink, absorbing almost a third of the carbon emissions of anthropogenic origin over the last decade (3.1 ± 0.6 GtC yr^{-1}) and for 2020 (2.9 ± 0.1 GtC) (Friedlingstein et al., 2022) from the so-called CO_2 Fertilization Effect.

Nevertheless, as detailed in the introduction chapter, plant development also depends on other factors such as water availability, nutrients and light intensity, with Nitrogen (N) playing a key limiting role in terrestrial productivity (Davies-Barnard et al., 2020). The terrestrial nitrogen limitation occurs when the biological demand exceeds the soil supply that is settled by nutrient input-output balances (Peng et al., 2020). For example, a site specific analysis across

Europe showed an apparent increase in ecosystem productivity with atmospheric N deposition, though only up to 2.5 gN m^{-2} yr^{-1} (Flechard, van Oijen, et al., 2020), while a meta-analysis of 126 experiments evaluated a limitation of above ground growth to an average of 29% growth in response to nitrogen deposition (LeBauer & Treseder, 2008). Overall, C sequestration to N deposition shows a nonlinear response across a large geographical and climate gradient (Flechard, van Oijen, et al., 2020), increasing the uncertainty of the terrestrial carbon uptake projections.

In this context, the incorporation of the nitrogen cycle and its impact on the carbon cycle in ESM, strongly impacts the net C sink sensitivity to key environmental drivers. This is mainly because the coupled C-N cycles lead to a CO_2 fertilization response over 50% weaker relative to C-only models due to the limitation (Huntzinger et al., 2017). With the reduction in the overall sink of carbon, comes along an additional uncertainty due to uncertainties in future nitrogen fertilization and nitrogen deposition.

In the previous IPCC Fifth Assessment Report (AR5), (Ciais et al., 2013) reported an important carbon sink on terrestrial ecosystems between 120 and 270 GtC over the 1860-2100 period, from the Coupled Model Intercomparison Project (CMIP5). Among the global terrestrial ecosystems models (GTEM) embedded in the CMIP5 EMSs, only two included the nitrogen cycle and carbon-nitrogen interactions (Thornton et al., 2009). However, when accounting - a posteriori - for a nitrogen limitation on carbon productivity, the terrestrial carbon sink was estimated to 40 to 80% of the original estimated range (Zaehle et al., 2015).

The representation of nitrogen-carbon interactions in the latest generation of climate models (CMIP6) is improved compared to the previous generation (CMIP5). A significant step forward happened in the last CMIP exercise (CMIP6) with at least ten GTEM versions including an explicit representation of the nitrogen cycle and of its impact on carbon productivity (Arora et al., 2020b). The study of (Arora et al., 2020b) found that the improved representation of nitrogen-carbon interactions in CMIP6 models leads to a better understanding of the role of carbon sinks in mitigating climate change and more accurate estimates of the potential for carbon storage in ecosystems (Figure 4.1).

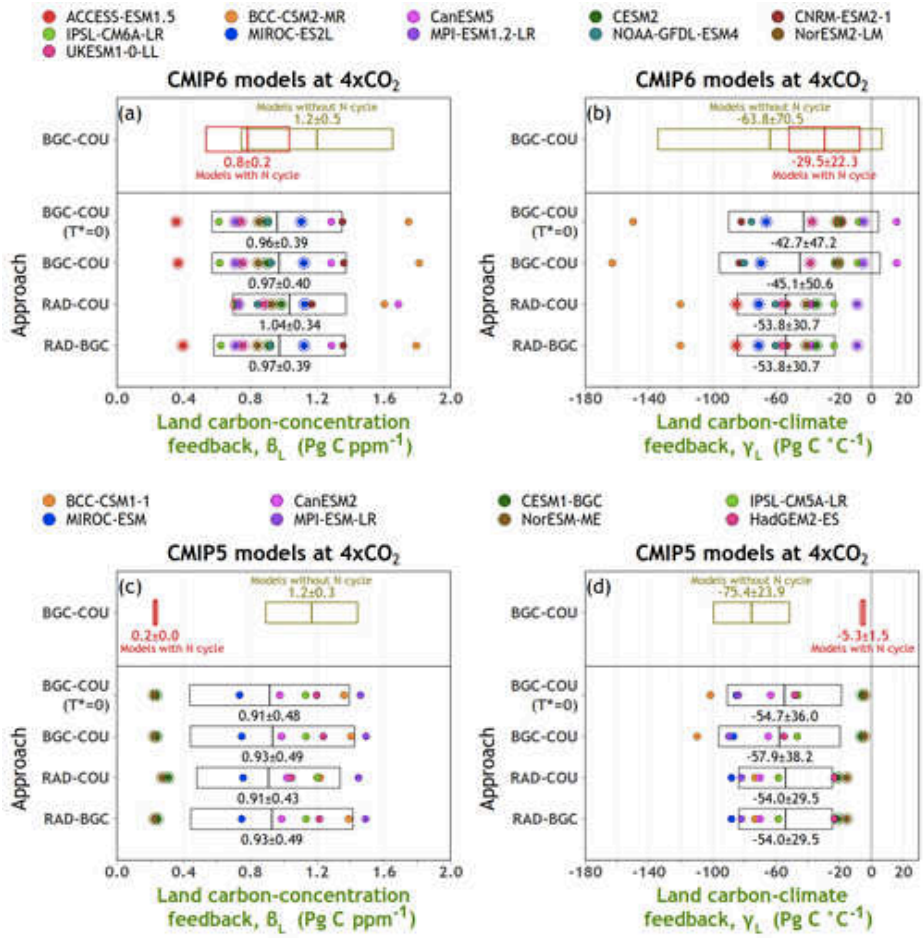

Figure 4.1 - Carbon–concentration (a) and carbon–climate (b) feedback parameters over land from participating CMIP6. The boxes show the mean ± 1 standard deviation range, and the individual colored dots represent individual models. Models which include a representation of the land nitrogen cycle are identified with a circle around their dot. The model mean ± 1 standard deviation range of feedback parameters is also separately shown for models which do and do not represent the land nitrogen cycle using the BGC–COU approach. Results from participating CMIP5 models in the A13 study are shown in (c) and (d) (Arora et al., 2020a).

The inclusion of nitrogen representation in the models showed a reduction in the absolute strength of feedback parameters and reduced spread among land models. The diverse response of land models is primarily due to differences in the strength of CO_2 fertilization, NPP conversion, and residence times of carbon in vegetation and soil. The uncertainty in the total carbon response in the Earth system (TCRE) on centennial timescales is dominated by physical processes, but a reduction in the carbon uptake uncertainty across models can reduce the TCRE uncertainty. The use of fully and biogeochemically coupled configurations of 1pctCO_2 simulations in Earth system models provides consistency and continuity for future comparisons (Arora et al., 2020a).

Phase 6 (CMIP6) concluded that the land and ocean will continue to absorb increasing amounts of carbon dioxide (CO_2) from the atmosphere in the coming decades, but at a slower rate than in the past. The land biosphere is projected to continue to absorb carbon with a projected carbon sink from 2015 to 2100 of 56.3 to 206.6 Pg C, a multi-model mean estimate

of 144.7 Pg C, and an intermodel standard deviation of 47 Pg C (Padrón et al., 2022), but the rate of uptake is uncertain and depends on factors such as land use change and changes in climate.

The Shared Socio-economic Pathways (SSPs) are projected global trajectories for the 21st century employed to foresee future climates through greenhouse gas emission predictions driven from climate policies and socioeconomic growths. They are complemented by quantitative elements such as national population, urbanization, and GDP per capita (O'Neill et al., 2016). The Integrated Assessment Models (IAMs) community uses the SSPs framework for estimating the projected trends of carbon fluxes, land-use change, emission and deposition of nitrogen compounds, and synthetic mineral fertilization rates for agriculture practices (Ciais et al., 2013). Hereby, the projected uncertainty of the reduction in terrestrial carbon sink associated with nitrogen limitation depends in conjunction with the possible SSP trajectories for the 21st century (Ciais et al., 2013).

In this context and following the work performed in the previous chapter on the historical period, I further use the latest version of ORCHIDEE (Organizing Carbon and Hydrology In Dynamic Ecosystems) (Vuichard et al., 2019), the land surface model of the Institut Pierre Simon Laplace (IPSL) earth system model (currently IPSL-CM6), to study the fate of ecosystem carbon budgets . The goal of this chapter is to continue the effort to assess and analyze the evolution of terrestrial productivity simulated by ORCHIDEE over the 21st century, as well as to quantify the uncertainties resulting from the combined effect of climate change, increased atmospheric CO_2 concentrations, land-use change, and the evolution of nitrogen contents of synthetic nitrogen fertilizer and nitrogen deposition.

The study's strategy consists of running various terrestrial production simulations to assess the influence of the overall uncertainty arising from the SSP dispersion as well as the variation within each SSP induced by IAM uncertainty. Key variables that serve as input to the ORCHIDEE model and that are provided by the IAMs are associated with large uncertainties and IAV-dependent (Sinha et al., 2019) It emphasizes the importance of disassociating the different forcings (i.e. through factorial simulations) in order to properly analyze their impact on the expected carbon sinks (Peng et al., 2022).

Most recent studies of the effect of nitrogen enrichment on the carbon sink, have a regional focus, with studies of the effect on temperate and boreal ecosystems (Kicklighter et al., 2019), on temperate forest (Cheng et al., 2018), and on semiarid grasslands (Zhao et al., 2020). Nevertheless, none specifically addressed the impact of uncertainties linked to the CMIP6 forcings and the nitrogen limitation (arising from the IAMs) on the global terrestrial C budget. This is an innovative study because on top of focusing on the global productivity of terrestrial ecosystems, it also aims to analyze the three main drivers separately, unlike the vast majority of studies that consider the effects of only one or two of the drivers (Tharammal et al., 2019),

unraveling the uncertainty from the modelisation of the future scenarios which poses major challenges for climate policies.

The core results of this chapter led to a scientific article that will be submitted very soon (before the Phd defense) and that is reported in section 4.3. The article describes the results of the impact of different SSP trajectories (through factorial simulations) on the terrestrial C budget up to the horizon 2100. In addition, in section 4.2, we present a brief description of the Shared Socioeconomic Pathways that are not heavily discussed in the scientific paper and how these SSPs scenarios were combined to define a factorial experiment investigating the uncertainties associated to key drivers (CO_2, N deposition and fertilization, Land use and climate change). We present the submitted article for the study of the SSP trajectories and the factorial simulations for the net carbon flux.

4.2 Shared Socioeconomic Pathways

Future anthropogenic climate change is a concern associated with uncertainties in all regions of the world. Scenarios have evolved as a valuable tool for investigating various outcomes in the absence of clear forecasts of future events (Lehtonen et al., 2021). Future climate change projections are critical for improved knowledge of the climate system, as well as its influence on societies and their responses. The Scenario Model Intercomparison Project (ScenarioMIP) is a major activity of Phase 6 of the Coupled Model Intercomparison Project (CMIP6), and it will produce multi-model climate forecasts based on various future emission scenarios (O'Neill et al., 2016).

ScenarioMIP is a component of a larger scenario process that will include a variety of research such as integrated assessment modeling (IAM), effects, and adaptation in vulnerable populations. This is a valuable tool for the IPCC assessment, providing crucial information on the effect of individual forcings on climate change. A design has been identified that consists of eight different 21st century scenarios grouped into two tiers based on relative priority. The new Shared Socioeconomic Pathways - SSP structure adds two crucial features to the scenarios system. It homogenizes the socioeconomic norms across all IAM models (such as population, GDP, and poverty, among others) and allows for a more distinct analysis of the many routes through which climate outcomes can be reached (Gidden et al., 2019).

These projections address the uncertainty in future societal conditions by describing societal futures that can be combined with climate change projections and climate policy assumptions to generate integrated scenarios that can be used to investigate mitigation, adaptation, and residual climate impacts in a consistent framework. Based on these, this framework incorporates the creation of new quantitative variables, such as future emissions and land use change trajectories (O'Neill et al., 2016).

The SSPs 1 and 5 anticipate a positive trend in human progress. While SSP1 (sustainability) emphasizes sustainable practices, SSP5 (fossil-fueled development) anticipates an energy-intensive, fossil-based economy. The SSP2 (middle of the road) follows the historical patterns without significant departure. The SSPs 3 and 4 predict a more pessimistic human development that would leave societies susceptible to climate change. The SSP3 (regional competition) stresses regional security, but the SSP4 (inequality) is based on wide disparities within and between nations (O'Neill et al., 2016) see Figure 4.2**.**

Figure 4.2 - Five shared socioeconomic pathways (SSPs) representing different combinations of challenges to mitigation and to adaptation (O'Neill et al., 2016).

Each of the five socioeconomic trends is associated with one or more radiative concentration pathways - RCP, thus completing eight possible trajectories corresponding to the baseline (1.9, 3.4, 4.5, 7, 8.5 W m^{-2} of additional radiative forcing in 2100) and the mitigation (6.0, 4.5, 2.6 W m^{-2}) scenarios. The eight possible trajectories have been simulated by several modeling groups or Integrated Assessment Models (IAMs), however, only one model was chosen to represent a given SPP trajectory.

For example, for the SSP1 (sustainability) trajectories (SSP1 with RCP of 1.9 and 2.6 W m^{-2}) the IMAGE modeling group (van Vuuren et al., 2017) trajectories were chosen (Riahi et al., 2017). For the rest of the SSPs, these are the selected IAMs: SSP2: MESSAGE-GLOBIOM (Fricko et al., 2017); SSP3: AIM (Fujimori et al., 2017); SSP4: GCAM (Calvin et al., 2019) and SSP5: REMIND-MAGPIE (Kriegler et al., 2017). Furthermore, because the outputs of the modeling groups are the consequence of distinct forcings and model structure, outputs were harmonized such that all trajectories begin at the same point in 2015 and continue a roughly similar trajectory, specially for parameters such as land use, through the land use harmonization project (G. C. Hurtt et al., 2020).

Four SSP were chosen for this study (*SSP1-1.9, SSP3-7.0, SSP4-3.4* and *SSP5-8.5*). This selection of SSPs corresponds to the most extreme values in the ensemble of SSPs, providing critical information on the possible range of outputs for the 21st century. In addition, the different forcings (CO_2, N deposition, N fertilization, Land use change) of the selected SSPs were further combined, using factorial simulations, to investigate the impact on the C projection of the uncertainty associated with each forcing. Ideally, for each SSP we should have taken the different forcing of all IAMs. Given that we could not easily access them, we took the range between SSPs for a given forcing, instead of the range between IAMs within a given SSPs (a hypothesis that we somehow justify below).

However, combining the different forcings across the selected SSPs might be a problem, given that NHx emissions are strongly tied to agricultural practices (Hertel et al., 2011), which in turn depend on land use change. A simulation with a low deforestation rate and a minor increase in crop lands (SSP1), for example, would not logically intersect with a high NHx emission (SSP4) trajectory.

Similarly, NOy emissions are mostly caused by the transportation and energy sectors (Hertel et al., 2011), hence a simulation perceptible for sustainable development (SSP1) will often not run into a high NOy emission (SSP3) trajectory. Nonetheless, as previously stated, many IAMs were used to quantify each SSP, and a single IAM (often referred as a marker scenario) was chosen as representative in each case (O'Neill et al., 2016), implying that there is significant uncertainty among markers (IAM dependent). It is evident that the presence of a diverse array of NHx and NOy emissions, in conjunction with land use change, can coexist within a specified Shared Socioeconomic Pathway (SSP), owing to the varying structural characteristics of the Integrated Assessment Models (IAMs), despite their comparable biogeochemical trajectory.

To quantify the high dispersion among the relationships between co-varying variables modeled by different IAMs and thus validate our factorial simulation approach, we analyze the correlation between NHx emission (Mt NH_3 yr^{-1}) and cropland area (million ha). These data were obtained from the non-harmonized outputs of the IAMs modeling groups available on the International Institute for Applied Systems Analysis (IIASA) (Riahi et al., 2017) as seen in (Figure 4.3).

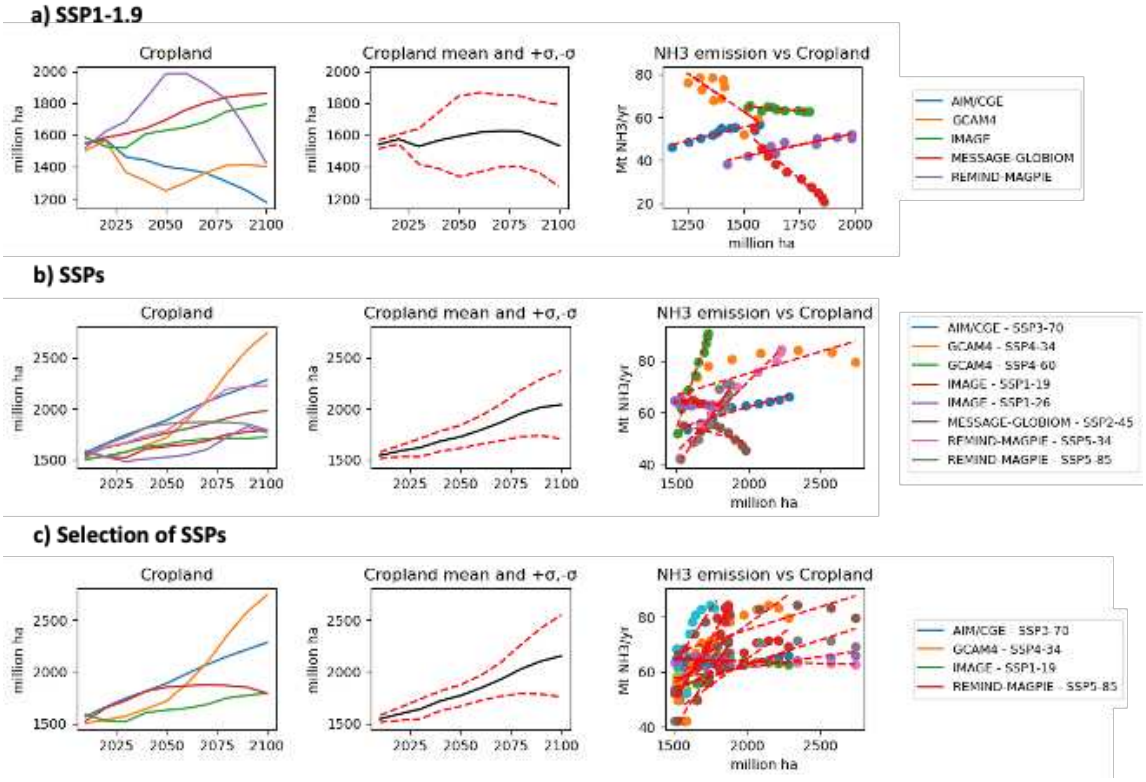

Figure 4.3 - Cropland evolution and scatter plot between NH_3 emission and cropland for a) all the IAMs outputs for the SSP1-1.9 as an example for all single SSP modeling outputs, b) the CMIP6 set of SSPs, in wich each SSP corresponds to a given IAM, and c) our selection of SSPs and combination of them (16 trajectories).

In Figure 4.3 we see that for a given SSP (SSP1-1.9) the future trajectory of land use (i.e. cropland expansion) varies a lot across the 5 IAMS, with increasing or decreasing trends. At the same time the relationship between NH_3 emission and cropland expansion, although mostly linear for each IAM, differ substantially with negative or positive slopes. Figure 4.4, further highlights that the range of variations for cropland expansion and the "NH_3 emission vs Cropland" regression between SSPs is similar to the uncertainty of the same factor within SSP1-1.9. Such features somehow justify that our approach (see the Article in the next section) of combining the factors of different SSPs to estimate the uncertainty of a given factor within a given SSP is plausible.

The boxplots of the slopes and robustness (R^2) derived from the correlations, as illustrated in (Figure 4.4), serve to further substantiate our methodology. These visualizations reveal that a significant degree of uncertainty arises from the utilization of a diverse set of substantially divergent IAM models in determining single SSP markers for the intercomparison exercise, for a single Shared Socioeconomic Pathway (SSP), the ScenarioMIP (CMIP6), and per consequence our selection of SSPs.

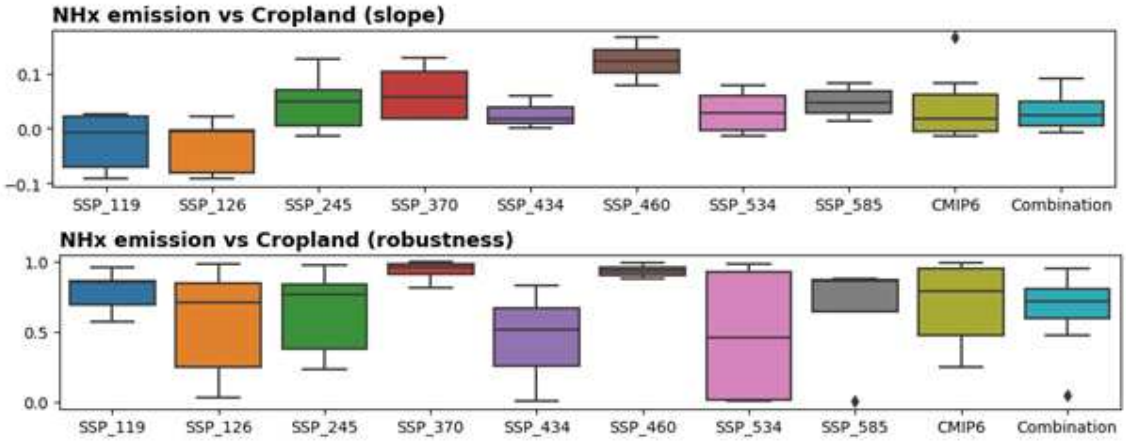

Figure 4.4 - Set of box plots for the slope and robustness (R2) for the correlation between NHx emission, and cropland evolution for the 21st for all the IAMs possible outcomes for each SSP, the selected markers for the scenarioMIP from CMIP6 and the combination of our selection of SSPs.

The slopes and robustness (R2) of the regression between NHx emissions and cropland expansion demonstrate a considerable range for each Shared Socioeconomic Pathway (calculated through the outputs of various IAMs), as well as for the CMIP-selected IAMs and our restricted selection of IAMs. This substantial variability warrants the consideration of the different forcing agents as possessing a degree of independence, thereby lending support to our approach of utilizing the range across SSPs as an indicator of uncertainty for a given factor.

4.3 Scientific Article - Projected changes in land carbon store over the 21st century: what contributions from land-use change and atmospheric nitrogen deposition?

Jaime A. Riano Sanchez[1], N. Vuichard[1], P. Peylin[1]

[1] Laboratoire des Sciences du Climat et de l'Environnement, LSCE-IPSL (CEA-CNRS-UVSQ), Université Paris-Saclay 91191 Gif-sur-Yvette, France

Correspondence to: Nicolas Vuichard (nicolas.vuichard@lsce.ipsl.fr)

Abstract. Earth System Models (ESM) represent the time evolution of the biophysical (energy, water cycles) and biogeochemical (carbon cycle) components of the Earth. When used for near-future projections in the context of the Coupled Model Intercomparison Project (CMIP), they use as forcings the evolution of greenhouse gas and other pollutant concentrations and land-use changes simulated by an ensemble of Integrated Assessment Models (IAMs) for a

combination of socio-economic pathways and mitigation targets (SSPs). More precisely, only one IAM output is used as representative of a single SSP while the inter-IAM spread is large for ammonia emissions and land-use changes, for instance. This makes the comparison of key ESM diagnostics among SSPs significantly noisy, without the capacity of disentangling SSP-driven and IAM-driven factors. In this paper, we quantify the projected change in land carbon store (CLCS) for the different SSPs with an advanced version of a land surface model embedded into IPSL-CM6 ESM. Through a set of land-only factorial simulations, we specifically aim at estimating the CLCS uncertainties associated with land-use change and nitrogen deposition trajectories. We showed that the spread of the simulated change in global land carbon store induced by the uncertainty on land-use changes is slightly larger than the one associated with the uncertainty on atmospheric CO_2. Globally, uncertainty associated with N depositions is responsible for a spread in CLCS lower by a factor three, than the one driven by atmospheric CO_2 or land-use changes. Our study calls for making available additional IAM scenarios for each SSP to be used in the next CMIP exercise, in order to specifically assess the IAM-related uncertainty impacts on the carbon cycle and the climate system.

1 Introduction

In the framework of the Phase 6 of the Coupled Model Intercomparison Project (CMIP6), the ScenarioMIP experiments (O'Neill et al., 2016) address the near-future evolution (2015-2100) of the Earth System for a combination of socio-economic and climate policy scenarios. Five shared socio-economic pathways (SSPs) are explored (Riahi et al., 2017) with contrasted assumptions regarding the future evolution of society in terms of population growth, economic development, urbanization and other factors. Driven by these five socio-economic pathways, an ensemble of Integrated Assessment Models (IAMs) simulate the evolution of energy and land-use systems and the associated emissions of GHG and other pollutants. In the context of ScenarioMIP, a selection of simulations are performed for the five socio-economic pathways with or without mitigation strategy (baseline scenario) leading to specific radiative forcings in 2100 (O'Neill et al., 2016). As defined in O'Neill et al. (2016), we label these eight scenarios as SSPx-y with x the selected SSP and y the 2100 radiative forcing. In the following, and by simplicity, we refer to these eight scenarios as SSPs. In order to be used by Earth System Models (ESM), IAMs outputs are harmonized to be consistent with the data used

for the historical period and downscaled from the IAMs large-region scale to a finer gridded one. Harmonization and downscaling are performed for land-use (Hurtt et al., 2020) and for emissions of GHG and other atmospheric compounds impacting climate (Gidden et al., 2019). Liddicoat et al. (2021) computed the compatible fossil fuel CO_2 emissions deduced from the historical and ScenarioMIP experiments of nine ESMs. They showed that the multimodel mean cumulative compatible fossil fuel CO_2 emissions over 1850-2100 were in closed agreement with the estimate based on observation (for the historical period) and the IAMs (for the period 2015-2100) for the different SSPs. The absolute relative difference between the multimodel mean and the observation/IAM-based estimate ranges from 1% (for SSP3-7.0) to 13% (for SSP1-1.9), proving the overall good consistency between ESM and IAM carbon cycle modellings. However, the model spread is large, with an intermodel standard deviation ranging from 5% (for SSP5-8.5) to 15% (for SSP4-3.4) of the multimodel mean compatible fossil fuel CO_2 emissions. This large disagreement between ESMs is primarily attributable to the land carbon response, with an intermodel standard deviation for the land carbon store between 1850 and 2100 of the order of 67% of the multimodel mean, while the one for the ocean carbon store does not exceed 6%.

In this paper, we focus on the projected ESM land carbon store for the different SSPs and in particular on another source of uncertainty directly related to the IAM forcings. Indeed, five IAMs simulated the evolution of the energy and land-use systems and associated gas emissions for each SSP but only outputs of a single IAM per SSP have been harmonized and downscaled to be further used as ESM inputs. These selected interpretations of SSPs are called "markers" and the other IAM scenarios for each SSP "non-makers" (Riahi et al., 2017). While the anthropogenic CO_2 emission trajectories simulated by the different IAMs for a given SSP are relatively similar (https://tntcat.iiasa.ac.at/SspDb, see also Bauer et al. (2017) for a specific analysis for fossil fuel emissions only), there are large inter-IAM spreads for land-use trajectories (Popp et al., 2017; Riahi et al., 2017) but also for nitrogen fertilizer usage (Sinha et al., 2019) and pollutant emissions (in particular ammonia, https://tntcat.iiasa.ac.at/SspDb).

This selection of marker IAMs as representatives of a single SSP while the inter-IAM spread is large, makes the comparison of key ESM diagnostics among SSPs significantly noisy, without the capacity of disentangling SSP-driven and IAM-driven factors (Monier et al., 2018; Sinha et al., 2019). While this difficulty gets support to the development of coupled human-Earth system (CHES) models (Monier et al., 2018) to gain in modelling consistency, this option does

not facilitate the assessment of an IAM-specific uncertainty and of its impact on the Earth system.

In this paper, we quantify the projected change in land carbon store (CLCS) for the different SSPs with an advanced version (ORCHIDEE-v3, Vuichard et al., 2019) of the land surface model embedded into IPSL-CM6 (Boucher et al., 2020). In addition, through a set of land-only simulations, we also aim at estimating the CLCS uncertainties associated specifically to land-use change and nitrogen deposition trajectories.

2 Methods

2.1 The ORCHIDEE-v3 model

ORCHIDEE (Organizing Carbon and Hydrology In Dynamic Ecosystems) is a global process-based terrestrial ecosystem model used to quantify energy, water, carbon and nitrogen flows and associated stocks in the soil-vegetation-atmosphere continuum (Krinner et al., 2005; Vuichard et al., 2019). For the last CMIP6 exercise, ORCHIDEE-v2, a carbon-only version of ORCHIDEE, has been used as the land component of the Earth System Model ESM of the Institut Pierre Simon-Laplace (IPSL-CM6). ORCHIDEE-v3 is an advanced version in which N cycle and the C-N interactions have been included (Vuichard et al., 2019). ORCHIDEEv3 needs as input data, information about climate (near-surface air temperature, precipitation, short and long-wave incoming radiation, specific air humidity), atmospheric CO_2 concentration, land cover, but also atmospheric N deposition (NHx and NOy) and N fertilizer rates on managed lands. ORCHIDEE-v3 showed good performance at simulating Gross Primary Productivity (GPP) and Leaf Area Index (LAI) both at site and global scales (Vuichard et al., 2019). It also ranked with a good score for a set of key land variables in a recent model benchmark study (Seiler et al., 2022) as well as in the TRENDY model inter-comparison project (Friedlingstein et al., 2022).

2.2 Model input datasets

Inputs related to atmospheric CO_2 concentration ($[CO_2]$), land-use, wood harvest, N-fertilizer and nitrogen deposition are those used for the historical and the different SSP CMIP6-related experiments and stored on input4MIPs nodes (https://esgf-node.llnl.gov/projects/input4mips/). The procedure needed for translating the original data for

land-use into the fifteen land classes of ORCHIDEE is described in Lurton et al. (2020). Climate data used as inputs of the land-only ORCHIDEE-v3 simulations correspond to the IPSL-CM6A-LR model outputs for the historical and the different SSP experiments (using for each experiment the r1i1p1f1 member).

2.3 Reference simulations

In order to get C and N vegetation and soil pools at equilibrium, we ran a spin-up simulation with the boundary conditions of year 1850 but recycling climate data for the period 1850-1869 in order to account for an inter-annual variability. From this equilibrium state, simulations ran for the historical period (1850-2014) and for each of the eight SSP experiments.

2.4 Land-use and Nitrogen-forcing related sensitivity simulations

In the absence of gridded harmonized data for the land-use and N deposition for non-marker scenarios of a given SSP *p*, we used the data from marker scenarios of selected alternative pathways to assess the sensitivity of the projected land carbon store for SSP *p* to land-use and N deposition. In other words, we used selected SSP markers spread as a proxy for the inter-IAM spread regarding the land-use and N deposition trajectories for any SSP. This is a strong assumption but supported by the comparison between inter-SSP markers and inter-IAM trajectories for the different SSPs (see Figures 1, 2, A1, A2 and A3). In particular, we showed that the inter-selected SSP markers spread of the forested global land area in 2100 is narrower than the inter-IAM spread for six out of eight SSPs (Fig. 1). Similarly, the inter-selected SSP markers spread of the global NH3 emissions in 2100 is narrower than the inter-IAM spread for seven out of the eight SSPs (Fig. 2). However, for some variables simulated by IAMs, the inter-selected SSP markers spread is significantly larger than the inter-IAM spread for many SSPs. This is particularly the case of NOy emissions (Fig. A3) for which the inter-selected markers spread is larger than the inter-IAM spread for any of the eight SSPs. Thus, depending of the driving variable considered (forested lands, pasture or croplands, NH3 or NOy emissions) and of the SSP considered, the use of the selected SSP markers spread as a proxy may translate into an upper or lower estimate of the inter-IAM spread.

2.5 Metrics assessing the change in land carbon store and its sensitivity to land-use and N-deposition uncertainties

We analysed specifically the projected change in land carbon store (CLCS) for the selected pathways SSP1-1.9, SSP3-7.0, SSP4-3.4 and SSP5-8.5 and its sensitivity to the different land-use and N-deposition marker trajectories for these four selected SSPs. We selected these four SSPs because 1/ they encompass a large spread of CO_2 level in 2100 ranging from 394 to 1135 ppm; and 2/ the inter-IAM spreads for land-use but also N-emission trajectories from this selection are comparable to those from the eight SSPs.

To perform this analysis, we ran a set of sixteen sensitivity simulations for each of the four selected reference simulations, where land-use and N-related data from the four SSPs is used independently as forcing (four land-use trajectories times four N-related trajectories), which resulted into an ensemble of sixty-four simulations. We expressed CLCS as a function of CO_2, LUC and NDEP trajectories (*CLCS(CO_2, LUC, NDEP)*) and computed mean (μ) and standard deviation (σ) metrics based on the following equations where X stands for μ or σ:

$$X_{CLCS,LUC}(i,k) = X\{CLCS(i,j,k)\}_{j=1-1.9,3-7.0,4-3.4,5-8.5}\ , (1)$$

$$X_{CLCS,NDEP}(i,j) = X\{CLCS(i,j,k)\}_{k=1-1.9,3-7.0,4-3.4,5-8.5}\ , (2)$$

$$X_{CLCS,LUC+NDEP}(i) = X\{CLCS(i,j,k)\}_{j,k=1-1.9,3-7.0,4-3.4,5-8.5}\ ,(3)$$

We quantified the mean CLCS and standard deviation associated specifically to different land-use (LUC), N-deposition (NDEP) and land-use and N-deposition (LUC+NDEP) trajectories, for each of the four selected SSPs. These metrics correspond to respectively $X_{CLCS,LUC}(i,i)$, $X_{CLCS,NDEP}(i,i)$ and $X_{CLCS,LUC+NDEP}(i)$ for i = 1-1.9,3-7.0,4-3.4,5-8.5.

We also aimed at comparing the CLCS spread induced by LUC or NDEP trajectories, relatively to the one induced by CO_2 level. As a consequence, similarly to $\sigma_{CLCS,LUC}$ and $\sigma_{CLCS,NDEP}$, we also computed $\sigma_{CLCS,CO2}$ as:

$$\sigma_{CLCS,CO2}(j,k) = \sigma\{CLCS(i,j,k)\}_{i=1-1.9,3-7.0,4-3.4,5-8.5}, (4)$$

In order to report on the overall dispersion of CLCS and the contribution from the three drivers (CO_2, LUC and NDEP), we first computed μ and σ accounting for all drivers:

$$X_{CLCS,TOT} = X\{CLCS(i,j,k)\}_{i,j,k=1-1.9,3-7.0,4-3.4,5-8.5}, (5)$$

We then computed the mean standard deviation, $\underline{\sigma}_{CLCS,D}$ in order to quantify the impact on CLCS of each of the three drivers (D) irrespective of the combinations of the two others:

$$\underline{\sigma}_{CLCS,D} = \mu\{\sigma_{CLCS,D}(i,j)\}_{i,j=1-1.9,3-7.0,4-3.4,5-8.5}, (6)$$

for D=CO_2, LUC and NDEP

Last, we expressed the relative impact on the CLCS spread of each of the three drivers, $r_{CLCS,D}$ as:

$$r_{CLCS,D} = \frac{\sigma_{CLCS,D}}{\sigma_{CLCS,CO2}+\sigma_{CLCS,LUC}+\sigma_{CLCS,NDEP}}, \quad (7)$$

for D=CO_2, LUC and NDEP

3 Results and discussion

The CLCS simulated by ORCHIDEEv3 over the historical period corresponds to a small carbon source of 7.7 PgC (table 1). Over the period 1850-2100 and depending on the SSP, the CLCS varies between a small source of 5.6 PgC (SSP4-3.4) to a sink of 115.5 PgC (SSP5-8.5). The CLCS simulated by ORCHIDEEv3 are in the low-end range of the values reported by Liddicoat et al. (2021) with an ensemble of nine ESMs. ORCIHDEEv3's CLCS is very similar to the one simulated by UKESM1-0-LL for the historical period and for any of the seven SSPs studied by this ESM (table 1 and table S3 of Liddicoat et al., 2021). The CLCS standard deviation induced by considering different N-related trajectories is relatively similar irrespective of the SPP considered with $\sigma_{CLCS,NDEP}$ varying between 10.9 and 13.6 PgC depending on the SSP (Table 1 and Figure 2). The effect of considering different LUC-related trajectories on the CLCS is more important with a standard deviation ($\sigma_{CLCS,LUC}$) going from 38.1 PgC (for SSP1-1.9) to 46.2 PgC (for SSP5-8.5). Accounting for both sources of uncertainty (LUC and NDEP) on CLCS leads to a similar dispersion than considering LUC uncertainty only with $\sigma_{CLCS,NDEP+LUC}$ varying between 37.2 and 45.3 PgC depending on the SSP. Expressed as a percentage of the mean CLCS, these values correspond to standard deviations between 43.8% and 114.1% of $\mu_{CLCS,NDEP+LUC}$. Although important, these uncertainties induced by the LUC and NDEP trajectories are a factor 2 to 3 less than those associated to the multi ESM ensemble assessed by Liddicoat et al. (2019) for the four studied SSPs (from 90 to 157 PgC for SSP1-1.9 and SSP5-8.5 respectively).

As shown on Figure 3, depending of the LUC and NDEP trajectories associated to the marker scenarios, the CLCS estimated for the marker may be in the very low-end range of values for all NDEP and LUC combinations (SSP4-3.4), in the high-end range (SSP1-1.9) or closed to the mean value $\mu_{CLCS,NDEP+LUC}$ (SSP3-7.0 and to some extent SSP5-8.5).

When accounting for all combinations of NDEP, LUC and CO_2 trajectories, the global CLCS at the end of the 21st century ranges from a source of 25 PgC to a sink of 175 PgC (Figures 3 and

4). The CLCS spread induced by the uncertainty on LUC ($\sigma_{CLCS,LUC}$) is slightly larger than the one related to the CO_2 trajectory ($\sigma_{CLCS,CO2}$). On average for all combinations of NDEP, LUC and CO_2, the relative impact of LUC on the CLCS spread ($r_{CLCS,LUC}$) amounts to 48% globally at the end of the 21st century, while $r_{CLCS,CO2}$ value is about 38% (Figure 4). The relative impact of NDEP on the CLCS spread is one third less, with a value of $r_{CLCS,NDEP}$ equals to 14%. The relative impacts of the three drivers on the CLCS spread at the end of the 21st century show contrasted results at regional scale. In Africa and Tropical Asia regions, where the strength of the land use change varies importantly from one SSP to another, the relative impact of LUC is far more important than the impact of CO_2 (and NDEP) with values of $r_{CLCS,LUC}$ of ~74% for both regions. As a consequence, the value of $r_{CLCS,CO2}$ in these two regions is less than 20% by 2100. They are the only two regions for which CLCS shifts significantly from source to sink depending of the LUC trajectories (Fig. 4) with regional $\mu_{CLCS,TOT} \pm \sigma_{CLCS,TOT}$ values of -10±43 PgC and -1±22 PgC by 2100, for Africa and Tropical Asia region respectively. Due to the strong impact of LUC on CLCS and its large area, Africa is the region that contributes the most to the overall dispersion of CLCS globally ($\sigma_{CLCS,TOT}$ of 43 PgC for Africa, to be compared to $\sigma_{CLCS,TOT}$ of 106 PgC for the globe). For the six other regions where the impact of LUC is less important, CO_2 is the factor that drives the most the CLCS dispersion with $r_{CLCS,CO2}$ values ranging from 37% (for Europe) to ~57.5% (for "Boreal Asia" and "Australia and New Zealand" regions). In these regions, the impact of NDEP on the CLCS dispersion varies significantly depending on how the NDEP trajectories are contrasted within a region but also on how the terrestrial ecosystems are N-limited regionally. In "South America" and "Australia and New Zealand" regions, the relative impact of NDEP is very small with $r_{CLCS,NDEP}$ values less than 10%. In the other four regions, $r_{CLCS,NDEP}$ values are more than 23% and up to 35% for the "Boreal Asia" region.

The time evolution of the relative impacts of the three drivers on the CLCS dispersion is not uniform over the 21st century (Fig. 4). Globally, $r_{CLCS,CO2}$ decreases over the two first decades (2015-2030, from values greater than 50% down to 7%) and increases the following decades with a kind of Michaelis-Menten curve shape. Mirroring the time evolution of the relative impact of CO_2, $r_{CLCS,NDEP}$ and $r_{CLCS,LUC}$ increase over the first decades of the 21st century and decrease after 2030 and 2040 for NDEP and LUC respectively. These specific temporal dynamics, which result from the combination of specific time evolution and time-response on the CLCS of the three studied drivers, are obtained globally but also for most large regions (eg

Temperate Asia, North America, South America). These first-decades dynamics are not analysed in more details here as they correspond to periods over which the CLCS overall dispersion remains small (see time evolution of $\mu_{CLCS,TOT} \pm \sigma_{CLCS,TOT}$ on Fig. 4).

The ensemble of sixty-four factorial simulations offers the advantage to isolate and quantify the effect of one specific driver among the three considered in this study (CO_2, LUC and NDEP) which are otherwise mixed up in the standard reference SSP simulations. We express CLCS in 2100 as a function of one driver (atmospheric [CO_2], Forested lands or N atmospheric deposition in 2100) for the sixteen simulations driven by the different combinations of the two other drivers (Fig. 5). The different relationships between CLCS and any of the three drivers are similar irrespective of the simulations considered meaning there is no strong co-varying effect across drivers. Only the CLCS baseline level differs between simulations, for the lowest value of atmospheric CO_2, forested lands area or N atmospheric deposition. The CLCS response curve to CO_2 shows a saturation effect for the highest CO_2 level (~1100 ppm) driven by the limitation of C assimilated by photosynthesis at high [CO_2]. Based on a simple linear regression, the CLCS response to CO_2 equals 0.1 PgC ppm^{-1} (Fig. 5a). We also highlight a relationship between the forested land area in 2100 and CLCS in 2100 (Fig. 5b). The forested land area in 2100 is inversely proportional to the deforestation trend (or proportional to the re/afforestation trend) experienced over the 21st century in the different SSPs. As a consequence, the higher forested land area, the higher CLCS. The relationship between CLCS and the forested land area is not strictly linear due to the different regions where the deforestation (or re/afforestation) acts in the SSPs, with different ecosystem productivity. However, on average, based on a linear regression, the CLCS response to the forested lands equals 13.85 PgC (Mkm^2 of forested lands)$^{-1}$ (Fig. 5b). Last, CLCS shows a nearly linear relationship with the global mean atmospheric N deposition rate in 2100. The 2100 rate reflects the average load of atmospheric N deposited on land over the 21st century and its fertilizing effect on terrestrial ecosystems. This results in a CLCS response to N deposition of 1 PgC (TgN yr^{-1})$^{-1}$.

To our knowledge, little attention has been paid to the co-effects of atmospheric CO_2, atmospheric nitrogen deposition and land-use change on the change in land carbon store in the CMIP6 framework and how these drivers interplay together. A 1pctCO_2 experiment was part of the DECK ensemble (Eyring et al., 2016) in order to analyse the effects of a 1% yr^{-1} increase in atmospheric CO_2 on the radiative (RAD) and carbon cycle (BGC) components with

pre-industrial atmospheric N deposition. In addition to the 1pctCO_2 experiment, two experiments (namely 1pctCO_2Ndep and 1pctCO_2Ndep-bgc) were planned in the Coupled Climate–Carbon Cycle Model Intercomparison Project (C4MIP, Jones et al., 2016) with time-increasing atmospheric N deposition, with the objective of quantifying the co-effects of atmospheric CO_2 and N deposition increases. Unfortunately, only three modelling groups performed these two additional experiments and no study made use of them so far. In the Land Use Model Intercomparison Project (LUMIP, Lawrence et al., 2016), the two experiments ssp370- ssp126Lu and ssp126-ssp370Lu, based on the ScenarioMIP ssp370 and ssp126 experiments but swapping their land-use datasets (ie. with land-use information associated to SSP 126 and 370, respectively , Hurtt et al., 2020), aim at quantifying the specific contribution from land-use change on the climate and carbon cycle over the 21st century. With this set of 2x2 experiments, Ito et al. (2020) quantified the impact of land-use change on the total soil carbon stock (cSoil) simulated by seven ESMs. Although limited to only two contrasted land-use trajectories, they reported large intermodel spread with change on cSoil due to land-use trajectory varying between -14 and +24 PgC. This highlights the need of performing the kind of multi-sensitivity analysis we proposed in this paper with an extended ensemble of models, in order to evaluate how our conclusions can be shared across models.

4 Conclusions

Our study ambitioned to quantify the impacts of the land-use and nitrogen-related IAM uncertainties on the change in land carbon store as simulated by the land component of an ESM. In the absence of harmonized and downscaled information for the IAMs other than the marker one of each SSP, we used the land-use and nitrogen trajectories of the different SSP markers as a surrogate of the trajectories simulated by the different IAMs for each SSP. We showed that the spread of the simulated change in global land carbon store induced by the uncertainty on land-use across SSPs is slightly larger than the one associated with the uncertainty on atmospheric CO_2. Globally, uncertainty associated with N emissions (and ultimately N depositions) is responsible for a spread in the change in land carbon store that is lower by a factor three, than the one driven by atmospheric CO_2 or land-use changes. The relative impact of these different uncertainties showed contrasted responses regionally. In regions with very contrasted land-use trajectories across SSPs, such as Africa, the spread in the

change in land carbon store is mainly driven by land-use change. In contrast, in regions where land-use trajectories are more similar across SSPs, the impact of the nitrogen deposition-related uncertainty on the change in land carbon store may be almost as large as the one induced by uncertainty on atmospheric CO_2 and land-use changes. Although we showed that the inter-marker spread and the inter-IAM spread for a given SSP were of the same order for the land-use trajectories but also for the N emissions trajectories globally, the two spreads are not strictly similar for each diagnostic variable by the IAMs or for each SSP. In this respect, there is a need for delivering harmonized and downscaled info about land-use changes, N emissions and N atmospheric deposition trajectories simulated by all IAMs for each SSP and not only by the marker IAMs. Performing sensitivity ESM or land-only experiments with these extra datasets is the only way to accurately assess the specific IAM-related uncertainty impacts on the carbon cycle and the climate system. While many GHG mitigation strategies imply more in more land-based solutions, this calls for facilitating the communication and evaluation between IAM and ESM modelling frameworks. Making available additional IAM scenarios to be used in the next CMIP exercise should contribute to this objective.

Appendix A

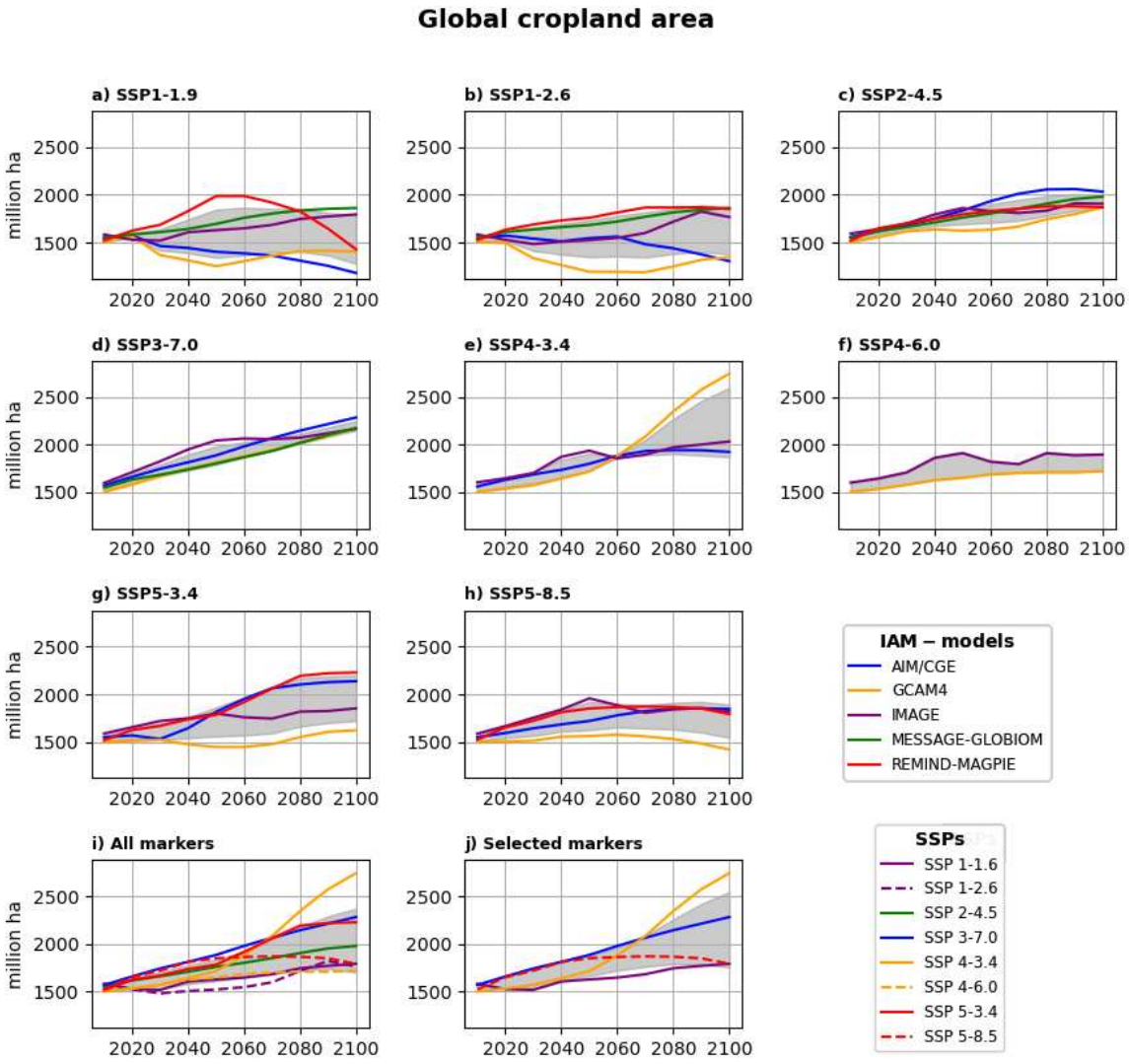

Figure A1: Time evolution (2015-2100) of the global cropland area (Mha) projected by (a to h) different Integrated Assessment Models (IAM) for different Shared Socio-economic Pathways,(i) all IAM markers and (j) the selected IAM markers.

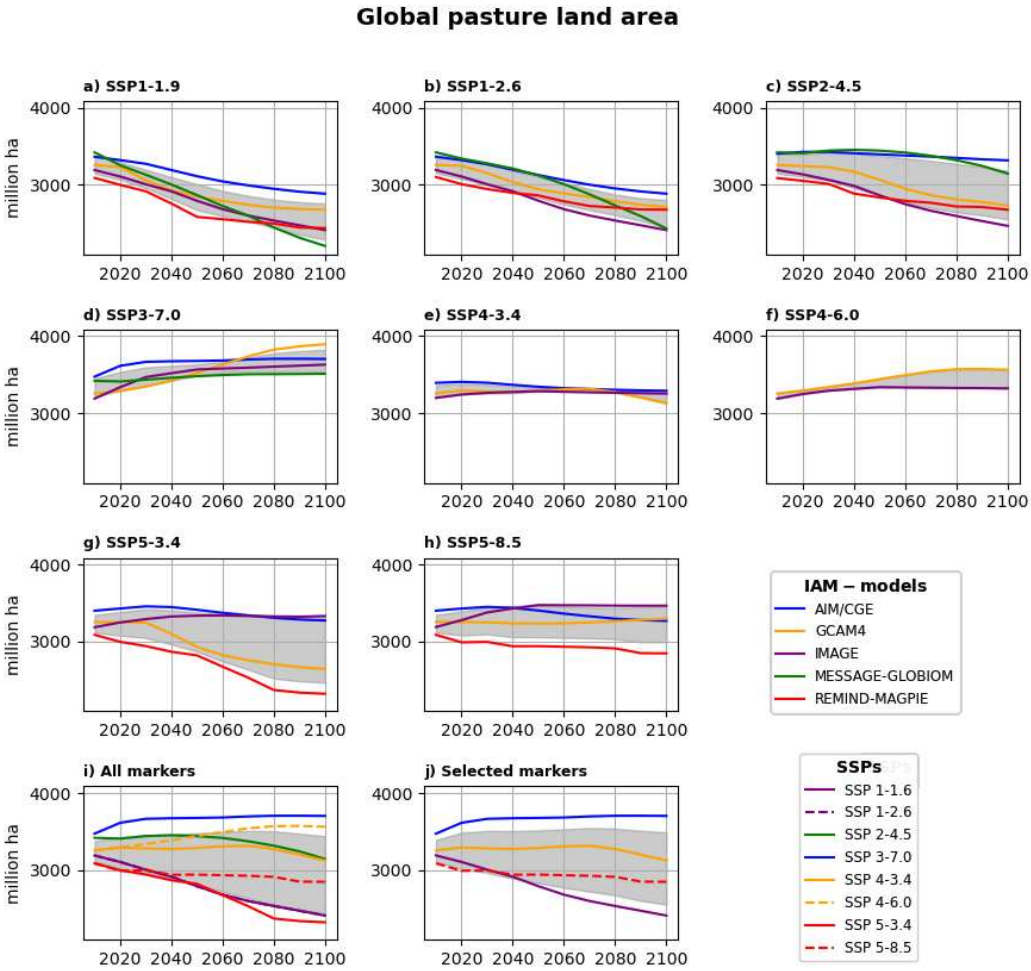

Figure A2: Time evolution (2015-2100) of the global pasture land area (Mha) projected by (a to h) different Integrated Assessment Models (IAM) for different Shared Socio-economic Pathways,(i) all IAM markers and (j) the selected IAM markers.

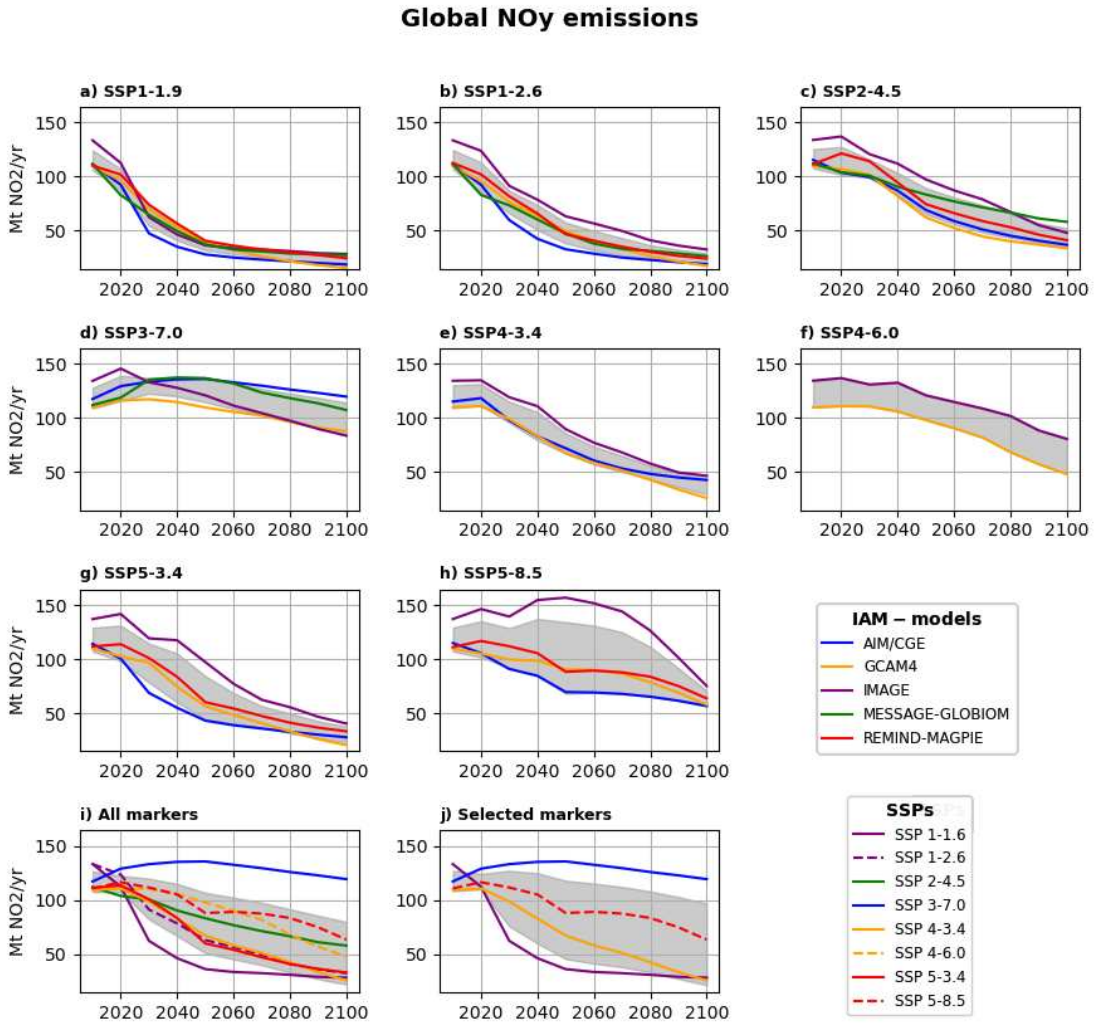

Figure A3: Time evolution (2015-2100) of the global NOy (NO_2) emissions ($Mt(NO_2)\ yr^{-1}$) projected by (a to h) different Integrated Assessment Models (IAM) for different Shared Socio-economic Pathways,(i) all IAM markers and (j) the selected IAM markers.

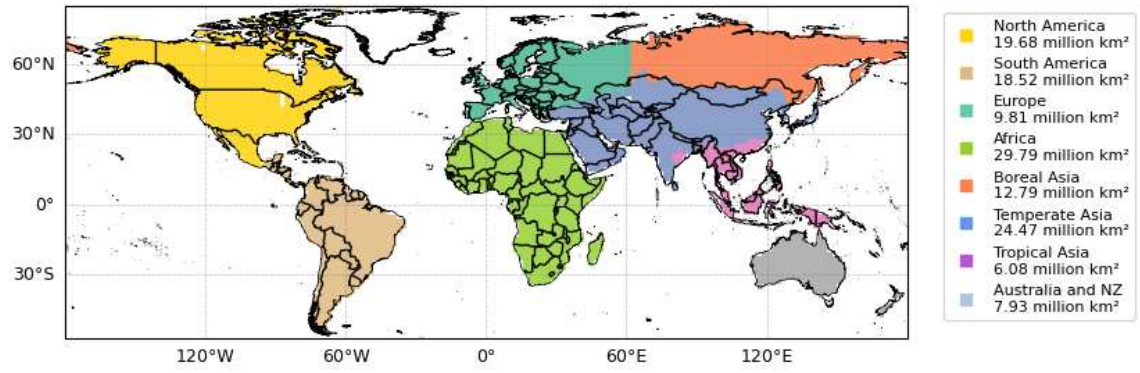

Figure A4: Spatial distribution and size area of the eight regions used in the study.

References

Bauer, N., Calvin, K., Emmerling, J., Fricko, O., Fujimori, S., Hilaire, J., Eom, J., Krey, V., Kriegler, E., Mouratiadou, I., Sytze de Boer, H., van den Berg, M., Carrara, S., Daioglou, V., Drouet, L., Edmonds, J. E., Gernaat, D., Havlik, P., Johnson, N., Klein, D., Kyle, P., Marangoni, G., Masui, T., Pietzcker, R. C., Strubegger, M., Wise, M., Riahi, K. and van Vuuren, D. P.: Shared Socio-Economic Pathways of the Energy Sector – Quantifying the Narratives, Glob. Environ. Chang., 42, 316–330, doi:10.1016/j.gloenvcha.2016.07.006, 2017.

Boucher, O., Servonnat, J., Albright, A. L., Aumont, O., Balkanski, Y., Bastrikov, V., Bekki, S., Bonnet, R., Bony, S., Bopp, L., Braconnot, P., Brockmann, P., Cadule, P., Caubel, A., Cheruy, F., Codron, F., Cozic, A., Cugnet, D., D'Andrea, F., Davini, P., de Lavergne, C., Denvil, S., Deshayes, J., Devilliers, M., Ducharne, A., Dufresne, J. L., Dupont, E., Éthé, C., Fairhead, L., Falletti, L., Flavoni, S., Foujols, M. A., Gardoll, S., Gastineau, G., Ghattas, J., Grandpeix, J. Y., Guenet, B., Guez, L. E., Guilyardi, E., Guimberteau, M., Hauglustaine, D., Hourdin, F., Idelkadi, A., Joussaume, S., Kageyama, M., Khodri, M., Krinner, G., Lebas, N., Levavasseur, G., Lévy, C., Li, L., Lott, F., Lurton, T., Luyssaert, S., Madec, G., Madeleine, J. B., Maignan, F., Marchand, M., Marti, O., Mellul, L., Meurdesoif, Y., Mignot, J., Musat, I., Ottlé, C., Peylin, P., Planton, Y., Polcher, J., Rio, C., Rochetin, N., Rousset, C., Sepulchre, P., Sima, A., Swingedouw, D., Thiéblemont, R., Traore, A. K., Vancoppenolle, M., Vial, J., Vialard, J., Viovy, N. and Vuichard, N.: Presentation and Evaluation of the IPSL-CM6A-LR Climate Model, J. Adv. Model. Earth Syst., 12(7), 1–52, doi:10.1029/2019MS002010, 2020.

Eyring, V., Bony, S., Meehl, G. A., Senior, C. A., Stevens, B., Stouffer, R. J. and Taylor, K. E.: Overview of the Coupled Model Intercomparison Project Phase 6 (CMIP6) experimental design and organization, Geosci. Model Dev., 9(5), 1937–1958, doi:10.5194/gmd-9-1937-2016, 2016.

Friedlingstein, P., Jones, M. W., Sullivan, M. O., Andrew, R. M., Bakker, D. C. E., Hauck, J., Quéré, C. Le, Peters, G. P. and Peters, W.: Global Carbon Budget 2021, , 1917–2005, 2022.

Gidden, M. J., Riahi, K., Smith, S. J., Fujimori, S., Luderer, G., Kriegler, E., Van Vuuren, D. P., Van Den Berg, M., Feng, L., Klein, D., Calvin, K., Doelman, J. C., Frank, S., Fricko, O., Harmsen, M., Hasegawa, T., Havlik, P., Hilaire, J., Hoesly, R., Horing, J., Popp, A., Stehfest, E. and Takahashi, K.: Global emissions pathways under different socioeconomic scenarios for use in CMIP6: A dataset of harmonized emissions trajectories through the end of the century, Geosci. Model Dev., 12(4), 1443–1475, doi:10.5194/gmd-12-1443-2019, 2019.

Hurtt, G. C., Chini, L., Sahajpal, R., Frolking, S., Bodirsky, B. L., Calvin, K., Doelman, J. C., Fisk, J., Fujimori, S., Goldewijk, K. K., Hasegawa, T., Havlik, P., Heinimann, A., Humpenöder, F., Jungclaus, J., Kaplan, J. O., Kennedy, J., Krisztin, T., Lawrence, D., Lawrence, P., Ma, L., Mertz, O., Pongratz, J., Popp, A., Poulter, B., Riahi, K., Shevliakova, E., Stehfest, E., Thornton, P., Tubiello, F. N., van Vuuren, D. P. and Zhang, X.: Harmonization of global land use change and management for the period 850-2100 (LUH2) for CMIP6., 2020.

Ito, A., Hajima, T., Lawrence, D. M., Brovkin, V., Delire, C., Jones, C. D., Malyshev, S., Materia, S. and Mcdermid, S. P.: Soil carbon sequestration simulated in CMIP6-LUMIP models: implications for climatic mitigation OPEN ACCESS Soil carbon sequestration simulated in CMIP6-LUMIP models: implications for climatic mitigation, 2020.

Jones, C. D., Arora, V., Friedlingstein, P., Bopp, L., Brovkin, V., Dunne, J., Graven, H., Hoffman, F., Ilyina, T., John, J. G., Jung, M. and Kawamiya, M.: C4MIP – The Coupled Climate – Carbon Cycle Model Intercomparison Project: experimental protocol for CMIP6, , (1), 2853–2880, doi:10.5194/gmd-9-2853-2016, 2016.

Krinner, G., Viovy, N., de Noblet-Ducoudré, N., Ogée, J., Polcher, J., Friedlingstein, P., Ciais, P., Sitch, S. and Prentice, I. C.: A dynamic global vegetation model for studies of the coupled atmosphere-biosphere system, Global Biogeochem. Cycles, 19(1), 1–33, doi:10.1029/2003GB002199, 2005.

Lawrence, D. M., Hurtt, G. C., Arneth, A., Brovkin, V., Calvin, K. V., Jones, A. D., Jones, C. D., Lawrence, P. J., Noblet-Ducoudré, N. De, Pongratz, J., Seneviratne, S. I. and Shevliakova, E.: The Land Use Model Intercomparison Project (LUMIP) contribution to CMIP6: Rationale and experimental design, Geosci. Model Dev., 9(9), 2973–2998, doi:10.5194/gmd-9-2973-2016, 2016.

Liddicoat, S. K., Wiltshire, A. J., Jones, C. D., Arora, V. K., Brovkin, V., Cadule, P., Hajima, T., Lawrence, D. M., Pongratz, J., Schwinger, J., Séférian, R., Tjiputra, J. F. and Ziehn, T.: Compatible fossil fuel CO_2 emissions in the CMIP6 earth system models' historical and shared socioeconomic pathway experiments of the twenty-first century, J. Clim., 34(8), 2853–2875, doi:10.1175/JCLI-D-19-0991.1, 2021.

Lurton, T., Balkanski, Y., Bastrikov, V., Bekki, S., Bopp, L., Braconnot, P., Brockmann, P., Cadule, P., Contoux, C., Cozic, A., Cugnet, D., Dufresne, J. L., Éthé, C., Foujols, M. A., Ghattas, J., Hauglustaine, D., Hu, R. M., Kageyama, M., Khodri, M., Lebas, N., Levavasseur, G., Marchand, M., Ottlé, C., Peylin, P., Sima, A., Szopa, S., Thiéblemont, R., Vuichard, N. and Boucher, O.:

Implementation of the CMIP6 Forcing Data in the IPSL-CM6A-LR Model, J. Adv. Model. Earth Syst., 12(4), doi:10.1029/2019MS001940, 2020.

Monier, E., Paltsev, S., Sokolov, A., Chen, Y. H., Gao, X., Ejaz, Q., Couzo, E., Schlosser, C. A., Dutkiewicz, S., Fant, C., Scott, J., Kicklighter, D., Morris, J., Jacoby, H., Prinn, R. and Haigh, M.: multi-sectoral climate impacts, Nat. Commun., (2018), 1–8, doi:10.1038/s41467-018-02984-9, 2018.

O'Neill, B. C., Tebaldi, C., Van Vuuren, D. P., Eyring, V., Friedlingstein, P., Hurtt, G., Knutti, R., Kriegler, E., Lamarque, J. F., Lowe, J., Meehl, G. A., Moss, R., Riahi, K. and Sanderson, B. M.: The Scenario Model Intercomparison Project (ScenarioMIP) for CMIP6, Geosci. Model Dev., 9(9), 3461–3482, doi:10.5194/gmd-9-3461-2016, 2016.

Popp, A., Calvin, K., Fujimori, S., Havlik, P., Humpenöder, F., Stehfest, E., Bodirsky, B. L., Dietrich, J. P., Doelmann, J. C., Gusti, M., Hasegawa, T., Kyle, P., Obersteiner, M., Tabeau, A., Takahashi, K., Valin, H., Waldhoff, S., Weindl, I., Wise, M., Kriegler, E., Lotze-Campen, H., Fricko, O., Riahi, K. and Vuuren, D. P. va.: Land-use futures in the shared socio-economic pathways, Glob. Environ. Chang., 42, 331–345, doi:10.1016/j.gloenvcha.2016.10.002, 2017.

Riahi, K., van Vuuren, D. P., Kriegler, E., Edmonds, J., O'Neill, B. C., Fujimori, S., Bauer, N., Calvin, K., Dellink, R., Fricko, O., Lutz, W., Popp, A., Cuaresma, J. C., KC, S., Leimbach, M., Jiang, L., Kram, T., Rao, S., Emmerling, J., Ebi, K., Hasegawa, T., Havlik, P., Humpenöder, F., Da Silva, L. A., Smith, S., Stehfest, E., Bosetti, V., Eom, J., Gernaat, D., Masui, T., Rogelj, J., Strefler, J., Drouet, L., Krey, V., Luderer, G., Harmsen, M., Takahashi, K., Baumstark, L., Doelman, J. C., Kainuma, M., Klimont, Z., Marangoni, G., Lotze-Campen, H., Obersteiner, M., Tabeau, A. and Tavoni, M.: The Shared Socioeconomic Pathways and their energy, land use, and greenhouse gas emissions implications: An overview, Glob. Environ. Chang., 42, 153–168, doi:10.1016/j.gloenvcha.2016.05.009, 2017.

Seiler, C., Melton, J. R., Arora, V. K., Sitch, S., Friedlingstein, P., Anthoni, P., Goll, D., Jain, A. K., Joetzjer, E., Lienert, S., Lombardozzi, D., Luyssaert, S., Nabel, J. E. M. S., Tian, H., Vuichard, N., Walker, A. P., Yuan, W. and Zaehle, S.: Are Terrestrial Biosphere Models Fit for Simulating the Global Land Carbon Sink?, J. Adv. Model. Earth Syst., 14(5), doi:10.1029/2021MS002946, 2022.

Sinha, E., Michalak, A. M., Calvin, K. V. and Lawrence, P. J.: Societal decisions about climate mitigation will have dramatic impacts on eutrophication in the 21 st century, Nat. Commun., 10(1), doi:10.1038/s41467-019-08884-w, 2019.

Vuichard, N., Messina, P., Luyssaert, S., Guenet, B., Zaehle, S., Ghattas, J., Bastrikov, V. and Peylin,

P.: Accounting for carbon and nitrogen interactions in the global terrestrial ecosystem model ORCHIDEE (trunk version, rev 4999): multi-scale evaluation of gross primary production, Geosci. Model Dev., 12(11), 4751–4779, doi:10.5194/gmd-12-4751-2019, 2019.

Simulation	SSP								
	Hist	**1-1.9**	**1-2.6**	**2-4.5**	**3-7.0**	**4-3.4**	**4-6.0**	**5-3.4os**	**5-8.5**
Marker	-7.7	58.6	83.1	103.8	86.9	-5.6	71.0	75.8	115.5
Ndep sensitivity	/	74.1±12.2	/	/	70.7±13.6	-1.1±10.9	/	/	111.1±13.5
LUC sensitivity	/	11.66±38.1	/	/	70.4±44.5	30.0±40.3	/	/	78.9±46.2
LUC and Ndep sensitivity	/	24.9±37.2	/	/	86.5±43.6	47.1±39.3	/	/	95.7±45.3

Table 1: Change in land carbon store (PgC) for the historical period from 1850 to 2015 (Hist) and for the SSPs from 1850 to 2100 by using the marker simulation (Marker) or an ensemble of simulations (mean±sigma) with different nitrogen deposition trajectories (Ndep sensitivity), different land-use change trajectories (LUC sensitivity) or different LUC and Ndep trajectories (LUC and Ndep sensitivity).

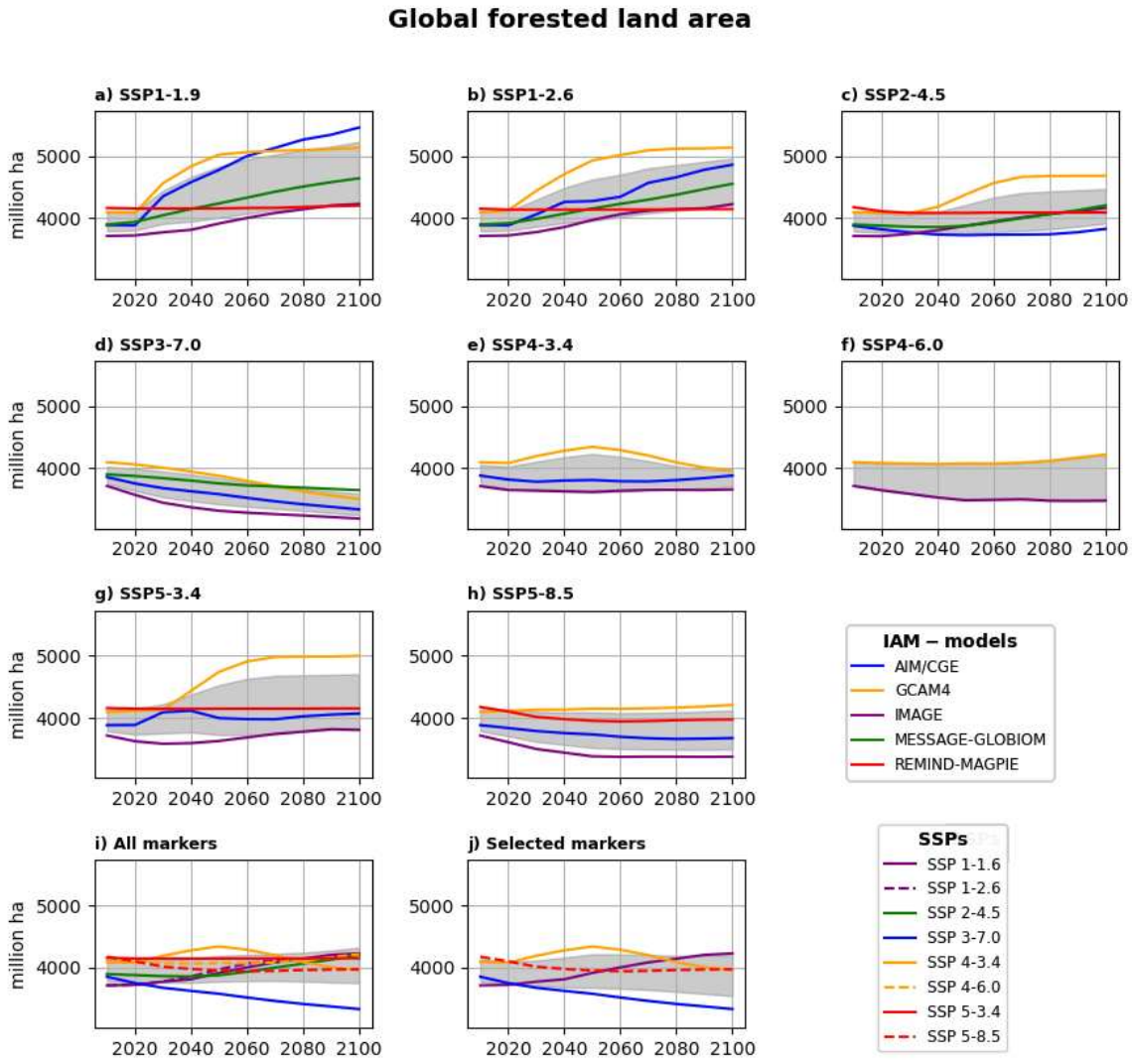

Figure 1: Time evolution (2015-2100) of the global forested land area (Mha) projected by (a to h) different Integrated Assessment Models (IAM) for different Shared Socio-economic Pathways,(i) all IAM markers and (j) the selected IAM markers.

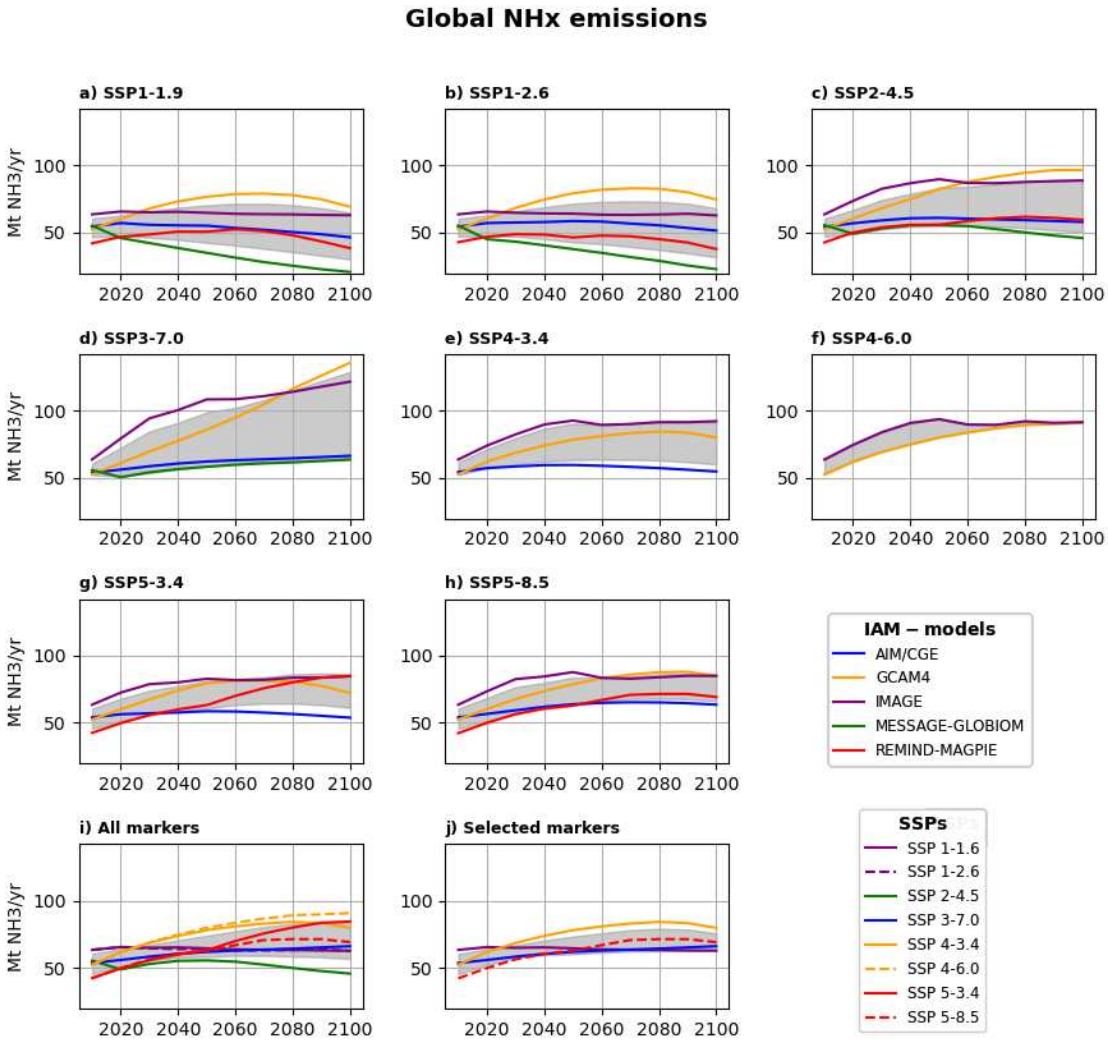

Figure 2: Time evolution (2015-2100) of the global NHx (NH_3) emissions (Mt(NH_3) yr^{-1}) projected by (a to h) different Integrated Assessment Models (IAM) for different Shared Socio-economic Pathways,(i) all IAM markers and (j) the selected IAM markers.

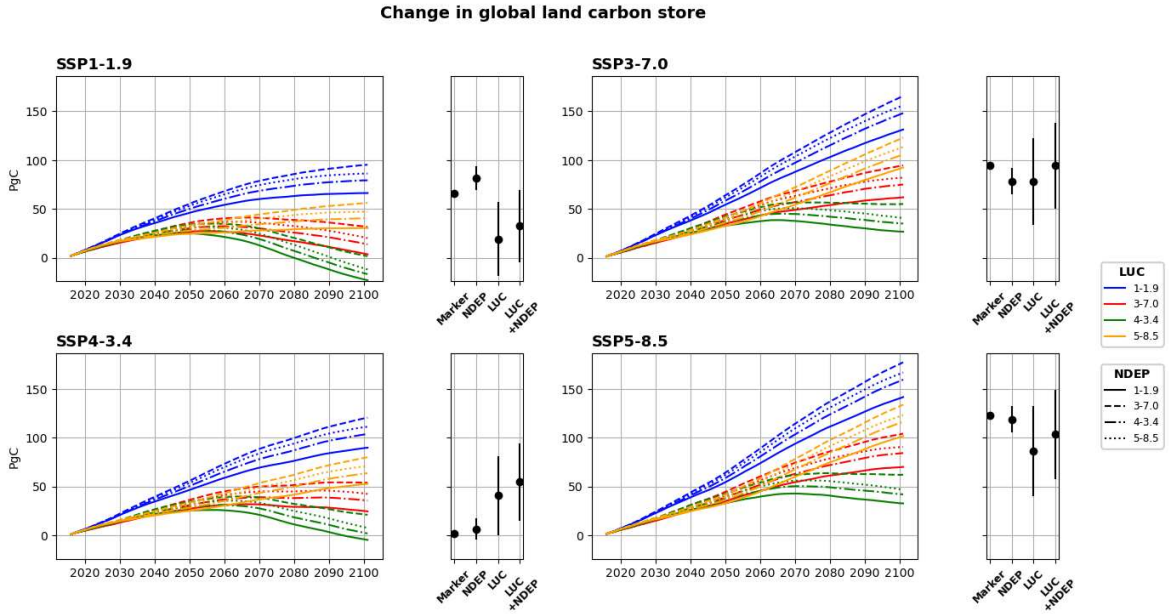

Figure 3: Time evolution (2015-2100) of the global change in land carbon store (PgC) for the historical period from 1850 to 2015 and for the SSPs from 1850 to 2100 by using the marker simulation (Marker) or an ensemble of simulations (mean±sigma) with different nitrogen deposition trajectories (Ndep sensitivity), different land-use change trajectories (LUC sensitivity) or different LUC and Ndep trajectories (LUC and Ndep sensitivity).

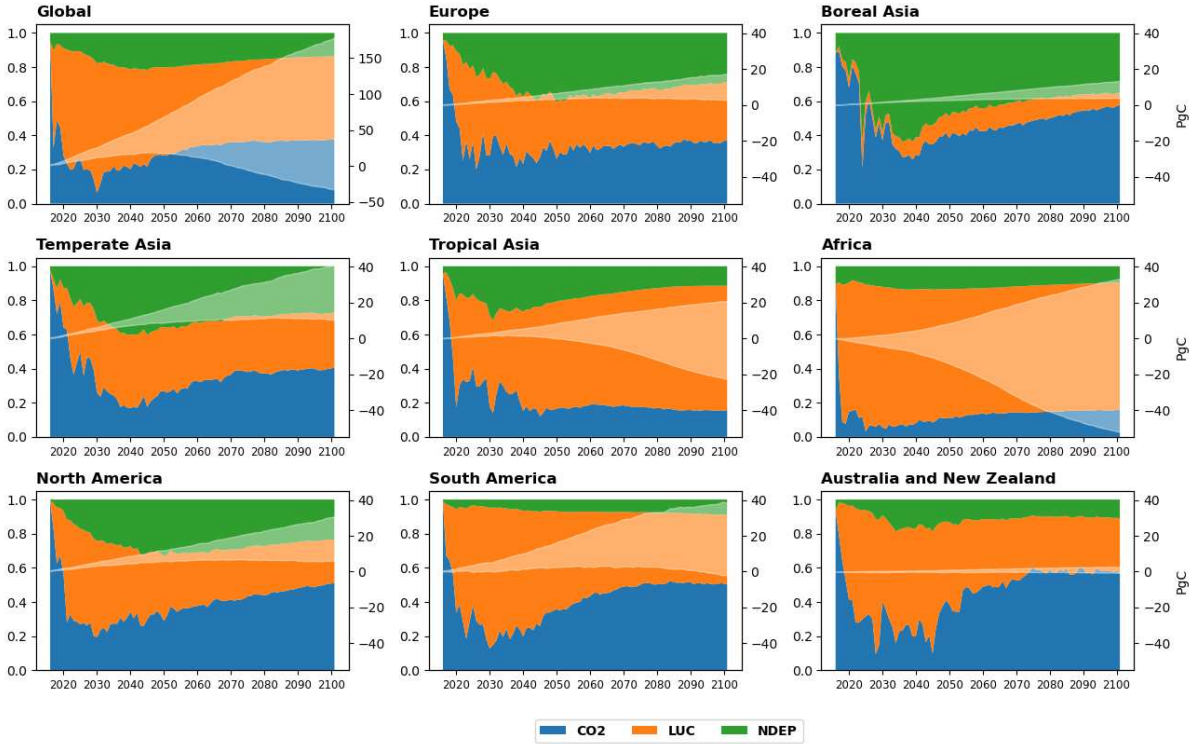

Figure 4: Time evolution (2015-2100) of the change in land carbon store accounting for uncertainty on atmospheric CO_2 (CO_2), land-use change (LUC) and atmospheric N

deposition (NDEP) trajectories (mean±sigma, in PgC, right y-axis, white area) and the relative impact on the CLCS dispersion of the three drivers (unitless, with CO_2 in blue, LUC in orange and NDEP in green).

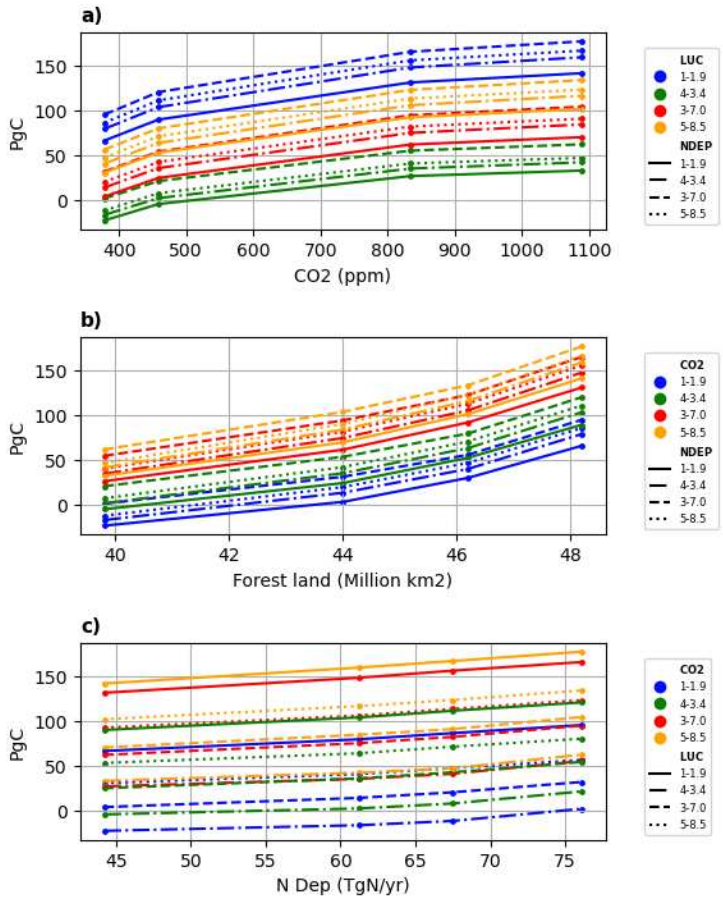

Figure 5: CLCS in 2100 as a function of one of the studied drivers (ie a) atmospheric CO_2 level for CO_2, b) Forested lands for LUC and c) Atmospheric N deposition for NDEP in 2100) for an ensemble of sixteen simulations driven by the different combinations of the two other drivers.

"*The future of carbon and nitrogen uptake is inextricably linked, as the balance between these two elements is critical for the health of ecosystems and the planet as a whole*".

Dr. Fakhri Bazzaz

CHAPTER 5

Modeling Biological Nitrogen Fixation within the global land surface model ORCHIDEE

5.1 Introduction

As previously stated, BNF was the major producer of reactive nitrogen (Nr) in terrestrial ecosystems at pre-industrial time, with approximately 58 TgN yr^{-1} (Fowler et al., 2013). Present-day global BNF best estimate amounts to 120 TgN yr^{-1}, equally shared between natural ecosystems and agricultural ones, which is equivalent to the global annual production of Nr by the Haber-Bosch process (Fowler et al., 2013, Clais et al. 2013). It plays, thus, an important role in the availability of Nr in soils and, as a consequence, on the terrestrial ecosystem carbon productivity. BNF consists in the reduction of dinitrogen (N_2) with either oxygen (O_2) or hydrogen (H) to create ammonia (NH_3) (Equation 5.1) through organic molecules that function as nitrogenases as catalysts.

$$N_2 + 8H^+ + 8\,e^- + 16\,Mg\,ATP \rightarrow 2NH_3 + H_2 + 16\,Mg\,ADP + 16\,P_i \qquad (5.1)$$

BNF is carried out by a wide range of bacteria and algae, both symbiotic and free-living (Jaffe, 2003). Free-living nitrogen fixation (FLNF) refers to nitrogen fixation by heterotrophs in the soil without direct interaction with other organisms. Some examples of this type of nitrogen-fixing bacteria include *Azotobacter*, *Bacillus*, *Clostridium*, and *Klebsiella* species. These organisms find their own energy source by oxidation of organic molecules released by other organisms or by decomposition. Some free-living organisms can use inorganic compounds as a source of energy.

On the other hand, many organisms fix nitrogen symbiotically in association with a plant host. In this case, the plant provides the energy source in the form of sugars generated through photosynthesis necessary to fix nitrogen. In return, the bacteria provide the nitrogen the plant needs to sustain its growth. Both free-living and symbiotic microorganisms are diazotrophs, meaning that they convert atmospheric nitrogen gas into a more useful form. In other words, these microorganisms can develop in the absence of fixed nitrogen sources (see Figure 5.1).

FLNF is maintained by Dissolved Organic Carbon (DOC) in the soil, a variable, and complicated C source. In contrast, symbiotic N fixers receive a continuous supply of simple C molecules (i.e., succinate) straight from the host plant. Oxygen content in the rhizosphere for FLNF organisms is changeable, influenced by soil structure and texture, as well as microbial and root respiration. Conversely, symbiotic N fixers receive low quantities of oxygen from their host plant. The diazotroph must obtain the nutrients required to promote FLNF (e.g., P, Fe, Mo, and V). The host plant, on the other hand, delivers these nutrients to symbiotic N fixers. In the rhizosphere, diazotrophs may receive N from soil and FLNF, and all symbiotically fixed N is supplied to the plant (Smercina et al., 2019).

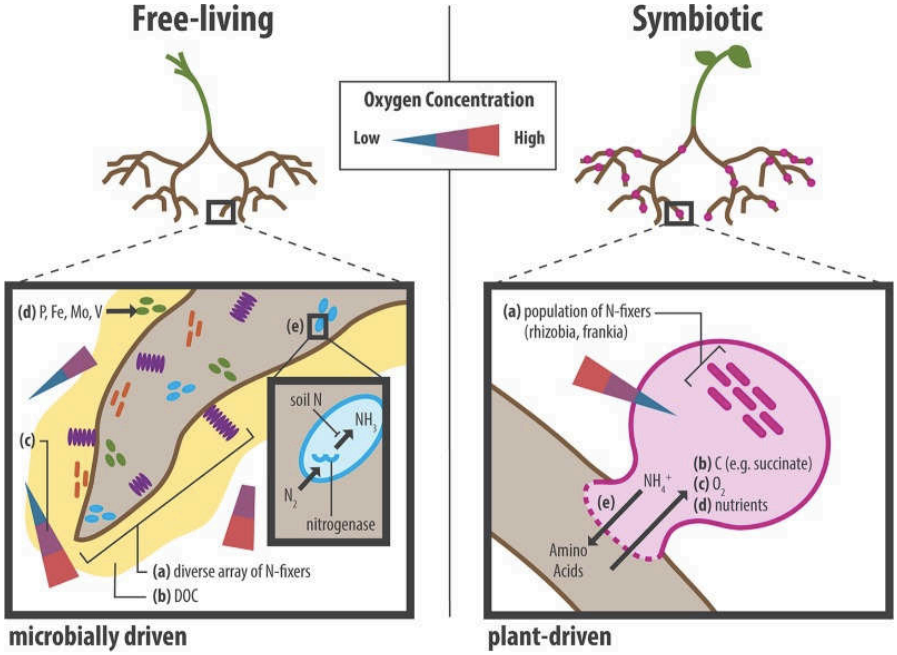

Figure 5.1 – Contrasting habitats of free-living and symbiotic nitrogen fixation.

As studied by Peters & Szilagyi. (2006), three distinct types of nitrogenase have been demonstrated to exist in diazotrophs: the Mo-nitrogenase, the V-nitrogenase, and the Fe-only nitrogenase. Despite the metal content, the three enzymes are related. Mo-nitrogenase, which can be found in legume associated *rhizobia*, is the most extensively studied and characterized.

The catalytic process caused by Mo-nitrogenase is the product of two components interacting: the iron protein (Fe protein) or dinitrogenase reductase (NifH protein), which is an ATP-dependent electron donor to the bigger heterotetrameric component (Hoffman et al., 2014), known as the molybdenum–iron (MoFe) protein or dinitrogenase that reduces N_2 to NH_3 (Mus et al., 2018) as could be seen in Figure 5.2**,** BNF requires minimally 16 magnesium ATP (MgATP), eight protons, and eight electrons (Equation 5.1) to fix one molecule of N_2.

As explained by Seefeldt et al. (2009), the Fe protein delivers electrons to the MoFe protein in a process coupled to the hydrolysis of two MgATP molecules in a three states cycle. At the time when the Fe protein binds with the two MgATP molecules it is reduced ($[4Fe\text{-}4S]^{1+}$) and temporarily associated with the MoFe protein. During this association, the two MgATP molecules are hydrolyzed into two MgADP molecules and an electron is transferred from the Fe protein group ($[4Fe\text{-}4S]^{1+}$) to the MoFe protein. The oxidized Fe protein ($[4Fe\text{-}4S]^{2+}$) with two attached MgADP molecules dissociates from the MoFe protein. The released Fe protein is then regenerated in two steps: MgADP molecules are replaced by MgATP and the $[4Fe\text{-}4S]^{2+}$ protein is reduced to the (1+) oxidation state.

$$C_2H_2 + 2e^- + 2H^+ \rightarrow C_2H_4 \tag{5.2}$$

Throughout the MoFe protein cycle as described by Kästner & Blöchl. (2005), the FeMo cofactor contained in the protein itself is successively reduced by the electron ceded during the Fe protein cycle in eight steps. When it reaches the E2 state, it uses acetylene reduction (C_2H_2) as a substrate (Equation 5.2) to oxidize the molecular nitrogen (N_2) into two molecules of ammonia (NH_3) in later stages of the cycle (E5 and E7) (see Figure 5.2).

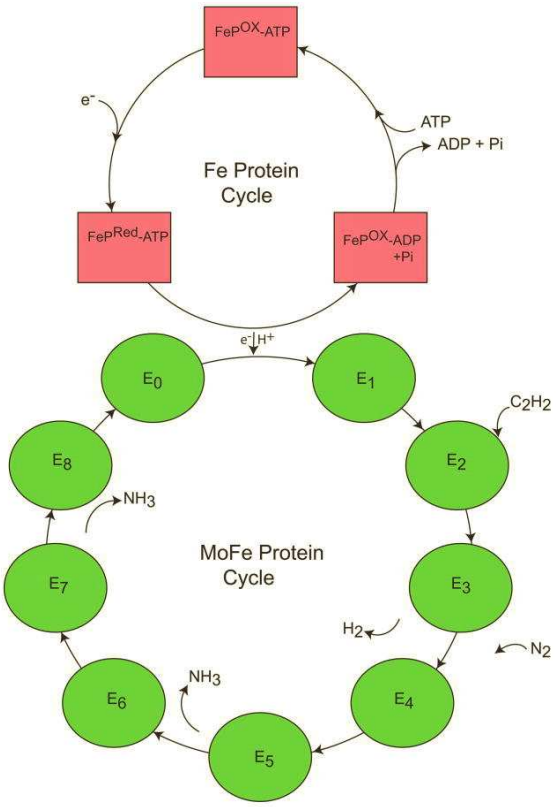

Figure 5.2 - Fe and MoFe protein catalytic cycles: three cycle states for the Fe protein (top) and eight cycle states for the MoFe protein (bottom). For the Fe protein (abbreviated FeP). The exchange of an electron occurs upon association of the Fe protein with the MoFe protein at the bottom of the cycle. In the MoFe protein cycle, the MoFe protein is successively reduced by one electron from (Seefeldt et al., 2009).

Despite the fact that the BNF is thoroughly studied at the molecular level, worldwide estimates are mostly unclear because of the difficulties in defining and quantifying the bacteria involved, as well as the restrictions of global monitoring (Vitousek et al., 2013). The fixing rate has often been measured or calculated at specific observation sites using methods such as the acetylene reduction assay method (ARA), which consists in measuring the reduction of C_2H_2 (acetylene) to C_2H_4 (ethylene) directly from nitrogenase oxidation to calculate the BNF activity (Dilworth, 1966). Such a method has been used for on-site measurements in boreal forests in Ontario, Canada (Hendrickson, 1990), Sweden (Nohrstedt, 1985) or in tropical forests in Hawaii (Ley & D'Antonio, 1998) and in Guadeloupe (Sheridan, 1991).

Another well-established method is to quantify the BNF rate by measuring the cation accumulation in a certain environment over time. It is recognized as the simplest method for calculating BNF rates. Jarrell & Virginia. (1990), used this approach to examine xeric shrubland in Arizona, while (Baker et al., 1986) used it to study temperate forests in New Zealand. Additionally, another method for calculating BNF rate is based on ^{15}N isotope data, such as in the work of (Bowman et al., 1996) for tundra in Colorado. It consists in detecting the natural ratio of nitrogen isotopes ^{15}N:^{14}N in soils and comparing the ratios of fixing and non-fixing plants (Smith et al., 2004). Overall, the ^{15}N approach is more expensive yet more trustworthy,

whereas alternative methods, such as cation buildup, do not produce accurate estimations (Davies-Barnard & Friedlingstein, 2020).

The most extensive meta-analysis of BNF rates has been established by (Davies-Barnard & Friedlingstein, 2020). It gathers 253 global measurements (47 for symbiotic BNF and 206 global measurements for free-living BNF). Measurements have been collected in boreal and temperate forests in the US (22 measurements), tropical and subtropical forests in South America and Africa (18 measurements) and few others (6 measurements) in Europe, Asia and Australia as seen in (Figure 5.3).

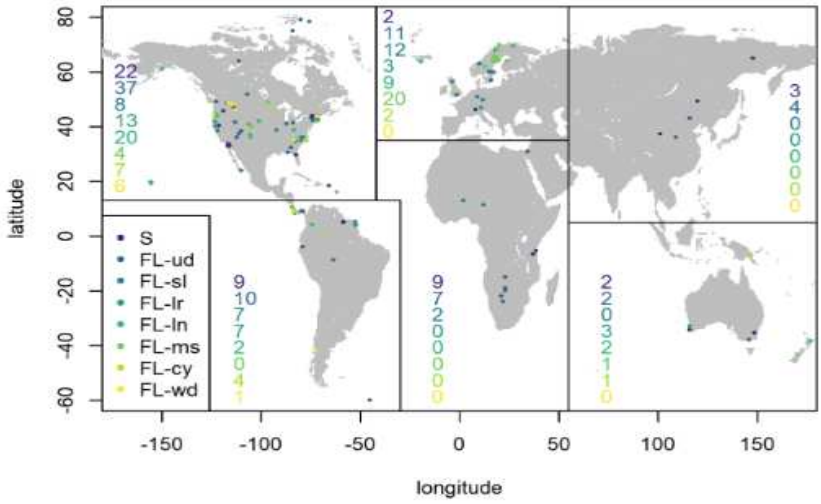

Figure 5.3 - Site location of BNF rate measurements gathered in the meta-analysis of (Davies-Barnard & Friedlingstein, 2020) for symbiotic (S) and different types of free-living (FL) organisms.

To quantify the BNF rate at the global scale, mechanistic models have been developed. The most often used approach for calculating terrestrial BNF includes the use of proxy variables, as demonstrated in the pioneering work of (Cleveland et al., 1999). In this study, the BNF fixation rate is determined using a simple linear regression of evapotranspiration fitted to few observation data. The relationship is based on observations (rather than a process knowledge) with greater BNF rates in humid environments with high evapotranspiration. Cleveland et al. (1999), proposed the following equation with BNF is expressed in gN m^{-2} yr^{-1} and the evapotranspiration rate (ET) in cm yr^{-1} (Equation 5.3):

$$BNF = 0.006 * (ET - 40) \quad (5.3)$$

The time-invariant BNF rate forcing used by ORCHIDEE-v3 by default, is based on the relationship with ET proposed by Clevelland et al. (1999) (see Chapter 2) (Equation 5.4). This implementation relies on the evapotranspiration simulated by a former version of ORCHIDEE for pre-industrial time to derive a constant BNF value of 83.4 TgN yr^{-1} (Figure 5.4) used for all current simulations of the coupled carbon-nitrogen version (Zaehle & Friend, 2010).

$$BNF = 0.1 * (0.0234 * ET + 0.172) \quad (5.4)$$

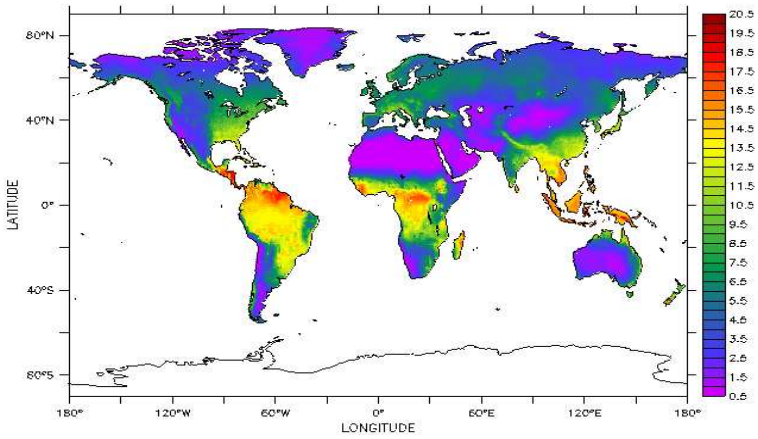

Figure 5.4 - Current BNF map for ORCHIDEE in kgN $ha^{-1}yr^{-1}$.

The second relationship proposed by (Cleveland et al., 1999) relates the BNF rate in gN m^{-2} yr^{-1} to the Net Primary Productivity (NPP in gC m^{-2} yr^{-1}) (Equation 5.5):

$$BNF_{NPP} = 1.8\,(1 - e^{-0.003*NPP})/(86400 * 365) \quad (5.5)$$

This method is used by the Community Land Model (CLM4.5), the land component of the Community Earth System Model (CESM) (Wieder et al., 2015). In a study[4] using the CLM4.5 model, when including the NPP-BNF relationship (Equation 5.5) the global BNF totaled 90 TgN yr^{-1} (Figure 5.5a), whereas when implementing the evapotranspiration ET-BNF relationship (Equation 5.4) the result totaled 77 TgN yr^{-1} (Figure 5.5b) for the 1990-2000 period.

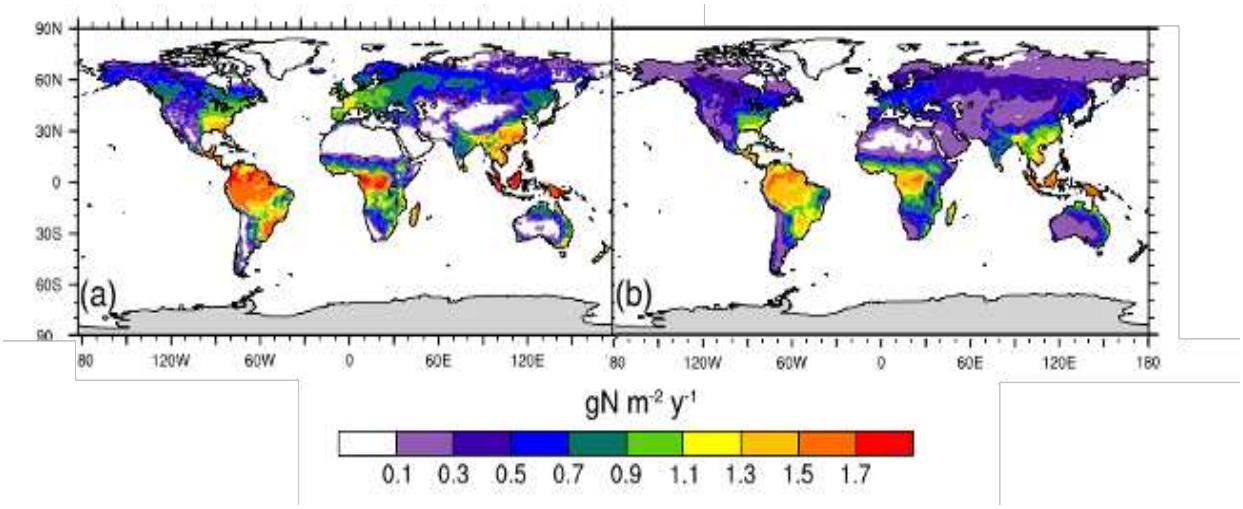

Figure 5.5 - Results for modeled BNF in (gN m^{-2} yr^{-1}) for (a) CLM4.5 using the standard NPP structure, (b) CLM4.5 using the standard evapotranspiration structure and (Wieder et al., 2015).

[4] The forcings used for this study were 1900–1919 meteorology and 1850 [CO2], N deposition, and land cover.

Some other models use a process-based approach, as the CASA-CNP model (Bai & Houlton, 2009). It estimates global rates of free-living and symbiotic BNF by taking into account light availability, nitrogen and phosphorus supply and demand, as well as presumed nitrogen fixer abundance (Wang & Houlton, 2009). This model yielded to a global BNF rate of 142 TgN yr^{-1} for the same time period with a spatial pattern that indicates higher responses in tropical zones compared to the CLM-ET and CLM-NPP implementation (Figure 5.6).

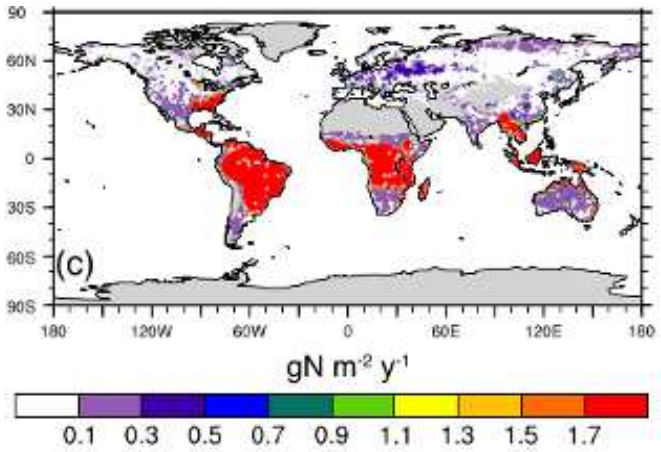

Figure 5.6 - Results for modeled BNF in (gN m-2 yr-1) for CASA-CNP using a process-based approach including light availability, N and phosphorus (P) supply and demand from (Wieder et al., 2015).

Another processed-based approach is the one of the recent model of (Yu & Zhuang, 2020). It is based on ecosystems' maximal fixating potentials corrected by a set of environmental parameters such as nitrogen and carbon soil content, soil water content, and soil temperature (Figure 5.7). For the 1990-2000 decade, the model calculated worldwide nitrogen fixation in terrestrial ecosystems to be 61.5 Tg N yr^{-1} (Yu & Zhuang, 2020) with a very good agreement to precedent model responses.

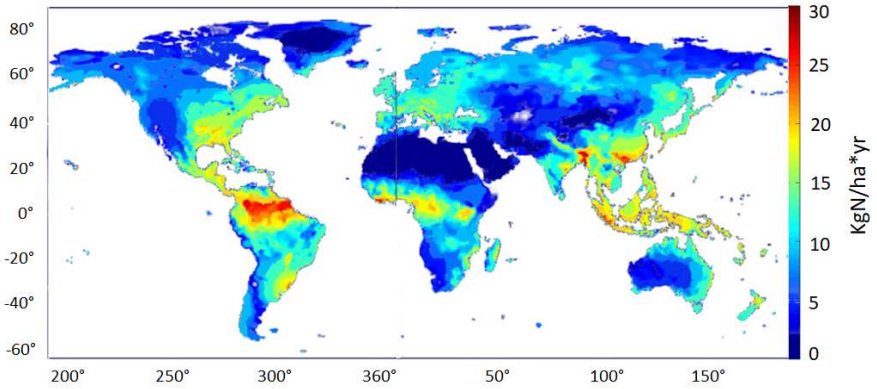

Figure 5.7 - Results from Yu and Zhuang simulated spatial distribution of BNF (kg N 2 ha −1 yr −1) in natural terrestrial ecosystems from 1990 to 2000 by considering the BNF effects (Yu & Zhuang, 2020).

A recent study from (Davies-Barnard & Friedlingstein, 2020) estimated total BNF at global scale at a value of 88 TgN yr^{-1} with a range of 52-120 TgN yr^{-1} (with at least one-third of BNF is

derived from free living sources) from an upscale enhanced biome approach that uses land cover groupings based only on measured data. This bottom-up estimate supports prior approaches, which indicate a similarly low estimate of BNF. A meta-analysis conducted in the same study, showed a large variability among the overall BNF values obtained for 12 different models, and revealed that there is no statistically significant link with variables such as evapotranspiration and BNF, invalidating global estimates such as (Cleveland et al., 1999) and (Cleveland et al., 2013), and thus overruling the current approach from an important set of models, including ORCHIDEE.

Because the nitrogen cycle limits the carbon cycle, it is critical to reduce the uncertainty associated with modeling key processes such as the BNF (Peng et al., 2020), allowing for more accurate estimates of carbon fluxes, all of which is critical for future and current understanding of the changing climate. For this purpose, the Y&Z model was implemented in ORCHIDEE, owing to the facility for collecting environmental data for computing the environmental factors as well as a straightforward correspondence between ecosystem classification and BNF potentials between models.

The model response was fine-tuned in two steps: 1) modifying the BNF potential correspondence by trial and error, and 2) calibrating the most relevant environmental parameters to get a spatial pattern as near to the Y&Z as possible. Once our model approximated the Y&Z model, it was dynamically implemented in ORCHIDEE, implying complete interaction between carbon and nitrogen pools. This new approach was used to examine the differences in carbon fluxes outputs for both the historical period (1850-2015) and future estimates (2015-2100).

5.2 BNF model from Yu and Zhuang (Y&Z model).

5.2.1 Y&Z model description

Yu and Zhuang. (2020) developed a process-based model to quantitatively estimate the global nitrogen fixation rate (Nfix, gN $m^{-2}yr^{-1}$) by symbiotic organisms in natural environments. The model is based on a maximum potential rate (Nfix pot, gN $m^{-2}yr^{-1}$) defined for each of the main ecosystems over the globe, and accounts for the impact of key environmental variables such as temperature and water availability which inhibit the development and functioning of free-living and symbiotic microorganisms, and hence the BNF (Lindemann, 2008). The equation defining the nitrogen fixation rate in a given gridcell for a given ecosystem is the following (Equation 5.6):

$$N_{fix} = N_{fix\,pot} * f_T * f_W * f_N * f_C \quad (5.6)$$

where f_T, f_W, f_N and f_C are the set of environmental factors (unitless) for respectively soil temperature, available soil water, soil nitrogen and soil carbon content. BNF rates were calibrated using 35 site-level observations and then extrapolated to an ecosystem for seven key ecosystem types throughout the world. The different environmental factors which control the BNF rate (Nfix) are detailed below.

Soil temperature factor:

Previous research from (Wu & McGechan, 1998; Yu & Zhuang, 2020) have revealed that the relationship between BNF and temperature is not strictly a Gaussian distribution. In the model, the optimal temperature for BNF is defined for each ecosystem with a bottom optimal temperature $t_{opt\ L}$ and top optimal temperature $t_{opt\ H}$ (see Table 5.1). The minimum and maximum temperatures for BNF activity are within a limited range of temperatures for all the ecosystems (t_{min} from 0°-2.5°C and t_{max} from 42.5°-45°C). The soil temperature factor is defined by the following equation where t is the soil temperature (°C) (see Figure 5.8 and Equation 5.7):

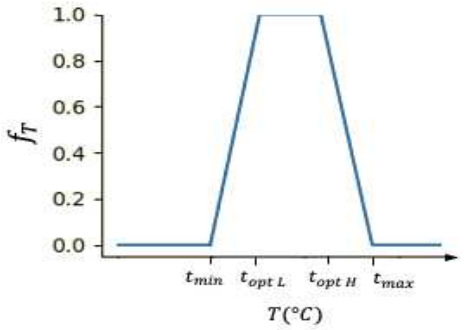

$$ft\begin{cases} 0\ when\ (t\ <t_{min}\ or\ t\ >\ t_{max}) \\ \dfrac{(t-t_{min})}{(t_{opt\ L}-t_{min})}\quad when\ (t_{min}\ \leq\ t<\ t_{opt\ L}) \\ 1\ when\ (t_{opt\ L}\ \leq\ t\ \leq\ t_{opt\ H}) \\ \dfrac{(t_{max}-t)}{(t_{max}-t_{opt\ H})}\quad when\ (t_{opt\ H}\ \leq\ t<\ t_{max}) \end{cases} \tag{5.7}$$

Figure 5.8 - Soil temperature factor (f_T) dependence on soil temperature (T) (°C) adapted from (Yu & Zhuang, 2020).

Available soil water factor:

Soil water is a major factor controlling BNF (Srivastava & Ambasht, 1993) since water shortfall inhibits nitrogen fixation due to drought stress and oxygen deficit (Marino et al., 2007) (See Figure 5.9 and Equation 5.8):

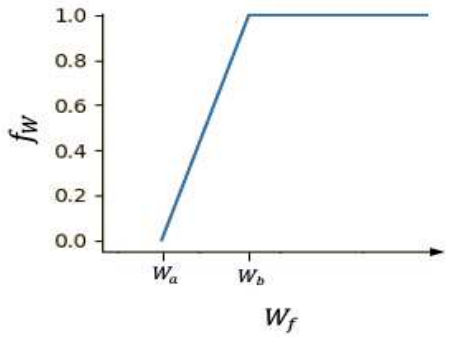

$$f_W\begin{cases} 0\ when\ (W_f\ \leq\ W_a\ ) \\ \dfrac{(W_f-W_a)}{(W_b-W_a)}\quad when\ (W_a<\ W_f<\ W_b) \\ 1\ when\ (W_f\ \geq\ W_b\ ) \end{cases} \tag{5.8}$$

Figure 5.9 - Available soil water factor (f_W) dependence on the ratio between soil water content and soil water at the field capacity (W_f) (unitless) adapted from (Yu & Zhuang, 2020).

Where W_f (unitless) is the relative soil water content, defined as the ratio of water content to that at the field capacity (unitless), W_a (unitless) the available water bottom threshold below which nitrogen fixation is totally inhibited by soil moisture (set to 0) and W_b (unitless) the available water upper threshold above which nitrogen fixation is not limited by soil moisture (set to 0.5) .

Soil nitrogen factor:

Nitrogen content in soils is also assumed to modulate BNF rate. When nitrogen is in excess, BNF is inhibited (Vitousek et al., 2013). The soil nitrogen content factor (fN) (See Figure 5.10 and Equation 5.9):

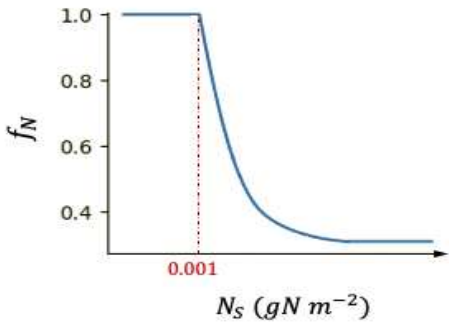

$$f_N \begin{cases} 1 - f_{Nup} * \ln(1000 - N_s)\ \boldsymbol{when}\ (N_s \geq 0.001) \\ 1\ \boldsymbol{when}\ (N_s < 0.001) \end{cases} \quad (5.9)$$

Figure 5.10 - Soil nitrogen factor (f_N) dependence on soil nitrogen content (N_s) (gN m^{-2}). Plants would uptake directly the nitrogen from the soil without the intermediate fixing microorganisms if there is abundant nitrogen (more than 0.001 gN m^{-2} which corresponds to the dashed red line). Adapted from (Yu & Zhuang, 2020).

Where N_s (gN m^{-2}) is the soil nitrogen content and f_{Nup} (unitless) is an ecosystem-dependent model parameter reflecting the sensitivity of BNF to N_s (see Table 5.1).

Soil carbon factor:

Nitrogen fixers get carbohydrates from plants. Every unit of fixed nitrogen depletes an amount of carbon, and so the lack of carbon constrains the fixation. The carbon requirement differs widely on environmental conditions and ecosystem types. The carbon effect (fC) is modeled following a Michaelis–Menten equation: (Boote et al., 1998) (See Figure 5.11 and Equation 5.10):

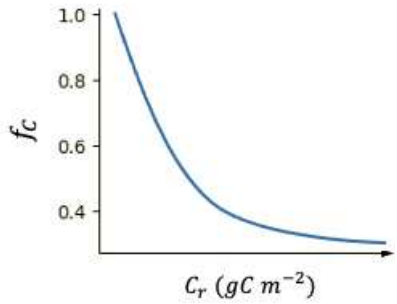

$$f_C = 1 + \left(\frac{K_C}{C_r}\right) \quad (5.10)$$

Figure 5.11 - Soil carbon factor (f_C) dependence on soil carbon content (C_r) (gC m^{-2}) adapted from (Yu & Zhuang, 2020).

Where C_r is the soil carbon content (gC m^{-2}) and K_c the Michaelis–Menten constant, which is plant species dependent and so varies by ecosystem (Yu & Zhuang, 2020) see Table 5.1.

5.2.2 Y&Z model: ecosystem dependent parameters

The classification of land cover and leguminous major ecosystems used by (Yu & Zhuang, 2020) derived from the combination of the International Geosphere and Biosphere (IGP) land cover classification system and the study of (Schrire et al., 2005). For each one of the 11 categories of ecosystem, ecosystem-specific parameter values are set to compute the environmental factors, as seen in Table 5.1.

Biome	*N pot* (gN/m^2*day)	*t optL* (°C)	*t optH* (°C)	*W upH* (J kg −1)	*f Nup*	*Kc* (g C m−2)
1. Wet tundra	0,00028	10	25	0,8	65	0,002
2. Alpine tundra and wet tundra	0,00028	10	25	0,8	65	0,002
3. Boreal forest	0,0012	12	25	0,8	70	0,008
4. Temperate coniferous forest	0,0055	16	35	0,6	80	0,01
5. Temperate deciduous forest	0,0055	18	35	0,6	80	0,01
6. Temperate evergreen forest	0,0055	18	35	0,6	80	0,01
7. Grassland	0,0005	18	35	0,5	60	0,012
8. Tropical forest	0,008	20	35	0,8	100	0,005
9. Xeric shrubland	0,007	15	35	0,4	65	0,016
10. Mediterranean shrubland	0,0008	19	35	0,5	65	0,016
11. Savanna	0,0005	20	35	0,5	60	0,012

Table 5.1 - Model parameters for various natural terrestrial ecosystems from the International Geosphere and Biosphere (IGP) land cover classification system from (Yu & Zhuang, 2020).

Historical Climate data was retrieved from the Climate Research Unit (CRU) (Mitchell & Jones, 2005). Other model parameters such as soil temperature (°C), and soil carbon (gC $m^{-2}yr^{-1}$) and soil nitrogen (gN $m^{-2}yr^{-1}$) contents were obtained from the Terrestrial Ecosystem Model – TEM (Chen & Zhuang, 2013) and (Zhuang et al., 2012).

5.2.3 Y&Z model results: BNF spatial variability

Y&Z model results in nearly half of the global BNF supplied by tropical forests and xeric shrubland. Low nitrogen fixation rates are found in high latitudes of eastern China, North America and Europe, mainly covered with temperate forests (**figure 5**). Compared to tropical areas, nitrogen fixation in temperate regions shows a larger variability depending on vegetation types. This spatial variation is partly explained by the distribution of legume plants (Yu & Zhuang, 2020), and by the difference in humidity and temperature conditions.

Most specifically, the model estimates that tropical forests have the highest fixation rate among all ecosystem types (Yu & Zhuang, 2020) with an average value of 18.2 kgN $ha^{-1}yr^{-1}$ which decreases from the Equator to the polar regions. This is then followed by temperate forests with an average BNF rate of 12.7 kgN $ha^{-1}yr^{-1}$. The Savanna ecosystems of the African

continent, Australia and large areas of South America have a mean fixation rate of 1.9 kgN $ha^{-1}yr^{-1}$, a much smaller rate compared to tropical forest and temperate ecosystems. Last, boreal ecosystem BNF rate averages 5.5 kgN $ha^{-1}yr^{-1}$ (from both tundra and boreal ecosystems). Overall, the Y&Z BNF model exhibits a strong spatial variability with low temperature and permafrost conditions limiting the activity of nitrogen fixers (Alexander & Bilington, 1986).

The Y&Z model response is comparable to the measured data (as listed in the introduction) for all major ecosystems with a mean coefficient of determination (R2) of 0.44 and a slope of 0.46 (Yu & Zhuang, 2020). By removing the outliers of observational data, the slope of regression increases up to 0.72. As shown by (Yu & Zhuang, 2020) soil temperature, rather than soil moisture and nutrient content, is the most dominant factor in controlling N_2 fixation in the Y&Z model.

5.3 Adaptation of the Y&Z model for ORCHIDEE

The adaptation of the Y&Z model in ORCHIDEE was carried out through three critical steps.

- **Step 1:** The Y&Z model classifies ecosystems differently from the ORCHIDEE model. ORCHIDEE defines 15 Plant Functional Types (PFTs) based on a conventional land surface classification, see for instance (Poulter et al., 2015). To do this, the ORCHIDEE PFTs were linked to those of the Y&Z main ecosystem model in order to specify a priori values for each model parameter.
- **Step 2**: Y&Z model is then applied on a monthly basis using the soil temperature, soil moisture, soil carbon and nitrogen stocks simulated by ORCHIDEE-v3 with the fixed BNF scheme over the period 1990-200, instead of those used in the original study of Yu and Zhuang (2020).
- **Step 3**: Based on the results obtained in Step 2, the potential N fixing rate and the parameters of environmental factors functions were adjusted to obtain a model result as close as those obtained by Yu and Zhuang (2020). We followed such an approach given that the results of Yu and Zhuang (2020) have already been evaluated against observations.

During this adaptation stage, the BNF was calculated off-line (ie. Out of ORCHIDEE), only using the values provided by ORCHIDEE for carbon and nitrogen contents and environmental conditions, with no interaction between the computed BNF and the other components of the ORCHIDEE model. To do so, I developed a Python version of the Y&Z model.

5.3.1 Correspondence between ORCHIDEE's PFTs and Y&Z ecosystem classification and first simulations

In ORCHIDEE, the land cover classification is based on the concept of Plant Functional Types (PFTs) with 15 classes (Table 5.2). The Y&Z major ecosystem classification was associated with ORCHIDEE PFTs categories based on common morphological characteristics and climate. Doing so, as can be seen in (Table 5.2), each ORCHIDEE PFT inherited the values for each variable necessary to run the model (N_{pot}, t_{optL}, t_{optH}, f_{Nup} and K_c). It is important to note that the correspondence and modeled BNF is done only for natural PFTs (or unmanaged lands) which excludes croplands.

PFT\Y&Z class.	1. Wet tundra	2. Alpine tundra and wet tundra	3. Boreal forest	4. Temperate coniferous forest	5. Temperate deciduous forest	6. Temperate evergreen forest	7. Grassland	8. Tropical forest	9. Xeric shrubland	10. Mediterranean shrubland	11. Savanna
1. Bare soil											
2. Tropical broad-leaved evergreen								X			
3. Tropical broad-leaved raingreen								X			
4. Temperate needleleaf evergreen				X							
5. Temperate broad-leaved evergreen						X					
6. Temperate broad-leaved summergreen					X						
7. Boreal needleleaf evergreen			X								
8. Boreal broad-leaved summergreen			X								
9. Boreal needleleaf deciduos			X								
10. Temparate natural (C3)							X				
11. Natural grassland (C4)							X				
12. Crops (C3)											
13. Crops (C4)											
14. Tropical Natural Grassland (C3)											X
15. Boreal Natural Grassland (C3)		X									

Table 5.2 - Equivalences from (Yu & Zhuang, 2020) major ecosystem classification into ORCHIDEE PFTs. Both crops and bare soil PFTs in ORCHIDEE are not included since the model is only used in natural lands.

When simulating the BNF with the ORCHIDEE climate, environmental data and PFT correspondences for the same decade (1990-2000) we obtained a BNF for natural lands of 74.2 TgN yr^{-1}, meaning a difference of almost 13 TgN yr^{-1} with the original Y&Z model. Most specifically, and as expected from optimal environmental factors (closer to one), the highest BNF was modeled in tropical ecosystems with 53 TgN yr^{-1}, almost 20 TgN yr^{-1} bigger than the original model. As could be seen in Figure 5.12, there is a larger distribution of the high-end range BNF values in Africa and Indonesia and the Amazonas, explaining this big gap between model responses.

This value was followed by temperate ecosystems with a BNF or 17.1 TgN yr^{-1}, showing a similar response covered by the ranges of the original model of 19.1 TgN yr^{-1}, but with a weaker response in the east coast of the United States, in Europe and in the east of China. For

the boreal ecosystems the estimated mean BNF rate was 2.4 TgN yr^{-1} (with an environmental factor correction ranging from 0.4 to 0.6) over the original BNF of 4.5 TgN yr^{-1}, this means that the modeled value is almost half as expected. In general, for this zone to have such a response, the potential should be significantly bigger, since factors such as soil temperature in effect reduce the response in these cold ecosystems.

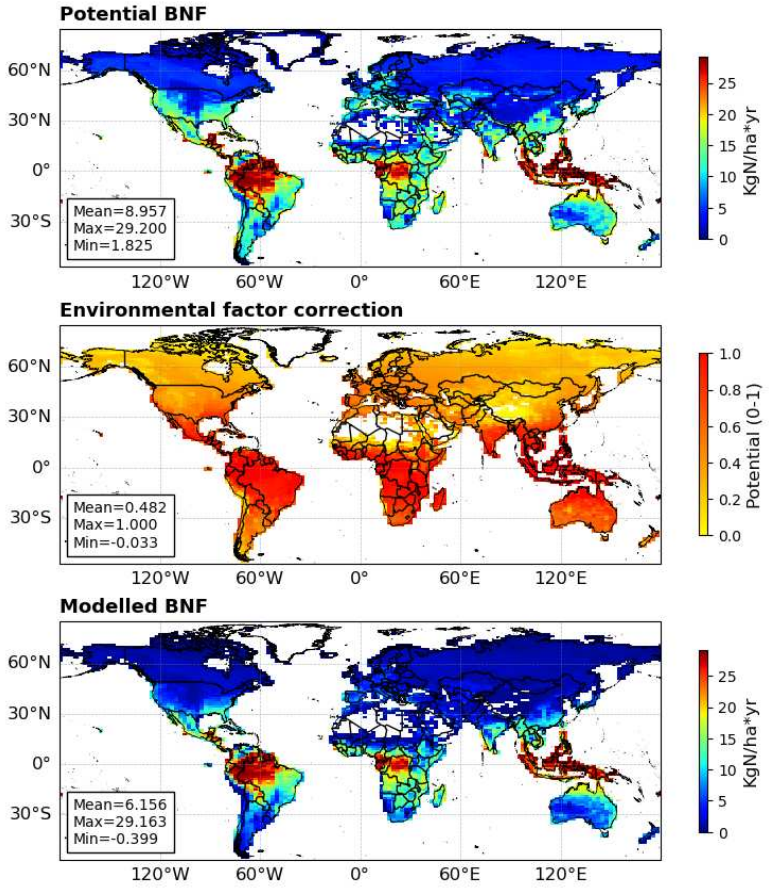

Figure 5.12 - Implementation of BNF with ORCHIDEE climate and environmental conditions for the period 1999-2000: a) potential BNF rate (kgN m^{-2} yr^{-1}), b) The environmental factor correction or (f_N*f_C*f_W*f_T) (0-1) and c) the modeled BNF (kgN m^{-2} yr^{-1}).

Figure 5.13, shows that the global mean of the soil available water factors is relatively high with 0.69, 0.68 and 0.68 respectively, while the soil temperature factor is 0.39, which is the most limiting factor as explained by (Yu & Zhuang, 2020). For tropical ecosystems (overestimation), it can be seen that all the factors are close to 1, while for boreal ecosystems the response is very high for the available soil water and carbon and nitrogen soil contents factors (from 0.8 to 1) and the limiting factor is soil temperature with a mean value of 0.2 to 0.4. This gives us an idea of which variables and parameters need to be adjusted in order to have an overall response more in line with current estimates.

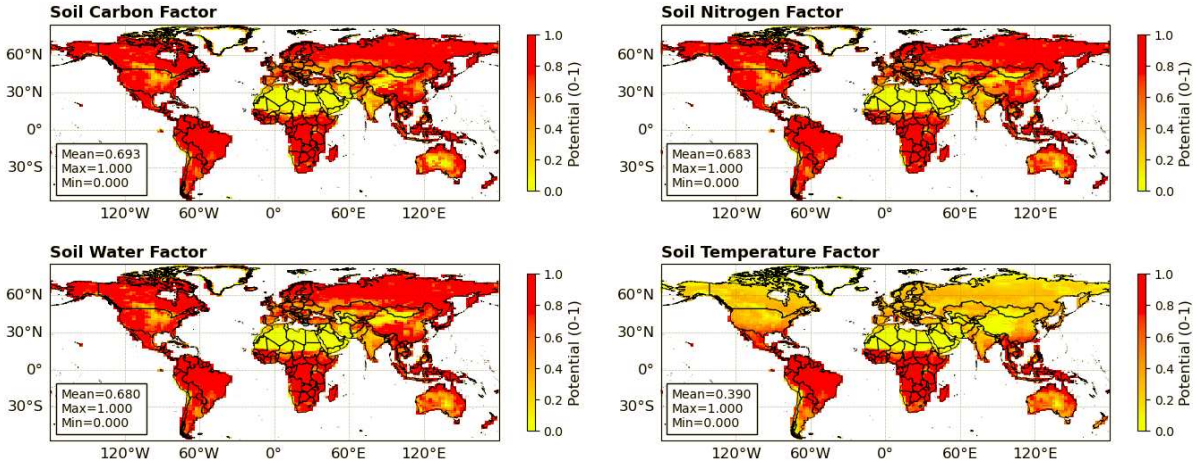

Figure 5.13 - Environmental factor responses for the 1990-2000 implementation with ORCHIDEEs climate and environmental data and PFTs correspondence for a) soil carbon factor, b) soil nitrogen factor, c) soil water factor and d) soil temperature factor.

5.3.2 Adjustment of the environmental factors and BNF potentials

From the above analysis, we thus choose to calibrate the two most limiting environmental factors, the nitrogen content and the soil temperature factors following three main axes:

- **Step 1:** The increase in the response for the soil temperature factor that reduces the response in temperate and boreal zones.
- **Step 2:** The decrease in the response for tropical zones for the soil nitrogen content factor.
- **Step 3:** The adjustment of potentials for boreal and temperate PFTs.

The adjustments on the soil temperature factor consisted in decreasing the minimum temperature from 2.5°C to 0°C, to encompass a larger area in cold regions of boreal and temperate ecosystems with temperatures below 2.5°C and above 0°C. On the optimal minimum and optimal maximum temperature for each ecosystem, since these values physically limit the BNF, there is not a very important calibration margin, and the values were kept untouched.

On the other hand, for the overestimation in the Congolese, Indonesian and Amazonian tropical forest regions, the calibration consisted in the creation of an intermediate variable ($N_{Threshold\ PFT}$ on Table 5.3) to reduce the response of the nitrogen factor and so reduce the overall reply of the environmental factors. The nitrogen factor correction consists in a formula derived from the model SOILN (Macduff et al., 1996) in which the nitrogen concentration decreases logarithmically with regards to the nitrogen fixation (see Figure 5.14). This means that for small concentrations of soil nitrogen, the biological fixation will be more relevant since there is no other source of the mineral. On the contrary, for high nitrogen concentration, the role of BNF is smaller since it is more energy carbon efficient for plants to take it directly from soils and not through BNF.

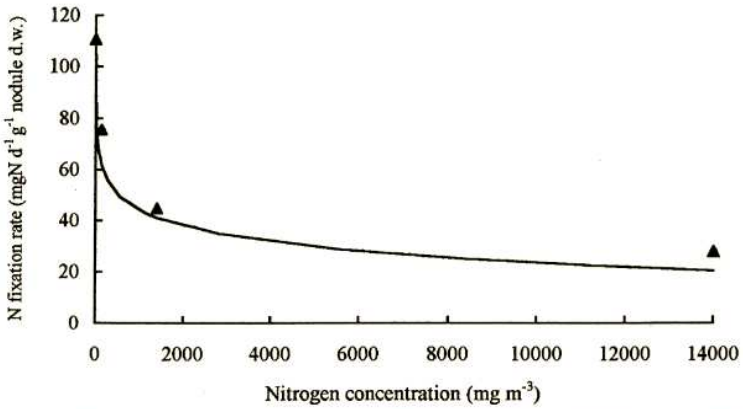

Figure 5.14 - Comparison of N_2 fixation rate with nitrogen concentration in soil. (Simulated; m, measured.) Data source: (Macduff et al., 1996).

In the adaptation of the soil nitrogen factor, given values are forced for each PFT ($N_{Threshold\ PFT}$). Below these values the factor response is equal to 1, thus indicating a high BNF or potential equal to modeled (see Figure 5.15 and Equation 5.11). In this way, for tropical PFTs, a relatively low value of $N_{Threshold\ PFT}$ as seen in (Table 5.3) was forced to decrease the factor response. Since tropical soils have a high nitrogen concentration (Liu et al., 2013), the factor response for tropical ecosystems would for most cases yield a value on the logarithmic curve (less than 1), reducing the maximum values in the zones described previously thus mimicking a behavior closer to the original model.

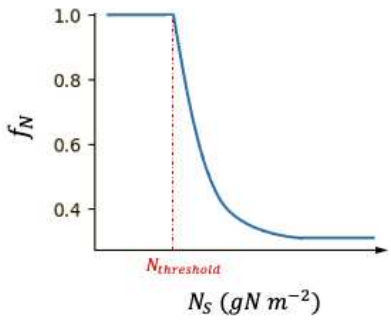

$$f_N \begin{cases} 1 - f_{Nup} * ln\,(1000 - N_s)\ \textbf{when}\ (N_s \geq N_{thresholdPFT}) \\ 1\ \textbf{when}\ (N_s < N_{thresholdPFT}) \end{cases} \quad (5.11)$$

Figure 5.15 - Soil nitrogen factor (f_N) dependence on soil nitrogen content (N_s) (gN m^{-2}) including the nitrogen threshold parameter (gN m^{-2}) in a dashed red vertical line. Adapted from (Yu & Zhuang, 2020).

The last calibration consisted of adjusting the potentials. As has already been discussed, the response values for certain ecosystems (specifically temperate and boreal ecosystems) is sometimes higher than the potential reported, representing a big incongruence, permitting us to adjust them for having a similar spatial outcome. The adjusted potentials can be seen in updated (Table 5.3).

	Plant Functional Type	*N pot* (gN/m^2*day)	*t optL* (°C)	*t optH* (°C)	*W upH* (J kg −1)	*f Nup*	*Kc* (g C m −2)	*N threshold* (gN/m^2)
1.	Bare soil	0	0	0	0	0	0	**0**
2.	Tropical broad-leaved evergreen	0,008	20	35	0,8	100	0,005	**0,1**
3.	Tropical broad-leaved raingreen	0,008	20	35	0,8	100	0,005	**0,4**
4.	Temperate needleleaf evergreen	**0,007**	16	35	0,6	80	0,01	**1,5**
5.	Temperate broad-leaved evergreen	**0,007**	18	35	0,6	80	0,01	**1,5**
6.	Temperate broad-leaved summergreen	**0,007**	18	35	0,6	80	0,01	**1,5**
7.	Boreal needleleaf evergreen	**0,0055**	12	25	0,8	70	0,008	**1,75**
8.	Boreal broad-leaved summergreen	**0,0055**	12	25	0,8	70	0,008	**1,75**
9.	Boreal needleleaf deciduos	**0,0055**	12	25	0,8	70	0,008	**1,75**
10.	Temparate natural (C3)	**0,00175**	18	35	0,5	60	0,012	**1,5**
11.	Natural grassland (C4)	0,0005	20	35	0,5	60	0,012	**1**
14.	Tropical Natural Grassland (C3)	0,0005	20	35	0,5	60	0,012	**1**
15.	Boreal Natural Grassland (C3)	**0,00175**	10	25	0,8	65	0,002	**1,75**

Table 5.3 - Calibrated nitrogen potential (bold) and inclusion of Nitrogen threshold parameter (bold).

As could be seen in Figure 5.16**,** after the calibration there is an increase in the response ranges for boreal and temperate areas for the soil temperature factor (from 0.390 to 0.404) and a decrease in the global response for the soil nitrogen content (from 0.68 to 0.66) resulting from the regional reduction of approximately 0.25 in the tropical regions of Amazonas, the Congolese tropical forest and Indonesia.

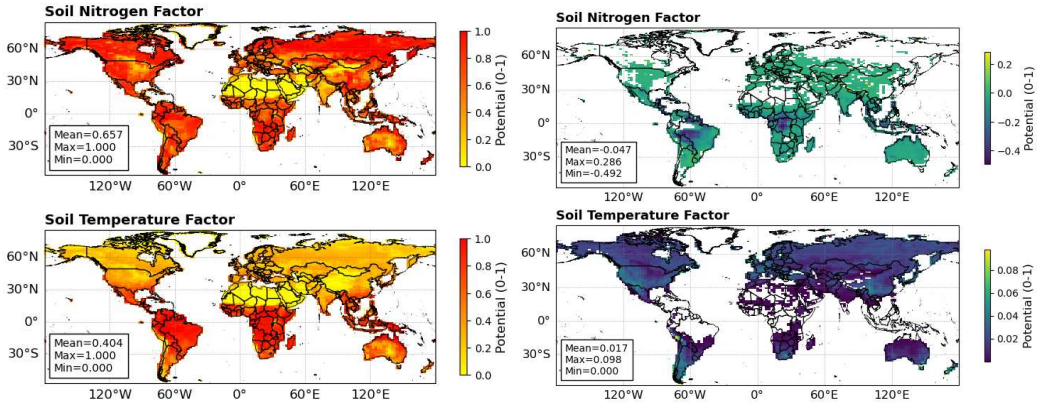

Figure 5.16 - Environmental factors as implemented in ORCHIDEE after calibration (left) and differences between initial and calibrated implementations (right) for Soil Nitrogen factor and soil temperature factor

This adjustment resulted in a closer response to the original results (Figure 5.17) reducing the BNF high-end rates in the tropical ecosystems and increasing the rates in boreal ecosystems in North America and Russia. The adjustment of the potentials also corrected the underestimation on rate on temperate zones of the United States, Europe, and Asia, with special emphasis on the hotspots of the east coast of the United States and Europe.

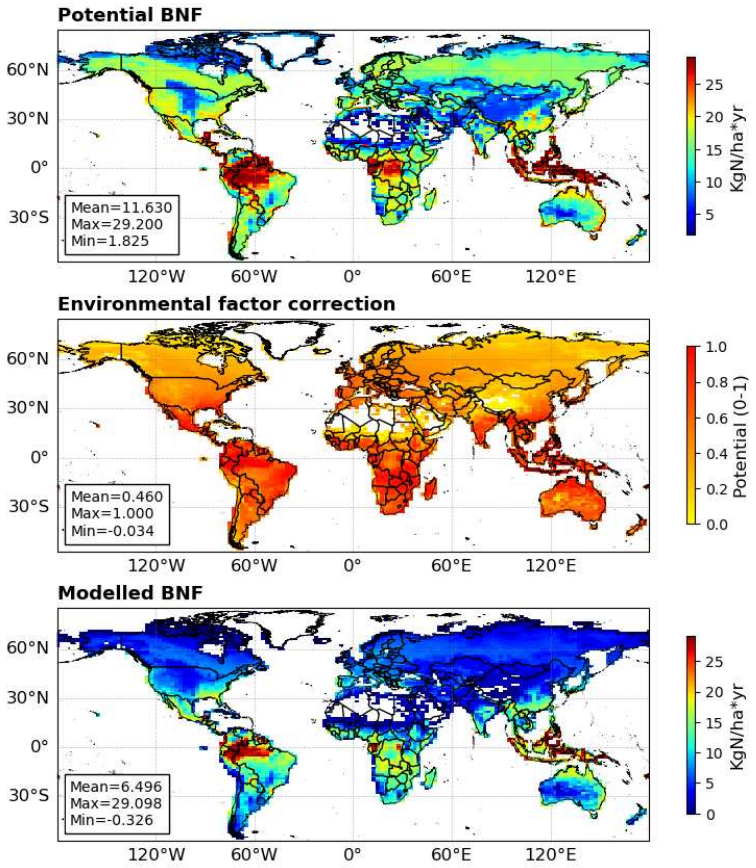

Figure 5.17 - Calibrated implementation of BNF with ORCHIDEE climate and environmental conditions and adjusted variables for the period 1999-2000: a) potential BNF rate (kgN m^{-2} yr^{-1}), b) The environmental factor correction or (f_N*f_C*f_W*f_T) (0-1) and c) the modeled BNF (kgN m^{-2} yr^{-1}).

The total value of post-calibration BNF was 86.36 TgN yr^{-1}, against the initial implementation value of 74.22 TgN yr^{-1}, thus showing an increase of about 12 TgN yr^{-1}, still bigger than the original value of 62 TgN yr^{-1} (Yu & Zhuang, 2020) yet much closer to the recent meta-analysis of (Davies-Barnard & Friedlingstein, 2020) with a value of 88 TgN yr^{-1}.

Tropical ecosystems, in particular, contributed a total of 38.86 TgN yr^{-1}, compared to the previous implementation's 53 TgN yr^{-1}, suggesting an adjustment in the hotspots but still having a larger response compared to the original value of 32 TgN yr^{-1}. Temperate ecosystems yielded a value of 20.03 TgN yr^{-1}, slightly higher compared to the previous 17.12 TgN yr^{-1}, indicating a considerable increase in values, correcting the initial miscalculation, and yielding a value closer to the original model value of 19.14 TgN yr^{-1}. Finally, for boreal ecosystems, the modeled BNF equaled 7.51 TgN yr^{-1} compared to the original model's reported 4.53 TgN yr^{-1}. This means that the BNF is bigger than the reported one, but since this region presents an inconsistency regarding the potentials, our results are similar to the Y&Z graphical distribution reported on (Figure 5.7).

5.4. Result of the new dynamic BNF in ORCHIDEE

5.4.1 On-line implementation in ORCHIDEE

After calibrating the model off-line, we proceeded to its integration into ORCHIDEE, in order to get a dynamical computation of the BNF (dBNF). This means that the interactive model takes the nitrogen and carbon amounts from ORCHIDEE, computes the BNF from these, and then adds it to the mineral nitrogen pool (NH_4^+) which will further impact on the plant N uptake and the C productivity . As a result, at each modeling step, the carbon and nitrogen pools interact with the BNF, considering the possibility of a major surge and decrease in BNF flux. Also, the model was calibrated using monthly data for the environmental variable, whereas ORCHIDEE simulations use a half-hourly time step, which might have a considerable influence on the flow due to the nonlinearity of the equations used. We first analyze the impact of our new dynamical computation of the BNF on the spin-up process and then on the historical and near-future periods.

5.4.2 Impact of the dynamic BNF modeling on the SPIN-UP procedure

As indicated in previous chapters, the spin-up simulation attempts to establish a steady state under specified forcing conditions. This steady state will then be used as the starting point for a simulation in which the forcing conditions alter throughout time. We frequently began simulations in 1850 from a pre-industrial steady state to study the human-driven disturbances of the terrestrial carbon cycle. As mentioned in the introduction of this chapter, BNF was the major pathway of Nr production at pre-industrial time and the main Nr input for terrestrial ecosystems (Global atmospheric N deposition at pre-industrial time totaled 20 TgN yr^{-1}).

Thus, changing from a constant BNF rate (provided as a forcing) to a BNF rate dynamically computed based on the Y&Z model (dBNF) may have a significant impact on the steady state values of the the BNF value and C pools obtained from the spin-up process. The purpose of this section is to evaluate how dBNF modeling impacts on these steady-state fluxes and pools.

The outputs of the spin-up with the current ORCHIDEE implementation with a static BNF[5] (sBNF) and with the new fully implemented dynamic BNF (dBNF) for global mean BNF, global mean gross primary production (GPP), total carbon in soils, and global net biospheric productivity (NBP) are shown in (Figure 5.18).

[5] The current version of ORCHIDEE, as mentioned in the introduction, employs a static BNF value for the year 1850 that does not depend on the changing nitrogen and carbon pools throughout the simulations.

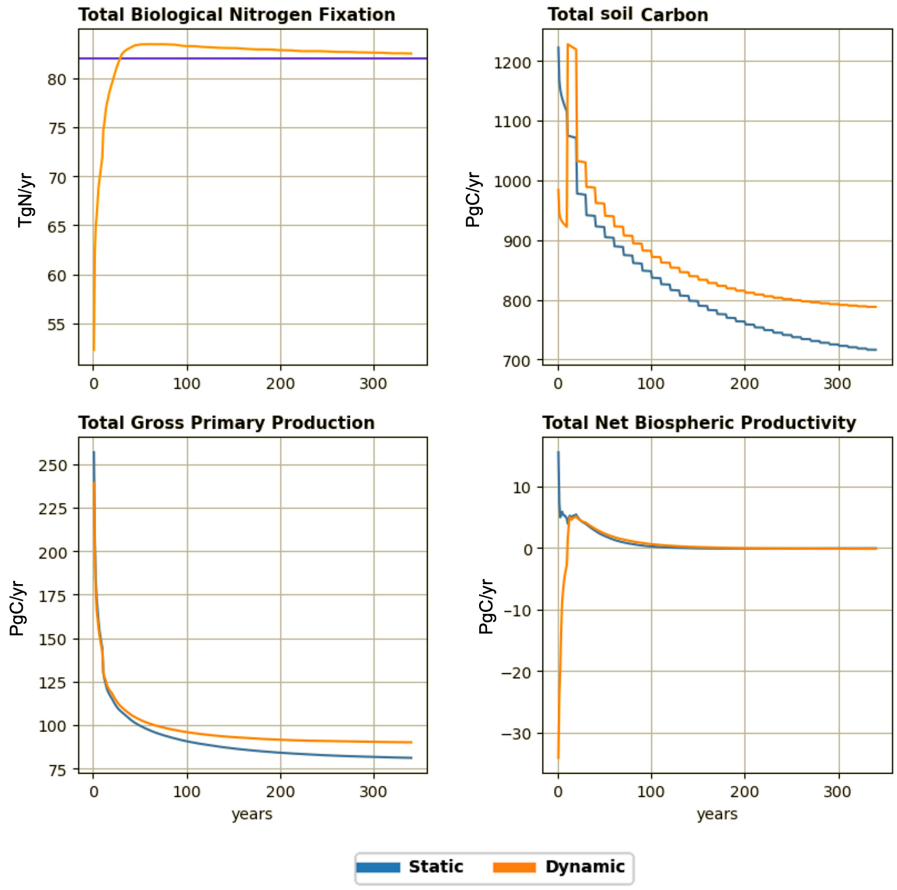

Figure 5.18 - Time evolution of a) Total biological nitrogen fixation (TgN yr^{-1}), b) Carbon in soil pool (PgC yr^{-1}), c) Total gross primary productivity (PgC yr^{-1}) and d) net biospheric productivity (PgC yr^{-1}) over the 350 years of spin-up for simulations with static (blue) and dynamic (orange) BNF.

At the start of the simulation, the dBNF values are minimal and significantly lower than the ORCHIDEE baseline sBNF. Nevertheless, this value of roughly 52 TgN yr^{-1} rapidly climbs throughout the first decades of the spin-up, reaching an equilibrium of 83 TgN yr^{-1}, slightly higher than the sBNF value.

The dynamical implementation has a direct influence on the simulated GPP. Starting values of global GPP amounts to 240 PgC yr^{-1} and 260 PgC yr^{-1} for static and dynamic BNF simulations respectively. Initial values for GPP are very high. This is explained by the model's initialization of the N pools with very high values, resulting in large mineralization rates. N pools decrease when they deviate from their original values, as does GPP. When the simulated BNF generated by the dBNF exceeds the sBNF baseline value, the GPP for the dBNF simulation surpasses that of the sBNF simulation, finding an equilibrium at approximately 90 PgC yr^{-1}. The objective of the spin-up simulations is to put the state variables at equilibrium, implying that the quantity of carbon entering the system equals the amount of carbon leaving it. This corresponds to getting the NBP flux equal to zero. As can be seen, both simulations attain this criteria for NBP, although via different trajectories. The values in the sBNF simulation begin above 10 PgC yr^{-1}, while the values in the dBNF simulation begin below -30 PgC yr^{-1}. This might be owing to early

nitrogen deficiency and the difference in the GPP. By the end of the first century of simulations the NBP flux is close to zero, a value that is reached after 350 years of simulation.

We predicted a significant interaction effect between the carbon and nitrogen pools, with either a large dampening or boosting influence on the fluxes, with the addition of another layer of complexity between the biogeochemical cycle interactions via the dBNF. The overall effect is not as critical to preclude an equilibrium state for the spin-up simulation comparable to the sBNF implementation. In this way, the implementation of a dBNF is validated allowing us to carry on with analysis over the historical period and the projections for the 21st century.

5.4.3 Revised BNF the dynamic BNF implementation for the historical and future periods

Before examining the influence of dynamic implementation on the temporal evolution of the BNF across the time range of the prior chapters (from 1850 to 2100, including the SSP trajectories of the 21st century), we compare the behavior of dynamical BNF with that of previously calibrated one (called offline model). This comparison is made between 1990 and 2000, the decade in which the model was calibrated.

Comparison to the calibrated off-line simulation:

The dBNF implementation yielded a global mean value of 79.3 TgN yr^{-1} vs 86.36 TgN yr^{-1} for the previous calibrated off-line model during the same original decade of study (1990-2000). The damping in the tropics, notably in the Amazon, the tropical forest of Gabon and the eastern half of the Democratic Republic of the Congo, and some hotspots in Indonesia, explain this discrepancy of around 7 TgN yr^{-1} (see Figure 5.19).

This is primarily due to the fact there is a reduction in reactive nitrogen through high regional nitrogen loss (Cusack et al., 2009) that has an amplified effect on the amount of assimilated carbon which in turn returns to have an negative effect on carbon pools in the soil, thus limiting our BNF value.

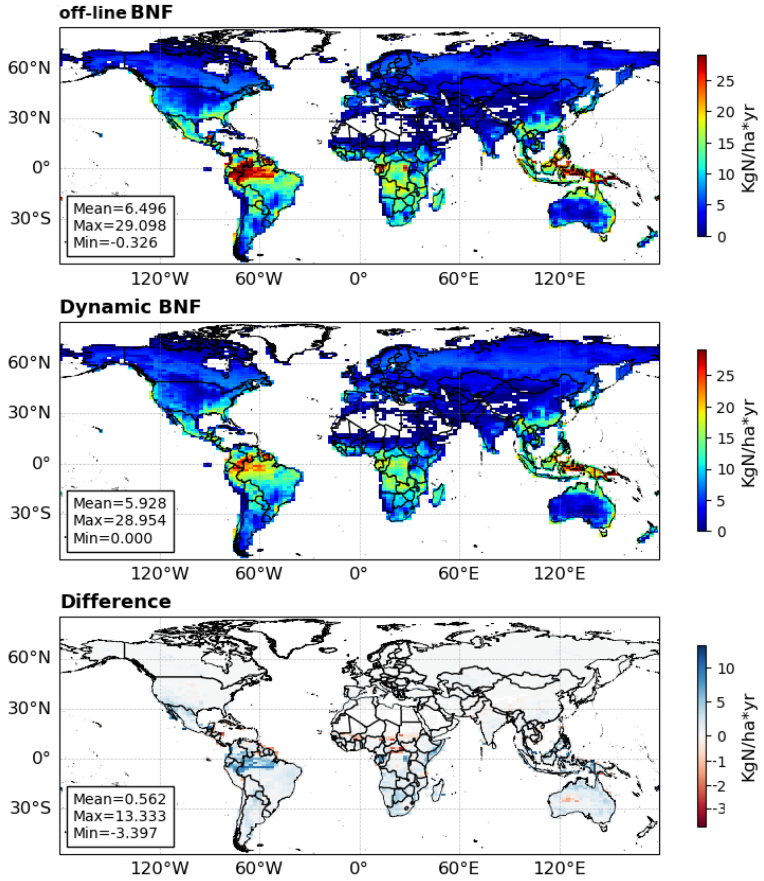

Figure 5.19 - Simulated BNF rate (kgN $ha^{-1}yr^{-1}$) with a) the off-line model version of Y&Z , b) the dBNF model and c) the difference between the offline and dBNF implementations. The values reported are annual mean values over 1990-2000.

Historical and future scenarios simulation:

The analysis is separated into two eras from the full simulation 1850 to 2100 (Figure 5.20): the historical period (1850 to 2015) and the future period (2015 to 2100). We first report on the BNF rate expressed in kgN per year and per hectare of land where the BNF acts (ie. All PFTs except croplands). A worldwide trend of BNF rise may be noticed during the historical era (from 8.5 to 9 kgN $ha^{-1}yr^{-1}$). More precisely, from 1920 to 2015, there was a global considerable rise for regions such as Europe (increase of 1.3 kgN $ha^{-1}yr^{-1}$), South America (growth of 1.45 kgN $ha^{-1}yr^{-1}$ from 1970 to 2015), and North America (increase of 1.3 kgN $ha^{-1}yr^{-1}$). Unlike the other regions investigated, Africa has a minor drop from 1940 to 1970 of roughly 0.7 kgN $ha^{-1}yr^{-1}$, and then stabilizes until 2015.

The trajectories of the BNF rate are different for each region for the different SSPs in the future, but certain worldwide trends can be detected, such as a generalized rise in the SSP5-8.5 and SSP3-7.0 trajectories and a reduction in the SSP4-3.4 and SSP1-1.9 trajectories of. Globally, there is a spread of 1.4 kgN $ha^{-1}yr^{-1}$ between the biggest (SSP5-8.5) and smallest (SSP4-3.4) SSPs trajectories, which show how large the impacts of the different climate evolutions in the SSP are. Some regions, such as Boreal Asia and Europe, have a continuous increase in all SSPs

at various rates, while in regions like Africa, Asia, and North America the trend is very similar to the worldwide one.

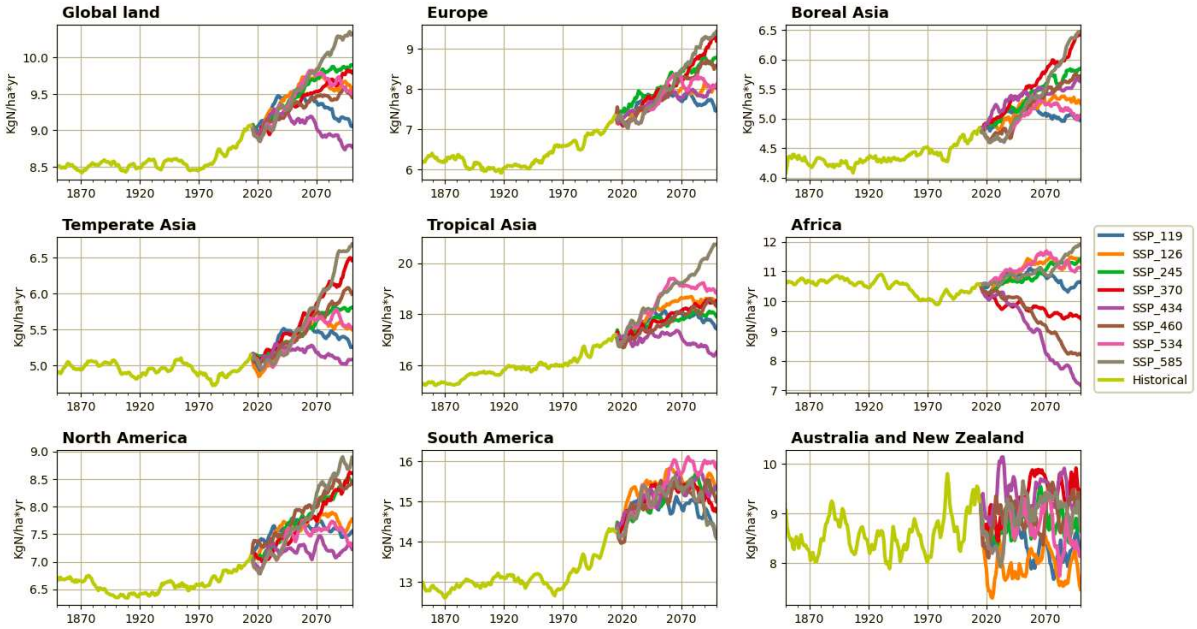

Figure 5.20 - dBNF in kgN ha^{-1} yr^{-1} from 1850 to 2100.

Although soil temperature has been identified as a major driver of BNF (following the original Y&Z model), the mean soil temperature trajectories from 1850 to 2100 (Figure A 3) reveal that there is no direct relationship between BNF rate and mean soil temperature trajectories. This might be owing to the dynamic interaction of other factors such as carbon and nitrogen content, which could have a higher influence on the final BNF. Temperature trajectories, on the other hand, can explain certain SSP behaviors, such as SSP5-8.5, which has a greater BNF rate in most areas due to rising soil temperatures.

Deforestation and afforestation explain some SSP trajectories since forest areas have the greatest related BNF rates of all ecosystems (Davies-Barnard & Friedlingstein, 2020). For example, the global fall in BNF associated with SSP4-3.4 can be attributed to massive deforestation in temperate and tropical Asia, Africa, and North America over the 20th century (regions that are marked by a significant decrease on BNF rates even if the temperature increase is significant).

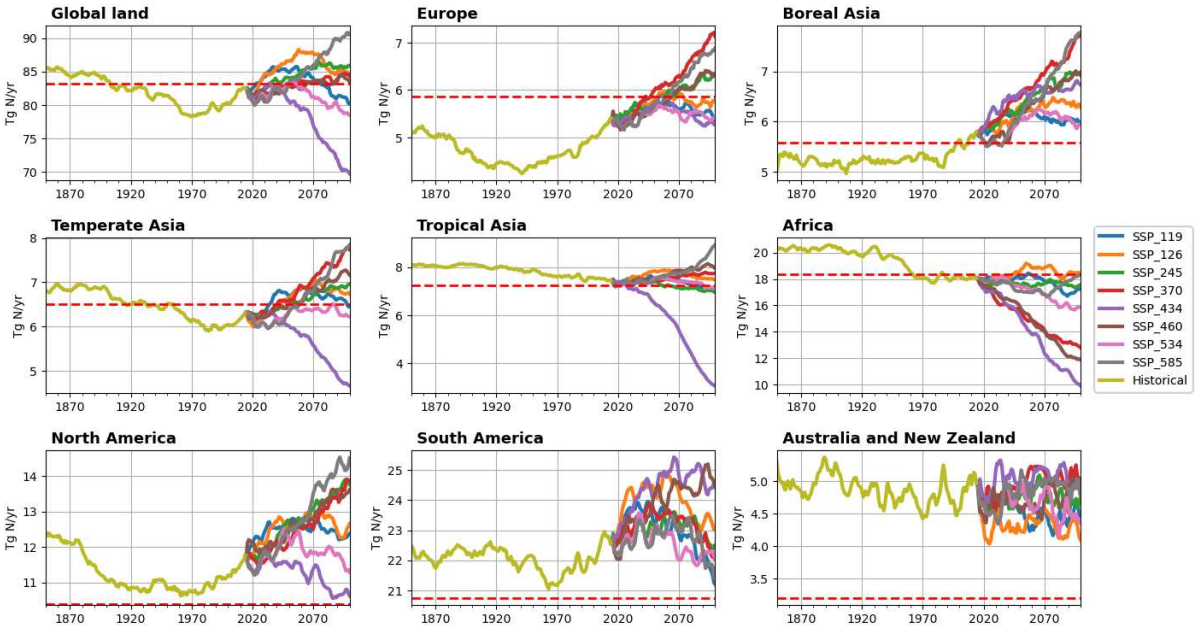

Figure 5.21 - Global- and regional-mean natural BNF (TgN yr^{-1}) simulated by the dynamic implementation from 1850 to 2100. The dashed line represents the current ORCHIDEE static implementation (sBNF).

Regarding the BNF totals in TgN yr^{-1}, as can be seen in (Figure 5.21), there is a clear similarity with the trajectories of the forest lands (Figure A 14). This is explained again by the importance of these ecosystems (relative to grasslands) in the total values of BNF and by the fact that natural BNF is not acting over croplands. Most specifically, in the tropical regions of Africa, South America and tropical Asia, the trajectories are almost equal between forest land and total BNF evolution, whereas for temperate and boreal regions, there is a similar behavior, but also driven by the evolution of soil temperature, adding relevance to non-deforested SSPs but rather those with higher soil temperature evolution such as in boreal Asia.

The global BNF value in the dBNF simulation was lower than the sBNF one over 1900-2020, a period during which dBNF decreased to a value close to 78 TgN yr^{-1} due to high deforestation in the last decades of the XXth century. All future trajectories start in 2015 with a value lower than the sBNF one. By the end of the 21st century, only global dBNF for SSP4-3.4, SSP5-3.4 and SSP1-1.9 remained below the values with the sNF implementation. Global dBNF values for other SSPs increase to reach up to 90 TgN yr^{-1} for the highest trajectory (SSP5-8.5).

The dBNF rate is greater than the sBNF rate in North America, South America, Australia, and New Zealand. Other locations, such as Africa and Tropical Asia, have model responses with dBNF that are more similar to the current sBNF (excluding the trajectories of the SSPs with deforestation). All of this shows that, while the model response differs from the expected sBNF value due to the interaction with the ambient variables affecting dBNF, there are no significant differences in the realized BNF value.

5.4.4 Impacts of dBNF on the carbon cycle

5.4.4.1 Historical period

Gross Primary Production for unmanaged land:

The global GPP expressed in kgC $m^{-2}yr^{-1}$ for unmanaged lands (ie. Where natural BNF acts) is higher for the dBNF simulation than for the sBNF simulation, with a difference of 0.1 kgC m^{-2} yr^{-1} for the whole period from 1850 to 2015 (Figure 5.22). In most circumstances, the GPP difference between the two implementations is consistent and lower in temperate and boreal zones, ranging from 0.01 to 0.07 kgC $m^{-2}yr^{-1}$, than in tropical zones (30°N-30°S), where the difference varies from 0.1 to 0.15 kgC $m^{-2}yr^{-1}$.

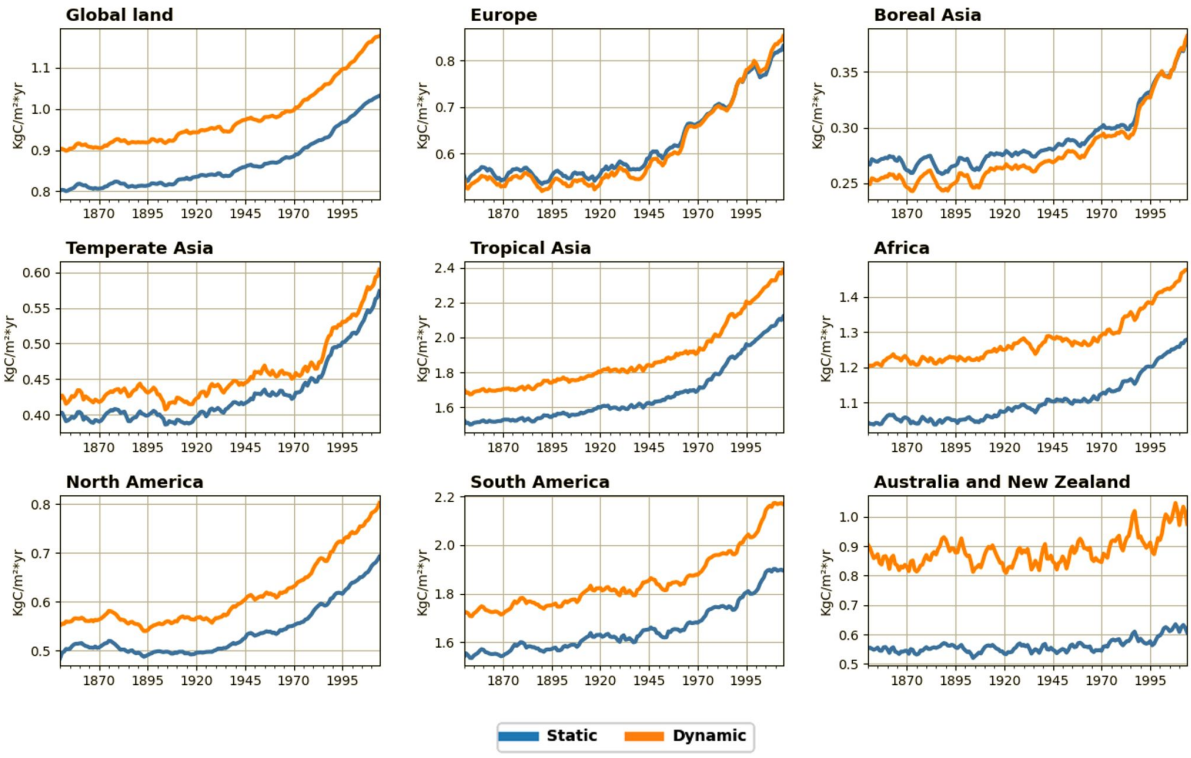

Figure 5.22 - GPP for natural lands in kgC $m^{-2}yr^{-1}$ for a dynamic and static BNF implementation from 1850 to 2100.

In Europe and Boreal Asia (Figure 5.22), dBNF values were lower than the sBNF values during the whole historical era, resulting in a lower GPP. In Temperate Asia, dBNF was larger than sBNF from 1850 to 1950 and lower from 1950 to 2015, explaining why the GPP in the dBNF simulation is larger than in the sBNF simulation during the first decades and then tends to the same value than in the sBNF simulation by the end of the historical era. In temperate and boreal forests one of the main supplies of reactive nitrogen comes from BNF (Flechard, Ibrom, et al., 2020; Vitousek et al., 2013). As a result, GPP in the dBNF simulation is smaller when the dBNF simulation yields to smaller BNF values than in the sBNF simulation. For the tropical and subtropical regions of South America, Africa, Australia, and Asia, as well as North America, the dBNF simulation yields to a higher GPP value than the sBNF simulation. Because these areas

are N limited at some point, as seen in Chapter 3, this increases in reactive nitrogen via BNF resulted in an increase in GPP.

Looking at the annual mean GPP over 2001-2010 (Figure 5.23), we simulated higher GPP values with the dBNF implementation than with the sBNF implementation. Pixel-average GPP amounts to 1.15 kgC $m^{-2}yr^{-1}$ in the sBNF simulation to be compared to 1.01 kgC $m^{-2}yr^{-1}$ in the dBNF simulation. Higher GPP are located primarily in the tropics (30°N-30°S), with a special emphasis on the Amazon, Central America, southern Africa, and Indonesia, as well as some specific hot spots on the southeast coast of Australia and southern China, and a slight increase on the west coast of North America. As indicated in (Figure 5.23), the largest rise in BNF from dBNF occurred in these locations, explaining this GPP increase, although in other boreal and temperate zones of Eurasia, dBNF implementation generated lower BNF than sBNF, resulting in a small reduction in GPP.

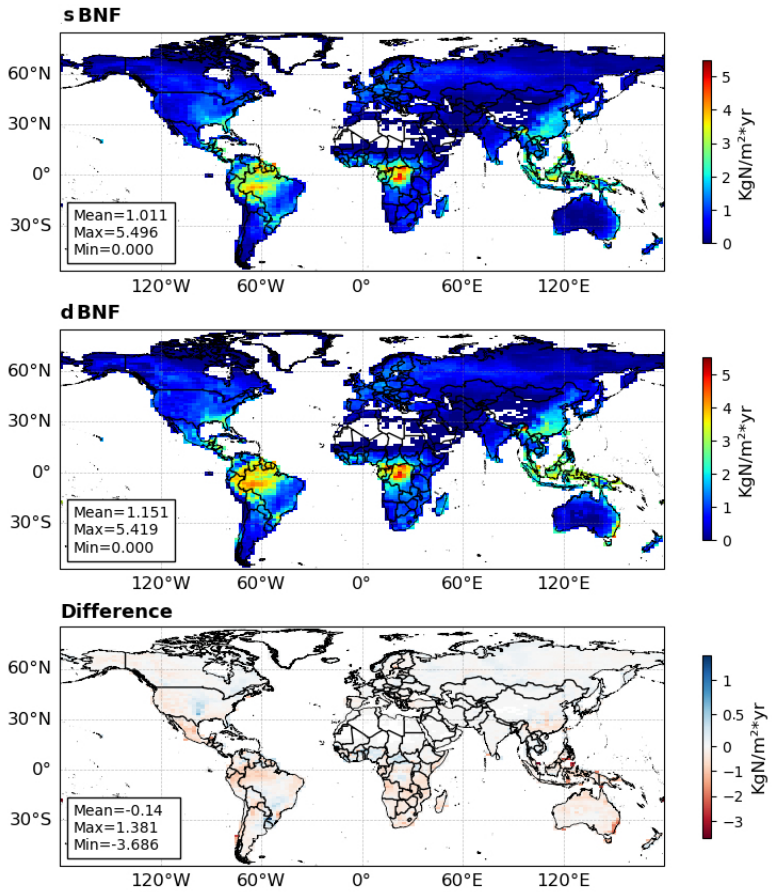

Figure 5.23 - Annual mean GPP in kgC $m^{-2}yr^{-1}$ between 2000 and 2015 simulated with a) the sBNF implementation, b) the dBNF implementation and c) the difference between the sBNF and dBNF implementation.

The dBNF shows a global constant increase of 12 PgC yr^{-1} throughout the simulated period with respect to the sBNF (Figure 5.24). For all regions except Europe and Boreal Asia, the total dBNF GPP is bigger than the sBNF GPP and ranges from 0.8 to 3.5 PgC yr^{-1}, with the largest

regional difference experienced in South America and the smallest in Temperate Asia, this latter explained by reduction of dBNF with respect to sBNF from 1950 onwards as explained before.

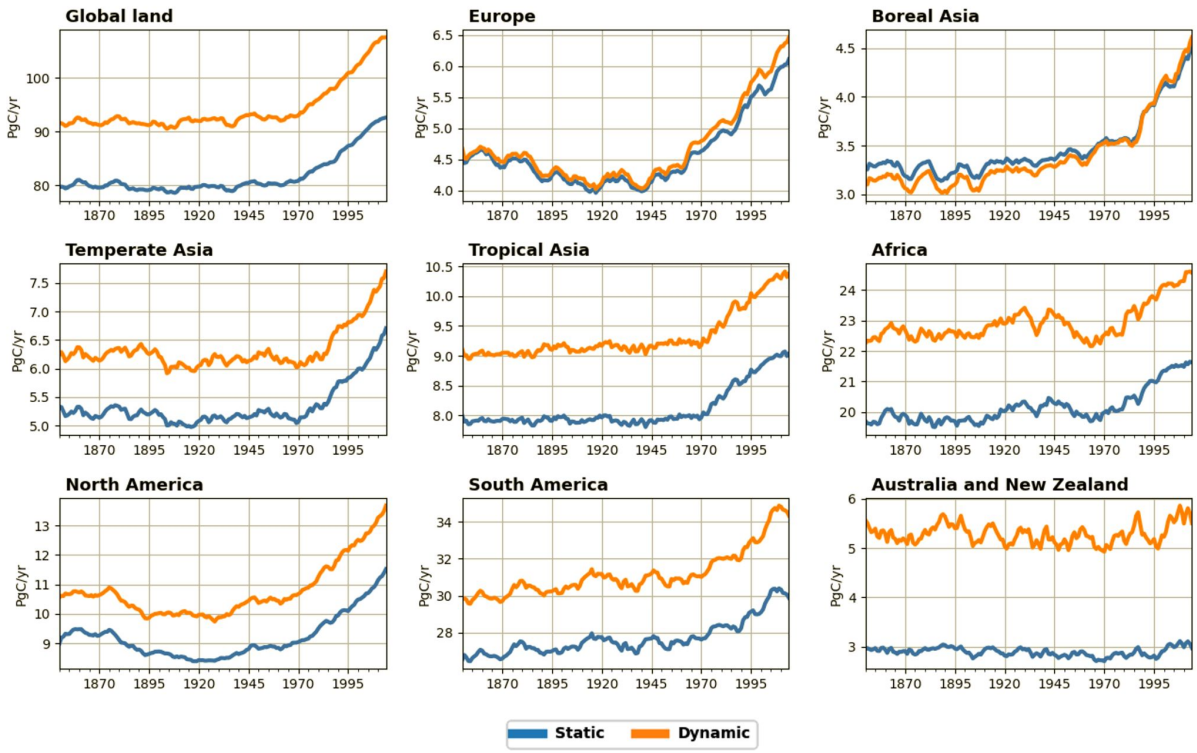

Figure 5.24 - Global- and regional-mean GPP for natural lands (PgC yr^{-1}) simulated with the dBNF implementation (orange) and the sBNF implementation (blue) from 1850 to 2015.

Net Biospheric Productivity:

For net biosphere production, the trends are very similar between the different implementations, with minor regional variations. It is observed that dBNF yields to lower NBP values than the sBNF approach worldwide for the whole simulation period (Figure 5.25). This means that until 1970 there was a carbon emission up to 0.005 kgC m^{-2} yr^{-1} for sBNF, while for dBNF the mean emission followed a very similar trend but with bigger emissions reaching up to 0.0085 kgC m^{-2} yr^{-1} in 1950-1965 (Figure 5.25) This emission is mainly due to land use change (Tharammal et al., 2019) and since dBNF provides higher GPP, the higher carbon stocked during photosynthesis makes the difference therefore more significant.

From 1970 to the present day, the land has acted as a carbon sink (Ciais et al., 2013), and the same can be corroborated in our simulations due to the CO_2 fertilization effect, increase in nitrogen deposition and a stabilization in deforestation in boreal and temperate regions. This is why the total dBNF NBP increased in the recent decades. With the preservation of natural lands and the rise in GPP owing to increased atmospheric CO_2 and nitrogen availability, the absorbed carbon remains in the system, leading to higher C stocks.

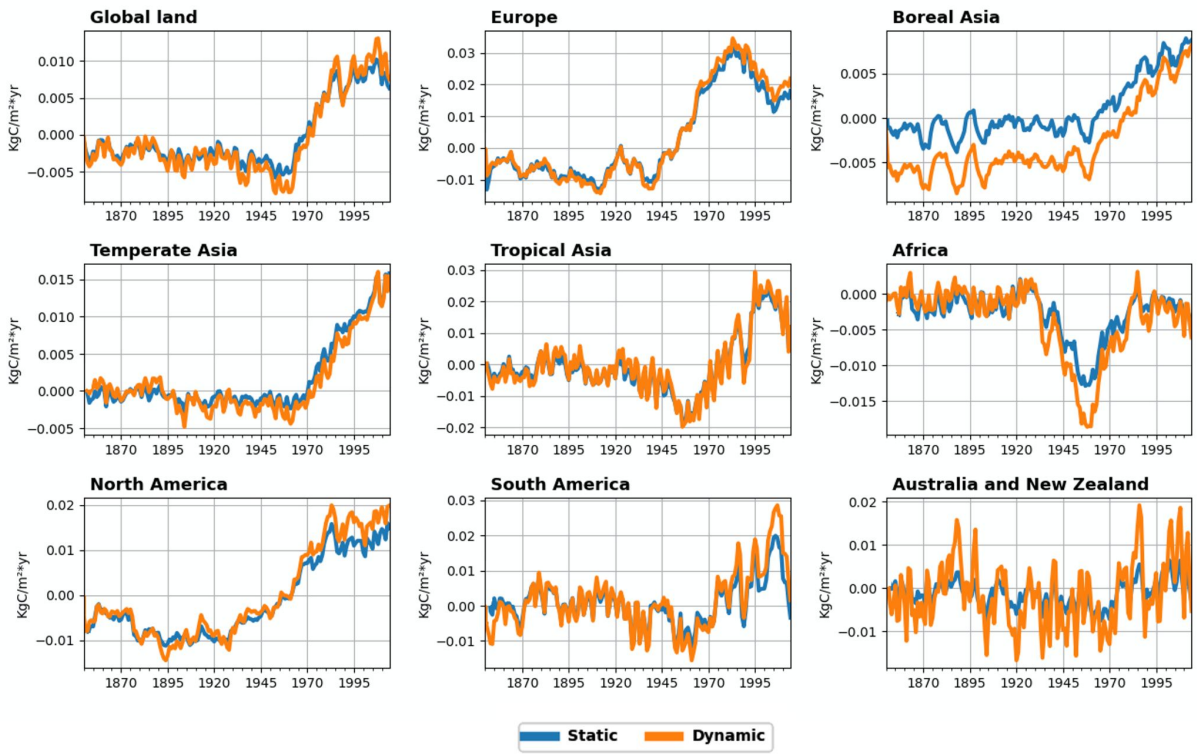

Figure 5.25 - NBP in kgC $m^{-2}yr^{-1}$ for a dynamic and static BNF implementation from 1850 to 2100.

Analyzing the evolution of the NBP regionally is challenging because of the overlapping of the fluxes due to important seasonal variability. We studied the spatial distribution of past decade simulated NBP as well as accumulated NBP. When zooming in the period 2001 to 2010, it can be seen that the dBNF shows a higher mean NBP value (0.010 kgC $m^{-2}yr^{-1}$) than the sBNF (0.008 kgC $m^{-2}yr^{-1}$) (Figure 5.26).

By adding more reactive nitrogen to the system, which accounts for an important part of the productivity, and by having a stabilization in deforestation, we find an increase NBP in Eurasia and North America for the dNBP in comparison to the sBNF. Other hotspots obtained from the difference in BNF implementations are seen in tropical zones of Amazonas, Indonesia, and Africa, where even though deforestation continued during the simulated period, the dBNF provided larger reactive nitrogen than the sBNF that boosted the net carbon storage capability.

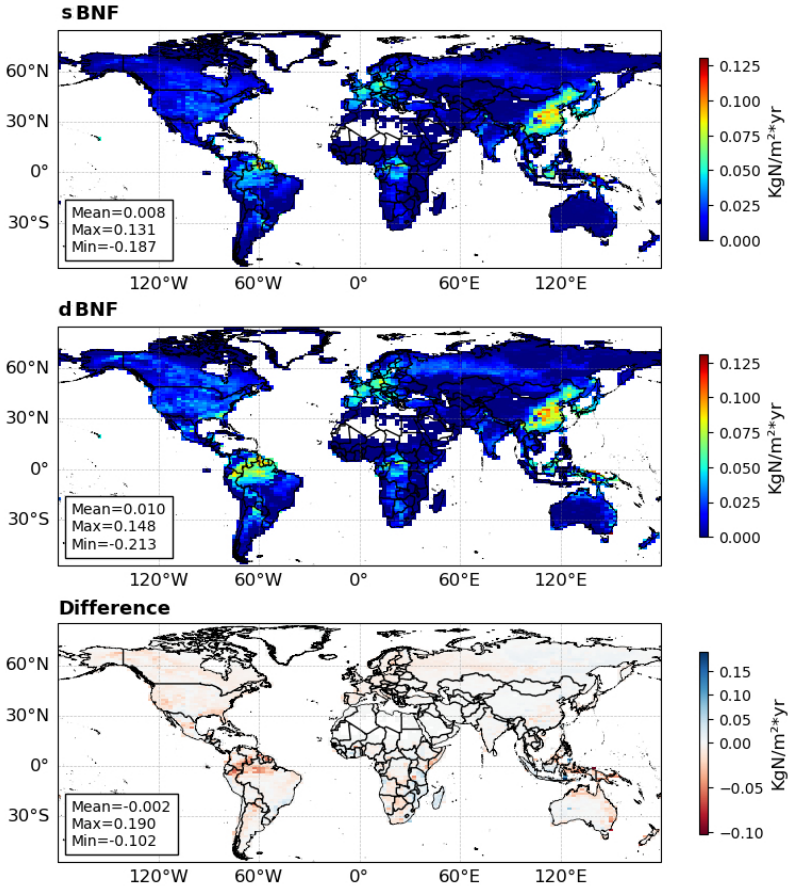

Figure 5.26 -Mean NBP in kgC $m^{-2}yr^{-1}$ from 2000 to 2015 for a) sBNF implementation, b) dBNF implementation and c) Difference between the sBNF and the dBNF.

The beginning NBP point is zero, as predicted from the equilibrium attained during spin-up. The worldwide paths of total cumulative NBP reveal that both BNF implementations resulted in large carbon emissions until 1970 (Figure 5.27). In 1970, the total net carbon emitted since 1850 in the sBNF scenario was 43 PgC, whereas the dBNF emitted 55 PgC. As previously stated, the quantity of carbon absorbed by photosynthesis was higher for the dBNF throughout this time period from 1850 to 1970, explaining the discrepancy of 12 PgC from the global deforestation. After 1970, we simulate a rise in both GPP and cumulative NBP for both scenarios. This is due to an increase in atmospheric CO_2 as well as an increase in reactive nitrogen. Globally, more carbon is sequestered between 1970 and 2015 in the dBNF scenario but because more carbon was lost in the dBNF scenario than in sBNF up to 1970, the total carbon store from 1850 to 2015 in the dBNF scenario fails to reach the sBNF carbon store value, with a difference of around 8 PgC by 2015.

In Boral Asia the sBNF was higher than the dBNF making the sBNF GPP higher. Since this region experienced the least global deforestation during this time, the dBNF cumulated NBP was higher than that of the dBNF implementation. For the rest of the regions the trajectories are similar. However, in Africa, South America, and Australia the emissions with the dBNF are

higher than those with the sBNF even if the dBNF GPP is larger than the sBNF, as a result of higher deforestation rates, especially after 1945 in Africa.

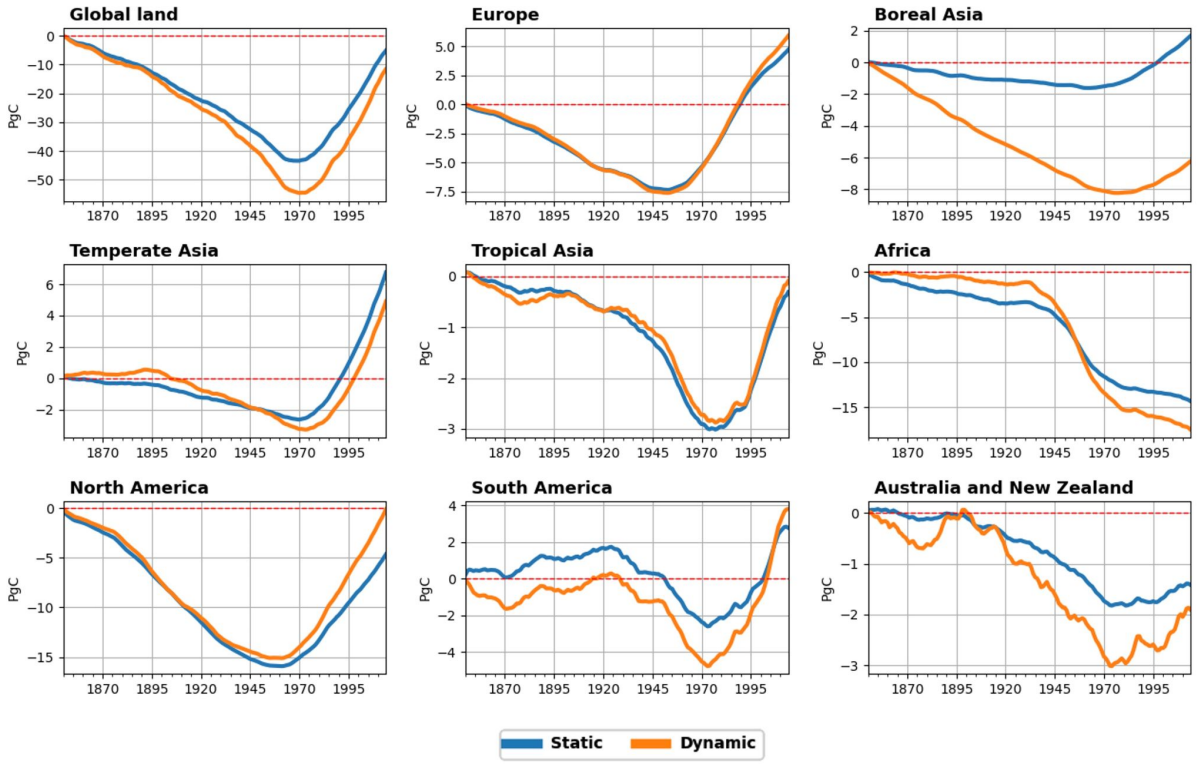

Figure 5.27 - Total accumulated NBP in PgC for a dBNF and and sBNF implementation from 1850 to 2100.

5.4.4.2 Future SSPs scenarios

As mentioned in the previous chapter, the alternative pathways for the 21st century are structured in the form of SSPs, reflecting different degrees and types of socioeconomic growth. Simulations were run in ORCHIDEE with the SSP forcings (same as in the previous chapter) to investigate how it affects the ability of terrestrial ecosystems to store or release carbon.

Gross Primary Production for unmanaged land:

(Figure 5.28) depicts the range of GPP in 164stima^{-1} for the trajectories of natural lands for the different SSP over the 21st century. Following the historical trajectory analysis, the implementation of the dBNF yields a greater response in GPP than the existing ORCHIDEE implementation with a sBNF. Implementing a dBNF expands the GPP response range in 2100 of 60 PgC yr^{-1} between SSPs against 44 PgC for the sBNF, as a result of the higher total biological fixation in the dBNF scenario than in the sBNF for most SSPs as seen in Figure 5.21.

The same is true for Europe, Boreal Asia, and Temperate Asia, where the total BNF for most of the high-end range SSPs is larger, resulting in a roughly similar trajectory for the lower GPP value but an increase in maximum values. In 2100, the rise in maximum GPP values will equal 0.87 PgC yr^{-1} for Europe, 1.11 PgC yr^{-1} for Boreal Asia, and 0.72 PgC yr^{-1} for Temperate Asia.

For the lower GPP values, it can be seen that the response is similar between the dBNF and sBNF, even if the bottom range SSP trajectories have a lower amount of dBNF than the sBNF value. The dBNF GPP for all SSPs is greater than the sBNF one in North America, South America, and Australia, reflecting an increase in GPP range of around 3 PgC yr^{-1}, 4.5 PgC yr^{-1} and 1 PgC yr^{-1} respectively for 2100. This means that these regions are not nitrogen-limited, and that increasing BNF equates to an increase in GPP.

In the case of Tropical Asia, the dBNF GPPs are above the sBNF ones for most of the 21st century SSPs, which explains the difference of about 2.5 PgC for the GPP upper range in 2100. However, the dBNF GPP for SSP4-3.4 is well below the sBNF GPP value due to the associated high deforestation, yet the GPP bottom range is very similar. This is because the GPP for this trajectory is explained by deforestation and not by the amount of BNF associated with the system as expected.

This is also the case in Africa, where the dBNF is lower than the sBNF for most of the SSPs and yet the bottom range of the GPP is very similar, since in Africa these SSP trajectories are related to deforestation. The increase in the upper range of about 8 PgC yr^{-1} is due to the fact that the only SSP that is above the sBNF is the one associated with afforestation (SSP1-2.6), and since tropical ecosystems are the most productive, an increase in BNF implies a significant increase in GPP.

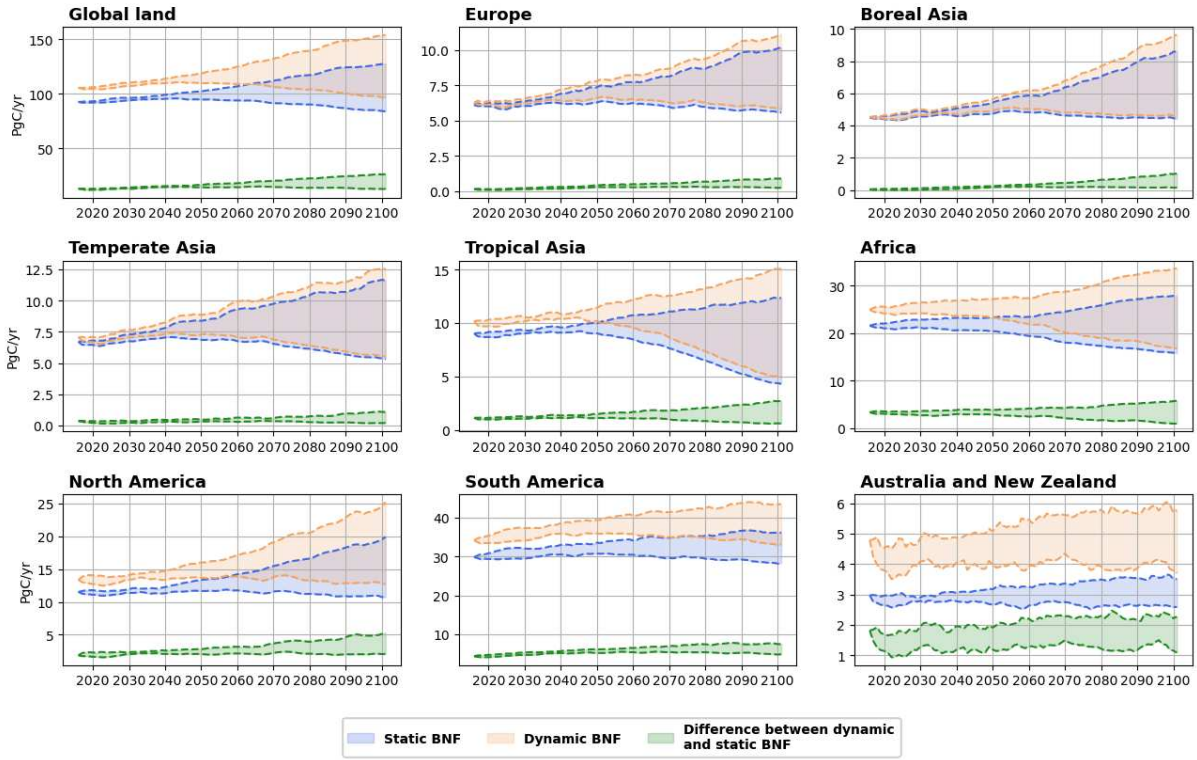

Figure 5.28 - Range of GPP for natural lands in PgC yr^{-1} from 2015 to 2100 for a dBNF, sBNF implementation, and the difference between the dBNF and the sBNF implementation. The range gathers the possible eight SSPs trajectories from the CMIP6 exercise.

Cumulated Net Biospheric Productivity:

The accumulated NBP values for the 21st century simulations in the form of SSPs (with the equivalent starting point at the end of the historical period) show that dBNF results in a range of 200 to 2 PgC for the upper range of the SSPs, whereas sBNF results in a range of 118 to -6 PgC for the upper range of the SSPs (Figure 5.29). This suggests that implementing dBNF can generate an additional store of around 80 PgC for the higher range of SSPs resulting from SSP5-8.5 and additional 8 PgC for the lower range of SSPs coming from SSP4-3.4, allowing terrestrial ecosystems to act as carbon stocks throughout the 21st century for every possible SSPs. On average, considering the eight SSP scenarios, the difference on the land carbon store due to the BNF scheme (dynamic vs. static) is equal to ~50 PgC. This is of the same order as the standard deviation associated with the uncertainty on the land-use scenario which has been166stimateed in Chapter 4. It is also three times larger than the standard deviation associated with the uncertainty regarding the evolution of the N deposition. A recent study from (Davies-Barnard et al., 2020) has shown that BNF does not add uncertainty to the flows of carbon for the CMIP6 exercise, nevertheless, the method of measuring the impact is carried out in ET and NPP linear approaches, and not in process-based models as the one we implemented, from which may reside the increase of uncertainty in our results.

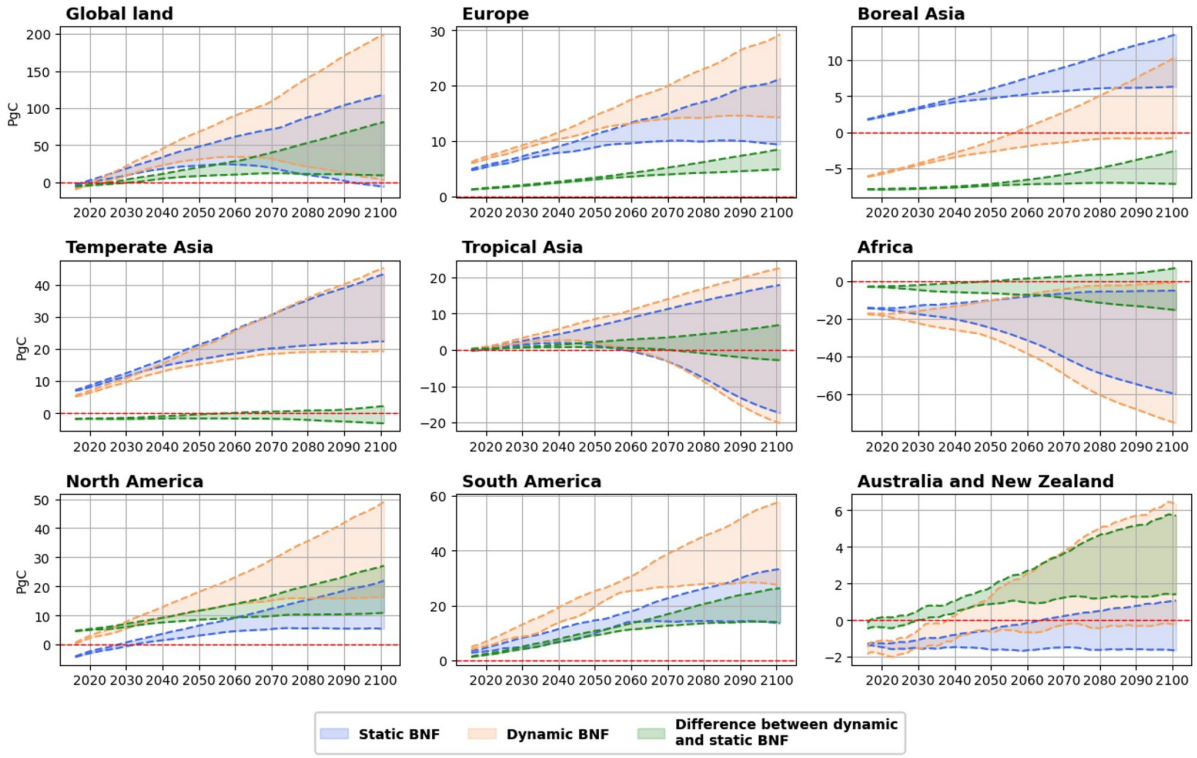

Figure 5.29 - Range of cumulated NBP in PgC from 2015 to 2100 for a dBNF, sBNF implementation, and the difference between the dBNF and the sBNF implementation. The range gathers the possible eight SSPs trajectories from the CMIP6 exercise. The starting accumulated values correspond to those of the end of the historical period.

The rise in the dBNF's storage capacity is due to an increase in GPP and hence the accumulated NBP in South America, North America, Australia, and Europe, where the ranges are larger than those of the sBNF. This is because our sBNF for all SSPs is greater than sBNF. This also means that the range is larger because, while the top range expands, the lower range also does because deforestation emits more carbon.

In Africa on the other hand there is a significant carbon emission projected for the entire range of SSPs and for both BNF implementations. For the dBNF there is an upper range with a lower emission than for the sBNF because the upper range of the SSPs experience a higher value of BNF than the sBNF and because for these trajectories (SSP1) deforestation is stabilized so the carbon emitted is lower.

5.5 Conclusion

We aimed to integrate a dynamic computation of biological nitrogen fixation (dBNF) into the ORCHIDEE model in order to better represent its impact on the mineral nitrogen pools and carbon productivity. The results show that the dBNF model has a significant impact on the evolution of BNF, gross primary production, carbon in soils, and net biospheric productivity, during the spin-up simulation. The dBNF model starts with lower values than the static BNF model, but rapidly increases and reaches an equilibrium slightly higher than the static BNF implementation (sBNF). This leads to higher steady state values for GPP. Overall, the dBNF model provides a more accurate representation of the BNF process and its impact on the carbon and nitrogen cycles.

Most of the models estimate the BNF at a range between 80 and 130 Tg N yr^{-1}. Nevertheless, a recent study has found no statistical relationship between these proxy variables and BNF, invalidating a significant number of existing land surface model implementations, including our study model, ORCHIDEE. By implementing a process-based BNF model in ORCHIDEE with full interaction between the carbon and nitrogen cycles we found a mean symbiotic BNF of 79.3 TgN yr^{-1} for a recent decade from 1990 to 2000. Considering that symbiotic BNF accounts for two-thirds of total BNF, our approximate total BNF value (120 TgN yr^{-1}) is in the range of the most recent study using available upscaling of symbiotic and measured free-living values obtained from natural ecosystems, by land cover, of 52-130 TgN yr^{-1}.

The analysis of the BNF rate from 1850 to 2100 shows a worldwide trend of BNF rise during the historical era, with regions such as Europe, South America, and North America showing a considerable increase. However, Africa had a minor drop from 1940 to 1970, and then stabilized until 2015. The damping in the tropics of the dBNF compared to the sBNF, notably in the Amazon, the tropical forest of Gabon and the eastern half of the Democratic Republic of the Congo, and some hotspots in Indonesia, explain this discrepancy. This is primarily due to the reduction in reactive nitrogen through high regional nitrogen loss that has an amplified effect on the amount of assimilated carbon, which in turn limits BNF value.

The future BNF rate trajectories are different for each region for the different SSPs, with a generalized rise in the SSP5-8.5 and SSP3-7.0 trajectories, and a reduction in the SSP4-3.4 and SSP1-1.9 trajectories. The BNF rate is found to be highly influenced by deforestation and afforestation, with forest areas having the greatest related BNF rates of all ecosystems. The study also finds that there is no direct relationship between BNF rate and mean soil temperature trajectories, which might be owing to the dynamic interaction of other factors such as carbon and nitrogen content, which could have a higher influence on the final BNF.

The influence of a BNF on Gross Primary Production (GPP) for unmanaged lands show that the global GPP expressed in kgC m^{-2} yr^{-1} is higher for the dynamic dBNF simulation than for the sBNF simulation, with a difference of 0.1 kgC m^{-2} yr^{-1} for the whole period from 1850 to 2015. The difference is consistent and lower in temperate and boreal zones, ranging from 0.01 to 0.07 kgC m^{-2} yr^{-1}, than in tropical zones, where the difference varies from 0.1 to 0.15 kgC m^{-2} yr^{-1}. In terms of total GPP (i.e. for both unmanaged and managed lands), the dBNF simulation yielded a global constant increase in GPP of 12 PgC yr^{-1} throughout the simulated period with respect to the static BNF simulation. For all regions except Europe and Boreal Asia, the total dBNF GPP is bigger than the sBNF GPP, and ranges from 0.8 to 3.5 PgC yr^{-1}, with the largest regional difference experienced in South America and the smallest in Temperate Asia. This latter difference can be explained by the reduction of dBNF with respect to sBNF from 1950 onwards. The study highlights the importance of considering dBNF in the modeling of GPP, and the potential for significant regional differences in the impacts of dBNF on GPP

For the future scenarios, the total dBNF GPP is bigger than the sBNF GPP and ranges from 0.8 to 3.5 PgC yr^{-1}, with the largest regional difference experienced in South America and the smallest in Temperate Asia. The dBNF also expands the response range in 2100 of 60 PgC yr^{-1} against 44 PgC for the sBNF for the different SSPs over the 21st century.

The results show that for net biosphere production, the trends are very similar between the different implementations, with minor regional variations. The dBNF approach yielded lower NBP values worldwide for the whole simulation period compared to the sBNF approach. This is mainly due to land use change and the higher gross primary productivity (GPP) provided by dBNF.

From 1970 to the present day, the land has acted as a carbon sink, and the same can be seen in the simulations due to the CO_2 fertilization effect, increase in nitrogen deposition, and stabilization in deforestation in boreal and temperate regions. This is why the total dBNF NBP increased in the recent decades.

When analyzing the spatial distribution of NBP from 2001 to 2010, it was found that the dBNF shows a higher mean NBP value than the sBNF. This increase was observed in Eurasia and North America and in tropical zones of Amazonas, Indonesia, and Africa. This is due to the addition of more reactive nitrogen to the system and the stabilization of deforestation in these regions.

In terms of the accumulated Net Biospheric Productivity, the results show that both BNF implementations resulted in large carbon emissions until 1970. From 1970 to present day, the land has acted as a carbon sink due to the CO_2 fertilization effect, increase in nitrogen deposition, and stabilization in deforestation in boreal and temperate regions. The results also show that the dBNF approach resulted in lower NBP values worldwide for the whole simulation period compared to the sBNF approach. However, in some regions such as Boral Asia, sBNF had higher values than dBNF, and in Africa, South America, and Australia, the emissions with the dBNF were higher than those with the sBNF.

The simulations for the 21st century (SSPs) show that dBNF results in a range of 200 to 2 PgC for the upper range of the SSPs, whereas sBNF results in a range of 118 to -6 PgC for the upper range of the SSPs. This suggests that implementing dBNF can generate an additional store of around 80 PgC for the higher range of SSPs and additional 8 PgC for the lower range of SSPs, allowing terrestrial ecosystems to act as carbon stocks throughout the 21st century for every possible SSPs.

Overall, this research has provided insights into the potential of terrestrial ecosystems to mitigate climate change through carbon sequestration and the importance of the nitrogen cycle in this process. The results of this study will contribute to the development of more accurate and reliable projections of future carbon sequestration potential of these ecosystems and help inform decision-making regarding climate change mitigation and adaptation.

"The future of carbon uptake is closely linked with nitrogen deposition and nitrogen fertilization. If we want to maintain or increase carbon sequestration, we must also address the impacts of nitrogen on ecosystems".

Dr. Jerry Melillo

CHAPTER 6

General conclusions and perspectives

In conclusion, this Ph.D. research has investigated the impact of nitrogen deposition and nitrogen fertilization on carbon uptake in terrestrial ecosystems. Through a combination of modeling experiments, we have shown that nitrogen deposition and fertilization can have a significant impact on carbon sequestration in ecosystems, depending on the rate and timing of nitrogen inputs and the characteristics of the ecosystem.

Contribution of atmospheric CO_2 and Nitrogen deposition to the evolution of land productivity over the historical period:

This study aimed to understand the interactions between carbon and nitrogen cycles and their impacts on ecosystem primary production and net ecosystem carbon storage or release during the historical era. We found that irrespective of the land-use change fluxes that had led to a decline in carbon stocks during the historical period, the rise in CO_2 and nitrogen deposition, combined with the consequent synergistic impact, produced a positive contribution on both the gross primary production and the net land carbon uptake from 1850 to 2015.

We found that the effect of the rise in atmospheric CO_2 represented 15% of the gross primary production (GPP) flux in 2015 globally (i.e., the increase of GPP due to CO_2 increase is equal in 2015 to 15% of a reference GPP that would have evolved only through land use and climate changes), while the nitrogen deposition increase contributed to 6% and the synergy between carbon and nitrogen to 3%, showing the importance of these factors to explain the evolution of carbon assimilation during the last decades. When expressing these contributions relatively to the change in the GPP flux between 1850 and 2015, our modeling study found that the rise in atmospheric CO_2 contributed to 53%, while the contribution from nitrogen deposition increase corresponded to 21% and the synergy between carbon and nitrogen to 9%, in line with literature reported contributions to these factors. The remaining (up to 100%) being due to climate and land use changes.

Overall, the model displays bimodality, meaning that there is a reaction (i.e., a change in both gross and net carbon fluxes) to increase either nitrogen or atmospheric carbon dioxide, but rarely both in equal proportion. Due to CO_2 increase during the historical period and owing to the fact that such CO_2 increase still lies in a photosynthetic suboptimal point, the increase in GPP was substantial and it was in turn boosted by increased nitrogen deposition. Nitrogen deposition makes more efficient the carbon assimilation (GPP) to increasing CO_2, by systematically improving the slope of the regional $ACUE^{+}_{GPP}$ curves.

The local increase in nitrogen deposition raised the maximum carbon assimilation rates in the grasslands of South America and Africa, as well as in agriculturally developed regions of South Asia and Europe and North America over the historical era. We also found that the increase of CO_2 enhances the maxima of carbon assimilation, especially in the tropics which, not being nitrogen limited, benefit from a more important carbon-nitrogen synergistic effect. Note that these large regional differences are important and contrast with the previous version of ORCHIDEE (used for the recent CMIP6 climate projection) that was showing a GPP response to "atmospheric CO_2 increase" that was directly proportional to the GPP itself.

We also examined the contributions of CO_2 increase to the overall rise in net biome production (NBP) from 1850 to 2015, and found that the contribution of CO_2 increase corresponded to 86% of the NBP flux in 2015 worldwide, while the contribution from nitrogen deposition increase corresponded to 29% and the synergy between carbon and nitrogen to 19%. The deviation between the aggregate of the contributing factors and the Net Biome Productivity (NBP) value is attributed to the alteration of land use which results in the release of extra carbon that was stored due to the positive impact of the contributing factors. These numbers show a larger contribution of the CO_2 increase to the net carbon uptake than for the GPP flux. The study identified a relationship between carbon storage and the increase in CO_2 and nitrogen deposition that exhibits a lower degree of linearity (than for GPP) due to the sensitivity of the flux to climate-induced changes.

The CO_2 rise led to an increase of net carbon uptake (NBP) of 1.2 PgC yr^{-1}, while the change in nitrogen deposition led to an increase of 0.41 PgC yr^{-1}. Additionally, the synergistic effect between the two factors contributed to an increase of 0.27 PgC yr^{-1}. The results also suggest that while nitrogen may be limiting the size of the carbon sink, climatic variations may also play a significant role. However, the response of the biosphere to recent climate variations is uncertain, and more research is needed to understand the possible biogeochemical interactions between carbon and nitrogen in future global change.

Contribution of CO_2, land-use and Nitrogen inputs to the future land productivity for different socio-economic scenarios:

The study aimed to quantify the impacts of land-use and nitrogen-related uncertainties on the change in land carbon storage as simulated by the land component of an Earth System Model (ESM) for the 21st century. The study used the land-use and nitrogen trajectories of different Shared Socioeconomic Pathways (SSP) markers, meaning a trajectory selected from Integrated Assessment Models (IAMs) to represent a SSP.

We found that the spread of the simulated change in global land carbon storage induced by the uncertainty on land-use across SSPs is slightly larger than the one associated with the uncertainty on atmospheric CO_2. Globally, the uncertainty associated with Nitrogen emissions (and ultimately Nitrogen depositions) is responsible for a spread in the change in land carbon store that is lower by a factor of three than the one driven by atmospheric CO_2 or land-use changes. The relative impact of these different uncertainties showed contrasted responses regionally. In regions with very contrasted land-use trajectories across SSPs, such as Africa, the spread in the change in land carbon store is mainly driven by land-use change. In contrast, in regions where land-use trajectories are more similar across SSPs, the impact of the Nitrogen deposition-related uncertainty on the change in land carbon store may be almost as large as the one induced by uncertainty on atmospheric CO_2 and land-use changes.

We also conclude that there is a need for delivering harmonized and downscaled information about land-use changes, Nitrogen emissions, and Nitrogen atmospheric deposition trajectories simulated by all IAMs for each SSP and not only by the marker IAMs. Performing sensitivity ESM or land-only experiments with these extra datasets is the only way to accurately assess the specific IAM-related uncertainty impacts on the carbon cycle and the climate system. As many greenhouse gas mitigation strategies imply more land-based solutions, this calls for facilitating the communication and evaluation between IAM and ESM modeling frameworks. Making available additional IAM scenarios to be used in the next Coupled Model Intercomparison Project (CMIP) exercise should contribute to this objective.

Modeling Biological Nitrogen Fixation within the global land surface model ORCHIDEE:

The study aimed to integrate a dynamic computation of biological nitrogen fixation into the ORCHIDEE model to better represent its impact on the carbon and nitrogen cycles. The results

show that the proposed dynamic BNF model (dBNF) has a significant impact on the steady state values of BNF, gross primary production and carbon in soils. The dBNF model starts with lower BNF values than the static BNF model, but rapidly increases and reaches an equilibrium slightly higher than the static BNF implementation during the spin-up procedure.

We highlight the worldwide trend of BNF rise during the historical era, with regions such as Europe, South America, and North America showing a considerable increase. However, Africa had a minor drop from 1940 to 1970, and then stabilized until 2015. The BNF rate is found to be highly influenced by deforestation and afforestation, forested lands having the greatest related BNF rates of all ecosystems. We found that there is no direct relationship between BNF rate and mean soil temperature trajectories, which might be owing to the dynamic interaction of other factors such as carbon and nitrogen content that explains the direct influence of land use change on the dBNF implementation.

The influence of BNF on Gross Primary Production (GPP) for unmanaged lands show that the global GPP was higher for the dynamic dBNF simulation than for the static BNF (sBNF, current ORCHIDEE's approach), with a difference of 0.1 kgC m^{-2} yr^{-1} for the whole period from 1850 to 2015 or equivalent to a difference of 12 PgC yr^{-1}. For the future scenarios, the dBNF expands the upper GPP response range throughout the simulated period with 60 PgC yr^{-1} from the dNBF against 44 PgC yr^{-1} from sBNF by 2100. For the lower range GPP values, it can be seen that the response is similar between the dBNF and sBNF, even if the bottom range SSP trajectories have a lower amount of dBNF than the sBNF implementation.

The data suggests that there are similar trends in net biosphere production across different implementations, with minor regional variations. The dBNF approach yields lower NBP values than the sBNF approach worldwide for the period before 1970. This is due to higher carbon emissions resulting from land use change until 1970. From 1970 to present day, the land has acted as a carbon sink due to the CO_2 fertilization effect, increase in nitrogen deposition, and stabilization of deforestation in boreal and temperate regions. This is why the total dBNF NBP increased in recent decades, with the preservation of natural lands and the rise in GPP owing to increased atmospheric CO_2 and nitrogen availability, leading to higher carbon stocks.

When analyzing the spatial distribution of NBP for the future period, our results suggest that implementing dBNF can generate a larger store of carbon for terrestrial ecosystems, compared to sBNF (Except for Boreal Asia). Overall, the study suggests that implementing dBNF can generate an additional store of around 80 PgC for the higher range of SSPs and additional 8 PgC for the lower range of SSPs, allowing terrestrial ecosystems to act as carbon stocks throughout the 21st century for every possible SSPs.

This increase in storage capacity is due to an increase in GPP (gross primary productivity) and accumulated NBP (net biome productivity) in certain regions such as South America, North

America, Australia, and Europe. However, the study also found that there will be significant carbon emissions projected for Africa for both BNF implementations and that implementing a dBNF may also induce larger carbon emissions than the sBNF.

Limitations of this research:

Some of the research's limitations include the need for longer term studies to better understand the impacts of nitrogen inputs on carbon sequestration, as well as the need for more data from diverse types of ecosystems. Our study focuses on the global effects of land-use and nitrogen-related uncertainty on changes in terrestrial carbon storage, but it does not go into depth on the regional effects. This is a constraint since regional impacts might vary substantially and have distinct consequences for land-use planning and climate change mitigation.

Our simulations do not account for other factors that may influence changes in terrestrial carbon storage, such as changes in land management techniques or changes in water resource availability. These variables may have a big influence on the carbon cycle and should be studied further. The study model is based on historical data and current assumptions, which may be revised for future scenarios for future CMIP exercises, potentially introducing uncertainty in the results. Future studies should include more advanced and better integrated models that can better account for future changes and scenarios.

Finally, the research does not investigate the economic and societal consequences of land-based mitigation options. When establishing sustainable land-use management plans, it is critical to address these consequences.

One of the most difficult aspects of this research will be simulating ecological responses to variations in atmospheric CO_2 levels. Because the rate of CO_2 fertilization varies depending on the kind of ecosystem investigated, it is difficult to incorporate this complexity in the model. This emphasizes the importance of more study to improve the model's portrayal of this process. To do this, we must calibrate our land surface model using both Fluxnet and FACE data. This might be dangerous since Fluxnet-only optimizations may not perform well under increased circumstances, which is crucial for estimating the terrestrial reaction to climate change.

Optimizing a nitrogen-cycle LSM is another key problem, since it is more difficult and complex than optimizing a carbon-only LSM due to higher model feedback. One crucial process to enhance is free living BNF since it accounts for a considerable fraction of total BNF and hence determines the overall quantity of accessible reactive nitrogen. We underline the need of using more observational data from multiple ecosystems in our model in order to enhance our estimates of available reactive nitrogen, resulting in improved carbon nitrogen feedbacks and better carbon assimilation responses.

Contribution of this research:

This research provides numerous important scientific contributions to the subject of land-use and nitrogen-related uncertainty in terrestrial carbon storage change. It sheds light on the relative implications of land-use and nitrogen related uncertainties on changes in terrestrial carbon storage against uncertainty associated with atmospheric CO_2. This data may be used to gain a better understanding of the possibilities for land-based mitigation techniques in the context of climate change. We emphasize the need of giving harmonized and downscaled information regarding land-use changes, nitrogen emissions, and nitrogen atmospheric deposition trajectories simulated by all IAMs, not just the marker IAMs, for each SSP.

We present a comprehensive analysis of the effects of land-use and nitrogen-related uncertainties on the global land carbon store, emphasizing the importance of improved coordination between Integrated Assessment Models and Earth System Models for a more accurate assessment of the carbon cycle and climate change. This might lead to a better understanding of the particular challenges and opportunities for carbon sequestration and mitigation in diverse places of the world. Our findings underscore the importance of further research into the potential synergies between land-based mitigation measures like afforestation and reforestation and other mitigation approaches like renewable energy and energy efficiency.

Next steps of the research:

Sensitivity testing Earth System Model or land-only experiments will give a more precise evaluation of the unique IAM related uncertainty consequences on the carbon cycle and the climate system for each SSP. Improving methods for downscaling and harmonizing information from IAMs in order to better coordinate between Integrated Assessment Models and Earth System Models will allow for more consistent and accurate projections of land-use and nitrogen related uncertainties in future climate change scenarios. Additional developments on the regional impacts of land-use and nitrogen-related uncertainty may provide better knowledge of the unique problems and possibilities for carbon sequestration and mitigation in various regions of the world.

Understanding the trade-offs and potential for sustainable development by analyzing the economic and social consequences of land-based mitigation solutions. The findings of the research may be used to guide policy choices such as land-use planning, carbon offset schemes, and emission reduction objectives. It is crucial to emphasize that this study serves as a starting point for future research that will entail more advanced models, richer data, and greater collaboration between academics and stakeholders.

ORCHIDEE is a vital tool for understanding the complicated relationships between the Earth's carbon and nitrogen cycles and climate. However, the model's depiction of these cycles still

has a lot of space for development. We describe various areas of future research and development concentration.

By addressing the constraints of the present Biological Nitrogen Fixation (BNF) model, the N cycle in ORCHIDEE may be enhanced. Despite recent improvements, the model remains essentially empirical, with few data limitations. To solve this, a more mechanistic approach to modeling BNF may be required, combining the most recent breakthroughs in our understanding of the nitrogen cycle and how it is impacted by climate, land use, and other variables.

The description of the C cycle, particularly the relationship between C availability and N availability, is another area of study for enhancing the ORCHIDEE model. Consider the possible advantages of adopting C:N ratios as a more flexible and accurate depiction of nutrients constraint in the model. This might be especially relevant in tropical locations where P may be scarce. The model should also be updated to accommodate other potential nutritents constraints. This might lead to the creation of a "*CNP version*" of ORCHIDEE, allowing for more nuanced depictions of nutrient restriction across diverse geographies and situations.

It is critical to calibrate the ORCHIDEE model using a range of data sources to guarantee that it correctly captures the dynamics of the C and N cycles. One interesting way is to use data from the FACE studies, which examine ecosystem responses to rising CO2 levels in the atmosphere. We can acquire a better knowledge of how the C and N cycles interact with one another and how they are altered by climate change by undertaking these studies.

Finally, fully coupled simulations with the *LMDZ-ORCHIDEE* model will be required to completely capture the feedback between the C and N cycles and the climate. This will help us to better understand the intricate interaction of these two key processes and develop more accurate predictions about how the Earth's land surface will adapt to changing climatic situations. There is a wide range of research opportunities for refining the representation of the C and N cycles in the ORCHIDEE land surface model. We can gain a deeper understanding of how the Earth's carbon and nitrogen cycles interact with the climate and make more accurate predictions about their future behavior by addressing the limitations of the current model and incorporating the most recent advances in our understanding of these processes.

Bibliography

Albani, M., Medvigy, D., Hurtt, G. C., & Moorcroft, P. R. (2006). The contributions of land-use change, CO_2 fertilization, and climate variability to the Eastern US carbon sink: PARTITIONING OF THE EASTERN US CARBON SINK. *Global Change Biology*, *12*(12), 2370–2390. https://doi.org/10.1111/j.1365-2486.2006.01254.x

Alexander, V., & Bilington, M. M. (1986). *Nitrogen fixation in the Alaskan taiga*. Springer.

Archer, D., Eby, M., Brovkin, V., Ridgwell, A., Cao, L., Mikolajewicz, U., Caldeira, K., Matsumoto, K., Munhoven, G., Montenegro, A., & Tokos, K. (2009). Atmospheric Lifetime of Fossil Fuel Carbon Dioxide. *Annual Review of Earth and Planetary Sciences*, *37*(1), 117–134. https://doi.org/10.1146/annurev.earth.031208.100206

Arora, V. K., Katavouta, A., Williams, R. G., Jones, C. D., Brovkin, V., Friedlingstein, P., Schwinger, J., Bopp, L., Boucher, O., Cadule, P., Chamberlain, M. A., Christian, J. R., Delire, C., Fisher, R. A., Hajima, T., Ilyina, T., Joetzjer, E., Kawamiya, M., Koven, C. D., … Ziehn, T. (2020a). Carbon–concentration and carbon–climate feedbacks in CMIP6 models and their comparison to CMIP5 models. *Biogeosciences*, *17*(16), 4173–4222. https://doi.org/10.5194/bg-17-4173-2020

Arora, V. K., Katavouta, A., Williams, R. G., Jones, C. D., Brovkin, V., Friedlingstein, P., Schwinger, J., Bopp, L., Boucher, O., Cadule, P., Chamberlain, M. A., Christian, J. R., Delire, C., Fisher, R. A., Hajima, T., Ilyina, T., Joetzjer, E., Kawamiya, M., Koven, C. D., … Ziehn, T. (2020b). Carbon–concentration and carbon–climate feedbacks in CMIP6 models and their comparison to CMIP5 models. *Biogeosciences*, *17*(16), 4173–4222. https://doi.org/10.5194/bg-17-4173-2020

Bai, E., & Houlton, B. Z. (2009). Coupled isotopic and process-based modeling of gaseous nitrogen losses from tropical rain forests: MODELING N GAS FLUXES FROM RAIN FORESTS. *Global Biogeochemical Cycles*, *23*(2), n/a-n/a. https://doi.org/10.1029/2008GB003361

Baker, T. G., Oliver, G. R., & Hodgkiss, P. D. (1986). Distribution and cycling of nutrients in Pinus radiata as affected by past lupin growth and fertiliser. *Forest Ecology and Management*, *17*(2–3), 169–187. https://doi.org/10.1016/0378-1127(86)90110-6

Bala, G., Devaraju, N., Chaturvedi, R. K., Caldeira, K., & Nemani, R. (2013). Nitrogen deposition: How important is it for global terrestrial carbon uptake? *Biogeosciences*, *10*(11), 7147–

7160. https://doi.org/10.5194/bg-10-7147-2013

Ballantyne, A. P., Alden, C. B., Miller, J. B., Tans, P. P., & White, J. W. C. (2012). Increase in observed net carbon dioxide uptake by land and oceans during the past 50 years. *Nature*, *488*(7409), 70–72. https://doi.org/10.1038/nature11299

Bleeker, A., Hicks, W. K., Dentener, F., Galloway, J., & Erisman, J. W. (2011). N deposition as a threat to the World's protected areas under the Convention on Biological Diversity. *Environmental Pollution*, *159*(10), 2280–2288. https://doi.org/10.1016/j.envpol.2010.10.036

Boahene, K. (1998). The challenge of deforestation in tropical Africa: Reflections on its principal causes, consequences and solutions. *Land Degradation & Development*, *9*(3), 247–258. https://doi.org/10.1002/(SICI)1099-145X(199805/06)9:3<247::AID-LDR278>3.0.CO;2-G

Bonan, G. B., Lombardozzi, D. L., Wieder, W. R., Oleson, K. W., Lawrence, D. M., Hoffman, F. M., & Collier, N. (2019). Model Structure and Climate Data Uncertainty in Historical Simulations of the Terrestrial Carbon Cycle (1850–2014). *Global Biogeochemical Cycles*, *33*(10), 1310–1326. https://doi.org/10.1029/2019GB006175

Boote, K. J., Jones, J. W., & Hoogenboom, G. (1998). Simulation of crop growth: CROPGRO model. In *Agricultural systems modeling and simulation* (Marcel Dekker, pp. 651–692).

Bowman, W. D., Schardt, J. C., & Schmidt, S. K. (1996). Symbiotic N2-fixation in alpine tundra: Ecosystem input and variation in fixation rates among communities. *Oecologia*, *108*(2), 345–350. https://doi.org/10.1007/BF00334660

Burnett, A. C., Rogers, A., Rees, M., & Osborne, C. P. (2018). Nutrient sink limitation constrains growth in two barley species with contrasting growth strategies. *Plant Direct*, *2*(11). https://doi.org/10.1002/pld3.94

Calvin, K., Patel, P., Clarke, L., Asrar, G., Bond-Lamberty, B., Cui, R. Y., Di Vittorio, A., Dorheim, K., Edmonds, J., Hartin, C., Hejazi, M., Horowitz, R., Iyer, G., Kyle, P., Kim, S., Link, R., McJeon, H., Smith, S. J., Snyder, A., … Wise, M. (2019). GCAM v5.1: Representing the linkages between energy, water, land, climate, and economic systems. *Geoscientific Model Development*, *12*(2), 677–698. https://doi.org/10.5194/gmd-12-677-2019

Canadell, J. G., Monteiro, P. M. S., Costa, M. H., Cotrim da Cunha, L., Cox, P. M., Eliseev, S., Henson, M., Ishii, S., Jaccard, C., Koven, A., Lohila, P. K., Piao, S., Rogeli, J., Syampungani, S., Zaehle, S., & Zickfeld, K. (2021). Global Carbon and other

Biogeochemical Cycles and Feedbacks. In *Climate Change 2021: The Physical Science Basis. Contribution of Working Group I to the Sixth Assessment Report of the Intergovernmental Panel on Climate Change* (pp. 673–816). Cambridge University Press.

Chen, M., & Zhuang, Q. (2013). Modelling temperature acclimation effects on the carbon dynamics of forest ecosystems in the conterminous United States. *Tellus B: Chemical and Physical Meteorology*, *65*(1), 19156. https://doi.org/10.3402/tellusb.v65i0.19156

Cheng, S. J., Hess, P. G., Wieder, W. R., Thomas, R. Q., Nadelhoffer, K. J., Vira, J., Lombardozzi, D. L., Gundersen, P., Fernandez, I. J., Schleppi, P., Gruselle, M.-C., Moldan, F., & Goodale, C. L. (2018). *Decadal impacts of nitrogen additions on temperate forest carbon sinks: A data-model comparison* [Preprint]. Biogeochemistry: Modelling, Terrestrial. https://doi.org/10.5194/bg-2018-505

Churkina, G., Brovkin, V., von Bloh, W., Trusilova, K., Jung, M., & Dentener, F. (2009). Synergy of rising nitrogen depositions and atmospheric CO_2 on land carbon uptake moderately offsets global warming: CO_2 , N, CARBON UPTAKE AND GLOBAL WARMING. *Global Biogeochemical Cycles*, *23*(4), n/a-n/a. https://doi.org/10.1029/2008GB003291

Ciais, P., Sabine, C., Bala, G., Bopp, L., Brovkin, V., Canadell, J. G., Chhabra, A., DeFries, R., Galloway, J. N., Heinimann, M., Jones, C., Le Quéré, C., Myneni, R. B., Piao, S., & Thornton, P. (2013). Carbon and Other Biogeochemical Cycles. In *Climate Change 2013: The Physical Science Basis. Contribution of Working Group I to the Fifth Assessment Report of the Intergovernmental Panel on Climate Change*. Cambridge University Press.

Cleveland, C. C., Houlton, B. Z., Smith, W. K., Marklein, A. R., Reed, S. C., Parton, W., Grosso, S. J. D., & Running, S. W. (2013). *Patterns of new versus recycled primary production in the terrestrial biosphere*. 16.

Cleveland, C. C., Townsend, A. R., Schimel, D. S., Fisher, H., Howarth, R. W., Hedin, L. O., Perakis, S. S., Latty, E. F., Von Fischer, J. C., Elseroad, A., & Wasson, M. F. (1999). Global patterns of terrestrial biological nitrogen (N_2) fixation in natural ecosystems. *Global Biogeochemical Cycles*, *13*(2), 623–645. https://doi.org/10.1029/1999GB900014

Cox, P. M., Betts, R. A., Jones, C. D., Spall, S. A., & Totterdell, I. J. (2000). Acceleration of global warming due to carbon-cycle feedbacks in a coupled climate model. *Nature*,

408(6809), 184–187. https://doi.org/10.1038/35041539

Cusack, D. F., Silver, W., & McDowell, W. H. (2009). Biological Nitrogen Fixation in Two Tropical Forests: Ecosystem-Level Patterns and Effects of Nitrogen Fertilization. *Ecosystems*, *12*(8), 1299–1315. https://doi.org/10.1007/s10021-009-9290-0

Danabasoglu, G., Lamarque, J. -F., Bacmeister, J., Bailey, D. A., DuVivier, A. K., Edwards, J., Emmons, L. K., Fasullo, J., Garcia, R., Gettelman, A., Hannay, C., Holland, M. M., Large, W. G., Lauritzen, P. H., Lawrence, D. M., Lenaerts, J. T. M., Lindsay, K., Lipscomb, W. H., Mills, M. J., … Strand, W. G. (2020). The Community Earth System Model Version 2 (CESM2). *Journal of Advances in Modeling Earth Systems*, *12*(2). https://doi.org/10.1029/2019MS001916

Davies-Barnard, T., & Friedlingstein, P. (2020). The Global Distribution of Biological Nitrogen Fixation in Terrestrial Natural Ecosystems. *Global Biogeochemical Cycles*, *34*(3). https://doi.org/10.1029/2019GB006387

Davies-Barnard, T., Meyerholt, J., Zaehle, S., Friedlingstein, P., Brovkin, V., Fan, Y., Fisher, R. A., Jones, C. D., Lee, H., Peano, D., Smith, B., Wårlind, D., & Wiltshire, A. J. (2020). Nitrogen cycling in CMIP6 land surface models: Progress and limitations. *Biogeosciences*, *17*(20), 5129–5148. https://doi.org/10.5194/bg-17-5129-2020

DeFries, R. S., Field, C. B., Fung, I., Collatz, G. J., & Bounoua, L. (1999). Combining satellite data and biogeochemical models to estimate global effects of human-induced land cover change on carbon emissions and primary productivity. *Global Biogeochemical Cycles*, *13*(3), 803–815. https://doi.org/10.1029/1999GB900037

Dentener, F., Stevenson, D., Ellingsen, K., van Noije, T., Schultz, M., Amann, M., Atherton, C., Bell, N., Bergmann, D., Bey, I., Bouwman, L., Butler, T., Cofala, J., Collins, B., Drevet, J., Doherty, R., Eickhout, B., Eskes, H., Fiore, A., … Zeng, G. (2006). The Global Atmospheric Environment for the Next Generation. *Environmental Science & Technology*, *40*(11), 3586–3594. https://doi.org/10.1021/es0523845

Devaraju, N., Bala, G., Caldeira, K., & Nemani, R. (2016). A model based investigation of the relative importance of CO_2-fertilization, climate warming, nitrogen deposition and land use change on the global terrestrial carbon uptake in the historical period. *Climate Dynamics*, *47*(1–2), 173–190. https://doi.org/10.1007/s00382-015-2830-8

Dewar, R. C., Tarvainen, L., Parker, K., Wallin, G., & McMurtrie, R. E. (2012). Why does leaf nitrogen decline within tree canopies less rapidly than light? An explanation from

optimization subject to a lower bound on leaf mass per area. *Tree Physiology*, *32*(5), 520–534. https://doi.org/10.1093/treephys/tps044

Dilworth, M. J. (1966). Acetylene reduction by nitrogen-fixing preparations from Clostridium pasteurianum. *Biochimica et Biophysica Acta (BBA) - General Subjects*, *127*(2), 285–294. https://doi.org/10.1016/0304-4165(66)90383-7

Drake, B. G., Gonzàlez-Meler, M. A., & Long, S. P. (1997). MORE EFFICIENT PLANTS: A Consequence of Rising Atmospheric CO_2? *Annual Review of Plant Physiology and Plant Molecular Biology*, *48*(1), 609–639. https://doi.org/10.1146/annurev.arplant.48.1.609

Ducoudré, N. I., Laval, K., & Perrier, A. (1993). SECHIBA, a New Set of Parameterizations of the Hydrologic Exchanges at the Land-Atmosphere Interface within the LMD Atmospheric General Circulation Model. *Journal of Climate*, *6*(2), 248–273. https://doi.org/10.1175/1520-0442(1993)006<0248:SANSOP>2.0.CO;2

Elser, J. J., Bracken, M. E. S., Cleland, E. E., Gruner, D. S., Harpole, W. S., Hillebrand, H., Ngai, J. T., Seabloom, E. W., Shurin, J. B., & Smith, J. E. (2007). Global analysis of nitrogen and phosphorus limitation of primary producers in freshwater, marine and terrestrial ecosystems. *Ecology Letters*, *10*(12), 1135–1142. https://doi.org/10.1111/j.1461-0248.2007.01113.x

Erisman, J. W., Sutton, M. A., Galloway, J., Klimont, Z., & Winiwarter, W. (2008). How a century of ammonia synthesis changed the world. *Nature Geoscience*, *1*(10), 636–639. https://doi.org/10.1038/ngeo325

Farquhar, G. D., von Caemmerer, S., & Berry, J. A. (1980). A biochemical model of photosynthetic CO_2 assimilation in leaves of C3 species. *Planta*, *149*(1), 78–90. https://doi.org/10.1007/BF00386231

Finzi, A. C., DeLucia, E. H., Hamilton, J. G., Richter, D. D., & Schlesinger, W. H. (2002). The nitrogen budget of a pine forest under free air CO_2 enrichment. *Oecologia*, *132*(4), 567–578. https://doi.org/10.1007/s00442-002-0996-3

Fisher, J. B., Badgley, G., & Blyth, E. (2012). Global nutrient limitation in terrestrial vegetation. *Global Biogeochemical Cycles*, *26*(3), 2011GB004252. https://doi.org/10.1029/2011GB004252

Fisher, R. A., & Koven, C. D. (2020). Perspectives on the Future of Land Surface Models and the Challenges of Representing Complex Terrestrial Systems. *Journal of Advances in*

Modeling Earth Systems, *12*(4). https://doi.org/10.1029/2018MS001453

Fisher, R. A., Koven, C. D., Anderegg, W. R. L., Christoffersen, B. O., Dietze, M. C., Farrior, C. E., Holm, J. A., Hurtt, G. C., Knox, R. G., Lawrence, P. J., Lichstein, J. W., Longo, M., Matheny, A. M., Medvigy, D., Muller-Landau, H. C., Powell, T. L., Serbin, S. P., Sato, H., Shuman, J. K., … Moorcroft, P. R. (2018). Vegetation demographics in Earth System Models: A review of progress and priorities. *Global Change Biology*, *24*(1), 35–54. https://doi.org/10.1111/gcb.13910

Flechard, C. R., Ibrom, A., Skiba, U. M., de Vries, W., van Oijen, M., Cameron, D. R., Dise, N. B., Korhonen, J. F. J., Buchmann, N., Legout, A., Simpson, D., Sanz, M. J., Aubinet, M., Loustau, D., Montagnani, L., Neirynck, J., Janssens, I. A., Pihlatie, M., Kiese, R., … Sutton, M. A. (2020). Carbon–nitrogen interactions in European forests and semi-natural vegetation – Part 1: Fluxes and budgets of carbon, nitrogen and greenhouse gases from ecosystem monitoring and modelling. *Biogeosciences*, *17*(6), 1583–1620. https://doi.org/10.5194/bg-17-1583-2020

Flechard, C. R., van Oijen, M., Cameron, D. R., de Vries, W., Ibrom, A., Buchmann, N., Dise, N. B., Janssens, I. A., Neirynck, J., Montagnani, L., Varlagin, A., Loustau, D., Legout, A., Ziemblińska, K., Aubinet, M., Aurela, M., Chojnicki, B. H., Drewer, J., Eugster, W., … Sutton, M. A. (2020). Carbon–nitrogen interactions in European forests and semi-natural vegetation – Part 2: Untangling climatic, edaphic, management and nitrogen deposition effects on carbon sequestration potentials. *Biogeosciences*, *17*(6), 1621–1654. https://doi.org/10.5194/bg-17-1621-2020

Fowler, D., Coyle, M., Skiba, U., Sutton, M. A., Cape, J. N., Reis, S., Sheppard, L. J., Jenkins, A., Grizzetti, B., Galloway, J. N., Vitousek, P., Leach, A., Bouwman, A. F., Butterbach-Bahl, K., Dentener, F., Stevenson, D., Amann, M., & Voss, M. (2013). The global nitrogen cycle in the twenty-first century. *Philosophical Transactions of the Royal Society B: Biological Sciences*, *368*(1621), 20130164. https://doi.org/10.1098/rstb.2013.0164

Fricko, O., Havlik, P., Rogelj, J., Klimont, Z., Gusti, M., Johnson, N., Kolp, P., Strubegger, M., Valin, H., Amann, M., Ermolieva, T., Forsell, N., Herrero, M., Heyes, C., Kindermann, G., Krey, V., McCollum, D. L., Obersteiner, M., Pachauri, S., … Riahi, K. (2017). The marker quantification of the Shared Socioeconomic Pathway 2: A middle-of-the-road scenario for the 21st century. *Global Environmental Change*, *42*, 251–267. https://doi.org/10.1016/j.gloenvcha.2016.06.004

Friedlingstein, P., Jones, M. W., O'Sullivan, M., Andrew, R. M., Bakker, D. C. E., Hauck, J., Le Quéré, C., Peters, G. P., Peters, W., Pongratz, J., Sitch, S., Canadell, J. G., Ciais, P., Jackson, R. B., Alin, S. R., Anthoni, P., Bates, N. R., Becker, M., Bellouin, N., … Zeng, J. (2022). Global Carbon Budget 2021. *Earth System Science Data*, *14*(4), 1917–2005. https://doi.org/10.5194/essd-14-1917-2022

Friedlingstein, P., Jones, M. W., O'Sullivan, M., Andrew, R. M., Hauck, J., Peters, G. P., Peters, W., Pongratz, J., Sitch, S., Le Quéré, C., Bakker, D. C. E., Canadell, J. G., Ciais, P., Jackson, R. B., Anthoni, P., Barbero, L., Bastos, A., Bastrikov, V., Becker, M., … Zaehle, S. (2019). Global Carbon Budget 2019. *Earth System Science Data*, *11*(4), 1783–1838. https://doi.org/10.5194/essd-11-1783-2019

Friedlingstein, P., Meinshausen, M., Arora, V. K., Jones, C. D., Anav, A., Liddicoat, S. K., & Knutti, R. (2014). Uncertainties in CMIP5 Climate Projections due to Carbon Cycle Feedbacks. *Journal of Climate*, *27*(2), 511–526. https://doi.org/10.1175/JCLI-D-12-00579.1

Friedlingstein, P., O'Sullivan, M., Jones, M. W., Andrew, R. M., Hauck, J., Olsen, A., Peters, G. P., Peters, W., Pongratz, J., Sitch, S., Le Quéré, C., Canadell, J. G., Ciais, P., Jackson, R. B., Alin, S., Aragão, L. E. O. C., Arneth, A., Arora, V., Bates, N. R., … Zaehle, S. (2020). Global Carbon Budget 2020. *Earth System Science Data*, *12*(4), 3269–3340. https://doi.org/10.5194/essd-12-3269-2020

Fujimori, S., Hasegawa, T., Masui, T., Takahashi, K., Herran, D. S., Dai, H., Hijioka, Y., & Kainuma, M. (2017). SSP3: AIM implementation of Shared Socioeconomic Pathways. *Global Environmental Change*, *42*, 268–283. https://doi.org/10.1016/j.gloenvcha.2016.06.009

Galloway, J. N., Dentener, F. J., Capone, D. G., Boyer, E. W., Howarth, R. W., Seitzinger, S. P., Asner, G. P., Cleveland, C. C., Green, P. A., Holland, E. A., Karl, D. M., Michaels, A. F., Porter, J. H., Townsend, A. R., & V�osmarty, C. J. (2004). Nitrogen Cycles: Past, Present, and Future. *Biogeochemistry*, *70*(2), 153–226. https://doi.org/10.1007/s10533-004-0370-0

Gavito, M. E. (2000). Atmospheric CO_2 and mycorrhiza effects on biomass allocation and nutrient uptake of nodulated pea (Pisum sativum L.) plants. *Journal of Experimental Botany*, *51*(352), 1931–1938. https://doi.org/10.1093/jexbot/51.352.1931

Gidden, M. J., Riahi, K., Smith, S. J., Fujimori, S., Luderer, G., Kriegler, E., van Vuuren, D. P., van

den Berg, M., Feng, L., Klein, D., Calvin, K., Doelman, J. C., Frank, S., Fricko, O., Harmsen, M., Hasegawa, T., Havlik, P., Hilaire, J., Hoesly, R., … Takahashi, K. (2019). Global emissions pathways under different socioeconomic scenarios for use in CMIP6: A dataset of harmonized emissions trajectories through the end of the century. *Geoscientific Model Development*, *12*(4), Article 4. https://doi.org/10.5194/gmd-12-1443-2019

Goll, D. S., Vuichard, N., Maignan, F., Jornet-Puig, A., Sardans, J., Violette, A., Peng, S., Sun, Y., Kvakic, M., Guimberteau, M., Guenet, B., Zaehle, S., Penuelas, J., Janssens, I., & Ciais, P. (2017). A representation of the phosphorus cycle for ORCHIDEE (revision 4520). *Geoscientific Model Development*, *10*(10), 3745–3770. https://doi.org/10.5194/gmd-10-3745-2017

Govind, A., & Kumari, J. (2014). Understanding the Terrestrial Carbon Cycle: An Ecohydrological Perspective. *International Journal of Ecology*, *2014*, 1–18. https://doi.org/10.1155/2014/712537

Gruber, N. (2008). *Nitrogen in the marine environment*. Academic Press.

Hamilton III, E. W., Heckathorn, S. A., Joshi, P., Wang, D., & Barua, D. (2008). Interactive Effects of Elevated CO_2 and Growth Temperature on the Tolerance of Photosynthesis to Acute Heat Stress in C3 and C4 Species. *Journal of Integrative Plant Biology*, *50*(11), 1375–1387. https://doi.org/10.1111/j.1744-7909.2008.00747.x

Hansell, D., Carlson, C., Repeta, D., & Schlitzer, R. (2009). Dissolved Organic Matter in the Ocean: A Controversy Stimulates New Insights. *Oceanography*, *22*(4), 202–211. https://doi.org/10.5670/oceanog.2009.109

Hedin, L. O., Brookshire, E. N. J., Menge, D. N. L., & Barron, A. R. (2009). The Nitrogen Paradox in Tropical Forest Ecosystems. *Annual Review of Ecology, Evolution, and Systematics*, *40*(1), 613–635. https://doi.org/10.1146/annurev.ecolsys.37.091305.110246

Hendrickson, O. Q. (1990). Asymbiotic nitrogen fixation and soil metabolism in three Ontario forests. *Soil Biology and Biochemistry*, *22*(7), 967–971. https://doi.org/10.1016/0038-0717(90)90137-O

Hertel, O., Reis, S., Skjøth, C. A., Bleeker, A., Harrison, R., Cape, J. N., Fowler, D., Skiba, U., Simpson, D., Jickells, T., Baker, A., Kulmala, M., Gyldenkærne, S., Sørensen, L. L., & Erisman, J. W. (2011). Nitrogen processes in the atmosphere. In M. A. Sutton, C. M. Howard, J. W. Erisman, G. Billen, A. Bleeker, P. Grennfelt, H. van Grinsven, & B.

Grizzetti (Eds.), *The European Nitrogen Assessment* (pp. 177–208). Cambridge University Press. https://doi.org/10.1017/CBO9780511976988.012

Hoffman, B. M., Lukoyanov, D., Yang, Z.-Y., Dean, D. R., & Seefeldt, L. C. (2014). Mechanism of Nitrogen Fixation by Nitrogenase: The Next Stage. *Chemical Reviews*, *114*(8), 4041–4062. https://doi.org/10.1021/cr400641x

Högberg, P., Näsholm, T., Franklin, O., & Högberg, M. N. (2017). Tamm Review: On the nature of the nitrogen limitation to plant growth in Fennoscandian boreal forests. *Forest Ecology and Management*, *403*, 161–185. https://doi.org/10.1016/j.foreco.2017.04.045

Holland, E. A., Braswell, B. H., Sulzman, J., & Lamarque, J.-F. (2005). NITROGEN DEPOSITION ONTO THE UNITED STATES AND WESTERN EUROPE: SYNTHESIS OF OBSERVATIONS AND MODELS. *Ecological Applications*, *15*(1), 38–57. https://doi.org/10.1890/03-5162

Houghton, R. A. (2003). The Contemporary Carbon Cycle. In *Treatise on Geochemistry* (pp. 473–513). Elsevier. https://doi.org/10.1016/B0-08-043751-6/08168-8

Houghton, R. A., & Castanho, A. (2022). *Annual emissions of carbon from land use, land-use change, and forestry 1850–2020* [Preprint]. ESSD – Land/Land Cover and Land Use. https://doi.org/10.5194/essd-2022-351

Houghton, R. A., & Nassikas, A. A. (2017). Global and regional fluxes of carbon from land use and land cover change 1850-2015: Carbon Emissions From Land Use. *Global Biogeochemical Cycles*, *31*(3), 456–472. https://doi.org/10.1002/2016GB005546

Huntzinger, D. N., Michalak, A. M., Schwalm, C., Ciais, P., King, A. W., Fang, Y., Schaefer, K., Wei, Y., Cook, R. B., Fisher, J. B., Hayes, D., Huang, M., Ito, A., Jain, A. K., Lei, H., Lu, C., Maignan, F., Mao, J., Parazoo, N., … Zhao, F. (2017). Uncertainty in the response of terrestrial carbon sink to environmental drivers undermines carbon-climate feedback predictions. *Scientific Reports*, *7*(1), 4765. https://doi.org/10.1038/s41598-017-03818-2

Hurtt, G. C., Chini, L., Sahajpal, R., Frolking, S., Bodirsky, B. L., Calvin, K., Doelman, J. C., Fisk, J., Fujimori, S., Goldewijk, K. K., Hasegawa, T., Havlik, P., Heinimann, A., Humpenöder, F., Jungclaus, J., Kaplan, J., Kennedy, J., Kristzin, T., Lawrence, D., … Zhang, X. (2020). *Harmonization of Global Land-Use Change and Management for the Period 850–2100 (LUH2) for CMIP6* [Preprint]. Climate and Earth System Modeling. https://doi.org/10.5194/gmd-2019-360

Hurtt, G., Chini, L., Sahajpal, R., Frolking, S., Bodirsky, B. L., Calvin, K., Doelman, J., Fisk, J.,

Fujimori, S., Goldewijk, K. K., Hasegawa, T., Havlik, P., Heinimann, A., Humpenöder, F., Jungclaus, J., Kaplan, J., Krisztin, T., Lawrence, D., Lawrence, P., … Zhang, X. (2017). *Harmonization of global land use scenarios (LUH2): Historical v2.1h 850 - 2015* (Version 20210201) [Application/x-netcdf]. Earth System Grid Federation. https://doi.org/10.22033/ESGF/INPUT4MIPS.1127

Jaffe, D. (2003). Nitrogen Cycle, Atmospheric. In *Encyclopedia of Physical Science and Technology* (pp. 431–440). Elsevier. https://doi.org/10.1016/B0-12-227410-5/00922-4

Janowiak, Connelly, Dante-Wood, Domke, Giardina, Kayler, Marcinkowski, Ontl, Rodriguez-Franco, Swanston, Woodall, & Buford. (2017). *Considering Forest and Grassland Carbon in Land Management*. https://doi.org/10.13140/RG.2.2.35421.20964

Jarrell, W. M., & Virginia, R. A. (1990). Soil cation accumulation in a mesquite woodland: Sustained production and long-term estimates of water use and nitrogen fixation. *Journal of Arid Environments*, *18*(1), 51–58. https://doi.org/10.1016/S0140-1963(18)30869-3

Jones, C. D., & Friedlingstein, P. (2020). Quantifying process-level uncertainty contributions to TCRE and carbon budgets for meeting Paris Agreement climate targets. *Environmental Research Letters*, *15*(7), 074019. https://doi.org/10.1088/1748-9326/ab858a

Jones, C., Robertson, E., Arora, V., Friedlingstein, P., Shevliakova, E., Bopp, L., Brovkin, V., Hajima, T., Kato, E., Kawamiya, M., Liddicoat, S., Lindsay, K., Reick, C. H., Roelandt, C., Segschneider, J., & Tjiputra, J. (2013). Twenty-First-Century Compatible CO_2 Emissions and Airborne Fraction Simulated by CMIP5 Earth System Models under Four Representative Concentration Pathways. *Journal of Climate*, *26*(13), 4398–4413. https://doi.org/10.1175/JCLI-D-12-00554.1

Joos, F., & Spahni, R. (2008). Rates of change in natural and anthropogenic radiative forcing over the past 20,000 years. *Proceedings of the National Academy of Sciences*, *105*(5), 1425–1430. https://doi.org/10.1073/pnas.0707386105

Jung, M., Reichstein, M., Margolis, H. A., Cescatti, A., Richardson, A. D., Arain, M. A., Arneth, A., Bernhofer, C., Bonal, D., Chen, J., Gianelle, D., Gobron, N., Kiely, G., Kutsch, W., Lasslop, G., Law, B. E., Lindroth, A., Merbold, L., Montagnani, L., … Williams, C. (2011). Global patterns of land-atmosphere fluxes of carbon dioxide, latent heat, and sensible heat derived from eddy covariance, satellite, and meteorological observations. *Journal of*

Geophysical Research, *116*, G00J07. https://doi.org/10.1029/2010JG001566

Kästner, J., & Blöchl, P. E. (2005). Model for Acetylene Reduction by Nitrogenase Derived from Density Functional Theory. *Inorganic Chemistry*, *44*(13), 4568–4575. https://doi.org/10.1021/ic0500311

Kattge, J., & Knorr, W. (2007). Temperature acclimation in a biochemical model of photosynthesis: A reanalysis of data from 36 species. *Plant, Cell & Environment*, *30*(9), 1176–1190. https://doi.org/10.1111/j.1365-3040.2007.01690.x

Kattge, J., Knorr, W., Raddatz, T., & Wirth, C. (2009). Quantifying photosynthetic capacity and its relationship to leaf nitrogen content for global-scale terrestrial biosphere models. *Global Change Biology*, *15*(4), 976–991. https://doi.org/10.1111/j.1365-2486.2008.01744.x

Kayler, Z., Janowiak, M., & Swanston, C. (2017). Global Carbon Cycle. In *Considering Forest and Grassland Carbon in Land Management*. United States Department of Agriculture.

Keeling, C. D., Bacastow, R. B., Bainbridge, A. E., Ekdahl, C. A., Guenther, P. R., Waterman, L. S., & Chin, J. F. S. (1976). Atmospheric carbon dioxide variations at Mauna Loa Observatory, Hawaii. *Tellus*, *28*(6), 538–551. https://doi.org/10.1111/j.2153-3490.1976.tb00701.x

Kennedy, D., Swenson, S., Oleson, K. W., Lawrence, D. M., Fisher, R., Lola da Costa, A. C., & Gentine, P. (2019). Implementing Plant Hydraulics in the Community Land Model, Version 5. *Journal of Advances in Modeling Earth Systems*, *11*(2), 485–513. https://doi.org/10.1029/2018MS001500

Kicklighter, D. W., Melillo, J. M., Monier, E., Sokolov, A. P., & Zhuang, Q. (2019). Future nitrogen availability and its effect on carbon sequestration in Northern Eurasia. *Nature Communications*, *10*(1), 3024. https://doi.org/10.1038/s41467-019-10944-0

Kolby Smith, W., Reed, S. C., Cleveland, C. C., Ballantyne, A. P., Anderegg, W. R. L., Wieder, W. R., Liu, Y. Y., & Running, S. W. (2016). Large divergence of satellite and Earth system model estimates of global terrestrial CO_2 fertilization. *Nature Climate Change*, *6*(3), 306–310. https://doi.org/10.1038/nclimate2879

Körner, C., Morgan, J., & Norby, R. (2007). CO_2 Fertilization: When, Where, How Much? In J. G. Canadell, D. E. Pataki, & L. F. Pitelka (Eds.), *Terrestrial Ecosystems in a Changing World* (pp. 9–21). Springer Berlin Heidelberg. https://doi.org/10.1007/978-3-540-32730-1_2

Kriegler, E., Bauer, N., Popp, A., Humpenöder, F., Leimbach, M., Strefler, J., Baumstark, L.,

Bodirsky, B. L., Hilaire, J., Klein, D., Mouratiadou, I., Weindl, I., Bertram, C., Dietrich, J.-P., Luderer, G., Pehl, M., Pietzcker, R., Piontek, F., Lotze-Campen, H., … Edenhofer, O. (2017). Fossil-fueled development (SSP5): An energy and resource intensive scenario for the 21st century. *Global Environmental Change*, *42*, 297–315. https://doi.org/10.1016/j.gloenvcha.2016.05.015

Krinner, G., Viovy, N., de Noblet-Ducoudré, N., Ogée, J., Polcher, J., Friedlingstein, P., Ciais, P., Sitch, S., & Prentice, I. C. (2005). A dynamic global vegetation model for studies of the coupled atmosphere-biosphere system: DVGM FOR COUPLED CLIMATE STUDIES. *Global Biogeochemical Cycles*, *19*(1). https://doi.org/10.1029/2003GB002199

Kronzucker, H. J., Siddiqi, M. Y., & Glass, Adm. (1996). Kinetics of NH4+ Influx in Spruce. *Plant Physiology*, *110*(3), 773–779. https://doi.org/10.1104/pp.110.3.773

Kronzucker, HerbertJ., Siddiqi, M. Y., & Glass, AnthonyD. M. (1995). Compartmentation and flux characteristics of nitrate in spruce. *Planta*, *196*(4). https://doi.org/10.1007/BF00197331

Lamarque, J.-F., Dentener, F., McConnell, J., Ro, C.-U., Shaw, M., Vet, R., Bergmann, D., Cameron-Smith, P., Dalsoren, S., Doherty, R., Faluvegi, G., Ghan, S. J., Josse, B., Lee, Y. H., MacKenzie, I. A., Plummer, D., Shindell, D. T., Skeie, R. B., Stevenson, D. S., … Nolan, M. (2013). Multi-model mean nitrogen and sulfur deposition from the Atmospheric Chemistry and Climate Model Intercomparison Project (ACCMIP): Evaluation of historical and projected future changes. *Atmospheric Chemistry and Physics*, *13*(16), 7997–8018. https://doi.org/10.5194/acp-13-7997-2013

Lawrence, D. M., Fisher, R. A., Koven, C. D., Oleson, K. W., Swenson, S. C., Bonan, G., Collier, N., Ghimire, B., Kampenhout, L., Kennedy, D., Kluzek, E., Lawrence, P. J., Li, F., Li, H., Lombardozzi, D., Riley, W. J., Sacks, W. J., Shi, M., Vertenstein, M., … Zeng, X. (2019). The Community Land Model Version 5: Description of New Features, Benchmarking, and Impact of Forcing Uncertainty. *Journal of Advances in Modeling Earth Systems*, *11*(12), 4245–4287. https://doi.org/10.1029/2018MS001583

LeBauer, D. S., & Treseder, K. K. (2008). NITROGEN LIMITATION OF NET PRIMARY PRODUCTIVITY IN TERRESTRIAL ECOSYSTEMS IS GLOBALLY DISTRIBUTED. *Ecology*, *89*(2), 371–379. https://doi.org/10.1890/06-2057.1

Lehtonen, H. S., Aakkula, J., Fronzek, S., Helin, J., Hildén, M., Huttunen, S., Kaljonen, M., Niemi, J., Palosuo, T., Pirttioja, N., Rikkonen, P., Varho, V., & Carter, T. R. (2021). Shared

socioeconomic pathways for climate change research in Finland: Co-developing extended SSP narratives for agriculture. *Regional Environmental Change*, *21*(1), 7. https://doi.org/10.1007/s10113-020-01734-2

Ley, R. E., & D'Antonio, C. M. (1998). Exotic grass invasion alters potential rates of N fixation in Hawaiian woodlands. *Oecologia*, *113*(2), 179–187. https://doi.org/10.1007/s004420050366

Lindemann, W. C. (2008). Nitrogen Fixation by Legumes. *College of Agriculture and Home Economics, New Mexico State University*, 4.

Liu, L., Zhang, T., Gilliam, F. S., Gundersen, P., Zhang, W., Chen, H., & Mo, J. (2013). Interactive Effects of Nitrogen and Phosphorus on Soil Microbial Communities in a Tropical Forest. *PLoS ONE*, *8*(4), e61188. https://doi.org/10.1371/journal.pone.0061188

Loehle, C. (1995). Anomalous Responses of Plants to CO 2 Enrichment. *Oikos*, *73*(2), 181. https://doi.org/10.2307/3545906

Long, S. P. (1991). Modification of the response of photosynthetic productivity to rising temperature by atmospheric CO_2 concentrations: Has its importance been underestimated? *Plant, Cell and Environment*, *14*(8), 729–739. https://doi.org/10.1111/j.1365-3040.1991.tb01439.x

Lu, X., Vitousek, P. M., Mao, Q., Gilliam, F. S., Luo, Y., Turner, B. L., Zhou, G., & Mo, J. (2021). Nitrogen deposition accelerates soil carbon sequestration in tropical forests. *Proceedings of the National Academy of Sciences*, *118*(16), e2020790118. https://doi.org/10.1073/pnas.2020790118

Macduff, J. H., Jarvis, S. C., & Davidson, I. A. (1996). Inhibition of N2 fixation by white clover (Trifolium repens L.) at low concentrations of NO3 in flowing solution culture. *KluwerAcademic Publishers*.

Marino, D., Frendo, P., Ladrera, R., Zabalza, A., Puppo, A., Arrese-Igor, C., & Gonzalez, E. M. (2007). *Nitrogen Fixation Control under Drought Stress. Localized or Systemic?1[OA]*. *143*, 7.

Matson, P., Lohse, K. A., & Hall, S. J. (2002). The Globalization of Nitrogen Deposition: Consequences for Terrestrial Ecosystems. *AMBIO: A Journal of the Human Environment*, *31*(2), 113–119. https://doi.org/10.1579/0044-7447-31.2.113

Meinshausen, M., Nicholls, Z. R. J., Lewis, J., Gidden, M. J., Vogel, E., Freund, M., Beyerle, U., Gessner, C., Nauels, A., Bauer, N., Canadell, J. G., Daniel, J. S., John, A., Krummel, P. B.,

Luderer, G., Meinshausen, N., Montzka, S. A., Rayner, P. J., Reimann, S., … Wang, R. H. J. (2020). The shared socio-economic pathway (SSP) greenhouse gas concentrations and their extensions to 2500. *Geoscientific Model Development*, *13*(8), 3571–3605. https://doi.org/10.5194/gmd-13-3571-2020

Melillo, J. M., Butler, S., Johnson, J., Mohan, J., Steudler, P., Lux, H., Burrows, E., Bowles, F., Smith, R., Scott, L., Vario, C., Hill, T., Burton, A., Zhou, Y.-M., & Tang, J. (2011). Soil warming, carbon–nitrogen interactions, and forest carbon budgets. *Proceedings of the National Academy of Sciences*, *108*(23), 9508–9512. https://doi.org/10.1073/pnas.1018189108

Mitchell, T. D., & Jones, P. D. (2005). An improved method of constructing a database of monthly climate observations and associated high-resolution grids. *International Journal of Climatology*, *25*(6), 693–712. https://doi.org/10.1002/joc.1181

Mus, F., Alleman, A. B., Pence, N., Seefeldt, L. C., & Peters, J. W. (2018). Exploring the alternatives of biological nitrogen fixation. *Metallomics*, *10*(4), 523–538. https://doi.org/10.1039/C8MT00038G

NOAA. (2022). *Trends in Atmospheric Carbon Dioxide*. Global Monitoring Laboratory Earth System Research Laboratories. https://gml.noaa.gov/ccgg/trends/monthly.html

Nohrstedt, H.-O. (1985). Biological Activity in Soil from Forest Stands in Central Sweden, as Related to Site Properties. *Springer-Verlag*, 259–266.

Norby, R. J., De Kauwe, M. G., Domingues, T. F., Duursma, R. A., Ellsworth, D. S., Goll, D. S., Lapola, D. M., Luus, K. A., MacKenzie, A. R., Medlyn, B. E., Pavlick, R., Rammig, A., Smith, B., Thomas, R., Thonicke, K., Walker, A. P., Yang, X., & Zaehle, S. (2016). Model–data synthesis for the next generation of forest free-air CO_2 enrichment (FACE) experiments. *New Phytologist*, *209*(1), 17–28. https://doi.org/10.1111/nph.13593

Norby, R. J., Warren, J. M., Iversen, C. M., Medlyn, B. E., & McMurtrie, R. E. (2010). CO_2 enhancement of forest productivity constrained by limited nitrogen availability. *Proceedings of the National Academy of Sciences*, *107*(45), 19368–19373. https://doi.org/10.1073/pnas.1006463107

Nowak, R. S., Ellsworth, D. S., & Smith, S. D. (2004). Functional responses of plants to elevated atmospheric CO_2 – do photosynthetic and productivity data from FACE experiments support early predictions? *New Phytologist*, *162*(2), 253–280. https://doi.org/10.1111/j.1469-8137.2004.01033.x

O'Neill, B. C., Tebaldi, C., van Vuuren, D. P., Eyring, V., Friedlingstein, P., Hurtt, G., Knutti, R., Kriegler, E., Lamarque, J.-F., Lowe, J., Meehl, G. A., Moss, R., Riahi, K., & Sanderson, B. M. (2016). The Scenario Model Intercomparison Project (ScenarioMIP) for CMIP6. *Geoscientific Model Development*, *9*(9), 3461–3482. https://doi.org/10.5194/gmd-9-3461-2016

O'Sullivan, M., Spracklen, D. V., Batterman, S., Arnold, S. R., Gloor, M., & Buermann, W. (2019). Have synergies between nitrogen deposition and atmospheric CO_2 driven the recent enhancement of the terrestrial carbon sink? *Global Biogeochemical Cycles*, 2018GB005922. https://doi.org/10.1029/2018GB005922

Padrón, R. S., Gudmundsson, L., Liu, L., Humphrey, V., & Seneviratne, S. I. (2022). Drivers of intermodel uncertainty in land carbon sink projections. *Biogeosciences*, *19*(23), 5435–5448. https://doi.org/10.5194/bg-19-5435-2022

Pan, Y., Birdsey, R. A., Phillips, O. L., & Jackson, R. B. (2013). The Structure, Distribution, and Biomass of the World's Forests. *Annual Review of Ecology, Evolution, and Systematics*, *44*(1), 593–622. https://doi.org/10.1146/annurev-ecolsys-110512-135914

Peng, J., Dan, L., Tang, X., & Yang, F. (2022). Trends in carbon sink along the Belt and Road in the future under high emission scenario. *Atmospheric and Oceanic Science Letters*, *15*(3), 100149. https://doi.org/10.1016/j.aosl.2022.100149

Peng, J., Wang, Y., Houlton, B. Z., Dan, L., Pak, B., & Tang, X. (2020). Global Carbon Sequestration Is Highly Sensitive to Model-Based Formulations of Nitrogen Fixation. *Global Biogeochemical Cycles*, *34*(1). https://doi.org/10.1029/2019GB006296

Peters, J. W., & Szilagyi, R. K. (2006). Exploring new frontiers of nitrogenase structure and mechanism. *Current Opinion in Chemical Biology*, *10*(2), 101–108. https://doi.org/10.1016/j.cbpa.2006.02.019

Postgate, J. R. (1982). Biology Nitrogen Fixation: Fundamentals. *Philosophical Transactions of the Royal Society of London. Series B, Biological Sciences*, *296*(1082,), 375–385.

Poulter, B., Frank, D., Ciais, P., Myneni, R. B., Andela, N., Bi, J., Broquet, G., Canadell, J. G., Chevallier, F., Liu, Y. Y., Running, S. W., Sitch, S., & van der Werf, G. R. (2014). Contribution of semi-arid ecosystems to interannual variability of the global carbon cycle. *Nature*, *509*(7502), 600–603. https://doi.org/10.1038/nature13376

Poulter, B., MacBean, N., Hartley, A., Khlystova, I., Arino, O., Betts, R., Bontemps, S., Boettcher, M., Brockmann, C., Defourny, P., Hagemann, S., Herold, M., Kirches, G., Lamarche, C.,

Lederer, D., Ottlé, C., Peters, M., & Peylin, P. (2015). Plant functional type classification for earth system models: Results from the European Space Agency's Land Cover Climate Change Initiative. *Geoscientific Model Development*, *8*(7), 2315–2328. https://doi.org/10.5194/gmd-8-2315-2015

Riahi, K., van Vuuren, D. P., Kriegler, E., Edmonds, J., O'Neill, B. C., Fujimori, S., Bauer, N., Calvin, K., Dellink, R., Fricko, O., Lutz, W., Popp, A., Cuaresma, J. C., Kc, S., Leimbach, M., Jiang, L., Kram, T., Rao, S., Emmerling, J., … Tavoni, M. (2017). The Shared Socioeconomic Pathways and their energy, land use, and greenhouse gas emissions implications: An overview. *Global Environmental Change*, *42*, 153–168. https://doi.org/10.1016/j.gloenvcha.2016.05.009

Ritchie, H., Roser, M., & Rosado, P. (2020). *CO_2 and Greenhouse Gas Emissions*. Our World in Data. https://ourworldindata.org/CO_2-and-other-greenhouse-gas-emissions

Schrire, B., Lewis, G., & Lavin, M. (2005). Biogeography of the Leguminosae. In *Legumes of the World* (pp. 21–54). Kew Publishing.

Seefeldt, L. C., Hoffman, B. M., & Dean, D. R. (2009). Mechanism of Mo-Dependent Nitrogenase. *Annual Review of Biochemistry*, *78*(1), 701–722. https://doi.org/10.1146/annurev.biochem.78.070907.103812

Seiler, C., Melton, J. R., Arora, V. K., Sitch, S., Friedlingstein, P., Anthoni, P., Goll, D., Jain, A. K., Joetzjer, E., Lienert, S., Lombardozzi, D., Luyssaert, S., Nabel, J. E. M. S., Tian, H., Vuichard, N., Walker, A. P., Yuan, W., & Zaehle, S. (2022). Are Terrestrial Biosphere Models Fit for Simulating the Global Land Carbon Sink? *Journal of Advances in Modeling Earth Systems*, *14*(5). https://doi.org/10.1029/2021MS002946

Sheridan, R. P. (1991). Nitrogenase Activity by Hapalosiphon flexuosus Associated With Sphagnum erythrocalyx Mats in the Cloud Forest on the Volcano La Soufriere, Guadeloupe, French West Indies. *Biotropica*, *23*(2), 134. https://doi.org/10.2307/2388298

Sinha, E., Michalak, A. M., Calvin, K. V., & Lawrence, P. J. (2019). Societal decisions about climate mitigation will have dramatic impacts on eutrophication in the 21st century. *Nature Communications*, *10*(1), 939. https://doi.org/10.1038/s41467-019-08884-w

Sitch, S., Huntingford, C., Gedney, N., Levy, P. E., Lomas, M., Piao, S. L., Betts, R., Ciais, P., Cox, P., Friedlingstein, P., Jones, C. D., Prentice, I. C., & Woodward, F. I. (2008). Evaluation of the terrestrial carbon cycle, future plant geography and climate-carbon cycle

feedbacks using five Dynamic Global Vegetation Models (DGVMs). *Global Change Biology*, *14*(9), Article 9. https://doi.org/10.1111/j.1365-2486.2008.01626.x

Smercina, D. N., Evans, S. E., Friesen, M. L., & Tiemann, L. K. (2019). To Fix or Not To Fix: Controls on Free-Living Nitrogen Fixation in the Rhizosphere. *Applied and Environmental Microbiology*, *85*(6), e02546-18. https://doi.org/10.1128/AEM.02546-18

Smith, B., Richards, R. L., & Newton, W. E. (Eds.). (2004). *Catalysts for nitrogen fixation: Nitrogenases, relevant chemical models and commercial processes*. Kluwer Academic Publishers.

Srivastava, A., & Ambasht, R. S. (1993). Soil Moisture Control of Nitrogen Fixation in Dry Tropical Causarina Plantation Forest. *Journal of Environmental Management*.

Taylor, J. A., & Orr, J. C. (2000). The natural latitudinal distribution of atmospheric CO_2. *Global and Planetary Change*, *26*(4), 375–386. https://doi.org/10.1016/S0921-8181(00)00050-3

Tharammal, T., Bala, G., Devaraju, N., & Nemani, R. (2019). A review of the major drivers of the terrestrial carbon uptake: Model-based assessments, consensus, and uncertainties. *Environmental Research Letters*, *14*(9), 093005. https://doi.org/10.1088/1748-9326/ab3012

Thornton, P. E., Doney, S. C., Lindsay, K., Moore, J. K., Mahowald, N., Randerson, J. T., Fung, I., Lamarque, J.-F., Feddema, J. J., & Lee, Y.-H. (2009). Carbon-nitrogen interactions regulate climate-carbon cycle feedbacks: Results from an atmosphere-ocean general circulation model. *Biogeosciences*, *6*(10), 2099–2120. https://doi.org/10.5194/bg-6-2099-2009

Tranvik, L. J., Downing, J. A., Cotner, J. B., Loiselle, S. A., Striegl, R. G., Ballatore, T. J., Dillon, P., Finlay, K., Fortino, K., Knoll, L. B., Kortelainen, P. L., Kutser, T., Larsen, Soren., Laurion, I., Leech, D. M., McCallister, S. L., McKnight, D. M., Melack, J. M., Overholt, E., … Weyhenmeyer, G. A. (2009). Lakes and reservoirs as regulators of carbon cycling and climate. *Limnology and Oceanography*, *54*(6part2), 2298–2314. https://doi.org/10.4319/lo.2009.54.6_part_2.2298

U.S. DOE. (2020). *Free-Air CO_2 Enrichment Experiments. FACE Results, Lessons, and Legacy*. U.S. Department of Energy Office of Science.

van Vuuren, D. P., Stehfest, E., Gernaat, D. E. H. J., Doelman, J. C., van den Berg, M., Harmsen, M., de Boer, H. S., Bouwman, L. F., Daioglou, V., Edelenbosch, O. Y., Girod, B., Kram, T.,

Lassaletta, L., Lucas, P. L., van Meijl, H., Müller, C., van Ruijven, B. J., van der Sluis, S., & Tabeau, A. (2017). Energy, land-use and greenhouse gas emissions trajectories under a green growth paradigm. *Global Environmental Change*, *42*, 237–250. https://doi.org/10.1016/j.gloenvcha.2016.05.008

Vilén, T., Cienciala, E., Schelhaas, M. J., Verkerk, P. J., Lindner, M., & Peltola, H. (2016). Increasing carbon sinks in European forests: Effects of afforestation and changes in mean growing stock volume. *Forestry*, *89*(1), 82–90. https://doi.org/10.1093/forestry/cpv034

Vitousek, P. M., Menge, D. N. L., Reed, S. C., & Cleveland, C. C. (2013). Biological nitrogen fixation: Rates, patterns and ecological controls in terrestrial ecosystems. *Philosophical Transactions of the Royal Society B: Biological Sciences*, *368*(1621), 20130119. https://doi.org/10.1098/rstb.2013.0119

Vivian, B. (1994). Agricultural dimensions of global climate change. H.M. Kaiser and T.E. Drennen (eds) 311pp. Hardback $59.95 ISBN 0-963-40303-6 St.Lucie Press: Florida, 1993. *Sustainable Development*, *2*(3), 23–23. https://doi.org/10.1002/sd.3460020305

Vuichard, N., Messina, P., Luyssaert, S., Guenet, B., Zaehle, S., Ghattas, J., Bastrikov, V., & Peylin, P. (2019). Accounting for carbon and nitrogen interactions in the global terrestrial ecosystem model ORCHIDEE (trunk version, rev 4999): Multi-scale evaluation of gross primary production. *Geoscientific Model Development*, *12*(11), 4751–4779. https://doi.org/10.5194/gmd-12-4751-2019

Wagner, S. (2011). *Biological Nitrogen Fixation*. https://www.nature.com/scitable/knowledge/library/biological-nitrogen-fixation-23570419/

Wang, Y.-P., & Houlton, B. Z. (2009). Nitrogen constraints on terrestrial carbon uptake: Implications for the global carbon-climate feedback. *Geophysical Research Letters*, *36*(24), L24403. https://doi.org/10.1029/2009GL041009

Wei, N., Xia, J., Wang, Y., Zhang, X., Zhou, J., Bian, C., & Luo, Y. (2022). Nutrient Limitations Lead to a Reduced Magnitude of Disequilibrium in the Global Terrestrial Carbon Cycle. *Journal of Geophysical Research: Biogeosciences*, *127*(5). https://doi.org/10.1029/2021JG006764

Weng, E., Farrior, C. E., Dybzinski, R., & Pacala, S. W. (2017). Predicting vegetation type through physiological and environmental interactions with leaf traits: Evergreen and

deciduous forests in an earth system modeling framework. *Global Change Biology*, *23*(6), 2482–2498. https://doi.org/10.1111/gcb.13542

Whitmarsh, J., & Gonvindjee. (1999). The Photosynthetic Process. In *Concepts in Pholobiology: Photosynthesis and Photomorphogenesis.* Narosa Publishing House.

Wieder, W. R., Cleveland, C. C., Lawrence, D. M., & Bonan, G. B. (2015). Effects of model structural uncertainty on carbon cycle projections: Biological nitrogen fixation as a case study. *Environmental Research Letters*, *10*(4), 044016. https://doi.org/10.1088/1748-9326/10/4/044016

Williams, D. R. (2021, December 21). *Earth Fact Sheet*. Earth Fact Sheet. https://nssdc.gsfc.nasa.gov/planetary/factsheet/earthfact.html

Wu, L., & McGechan, M. B. (1998). A Review of Carbon and Nitrogen Processes in Four Soil Nitrogen Dynamics Models. *Journal of Agricultural Engineering Research*, *69*(4), 279–305. https://doi.org/10.1006/jaer.1997.0250

Yin, X., & Struik, P. C. (2009). C_3 and C_4 photosynthesis models: An overview from the perspective of crop modelling. *NJAS: Wageningen Journal of Life Sciences*, *57*(1), 27–38. https://doi.org/10.1016/j.njas.2009.07.001

Yu, T., & Zhuang, Q. (2020). Modeling biological nitrogen fixation in global natural terrestrial ecosystems. *Biogeosciences*, *17*(13), 3643–3657. https://doi.org/10.5194/bg-17-3643-2020

Zaehle, S. (2013). Terrestrial nitrogen–carbon cycle interactions at the global scale. *Philosophical Transactions of the Royal Society B: Biological Sciences*, *368*(1621), 20130125. https://doi.org/10.1098/rstb.2013.0125

Zaehle, S., & Friend, A. D. (2010). Carbon and nitrogen cycle dynamics in the O-CN land surface model: 1. Model description, site-scale evaluation, and sensitivity to parameter estimates: SITE-SCALE EVALUATION OF A C-N MODEL. *Global Biogeochemical Cycles*, *24*(1), n/a-n/a. https://doi.org/10.1029/2009GB003521

Zaehle, S., Jones, C. D., Houlton, B., Lamarque, J.-F., & Robertson, E. (2015). Nitrogen Availability Reduces CMIP5 Projections of Twenty-First-Century Land Carbon Uptake*. *Journal of Climate*, *28*(6), 2494–2511. https://doi.org/10.1175/JCLI-D-13-00776.1

Zhao, G., Liang, C., Feng, X., Liu, L., Zhu, J., Chen, N., Chen, Y., Wang, L., & Zhang, Y. (2020). Elevated CO_2 decreases soil carbon stability in Tibetan Plateau. *Environmental Research Letters*, *15*(11), 114002. https://doi.org/10.1088/1748-9326/abbb50

Zhuang, Q., Lu, Y., & Chen, M. (2012). An inventory of global N2O emissions from the soils of natural terrestrial ecosystems. *Atmospheric Environment*, *47*, 66–75. https://doi.org/10.1016/j.atmosenv.2011.11.036

Annexes

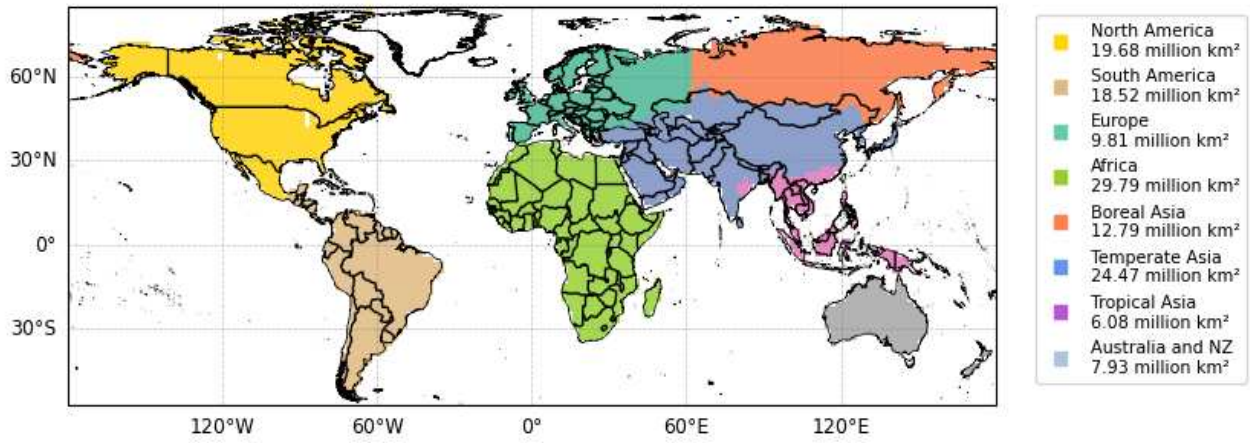

Figure A 1 – Area of the regional masks selected for the three-chapter analysis

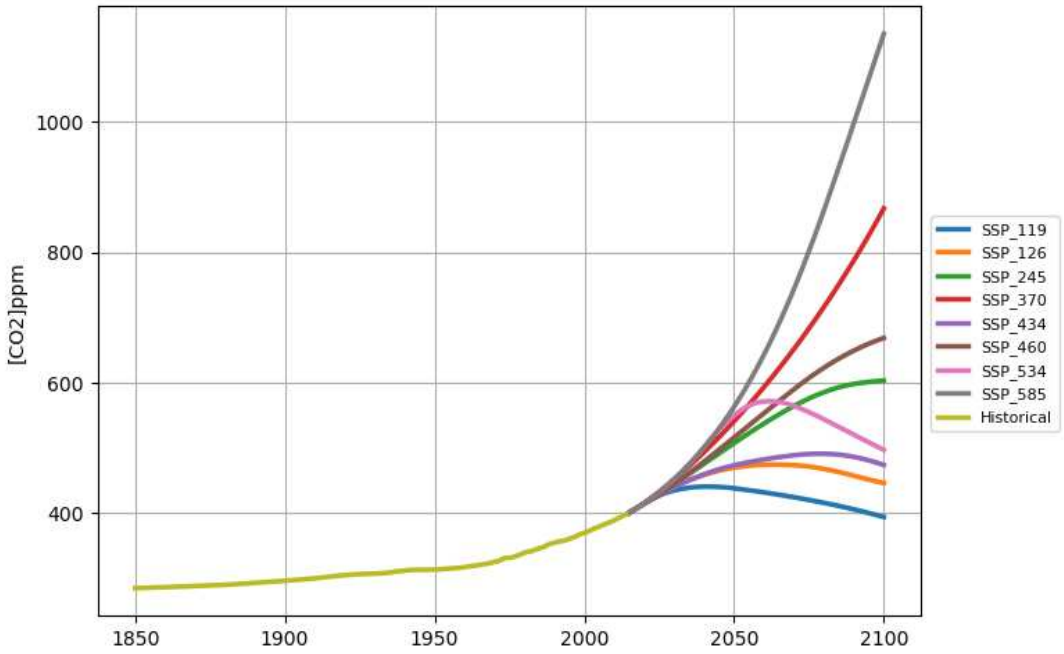

Figure A 2 - CO_2 annual global-mean surface concentration (ppm) was obtained from the consolidated database of historical and projected atmospheric greenhouse gasses concentration from the climate–carbon-cycle model MAGICC7.0 adapted from (Meinshausen et al., 2020).

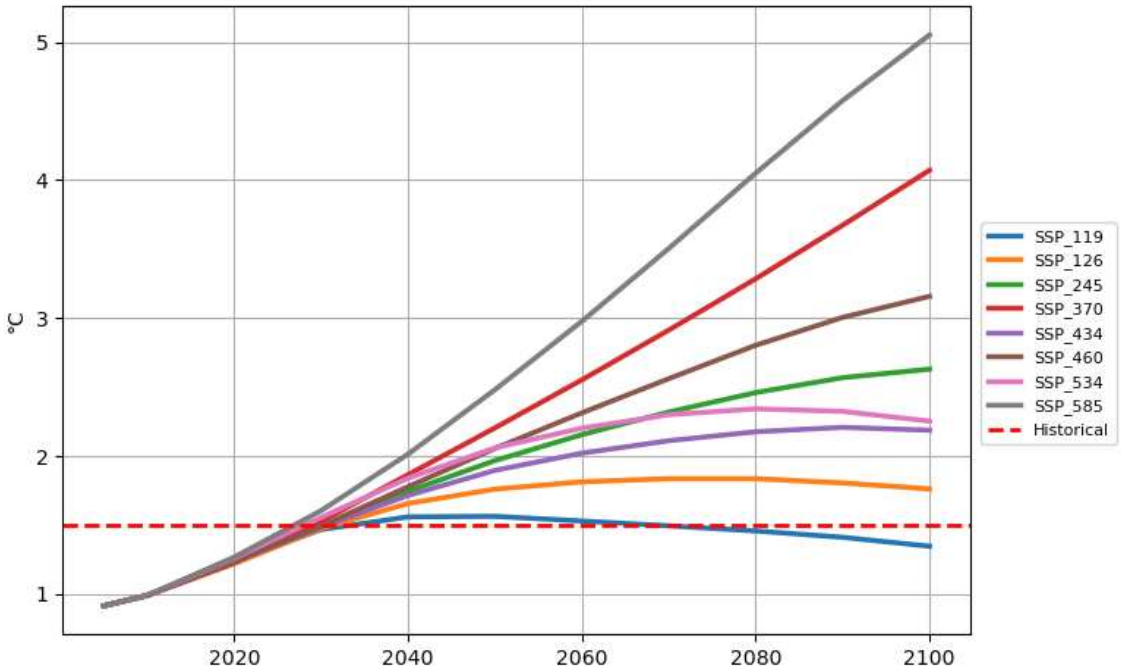

Figure A 3 - Global mean temperature increase from 2015 to 2100 from the SSP database adapted from (Riahi et al., 2017).

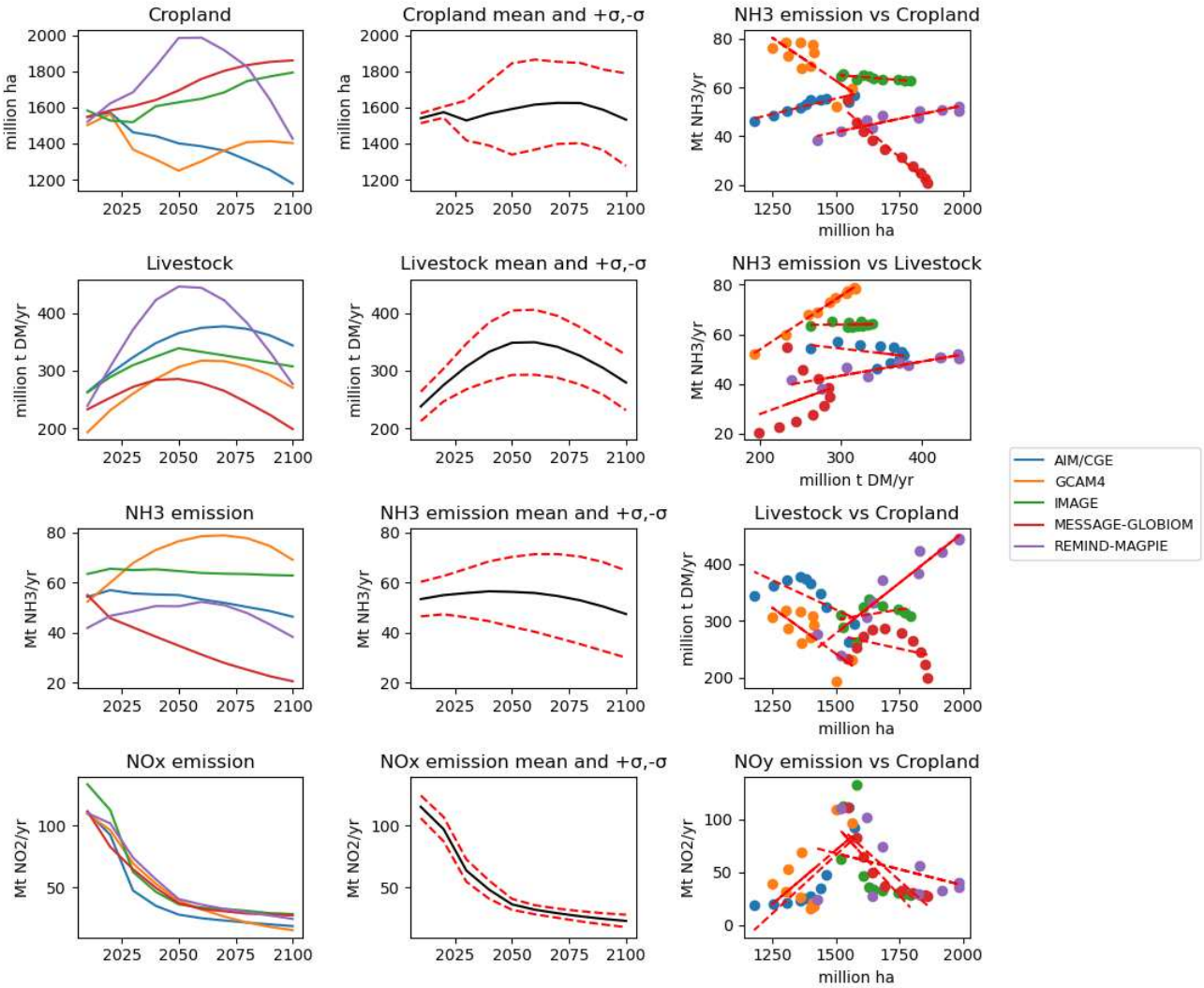

Figure A 4 – Trajectories of the evolution of cropland area (million ha), livestock (million t DM yr^{-1}), NH_3 emission (Mt NH_3 yr^{-1}) and NO_X emission (My NO_2 yr^{-1}) and their relationship for the IAM modelling groups for the SSP1-1.9.

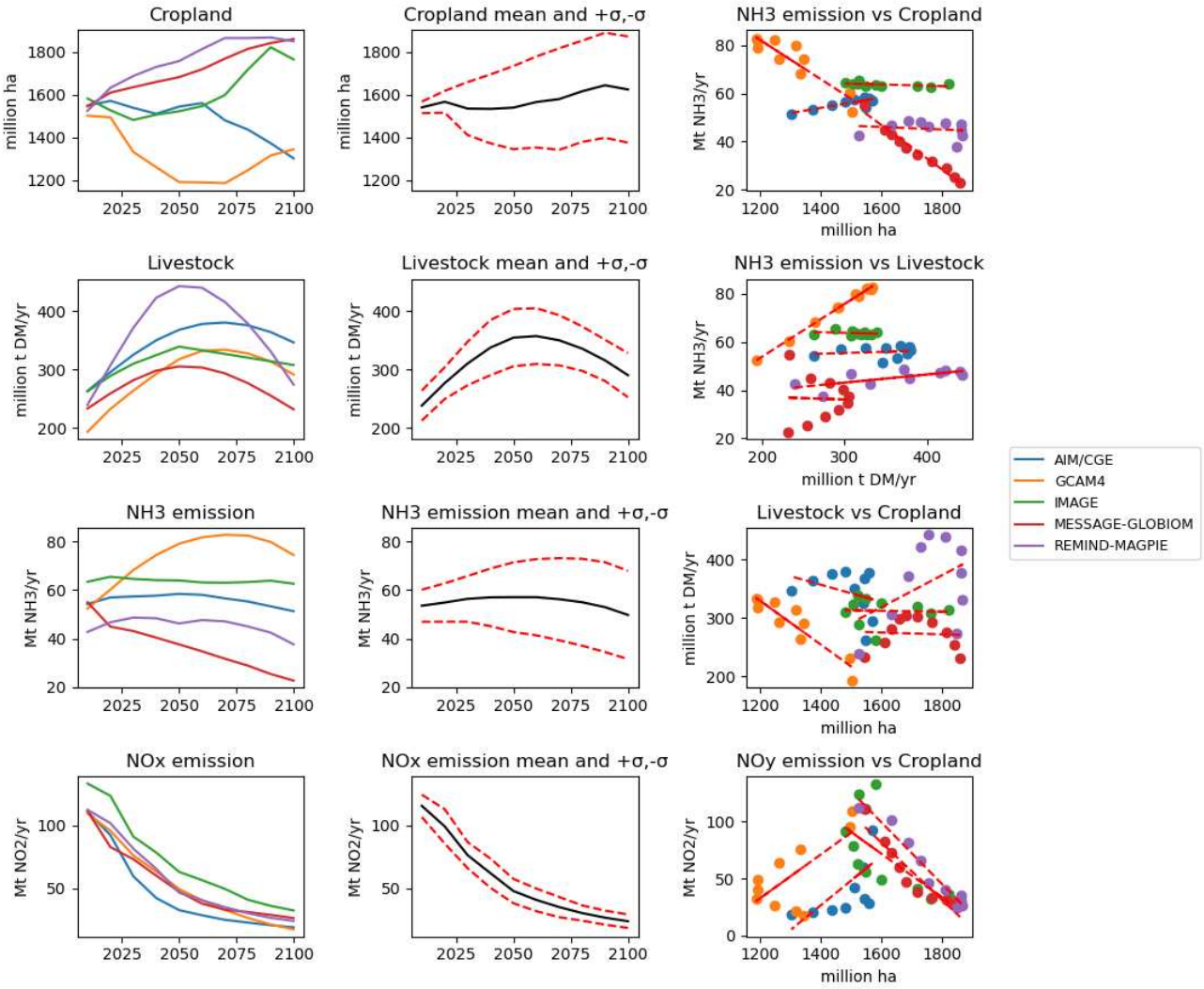

Figure A 5 – Trajectories of the evolution of cropland area (million ha), livestock (million t DM yr^{-1}), NH_3 emission (Mt NH_3 yr^{-1}) and NO_X emission (My NO_2 yr^{-1}) and their relationship for the IAM modelling groups for the SSP1-2.6.

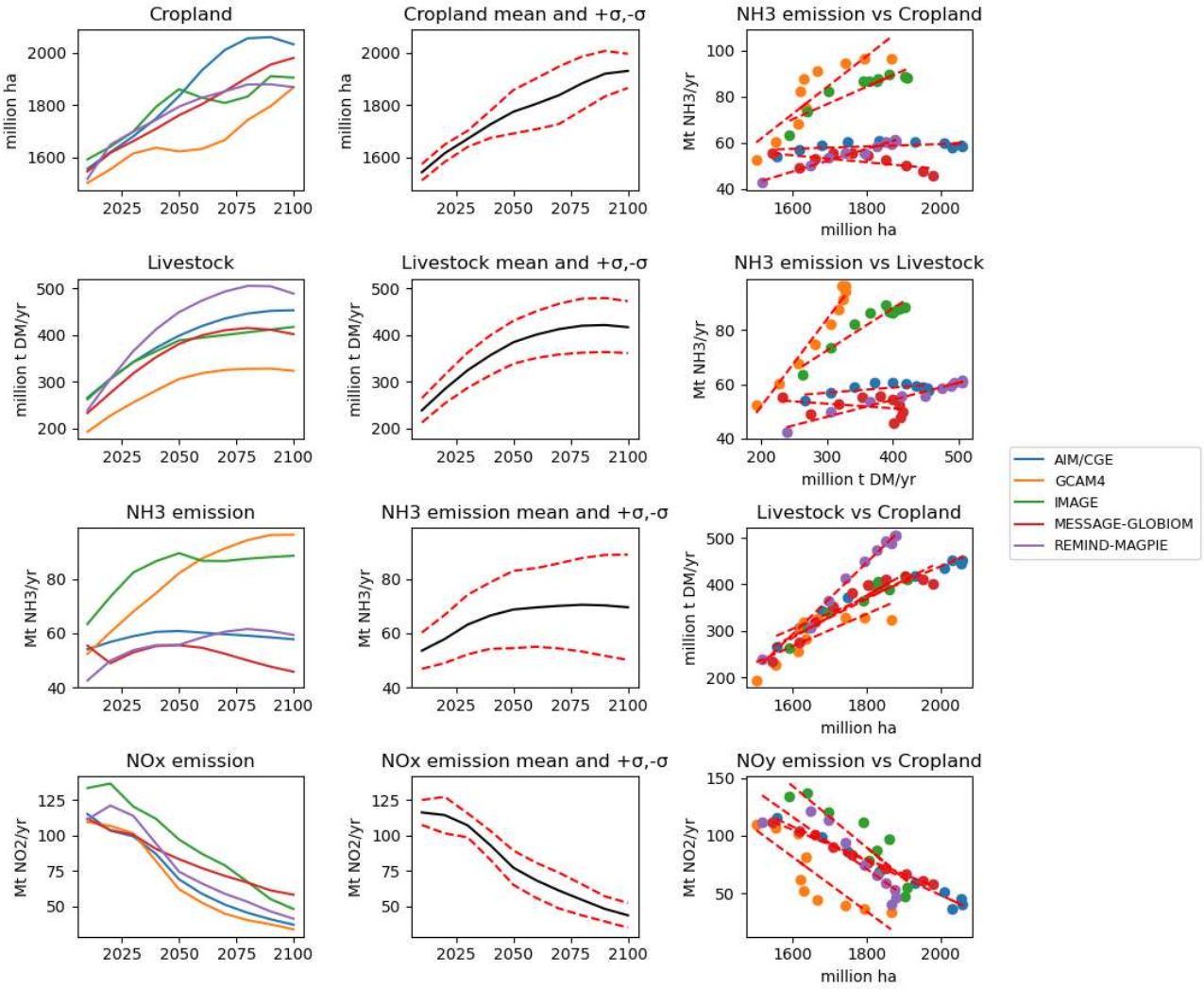

Figure A 6 – Trajectories of the evolution of cropland area (million ha), livestock (million t DM yr^{-1}), NH_3 emission (Mt NH_3 yr^{-1}) and NO_X emission (My NO_2 yr^{-1}) and their relationship for the IAM modelling groups for the SSP2-4.5.

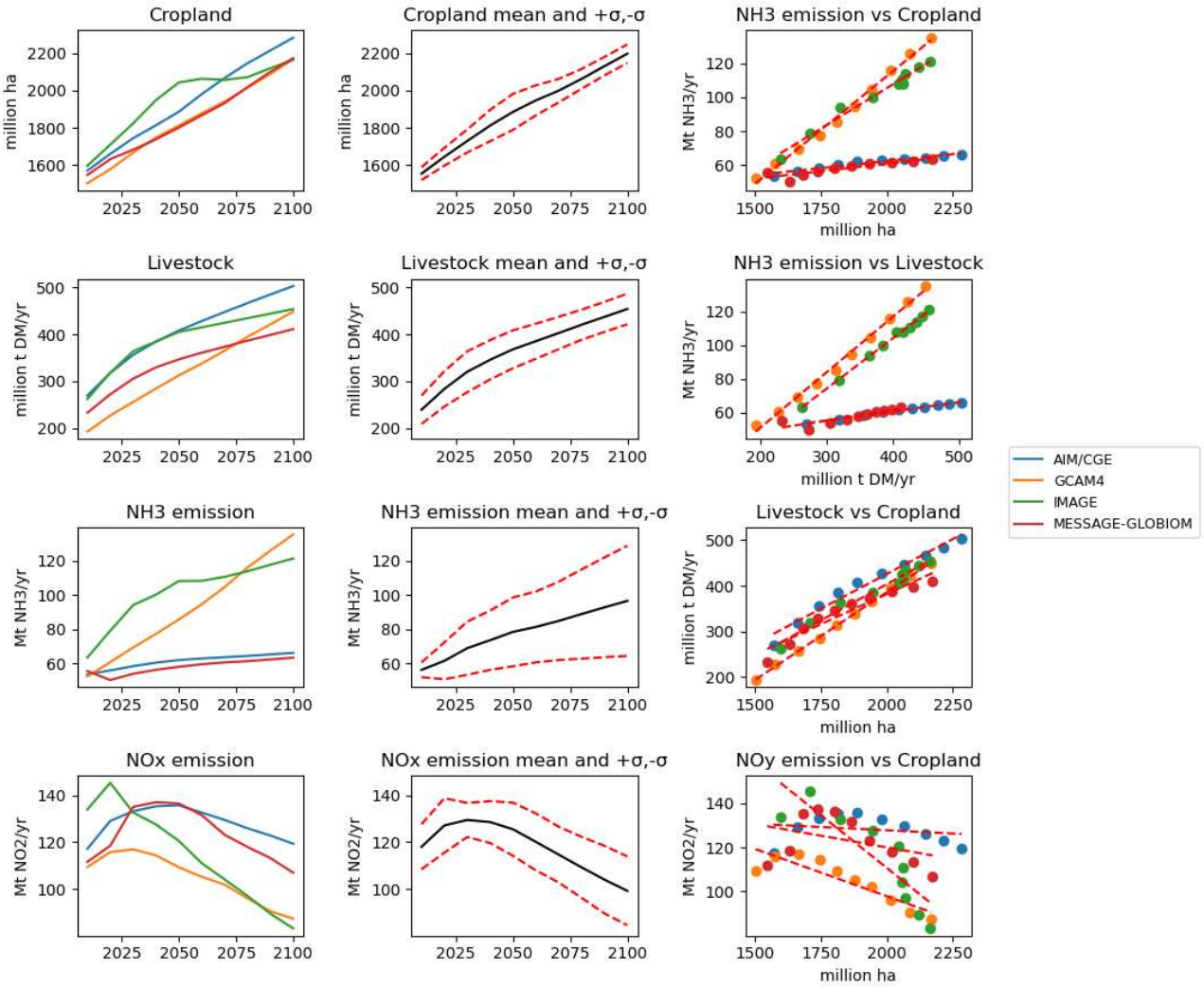

Figure A 7 – Trajectories of the evolution of cropland area (million ha), livestock (million t DM yr^{-1}), NH_3 emission (Mt NH_3 yr^{-1}) and NO_X emission (My NO_2 yr^{-1}) and their relationship for the IAM modelling groups for the SSP3-7.0.

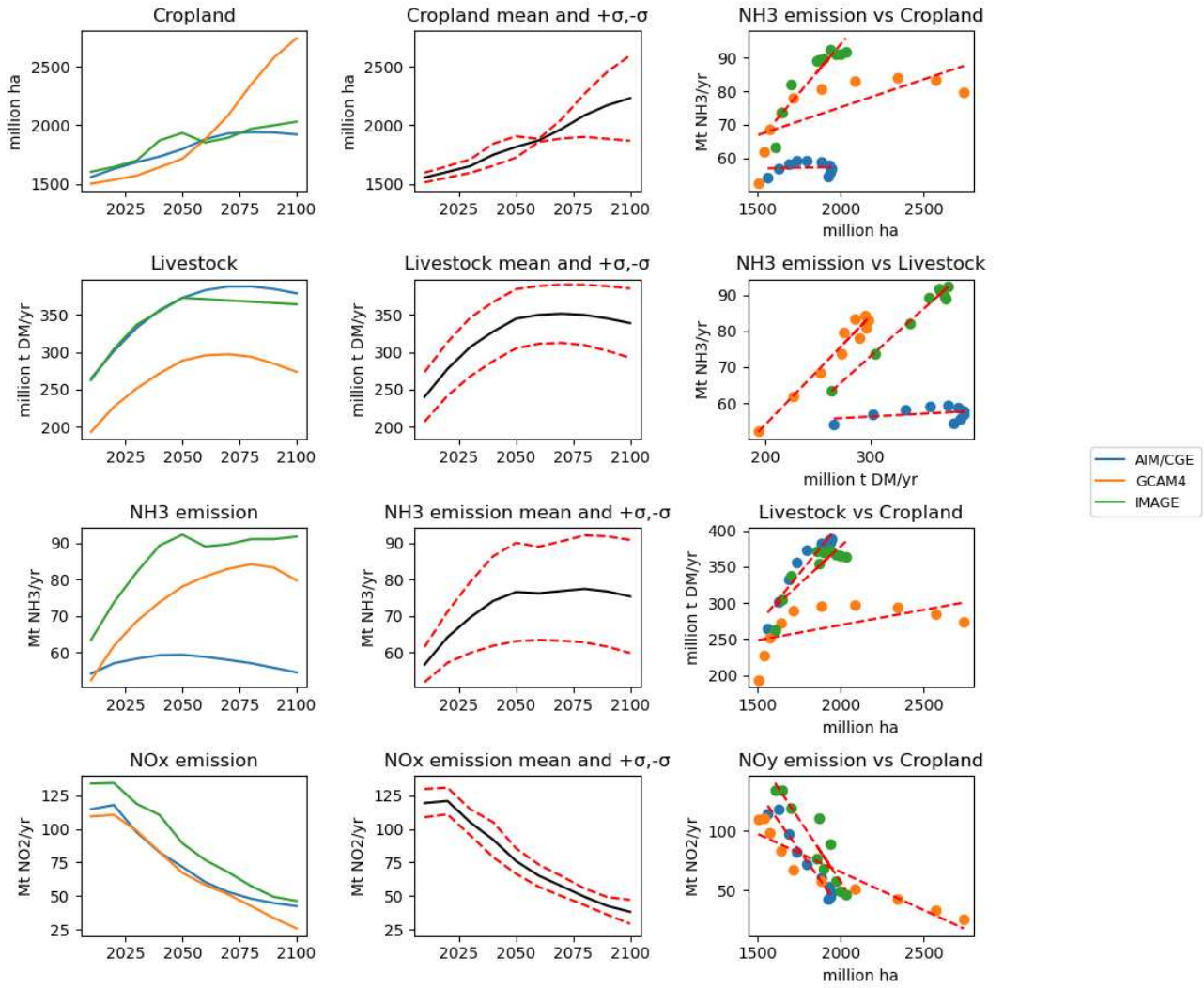

Figure A 8 – Trajectories of the evolution of cropland area (million ha), livestock (million t DM yr^{-1}), NH_3 emission (Mt NH_3 yr^{-1}) and NO_X emission (My NO_2 yr^{-1}) and their relationship for the IAM modelling groups for the SSP4-3.4.

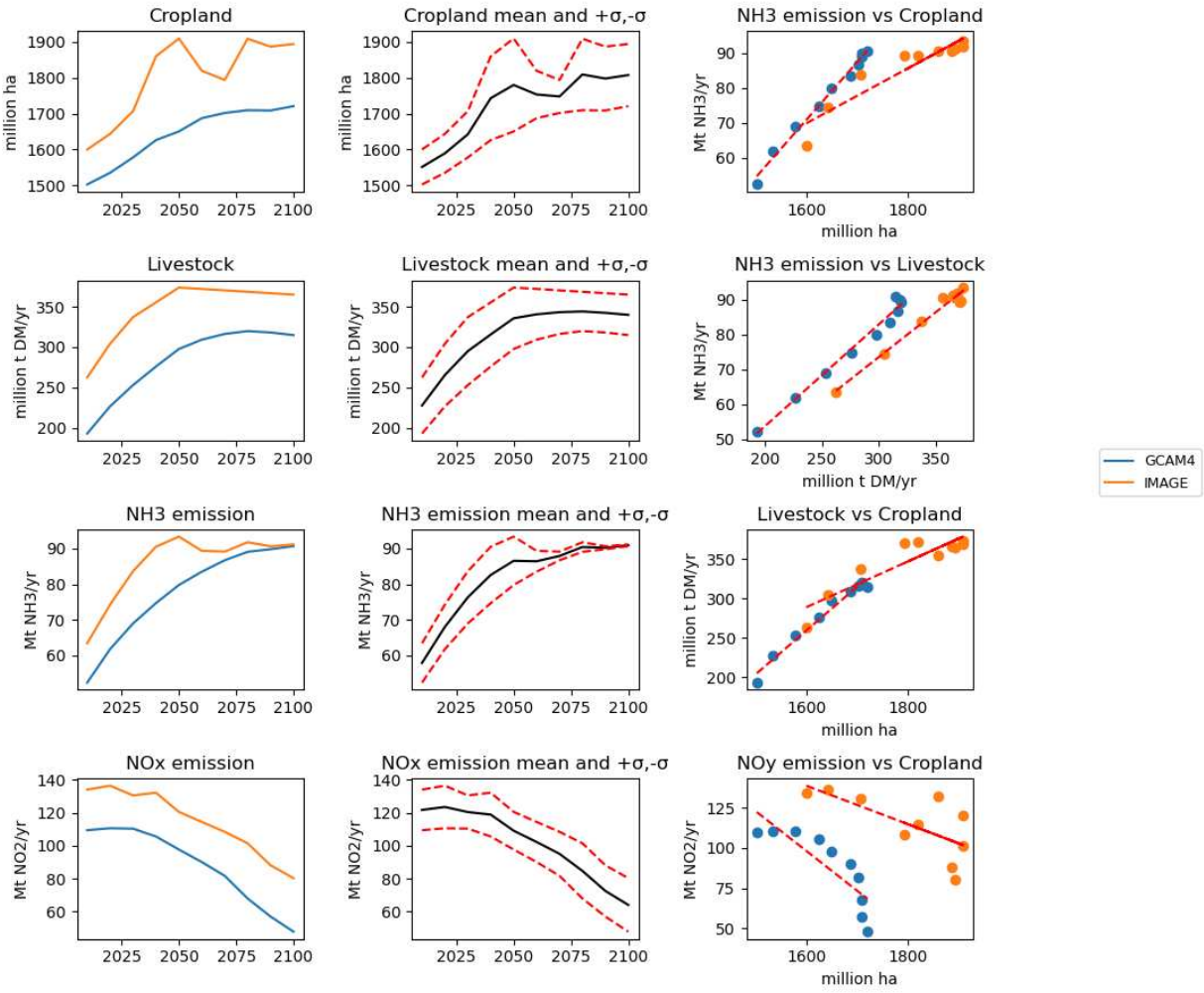

Figure A 9 – Trajectories of the evolution of cropland area (million ha), livestock (million t DM yr^{-1}), NH_3 emission (Mt NH3 yr^{-1}) and NO_X emission (My NO_2 yr^{-1}) and their relationship for the IAM modelling groups for the SSP4-6.0

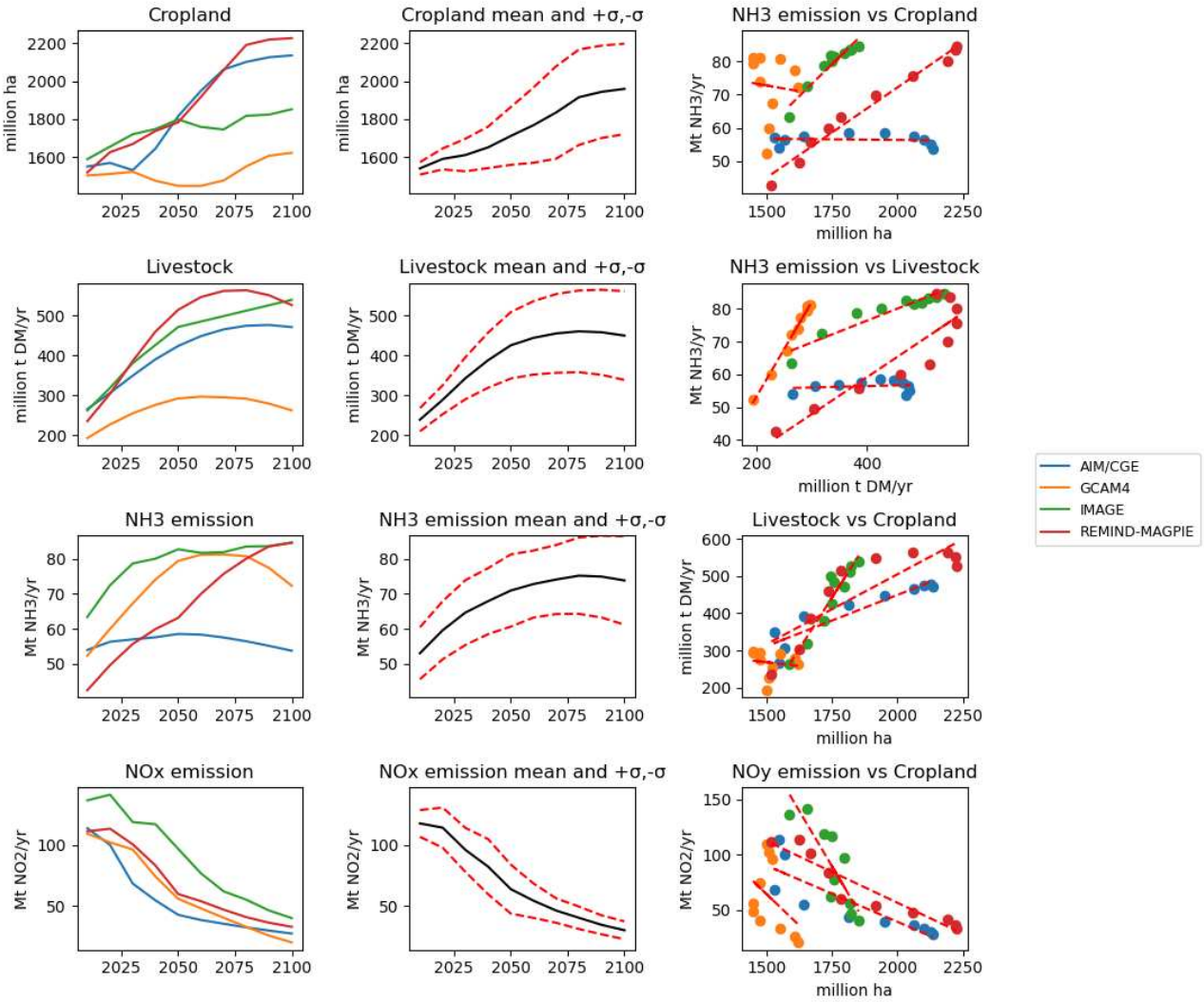

Figure A 10 – Trajectories of the evolution of cropland area (million ha), livestock (million t DM yr^{-1}), NH_3 emission (Mt NH_3 yr^{-1}) and NO_X emission (My NO_2 yr^{-1}) and their relationship for the IAM modelling groups for the SSP5-3.4.

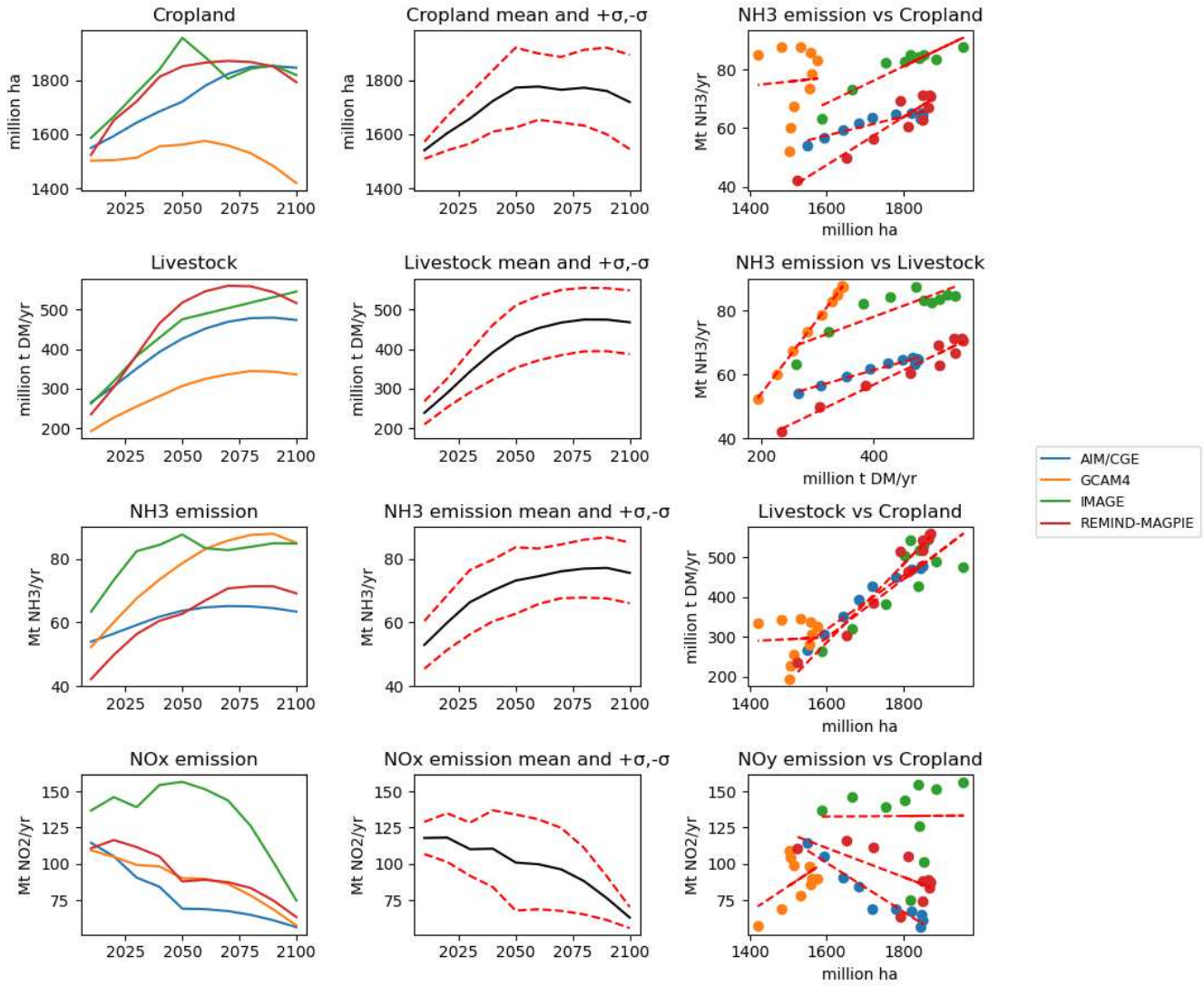

Figure A 11 – Trajectories of the evolution of cropland area (million ha), livestock (million t DM yr^{-1}), NH_3 emission (Mt NH_3 yr^{-1}) and NO_X emission (My NO_2 yr^{-1}) and their relationship for the IAM modelling groups for the SSP5-8.5.

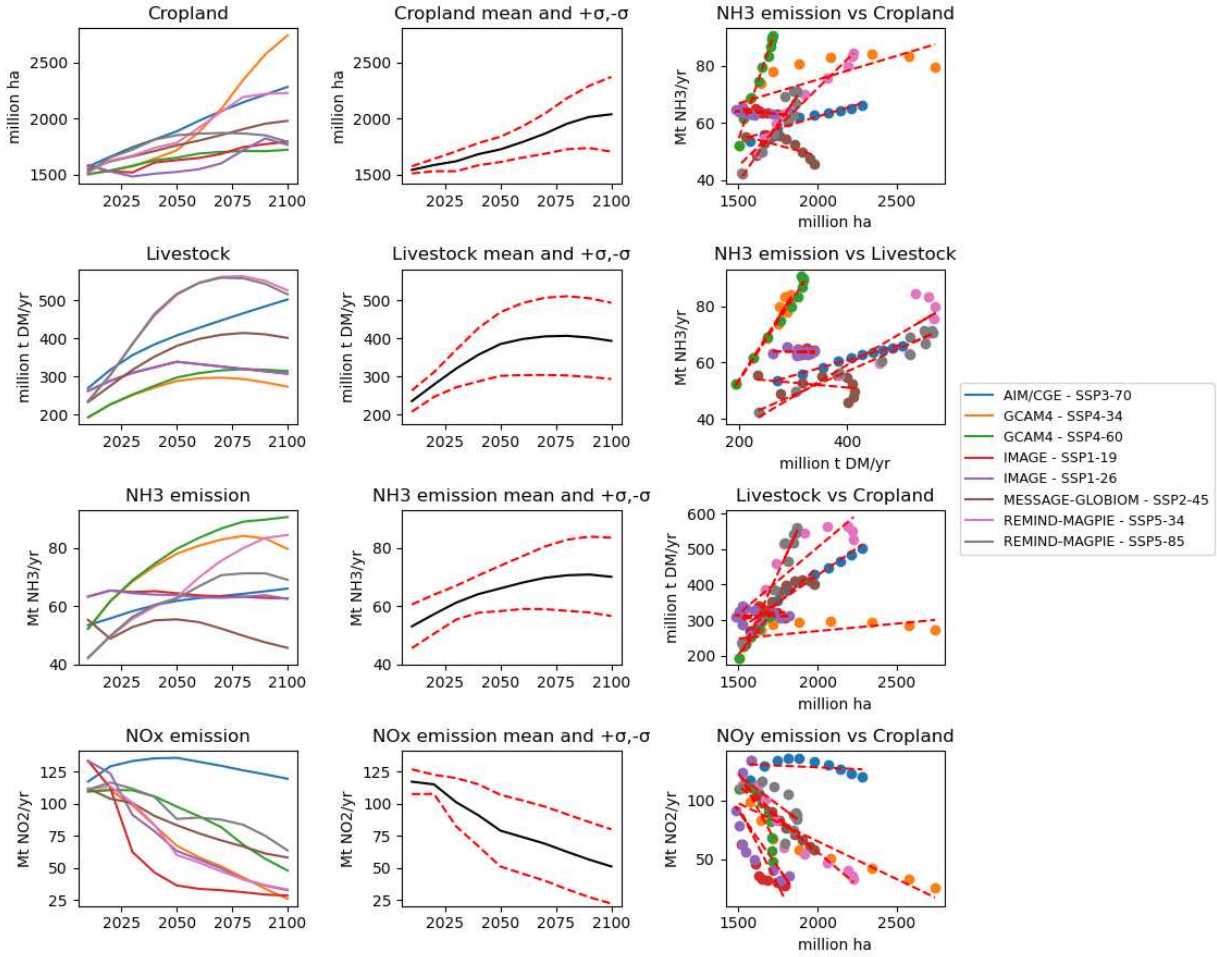

Figure A 12 – Trajectories of the evolution of cropland area (million ha), livestock (million t DM yr^{-1}), NH_3 emission (Mt NH_3 yr^{-1}) and NO_X emission (My NO_2 yr^{-1}) and their relationship for the IAM selected as a marker or the ScenarioMIP exercise.

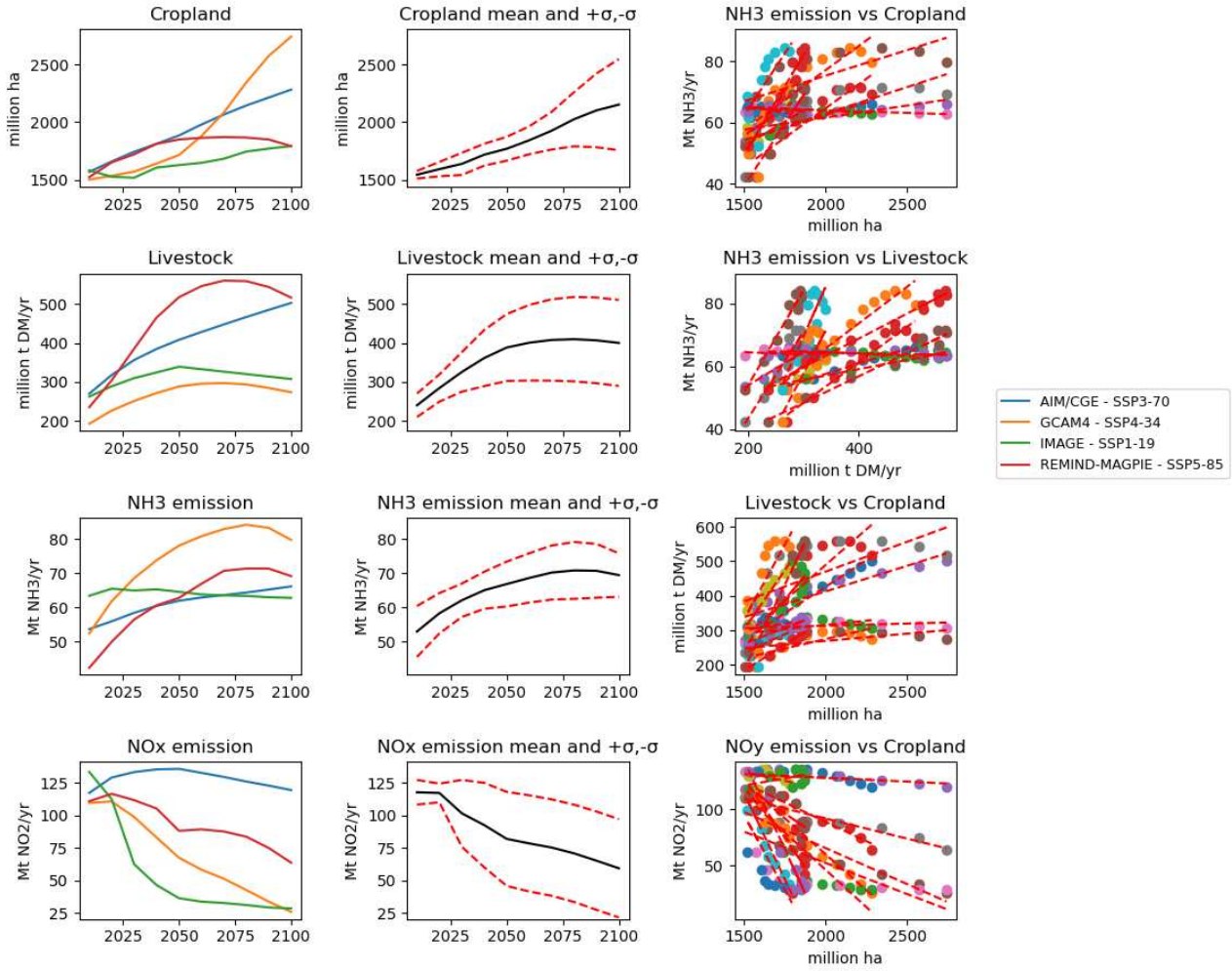

Figure A 13 – Trajectories of the evolution of cropland area (million ha), livestock (million t DM yr^{-1}), NH_3 emission (Mt NH_3 yr^{-1}) and NO_X emission (My NO_2 yr^{-1}) and their relationship for the IAM selected for our factorial simulation.

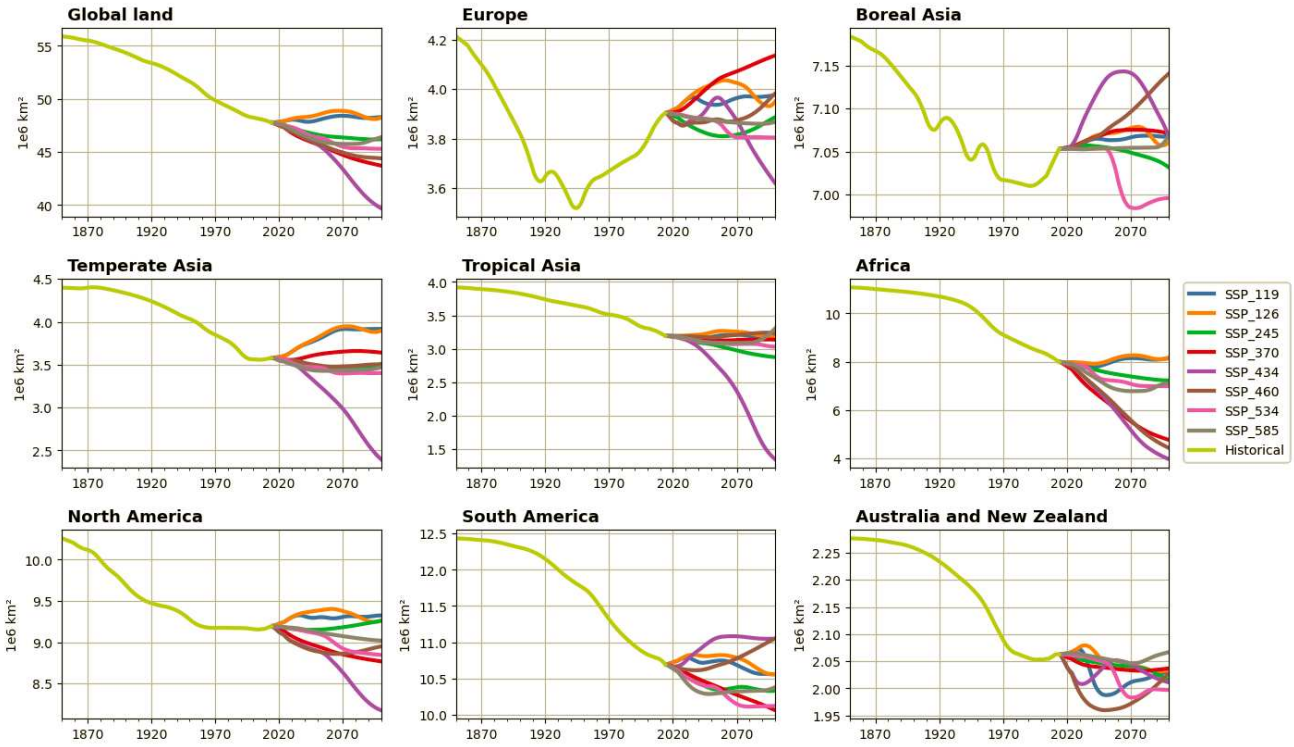

Figure A 14 - Forest land evolution in million km^2 from 1850 to 2100.

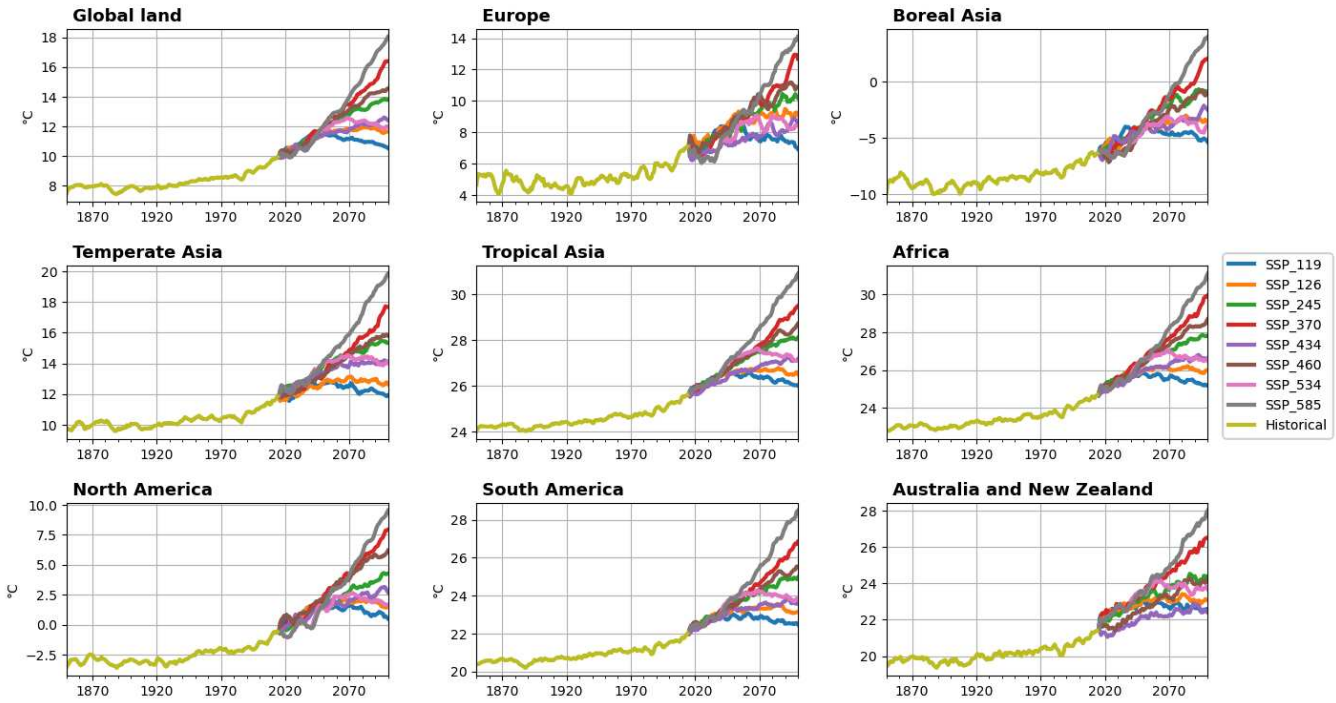

Figure A 15 - Mean soil temperature (°C) from 1850 to 2100.

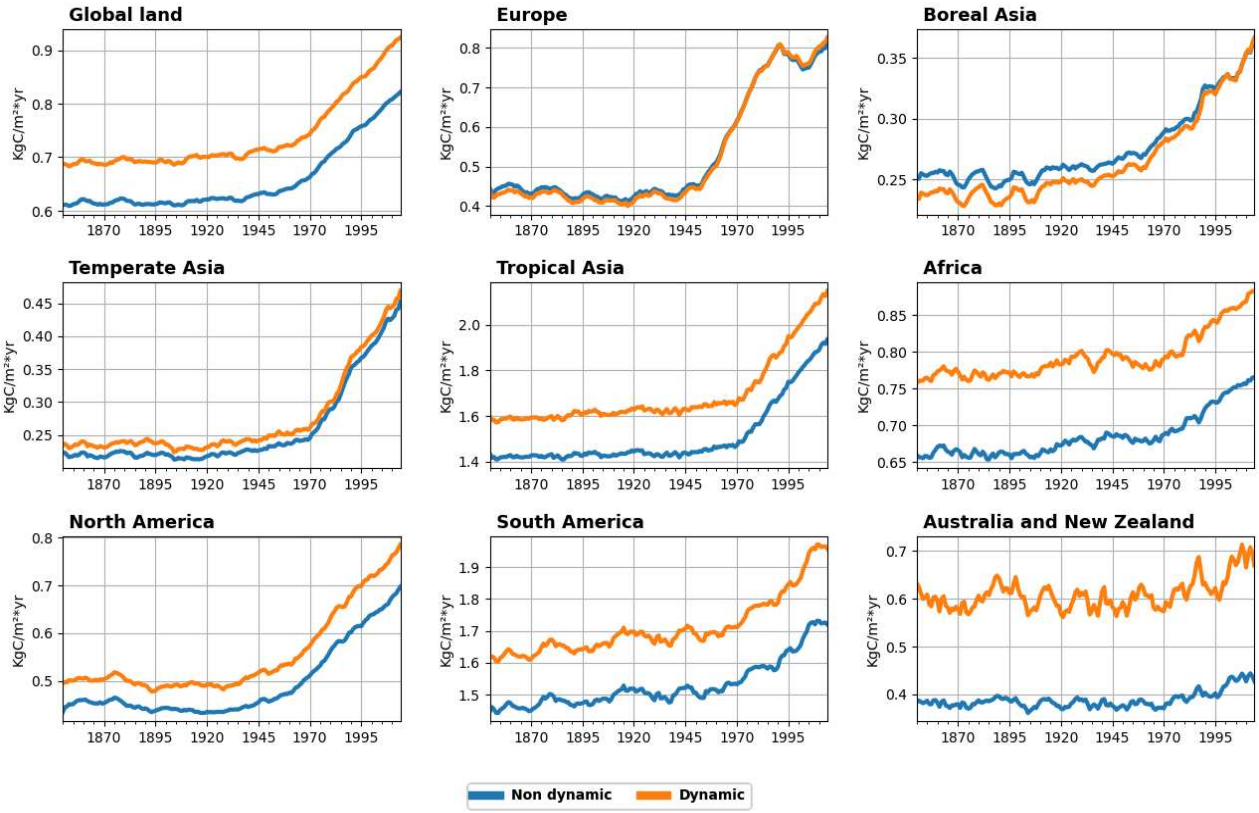

Figure A 16 - GPP for total lands in kgC m^{-2} yr^{-1} for a dynamic and static BNF implementation from 1850 to 2100.

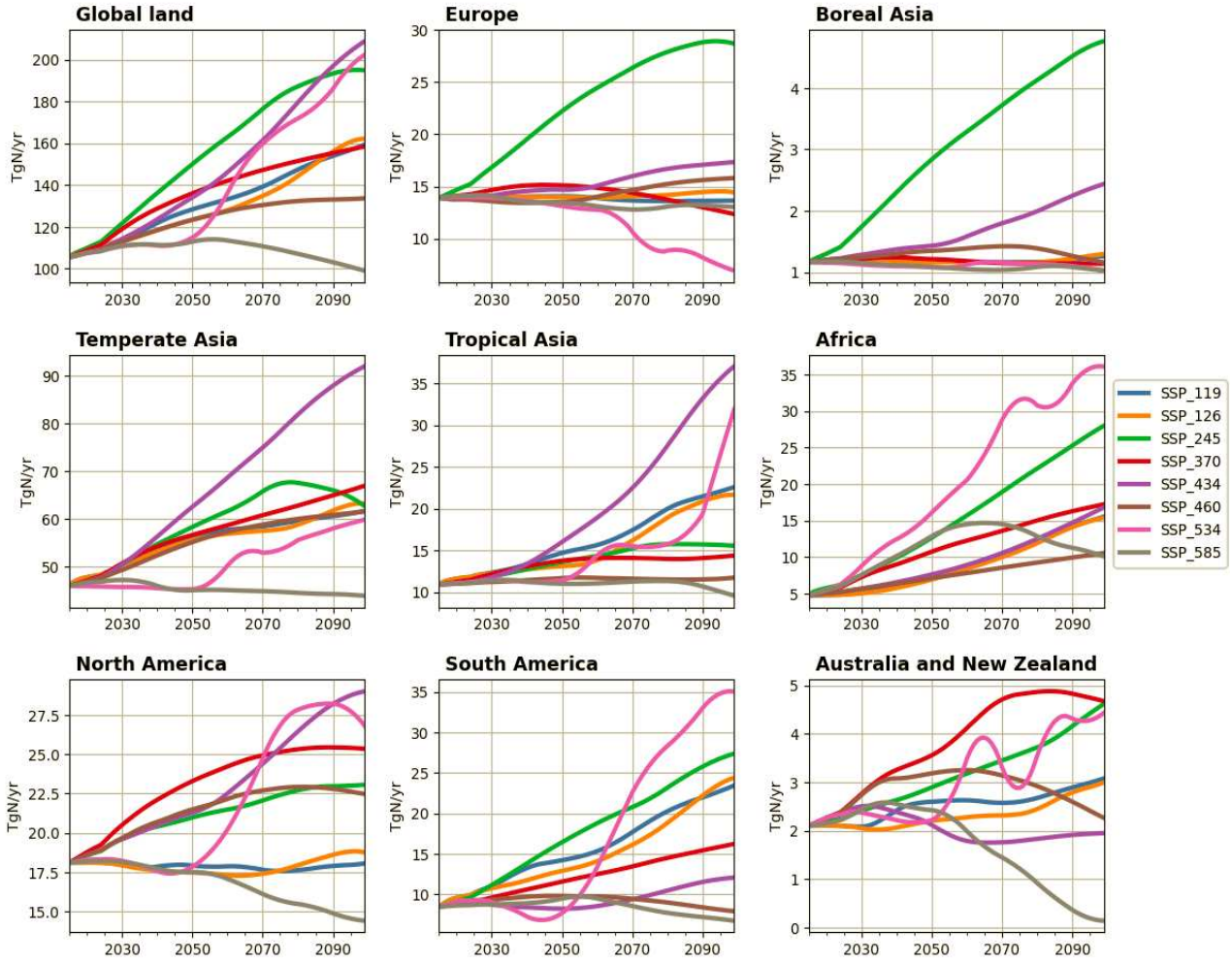

Figure A 17 – Total nitrogen application as fertilizer in TgN yr-1 for the projected scenarios SSPs.

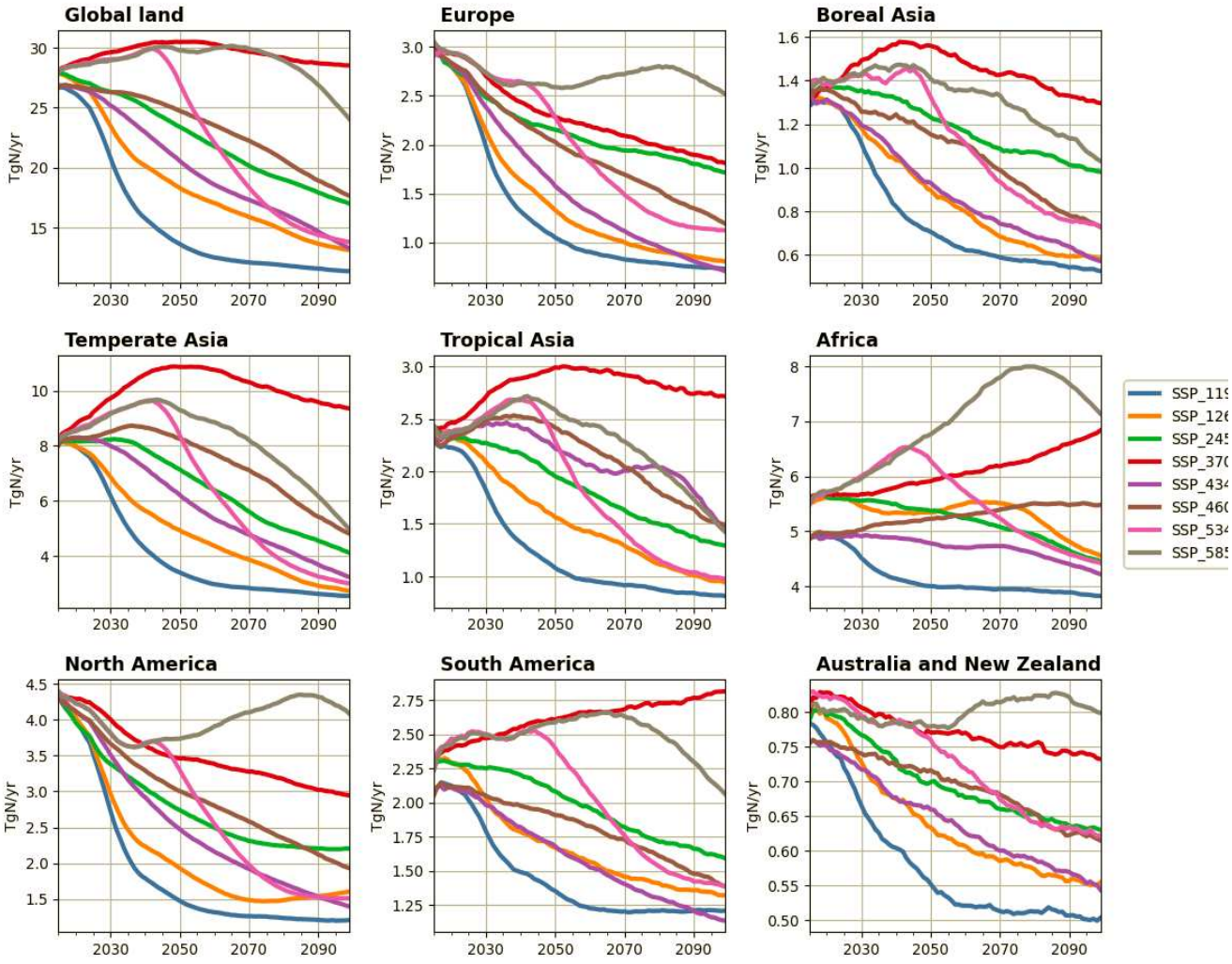

Figure A 18 – Total Noy deposition for all SSPs in TgN yr^{-1} from 2010 to 2100.

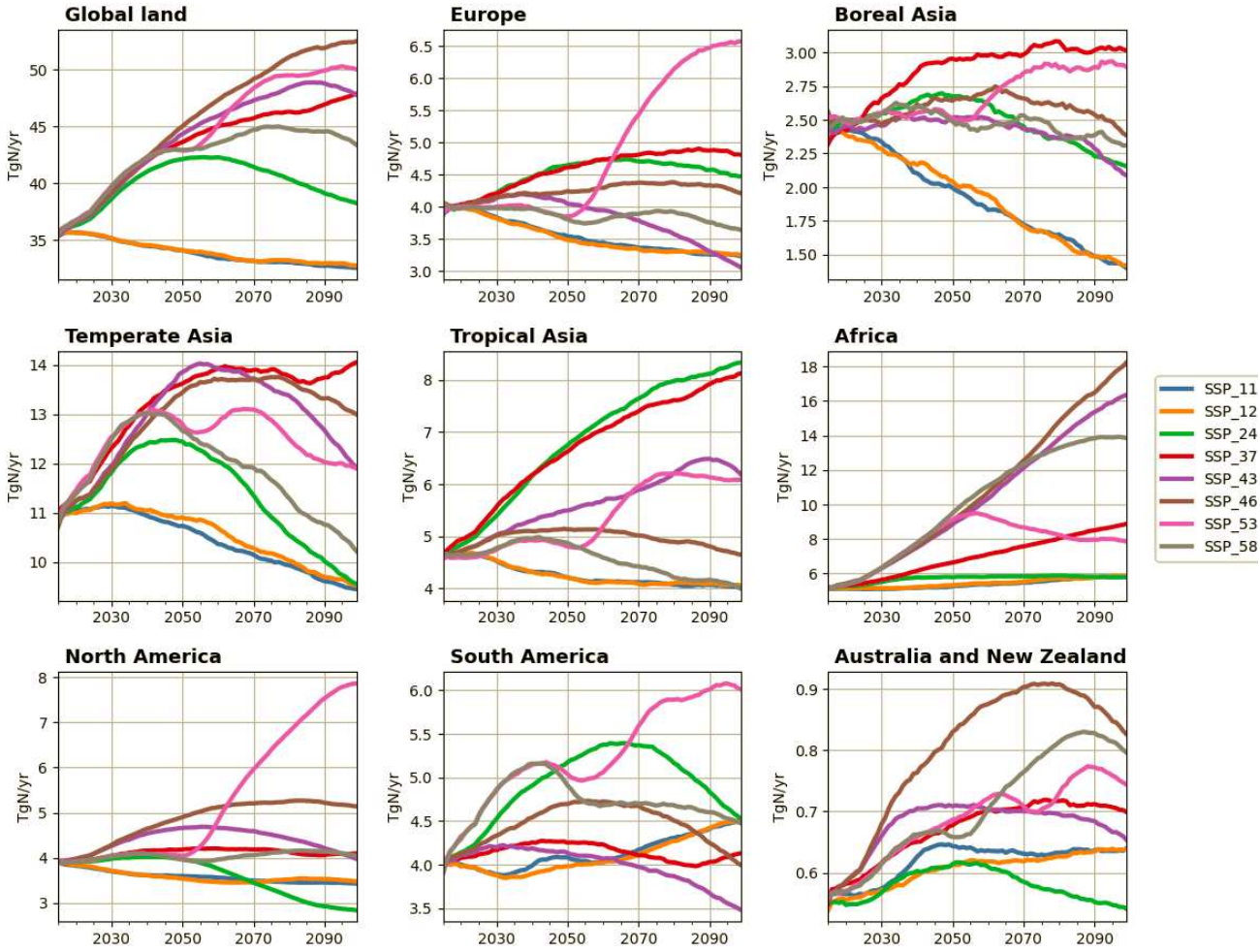

Figure A 19 – Total Noy deposition for all SSPs in TgN yr^{-1} from 2010 to 2100.

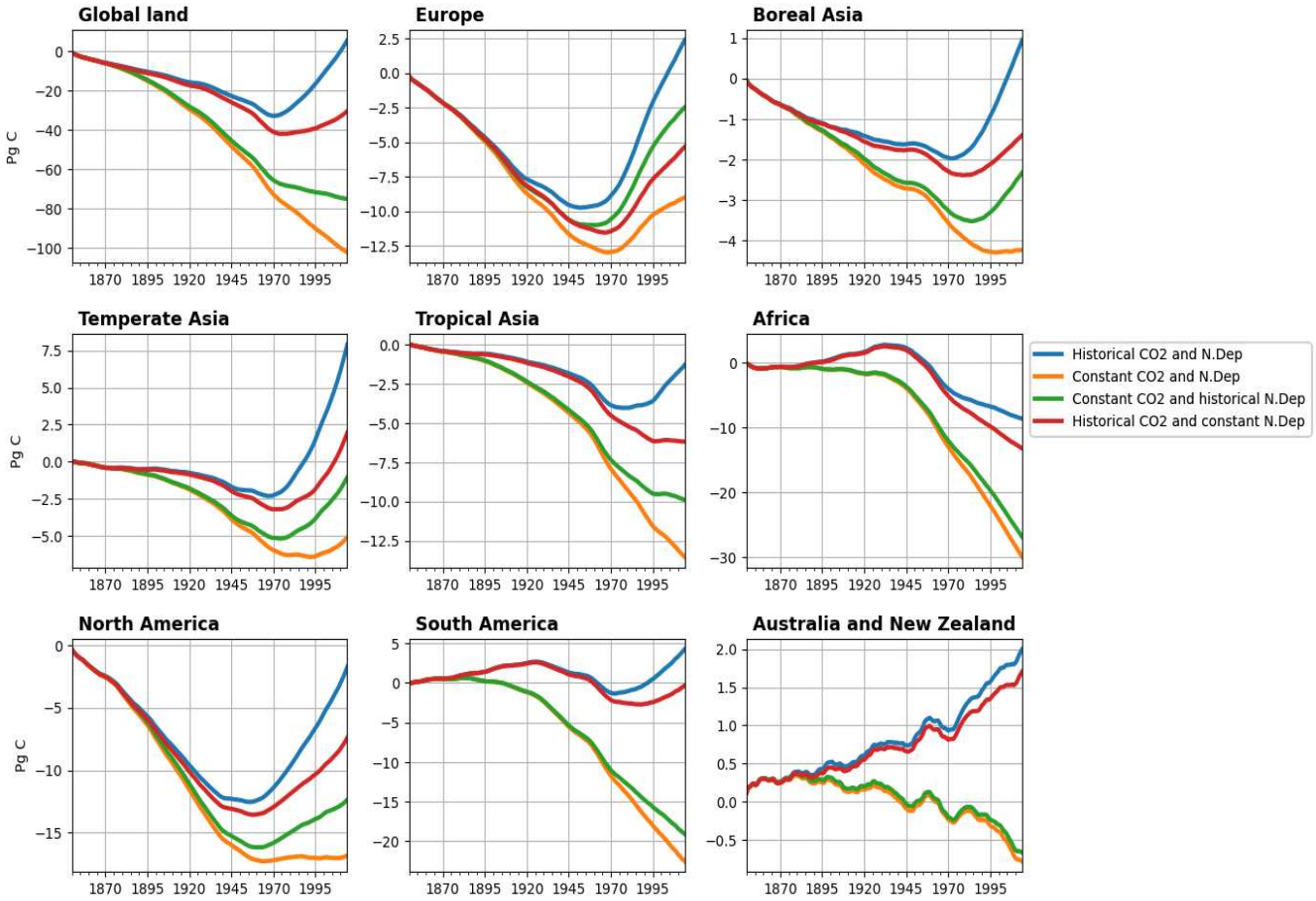

Figure A 20 - Accumulated NBP in PgC, also equivalent to Terrestrial Ecosystem Carbon TEC) for the protocol simulations from 1850 to 2015.

Site acronym	Site name, country	PFT[a] short name	Dominant vegetation	Forest age (2010)	H_{max}[b] (m)	LAI_{max}[c] ($m^2 m^{-2}$)	Lat. (° N)	Long. (° E)	Elevation[d] (m a.s.l.)	MAT[e] (°C)	MAP[f] (mm)	N_{dep}[g] ($g N m^{-2} yr^{-1}$)	GPP[h] ($g C m^{-2} yr^{-1}$)	R_{eco}[i] ($g C m^{-2} yr^{-1}$)	NEP[j] ($g C m^{-2} yr^{-1}$)
DE-Hai	Hainich, Germany	DB1	*Fagus sylvatica*	142	23	4.0	51.079	10.452	430	8.4	775	2.3	1553	1074	479
DK-Sor	Sorø, Denmark	DB2	*Fagus sylvatica*	91	31	4.6	55.487	11.646	40	8.9	730	2.2	1883	1581	301
FR-Fon	Fontainebleau-Barbeau, France	DB3	*Quercus petraea*	111	28	5.1	48.476	2.780	92	11.0	690	1.7	1850	1185	665
FR-Fgs	Fougères, France	DB4	*Fagus sylvatica*	41	20	6.0	48.383	−1.185	140	10.3	900	2.4	1725	1316	409
FR-Hes	Hesse, France	DB5	*Fagus sylvatica*	45	16	6.7	48.674	7.066	300	10.2	975	1.7	1634	1187	446
IT-Col	Collelongo, Italy	DB6	*Fagus sylvatica*	120	22	5.7	41.849	13.588	1560	7.2	1140	1.2	1425	776	650
CZ-BK1	Bily Kriz, Czech Rep.	EN1	*Picea abies*	33	13	9.8	49.503	18.538	908	7.8	1200	2.1	1548	767	781
DE-Hoe	Höglwald, Germany	EN2	*Picea abies*	104	35	6.3	48.300	11.100	540	8.9	870	3.2	1856	1229	627
DE-Tha	Tharandt, Germany	EN3	*Picea abies*	120	27	6.7	50.964	13.567	380	8.8	820	2.3	1997	1396	601
DE-Wet	Wetzstein, Germany	EN4	*Picea abies*	56	22	7.1	50.453	11.458	785	6.6	950	2.2	1809	1767	43
IT-Ren	Renon, Italy	EN5	*Picea abies*	111	29	5.1	46.588	11.435	1730	4.6	1010	1.3	1353	528	826
RU-Fyo	Fyodorovskoye, Russia	EN6	*Picea abies*	190	21	2.8	56.462	32.922	265	5.3	711	1.0	1488	1559	−70
UK-Gri	Griffin, UK	EN7	*Picea sitchensis*	29	12	6.5	56.617	−3.800	340	7.7	1200	0.7	989	677	311
BE-Bra	Brasschaat, Belgium	EN8	*Pinus sylvestris*	82	21	1.9	51.309	4.521	16	10.8	850	4.1	1272	1149	123
ES-ES1	El Saler, Spain	EN9	*Pinus halepensis*	111	10	2.6	39.346	−0.319	5	17.6	551	2.1	1552	960	593
FI-Hyy	Hyytiälä, Finland	EN10	*Pinus sylvestris*	48	18	3.4	61.848	24.295	181	3.8	709	0.5	1114	845	268
FI-Sod	Sodankylä, Finland	EN11	*Pinus sylvestris*	100	13	1.2	67.362	26.638	180	−0.4	527	0.3	551	598	−47
FR-Bil	Bilos, France	EN12	*Pinus pinaster*	9	4	0.5	44.522	−0.896	50	12.4	930	0.8	1178	989	189
FR-LBr	Le Bray, France	EN13	*Pinus pinaster*	41	22	1.9	44.717	−0.769	61	12.9	972	1.6	1906	1479	427
IT-SRo	San Rossore, Italy	EN14	*Pinus pinaster*	61	18	4.0	43.728	10.284	4	14.9	920	1.6	2256	1702	554
NL-Loo	Loobos, Netherlands	EN15	*Pinus sylvestris*	101	18	1.5	52.168	5.744	25	10.0	786	4.2	1617	1141	476
NL-Spe	Speulderbos, Netherlands	EN16	*Pseudotsuga menziesii*	51	32	7.5	52.252	5.691	52	10.0	834	4.3	1416	1015	401
SE-Nor	Norunda, Sweden	EN17	*Pinus sylvestris*	112	28	4.6	60.083	17.467	45	6.8	527	0.6	1414	1356	58
SE-Sk2	Skyttorp, Sweden	EN18	*Pinus sylvestris*	39	16	3.2	60.129	17.840	55	7.4	527	0.5	1235	953	282
ES-LMa	Las Majadas, Spain	EB1	*Quercus ilex*	111	8	0.6	39.941	−5.773	258	16.1	528	0.9	1091	958	133
FR-Pue	Puéchabon, France	EB2	*Quercus ilex*	69	6	2.9	43.741	3.596	270	13.7	872	1.1	1309	1030	279
IT-Ro2	Roccarespampani, Italy	EB3	*Quercus cerris*	21	16	3.8	42.390	11.921	224	15.7	876	1.8	1707	886	821
PT-Esp	Espirra, Portugal	EB4	*Eucalyptus globulus*	25	20	2.7	38.639	−8.602	95	16.1	709	1.2	1473	1163	311
PT-Mi1	Mitra, Portugal	EB5	*Quercus ilex, Quercus suber*	91	8	3.4	38.541	−8.000	264	14.5	665	0.9	870	817	53
BE-Vie	Vielsalm, Belgium	MF1	*Fagus sylvatica, Pseudotsuga menziesii*	86	30	5.1	50.305	5.997	450	8.1	1000	1.7	1792	1247	545
CH-Lae	Lägeren, Switzerland	MF2	*Fagus sylvatica, Picea abies*	111	30	3.6	47.478	8.365	689	7.7	1100	2.2	1448	757	692
DE-Meh	Mehrstedt, Germany	SN1	Afforested grassland	n/a	0.5	2.9	51.276	10.657	293	9.1	547	1.5	1171	1175	−4
ES-VDA	Vall d'Alinya, Spain	SN2	Upland grassland	n/a	0.1	1.4	42.152	1.448	1765	6.4	1064	1.2	669	528	140
FI-Lom	Lompolojänkkä, Finland	SN3	Peatland	n/a	0.4	1.0	67.998	24.209	269	−1.0	521	0.1	377	345	32
HU-Bug	Bugac, Hungary	SN4	Semi-arid grassland	n/a	0.5	4.7	46.692	19.602	111	10.7	500	1.4	1044	918	126
IT-Amp	Amplero, Italy	SN5	Upland grassland	n/a	0.4	2.5	41.904	13.605	884	9.8	1365	0.9	1241	1028	213
IT-MBo	Monte Bondone, Italy	SN6	Upland grassland	n/a	0.3	2.5	46.029	11.083	1550	5.1	1189	1.7	1435	1347	89
NL-Hor	Horstemeer, Netherlands	SN7	Peatland	n/a	2.5	6.9	52.029	5.068	−2	10.8	800	3.1	1584	1224	361
PL-wet	POLWET/Rzecin, Poland	SN8	Wetland (reeds, sedges, mosses)	n/a	2.1	4.9	52.762	16.309	54	8.5	550	1.4	937	642	295
UK-AMo	Auchencorth Moss, UK	SN9	Peatland	n/a	0.6	2.1	55.792	−3.239	270	7.6	1165	0.8	786	705	81

[a] PFT (plant functional types): DB – deciduous broadleaf forest; EN – evergreen needleleaf coniferous forest; EB – evergreen broadleaf Mediterranean forest; MF – mixed deciduous–coniferous forest; SN – short semi-natural, including moorland, peatland, shrubland and unimproved/upland grassland. [b] Maximum canopy height. [c] Maximum leaf area index, defined as one-sided or half of the total. [d] Above mean sea level. [e] Mean annual temperature. [f] Mean annual precipitation. [g] Nitrogen deposition. [h] Gross primary productivity. [i] Ecosystem respiration. [j] Net ecosystem productivity. n/a: not applicable.

Table A 1 - Forest measurement sites from the study from Flechard et al. 2020.

Region	*GPP(CO2) (PgC/yr)*	*% GPP(S1)*	*GPP(Ndep) (PgC/yr)*	*% GPP(S1)*	*GPP(Syn) (PgC/yr)*	*% GPP(S1)*	*Combined effect (PgC/yr)*	*Combined effect (%)*
1.World	14,71	53,24	5,74	20,76	2,43	8,8	22,88	82,8
2. Europe	0,68	16,31	1,07	25,88	0,33	7,87	2,08	50,06
3. Boreal Asia	0,34	24,61	0,36	26,64	0,1	7,22	0,8	58,47
4. Temperate Asia	2,14	31,2	0,81	11,76	0,55	8,04	3,5	51
5. Tropical Asia	1,51	44,54	1,1	32,53	0,43	12,69	3,04	89,76
6. Africa	3,62	119,11	0,73	24,13	0,36	11,8	4,71	155,04
7. North America	1,65	36,77	0,83	18,48	0,32	7,11	2,8	62,36
8. South America	4,24	103,02	0,81	19,67	0,31	7,45	5,36	130,14
9. Australia and NZ	0,53	182,79	0,01	4,71	0,04	13,81	0,58	201,31

Table A 2 - Impact of atmospheric CO_2 increase (GPP_{CO_2} in PgC yr^{-1}), Nitrogen deposition increase (GPP_{Ndep} in PgC yr^{-1}) , synergy between the two (GPP_{syn} in PgC yr^{-1}) and combined effect (GPP_{comb} in PgC yr^{-1}) and their percentage on the change of the total GPP (%) between 1850 and 2015.

Region	*NBP(CO2) (PgC/yr)*	*% NBP(S1)*	*NBP(Ndep) (PgC/yr)*	*% NBP(S1)*	*NBP(Syn) (PgC/yr)*	*% NBP(S1)*	*Combined effect (PgC/yr)*	*Combined effect (%)*
1.World	1,27	85,92	0,44	29,49	0,29	19,63	2	135,04
2. Europe	0,07	30,21	0,07	30,05	0,03	15,35	0,17	75,61
3. Boreal Asia	0,03	31,84	0,05	50,18	0,01	12,46	0,09	94,48
4. Temperate Asia	0,18	40,62	0,08	18,22	0,07	16,61	0,33	75,45
5. Tropical Asia	0,11	79,17	0,08	57,27	0,05	38,03	0,24	174,47
6. Africa	0,26	-373,07	0,04	-56,43	0,04	-53,99	0,34	-483,49
7. North America	0,17	49,94	0,06	18,31	0,04	11,62	0,27	79,87
8. South America	0,39	156,85	0,05	20,02	0,04	14,24	0,48	191,11
9. Australia and NZ	0,05	128,29	0,002	5,19	0,002	6,69	0,054	140,17

Table A 3 Impact of atmospheric CO_2 increase (NBP_{CO_2} in PgC yr^{-1}), Nitrogen deposition increase (NBP_{Ndep} in PgC yr^{-1}) , synergy between the two (NBP_{syn} in PgC yr^{-1}) and combined effect (NBP_{comb} in PgC yr^{-1}) and their percentage on the change of the total NBP (%) between 1850 and 2015.